34th International Gemmological Conference IGC

August 2015
Vilnius, Lithuania

34th International Gemmological Conference IGC

August, 2015
Vilnius, Lithuania

Dear Participants,

We are really honored for the first time to host IGC Conference here, in Lithuania – "Lonely Planet" Best in Travel destination for 2015. Thank you for taking this great opportunity to come to Europe's Northern Baroque pearl – capital Vilnius and our Amber land, Lithuania. Many of you are coming from afar to share great ideas and experiences, all in the single love to gemmology.

Since I joined IGC, I have been impressed by high level of intelligence and the pool of knowledge of great IGC community that was built almost 90-ty years ago and still continuing to grow. From Greenland to Japan, from France, Germany to India, Sri Lanka to Australia, from Tanzania, Switzerland to Vietnam, USA, Canada and many more – the community's in-depth research and awareness in science of gemmology shines through.

I am truly delighted that our worldwide dialogue and exchange in gemmological research will be held with the highest-level standard here, at Vilnius University, one of the oldest Alma Mater in Europe, developing its deep scientific traditions for over 430 hundred years.

I wish all of you an inspiring conference and great discoveries and emotions visiting our charming Vilnius and beautiful Lithuania – the country where World Amber Road starts.

Dr. Arūnas Kleišmantas
Chairman of 34th IGC 2015

Organising Committee for the 34th IGC Conference

Organisers

Dr. Arūnas Kleišmantas, Chairman of 34th IGC'2015, Vilnius – IGC programme development
Dr. Jayshree Panjikar, Executive Secretary – international coordination
Vilma Misiukonienė, Advisor to IGC – website, communication & public relations
Vilnius University, Department of Geology & Mineralogy and other units
Gem laboratory "Du Safyrai" & Gemmological Museum of Gemstones

Partners

Verslas ir poilsis Ltd, travel, event management and logistics
VTeX Ltd., scientific digital publishing solutions & services

Local planning

Dr. Arūnas Kleišmantas – general planning and coordination
Dr. Albertas Bitinas, Giedrius Bičkauskas – geological tours guides
Aušra Vadopalienė, Danutė Gricienė, Marius Krutkis, Verslas ir poilsis Ltd. – travel, event management & logistics
Kazimieras Dainovskis (IGC poster), Ieva Misiukonytė (brochures) – design

Review Board

Dr. Emmanuel Fritsch, University of Nantes and CNRS
Dr. Ulrich Henn, German Gemmological Association and Gemmological Training Centre
Dr. Hanco Zwann, Netherlands Gemmological Laboratory

Proceedings Layout & Editing

Ina Talandienė, Dr. Mirek Sheibak, VTeX Ltd.
Printed in Lithuania by Baltijos kopija Ltd.

Website

Vilma Misiukonienė, website content and project management
Dainius Kleišmantas, Web Admin
Technical solution by Citrus Ltd.

Special thanks

We'd like to give a big Thank to all our Patrons, Partners and Sponsors, and particulary to:

Dr. Antanas Smetona and Dr. Audrius Valotka, for their kind assistance to host IGC at Vilnius University
Karolina Zarankaitė and Citrus team for our website http://www.igc-gemmology.net/
Juozas Veilandas, photo artist for the availability of its facinating photos on Baltic Amber
Ina Talandienė for her restless hours and scrupulous work on book of Proceedings
Consular Department and its network at the Lithuanian Ministry of Foreign Affairs for great diplomatic services
Lithuanian State Department of Tourism for great help in setting important links and publicity

IGC Executive Board

Some of the members of Executive Committee with the Vice President of Vietnam at the IGC 2013 in Hanoi.

Dr. Jayshree Panjikar, Executive Secretary, India (fourth from the left)

Prof. Dr. Emmanuel Fritsch, France (first from the right)

Prof. Dr. Henry Hänni, Switzerland (third from the left)

Dr. Michael Krzemnicki, Switzerland

Dr. Karl Schmetzer, Germany

Dr. Dietmar Schwarz, Germany

Mr. Tay Thye Sun, Singapore

Mrs. Willow Wight, Canada

Mr. Gamini Zoysa, Sri Lanka (first from the left)

Dr. J.C. Hanco Zwaan, Netherlands (second from the left)

The Venue

In Lithuania, we do not waste time on things that do not matter. Few other capital cities in the world can offer you 15 minutes transfer time from the Vilnius airport to your downtown hotel. After you check in, you can be having drinks in Town Hall square five minutes later. After the hustle and bustle of the Old Town, it will take you another thirty minutes and you are in a lakeside sauna, or watching sunset immersed in a lake surrounded by dense forests.

This is how we do it. Get more space. Get more fun. Get more pictures. Get more. More life for every minute you spend in Lithuania.

In 2015 Lithuania became the newest member of the Eurozone and made the final step in the journey from reluctant Soviet republic to fully fledged European nation. Lithuania has been ranked third in Top 10 Lonely Planet's Best in Travel for 2015.

Lithuania – unexpected Amber Life

Ideal city break in vibrant Vilnius – the largest baroque old town in northern Europe – earned Lithuania one of its entries on the World Heritage list. The historic core of Lithuania's capital is an eye-pleasing assemblage, viewed from a hot air balloon and inviting with alleyways and colourful churches built around quiet courtyards. Tumble-down buildings hide designer boutiques and high-end handicraft shops lively pubs and bars, hidden terraces and romantic restaurants. As well, Vilnius proudly displays the world's only statue to Frank Zappa.

Amber – Lithuanian national symbol and pride – has also been used in folk medicine for its purported healing properties. Here you can start **World Amber Road** – an exclusive theme trip across the country with more than 100 amber stops inviting you to explore amber impressions in Lithuania: from the geographic old trade route of the Amber Road (98 km coastal strip) to amber SPA treatments (massages, saunas), getting to know the use of amber acid in cosmetic products and modern cooking, amber jewellery, design, incense. Try amber fishing in the Baltic Sea or listen to the Amber Quartet music played using unique instruments made from amber.

Basketball is called "Lithuania's second religion". The above-average height of Lithuanians is nearly 4 cm taller than the European norm – that's why we are called "Baltic Giants".

Curonian Spit – life changing experience, included into the World Heritage list and Lonely Planet's TOP-10 beaches in Europe for 2015. It is a 98 km long, thin, curved sand-dune spit that separates the Curonian Lagoon from the Baltic Sea coast. Visit one more World Heritage list object and get the-end-of-the-world feel and at a lonely, lovely strip of land topped by moving sand dunes, pines and tiny, charming villages.

Probably the most bizarre sight is Grūto parkas – known as Stalin World, with its statues of "heroic workers" and rescued busts of Lenin and Uncle Joe, spread around a forest park guarded by gulag-style watchtowers. The park exists not only to reflect the painful past of the nation, but also make fun of Communism. Lithuania was the first Soviet Republic to declare independence, leading the change in 1990. Around the country you'll find scattered more Soviet Union time remains: the most fascinating – and frightening – are former **Soviet nuclear missile base**, hidden among the forests and lakes of Žemaitija National Park and **Museum of Genocide Victims**, located in former headquarters of the Soviet KGB house in Vilnius.

Almost as strange is Šiauliai's Hill of Crosses, a collection of around 200,000 crucifixes of every imaginable kind and size, groaning under the weight of rosaries and devotional offerings. The first crosses appeared here after the 1831 uprising against Russian rule. Thousands of crosses left here over the years by pilgrims, visitors and newly-weds on their wedding day and the collection is constantly growing.

No visit to Lithuania would be complete without sampling some of the **native cooking**. The specialties of current Lithuanian cuisine are authentic, organic food and variety of seasonal, fresh products. The main course would probably be a cepelinai – nicknamed a "zeppelin" because of its elongated oval shape. These are big potato dumplings stuffed with meat or occasionally curd cheese, and served with sour cream and crispy bits of cubed bacon. In summer don't miss pink and cold beetroot soup – šaltibarščiai.

More information available at www.Lithuania.travel

The Conference Venue – Vilnius University

The Conference is held at the University of Vilnius, one of the oldest and most famous establishments of higher education in Eastern and Central Europe. The University of Vilnius was founded in 1579. Functioning for a long time as the only school of higher learning in Lithuania, it was a preserver of cultural and scientific traditions, and has played a significant part in the cultural life not only of Lithuania, but the neighboring countries as well. During more than four centuries of its existence, the University of Vilnius has seen periods of growth and decline, revival, and closure. The University is a unique witness to the history of the Lithuanian state. The University of Vilnius has 12 faculties, 7 institutes, 4 study and research centers. There are 20,6 thousands of students, where almost 1 thousand of them are internationals and 3,7 thousands of academia staff people are teaching there.

Organisers, Patrons, Partners and Sponsors

The organisers would like to thank the patrons, sponsors and partners, which have kindly contributed with their sponsorship to organise the 34th IGC Conference in Vilnius.

ORGANISERS:

PATRONS:

PARTNERS:

SPONSORS:

IGC 2015 Programme

23–25/08	Pre-conference tour "Feel Lithuania"
26–30/08	Conference, Central Building, Vilnius University
26–29/08	Guest programme
31/08 – 3/09	Post-conference tour "Towards Amber Road"

Conference Programme

Vilnius, Lithuania 26–30 August 2015

Wednesday 26 August

14.00–16.00	Excursion to Amber Museum Gallery and Church Heritage Museum
17.30	Registration at the Narutis Hotel (Columns Hall)
18.00–20.30	Ice Breaking Welcome Reception at the Narutis Hotel (Columns Hall)
20.30–21.30	Executive Committee (EXECO) Meeting

Thursday 27 August

8.30–9.00	Registration at the Small Aula, Central Building, Vilnius University
9.00–9.45	Opening ceremony at the Small Aula, Central Building, Vilnius University
9.45–10.15	Coffee break

Amber/Diamonds
Session at the Donelaitis Hall, Faculty of Philology, Vilnius University

Chairperson Dr. Ulrich Henn

10.15–10.35	Sigitas Podėnas: Crane flies (Diptera, Tipuloidea) from Baltic amber
10.35–10.55	Albertas Bitinas: Amber in the Southeast Baltic Sea region: Geological aspect
10.55–11.15	Jonas Satkūnas: Perspectives of amber production in Lithuania
11.15–11.30	Coffee break

Chairperson Dr. Henry Haenni

11.30–11.50	Willow Wight: Canadian Amber—History and significance to science
11.50–12.10	Lore Kiefert: Natural green amber from Ethiopia

12.10–12.30 Tay Thye Sun, Arunas Kleismantas, Thet Tin Nyunt, Zheng Minrui, Murali Krishnaswamy, Loke Hui Ying: Burmese amber from Hti Lin

12.30–14.00 Lunch

Chairperson Dr. Emmanuel Fritsch

14.00–14.20 Thomas Hainschwang, Franck Notari, Emmanuel Fritsch: Natural "lonsdaleite and CO_2 rich" diamonds

14.20–14.40 Hiroshi Kitawaki, Mio Hisanaga, Masahiro Yamamoto, Kentaro Emori: Type Ib yellow to brownish yellow CVD synthetic diamond

14.40–15.00 Joe C.C. Yuan: Identification and influence to the future market of synthetic diamond

15.00–16.00 Poster session (see below)

16.00–16.20 Coffee break

16.20 Conference day closes

16.30–18.00 Excursion to Palace of the Grand Dukes of Lithuania

19.30 Transfer to Belmontas park

20.00–22.00 Dinner at Belmontas restaurant

Friday 28 August

Coloured Stones/Testing Techniques
Corundum natural, treated
Session at the Donelaitis Hall, Faculty of Philology, Vilnius University

8.00–8.45 Executive Committee meeting

Chairperson Dr. Dietmar Schwarz

9.00–9.20 Anette Juul-Nielsen: Small scale mining of rubies and pink sapphires at Fiskenaesset, Greenland

9.20–9.40 Jayshree Panjikar, Aatish Panjikar: Investigation into the asterism observed in the star ruby from Neriya, Karnataka, India

9.40–10.00 Kentaro Emori, Hiroshi Kitawaki: Geographic origin determination of ruby and blue sapphire based on trace element analysis using LA-ICP-MS and 3D-plot

10.00–10.20 Emilie Elmaleh, Stefanos Karampelas, Susanne Theodora Schmidt, Federico Galster: Zircon inclusions in blue sapphires

10.20–10.40 Coffee break

Chairperson Mr. Tay Thye Sun

10.40–11.00 J.C. (Hanco) Zwaan, Eric Buter, Regina Mertz-Kraus, Robert E. Kane: Alluvial sapphires from Montana – Inclusions, geochemistry and indications for a metasomatic origin

11.00–11.20 E. Gamini, G. Zoysa: Sapphire deposits of Sri Lanka

11.20–11.40 K. Schmetzer, M.P. Steinbach, H.A. Gilg, A.R. Blake: Dual-color double stars in corundum and quartz

11.40–12.00 Visut Pisutha-Arnond, Chaniya Rochd, Wilawan Atichat, Pornsawat Wathanakul, Nalin Narudeesombat: Role of Be in reduction and oxidation heating of sapphire

12.00–13.30 Lunch

Chairperson Dr. Hanco Zwaan

13.30–13.50 Walter A. Balmer, Michael S. Krzemnicki: Be-detection by FTIR on corundum: A preliminary report

13.50–14.10 Thanong Leelawatanasuk, Nalin Naruedeesombat, Namrawee Susawee, Pantaree Lomthong, Pornsawat Wathanakul: "Surface de-leaded" ruby

14.10–14.30 Ahmadjan Abduriyim: Residual pressure distribution and visualization of mineral inclusions in corundum: application of photoluminescence spectroscopy in relation to sapphires from New England, New South Wales, Australia

14.30–14.50 S.I. Liu, C.M. Ouyang, F.Y. Ng: The application of VPSEM-Raman coupled system in studying Fei Cui

14.50–15.50 Poster session (see below)

15.50–16.10 Coffee break

16.10 Conference day closes

17.30 Departure by bus from Vilnius to Trakai

18.30 Family picture with all the participants at the Trakai Castle

20.00–23.00 Gala dinner at the Trakai Castle

Saturday 29 August

Coloured Stones/Pearls

Session at the Donelaitis Hall, Faculty of Philology, Vilnius University
Chairperson Dr. Lore Kiefert

9.00–9.20 Shane F. McClure: Brazilian emeralds from the Belmont mine

9.20–9.40 Masaki Furuya, Scott Davies: Gemmological features of pallasitic peridot of six different meteorites

9.40–10.00 R. Serov, Y. Shelementiev, A. Serova: Russian demantoid color origin

10.00–10.20 Andy H Shen, Zemin Luo, Mingxing Yang: Country of origin determinations of nephrite jades from East Asia Regions

10.20–10.40 Coffee break

Chairperson Dr. Jayshree Panjikar

10.40–11.00 Karen E. Fox: Opal Adventures in the Land of Never Never

11.00–11.20 Emmanuel Fritsch, Peter Megaw, Tyler L. Spano-Franco: Green-luminescing, gem hyalite opal from Zacatecas, Mexico

11.20–11.40 Ulrich Henn, Observations on some rare gem materials

11.40–12.00 Claudio C. Milisenda, Stefan Koch, Stefan Müller, Tom Stephan, Michael Wild: Gemstones with photochromism

12.00–12.20 Dietmar Schwarz: Colored gemstones – Mines and markets

12.20–14.00 Lunch

Chairperson Dr. Pornsawat Wathanakul

14.00–14.20 Elisabeth Strack: The present situation of freshwater pearls from Wisconsin

14.20–14.40 Michael S. Krzemnicki, Vincent Revol, Carina Hanser, Laurent Cartier, Henry A. Hänni: X-ray phase contrast and X-ray scattering images of pearls

14.40–15.00 Nicholas Sturman, Artitaya Homkrajae, Areeya Manustrong, Nanthaporn Somsa-ard: X-ray computed microtomography (μ-CT) structures of known natural and non-bead cultured *Pinctada maxima* pearls

15.00–15.20 Sutas Singbamroong, Nazar Ahmed, Ayesha Rashid Ahmed, Mohamed Karam, Ghaliah Hassan, Sameera Mohammed, Nahla Al Muhairi: Observations on natural non-nacreous pearls reportedly from Tridacna (clam) species

15.20–15.40 Coffee break

15.40 Conference day closes

15.40–16.30 Executive Committee meeting

19.00–21.00 Dinner at the City Hall

Sunday 30 August

8.00–8.45 Executive Committee meeting

Testing Techniques

Session at the Donelaitis Hall, Faculty of Philology, Vilnius University
Chairperson Dr. Karl Schmetzer

9.00–9.20 Lutz Nasdala, Chutimun Chanmuang, Tobias Häger, Wolfgang Hofmeister, Allen K. Kennedy, Peter W. Reiners, Tamás Váczi, John W. Valley, Bhuwadol Wanthanachaisaeng, Wu Fuyuan, Manuela Zeug, E. Gamini Zoysa: The scientific importance of gem zircon as analytical reference materials

9.20–9.40 Brendan M. Laurs: Modern mining methods for primary and secondary gem deposits in Mogok, Myanmar

9.40–10.00 Manfred Eickhorst: Technical progress report on LED, gemmology and sustainabily

10.00–10.05 Announcements

10.05–10.50 Coffee break

10.50–12.00 Conference closing ceremony. Conference ends

12.00–14.00 Lunch

POSTERS

- Gagan Choudhary: Emeralds from Jharkhand, India: An update
- Helmut Pristacz, Toshihiro Kogure, Vera M.F. Hammer, Gerald Giester, Manfred Wildner, Eugen Libowitzky, Lutz Nasdala: A review of synthetic turquoise
- Antonello Donini, Elena Gambini, Emanuela Castaman, Giuliano Radice: Unusual and curious gemological materials in laboratory
- Emmanuel Fritsch, Joel Ivey: Mustard Jasper or Bumble bee stone
- John M. Saul: "ELECTRUM": Why was the same word used for amber and also for the naturally occurring alloy of gold and silver?
- Guanghai Shi, Yan Wang, Wei Shi, Ruihua Wu: Infrared spectral characteristics of ambers from three main sources (Baltic Sea, Dominican Republic and Myanmar) and their implications
- Elizabeth Su: Jadeite markets in China
- Thanong Leelawatanasuk, Namrawee Susawee, Marisa Maneekrajangsaeng, Saengthip Saengbuangamlam, Supparat Promwongnan, Nicharee Atsawatanapirom, Pantaree Lomthong, Pornsawat Wathanakul: Treated black sapphire
- Supparat Promwongnan, Saengthip Saengbuangarmlum, Thanong Leelawatanasuk: Synthetic ruby overgrowth on natural corundum

Crane flies (Diptera, Tipuloidea) from Baltic amber

Sigitas Podenas

Department of Zoology of Vilnius University, Ciurlionio str. 21/27 and Nature Research Centre, Akademijos str. 2, LT-08412 Vilnius, Lithuania. E-mail: sigitas.podenas@ekoi.lt

The oldest deposits known today indicate that the Baltic amber forest must have already existed in the Lower Eocene (about 50 million years ago) (Weitschat, Wichard, 2002). The variety of animals and plants found in amber is associated with the distribution area of resin-producing trees (*Pinus succinifera*) and with conditions which prevailed in amber forest. As is the case with the majority of all fossil resin deposits, today Baltic amber is no longer found at the site where the resins were originally produced and deposited on the forest floor.

The most significant deposits of Baltic amber, also the largest known amber deposits in the world, are located in the northern and northwestern areas of the Samland Peninsula in the Kaliningrad district of Russia.

Crane flies from Baltic amber belong to the families Tipulidae (long-palped crane flies), Limoniidae (short-palped crane flies), Pediciidae and Cylindrotomidae. The taxonomic position of winter flies Trichoceridae is not yet solved (Bertone et al., 2008; Krzeminska et al., 2009). Crane flies make about 0.35 percent of all amber inclusions, but the percentage of them in different museum collections is higher and usually reaches to about 2 percent. About 80 percent of all amber crane flies belong just to the three commonest species *Trichoneura vulgaris* Loew, 1850, *Cheilotrichia minuta* Meunier, 1899 and *Rhabdomastix pulcherrima* Meunier, 1906. The remaining 20 percent is made up of more rare and interesting species. In total, 20 species of Tipulidae, 147 (and 1 subspecies) Limoniidae, 4 Pediciidae, 2 Cylindrotomidae (Evenhuis, 2014) and 11 Trichoceridae (Krzeminska et al., 2009) are known, but description of new taxa from Baltic amber is far from finished. Every year at least a few new species of Limoniidae from Baltic amber are described.

Eocenian species often share complexes of morphological features that do not occur together in recent taxa, thus subgenera of crane flies, in most cases, are comparatively young, they split from each other only during the post-Eocene period. That was shown for both long- and short-palped crane flies.

Ecological preferences of species met in amber show that most of them need decomposing organic material, such as fallen leaves, dead wood, and mud at the edges of water. It indicates that dead organic material had the tendency to aggregate in amber forest, when similar comparison with Dominican crane flies shows an opposite tendency, where decomposition of dead plant material was too fast for accumulations to occur. Probably that also explains why black Baltic amber, rich in humus, is so common.

References

Bertone, M.A., Courtney, G.W., Wiegmann, B.M. 2008. Phylogenetics and temporal diversification of the earliest true flies (Insecta: Diptera) based on multiple nuclear genes. Systematic Entomology 33: 668-687.

Evenhuis, N. L. , 2014. Catalog of fossil Diptera of the world (Version 2.0). http://hbs.bishopmuseum.org/fossilcat/.

Krzeminska, E., Krzeminski, W., Dahl, C., 2009. Monograph of fossil Trichoceridae (Diptera) over 180 million years of evolution. Institute of Systematics and Evolution of Animals, Polish Academy of Sciences, Krakow, 171 pp.

Weitschat, W., Wichard, W., 2002. Atlas of plants and animals in Baltic amber. Verlag Dr. Friedrich Pfeil, Munchen, 256 pp.

Figure 1. *Paradelphomyia* (*Ohyrhiza*) *antiqua* Podenas, 1999 from Baltic amber. This genus has a very wide distribution in recent fauna, but is very rare in fossil material.

Figure 2. *Trichoneura vulgaris* Loew, 1850. Genus *Trichoneura* was described from Baltic amber and was thought to be extinct. However, later on it was found to be still alive.

Amber in the Southeast Baltic Sea region: Geological aspect

Albertas Bitinas

Open Access Center for Marine Research, Klaipeda University; albertas.bitinas@jmtc.ku.lt

Keywords Amber, Semba Peninsula, Lithuania, Curonian Lagoon, exploitation

Information about the amber origin, geological setting of amber-bearing deposits and some peculiarities of exploitation in the Southeast Baltic Sea region (the territory of the recent Kaliningrad Oblast of the Russian Federation and maritime areas along the Baltic Sea Lithuanian coast) are presented in this brief overview.

The origin of amber, also known as natural organic mineral succinite, is related to the Paleogene period which lasted from 65 to 23.5 million years (MA) before present (BP). During the middle part of this period – at the end of Eocene (53-33.7 MA BP) – when the climate in North Europe was humid, the territory of Southern and Central Sweden was covered with pine forests (Grigelis, 2001). The pine trees (*Pinus succinifera*) produced a big amount of resin that later, after fossilization, became amber (Katinas, 1971, 1983). During the Late Eocene, due to the activity of rivers, the amber was dislocated from Scandinavia to the territory of the present-day Semba Peninsula. The amber was accumulated in the deposits of the river delta that existed there about 37-33.7 MA BP. The amber-bearing deposits in the Semba Peninsula were defined as Prussian Formation, or, in other words, as "Blue Earth" (Grigelis, 2001). These deposits are presented by a layer of brownish-green sandy silt with amber pieces, up to 10-meters thick (Figure 1). The top of amber-bearing deposits of the Prussian Formation *in situ* is lying about 7 meters below the present sea level and is covered with 35-40 meters-thick deposits of other formations, including Quaternary glacial deposits. During the Holocene, when the Baltic Sea level raised (Litorina Sea stage) and reached the amber-rich deposit layers in the Semba Peninsula, a particular amount of amber was washed out due to coastal abrasion. The amber was transported by sea currents and accumulated in the sandy deposits below the recent Curonian Spit and the Curonian Lagoon bottom, as well as in the coastal and lagoon sediments along the entire eastern Baltic Sea. Some pieces of amber were transported to the recent Saaremaa Island, Estonia.

Figure 1. Amber in the "Blue Earth", Kaliningrad Oblast, Yantarnoye quarry (photo A. Damušytė).

Despite that amber was known and used for human needs in the Baltic Sea region from the Paleolithic period, the industrial exploitation of this mineral started only in the XIXth century in the Curonian Lagoon near Juodkrantė settlement. About 2250 tons of amber were extracted from 1890 to 1899 (about 60-80 tons per year) by Prussian "Stantient & Becker Company" (Ar Lietuva gintaro šalis?, 1995). Moreover, some amounts of amber had been excavated from the peat bogs (former marine bays and lagoons) to the north of Palanga, near Priekulė, dragging the harbor in the Klaipėda Strait, and digging the King Wilhelm's Channel (Klaipėda Channel). Later, when the amber-bearing deposits were discovered at the Semba Peninsula, industrial exploitation of amber was removed to the latter location. At the end of the XIXth century amber was exploited in mines, whereas since 1912 until recently it was excavated from the open quarries near the Yantarnoye (former Palvininkai, Palmicken) settlement (Figure 2). The concentration of amber in the "Blue Earth" reaches from 2.2-2.5 kg in the cubic meter. It has been determined that the amber-bearing deposits in the western part of Semba Peninsula are distributed in an area of about 700 sq. kilometers. The estimated total amount of extractable amber consists of several hundred thousands of tons – i.e. more that 90% of the world resources (Grigelis, 2001).

Figure 2. Recent exploitation of amber in the Yantarnoye quarry, Kaliningrad Oblast (photo A. Damušytė).

A few decades ago, the amber resources were prospected in the bottom sediments of the northern Lithuanian part of the Curonian Lagoon. A few prognostic areas were discovered; afterwards, one deposit of amber was investigated in detail. The total amount of extractible amber was estimated as a few hundred tons (Ar Lietuva gintaro šalis?, 1995). The possibilities of industrial exploitation of amber in the Curonian Lagoon water area and its influence on the environment, as well as cost effectiveness of such activities, are still under discussion.

References

Ar Lietuva gintaro šalis? 1995. LGT informacinis leidinys, 11 pp. [Is the Lithuania country of amber?].

Grigelis, A., 2001. Outline on geology of amber-bearing deposits in the Sambian Peninsula. In A. Butrimas, Ed., Baltic amber in natural sciences, archaeology and applied arts. Lithuania, pp. 35-40.

Katinas, V., 1981. Amber and amber-bearing deposits of the Southern Baltic area. Mintis, Vilnius, 156 pp. (In Russian).

Katinas, V., 1983. Baltijos gintaras. Mokslas, Vilnius, 110 pp. [Baltic amber].

Perspectives of amber production in Lithuania

Jonas Satkūnas

Lithuanian Geological Survey; jonas.satkunas@lgt.lt

In the territory of the present country of Lithuania industrial production of amber was carried out only in the XIX century, when 2250 tons of amber in total were excavated in the Curronian lagoon. The geological exploration of amber deposits in the Curonian lagoon was processed by the Lithuanian Geological Survey from 1992 to 1994. In the scope ot this work 74 boreholes (diameter 715 mm - 1000 mm, depth 7,4 m - 22,2 m) were drilled. Parallely, research regarding the impact of amber exploration on the ecosystems of the Curonian lagoon was carried out by the Institutes of Geology and Ecology.

Amber exploration in the Curonian lagoon resulted in the delimitation of 4 perspective areas and a preliminary explored deposit close to Juodkrantė. In this deposit amber resources in the amount of 112 tons were estimated. Amber occurs under the cover of 1.8 m thick lagoon sediments in this deposit. The depth of the lagoon is approximately 1.2 m, the average thickness of amber bearing sandy sediments 1.7 m; the concentration of amber is 81 g/m^3. The size of the Juodkrantė area deposit is 82 ha.

In the other prospected areas the amount of amber is approximately 230 tons. The distribution of amber pieces according to their sizes: ø > 40 mm – 10%; ø 40–20 mm – 30%; ø 20–10 mm – 29%; ø < 10 mm – 31%.

Figure 1. Amber from the deposit in the Curonian lagoon obtained during geological exploration in 1992-1994.

A preparatory work for launching a tender of amber exploitation in the Juodkrantė deposit was carried out by the Lithuanian Geological Survey in 2015.

Canadian amber—History and significance to science

Willow Wight
Canadian Museum of Nature, Ottawa, Canada; wwight@mus-nature.ca

Keywords Canada, amber, Chemawinite, retinite, resinite

Introduction

Canadian amber has never been considered seriously as a gem material, but it has contributed significantly to several branches of natural science. Amber occupies a unique position in the sciences—it is studied by gemmologists and mineralogists, but most research is done by geologists looking at the character and ages of the formations in which it is found; by entomologists studying fossil arthropods; by botanists interested in the plant remains, and increasingly by researchers such as analytical and organic geochemists, who are unravelling the mysteries of the trees that produced the resins that we now call amber.

Amber's history in Canada (See Map)

Chemawinite: "retinite" from Cedar Lake, Manitoba (Figure 1)

In the mid-1800s, the Geological Survey of Canada (GSC) explored vast areas of Canada searching for economic minerals. Mineral resins were known, associated with coal and lignite deposits in Western Canada. J.B. Tyrrell of the GSC learned of amber washed up on the shores of Cedar lake near the entrance of the Saskatchewan river (Tyrrell, 1892). His conclusion was that the "amber" was derived from a Cretaceous lignite occurring along the Saskatchewan river. The material was described and analysed by B.J. Harrington (1891). Because it did not contain succinic acid,

Figure. 1. Cedar Lake amber, Canadian Museum of Nature, Ottawa. Nodules have a tumble-polished appearance, because they have travelled long distances by river from their original site. Photo: W. Wight, CMN.

he referred to it as the "so-called Amber of Cedar Lake", and used the terms "retinite", and "Chemawinite" (for the local Chemahawin Indians). Only a few larger pieces were considered for ornamental use. The quantity available was such that it was considered for the production of varnish, but no commercial use was ever found. Polished "Retinite (Chemawinite)" from Cedar Lake was listed in the *Catalogue of Section One of the Museum of the Geological Survey* (Hoffmann, 1893), as presented by C.P. Willimott & Co., Ottawa. Seven polished pieces are now in the Gem Collection, Canadian Museum of Nature (CMN).

In 1934, T.L. Walker at the Royal Ontario Museum (ROM) in Toronto studied chemawinite extensively (Walker, 1934). Some material was polished; three cabochons and a necklace are in the ROM collections today. As a gem, chemawinite was disappointing, but Walker's report had great significance for palaeontologists. He reported for the first time that many larger pieces showed remains of insects (Figure 2). F.M. Carpenter, a paleoentomologist at Harvard University, was greatly excited, because Cedar Lake amber was the first really good source of arthropod fossils of Cretaceous age, thus allowing comparisons between modern and Cretaceous species. Walker sent inclusion-containing pieces to Carpenter for examination by specialists, who described many new species of insects and arachnids (Carpenter et al., 1937).

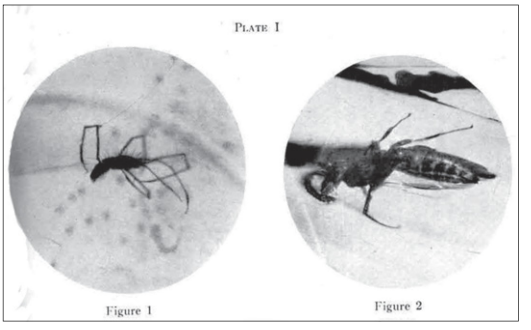

Figure 2. The first fossil inclusions observed in Cedar Lake amber. From Plate I (Walker, 1934).

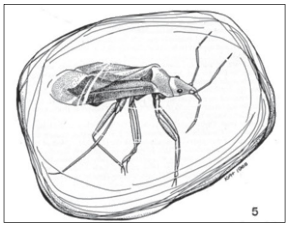

*Figure 3. Drawing of a minute pirate bug (*Hemiptera: Anthocoridae*) entombed in Cedar Lake amber. This fossil species was probably a predator of aphids infesting the amber-producing conifer. (By K.G.A. Hamilton, from McAlpine & Martin, 1969).*

Inclusions

A Paleontological Treasure-chest I

In the 1960s, J.F. McAlpine and J.E.H. Martin at the Central Experimental Farm in Ottawa were studying inclusions in Canadian amber (McAlpine & Martin, 1969). Inclusions of fossil fauna, as well as pollen grains, spores, and fragments of plants, yielded much information about life in the Cretaceous. These specimens, from a number of Canadian sites, are now part of the Canadian National Collection (CNC) of Insects, Arachnids & Nematodes. The Amber section includes two dozen primary type-specimens and nearly 1,300 inclusions (Figure 3).

A Paleontological Treasure-chest II

Cedar Lake amber occurs as a secondary deposit, having been transported from southern Alberta by the Saskatchewan river to Cedar Lake. Cretaceous ambers from Western Canada found *in situ* were analysed by R.C. McKellar and colleagues (McKellar, et al., 2008). The Grassy Lake outcrop in southeastern Alberta is the only known up-river amber occurrence that produces equivalent material. Grassy Lake amber contains significant arthropod inclusions; many species have been described by the group. Of more than 4,000 amber pieces with inclusions, eleven contained feather fossils. The resulting paper "A diverse assemblage of Late Cretaceous dinosaur and bird feathers from Canadian amber" by McKellar, Chatterton, Wolfe & Currie, in *Science* in 2011, provoked much attention (McKellar, et al., 2011).

Tree species associated with amber

There has been little data on fossil resins that can be definitively assigned to a specific species of tree, either extinct or extant. On Axel Heiberg Island, in the Canadian Arctic Archipelago, well-preserved fossil-forests of Eocene age occur in sediments. Resinite samples unambiguously associated with identifiable fossil woods were collected, and provided a unique opportunity for analysis, both chemically and taxonomically (Anderson & LePage, 1995). These resinites are associated with three different genera of trees: *Metasequoia, Pinus* and *Pseudolarix*.

Abundant wood fragments were recovered from the Panda kimberlite pit during mining at the Ekati diamond mine northeast of Yellowknife, NT. The Panda intrusion is dated at 53 million years (Wolfe et al., 2012). One specimen revealed an amber nodule upon splitting, and this offered the rare opportunity for parallel geochemical investigations of the wood and associated amber. The wood was identified conclusively to the genus *Metasequoia* (Cupressaceae). The amber is classified tentatively as Class Ib (see below) resinite, the most common in Canada. The authors also infer that Early Eocene paleoclimates in the western Canadian subarctic were 12-17°C warmer and four times wetter than present.

Chemical classification of ambers

Resinites are the result of the natural polymerization and fossilization of certain tree resins. Great strides have been made in determining their chemical compositions and details of the complicated polymer structures, using FTIR and combined Pyrolysis-Gas Chromatography-Mass Spectrometry (Pyr-GC-MS). On this basis, Anderson, et al. (1992) proposed five classes of resinites. The most common (Class I) have structures based on "polymers of labdanoid diterpenes". Baltic amber, which contains succinic acid, is Class Ia. Canadian amber has no succinic acid, and was called retinite—or now, resinite Class Ib. At the Canadian Conservation Institute (CCI) in Ottawa, J. Poulin and K. Helwig (2012, 2014) have pioneered a modified Pyr-GC-MS technique that has led to a greater understanding of the complex macrostructures. They described a new sub-class of Class I resinites, having a different configuration, and incorporating succinic acid. This new group, designated as Class Id, occurs at three localities in Canada. Two are in northern Nunavut: the fossil-forest site on Axel Heiberg Island, and near Lake Hazen on Ellesmere Island. The third is near François Lake, BC.

Discussion

Western and Northern Canada is rich with amber deposits that are of different geological ages and types. Since the mid-1930s, rare inclusions in Cedar Lake-Grassy Lake amber have provided a much-needed window to the Late Cretaceous world. Hundreds of species of arthropods that existed only in prehistoric times have been described. The more recent discovery of feather and "protofeather" traces (from a dinosaur) in Grassy Lake amber adds another dimension to our view of the prehistoric world. Ever more inventive combinations of analytical techniques have led to a better understanding of the complex organic geochemistry of the resinites, resulting in the description of a new sub-class of amber from Canada (Class Id). Amber associated with fossil woods in Canada's far North provided a rare opportunity to identify the trees that had secreted the original resin, and the climate that existed there in the Eocene.

Acknowledgments

The author thanks her colleagues at the CMN; Jennifer Poulin, CCI; and for information on Canadian amber in their respective collections: K. Dunnell, ROM, Dr. K.G.A. Hamilton, CNC, and M. Coyne and A. Therriault, GSC.

References

Anderson, K.B., Winans, R.E., Botto, R.E., 1992. The nature and fate of natural resins in the geosphere P II. Identification, classification and nomenclature of resinites. Organic Geochemistry, 18, 829P841.
Anderson, K.B., LePage, B.A., 1995. Analysis of fossil resins from Axel Heiberg Island, Canadian Arctic. In: Anderson, K.B.,

Crelling, J.C. (Eds.), Amber, Resinite, and Fossil Resins, Am. Chem. Soc. Symp. Ser., 617, 170-192.
Carpenter, F.M, Folsom, J.W., Essig, E.O., Kinsey, A.C., Brues, C.T., Boesel, M.W., Ewing, H. E., 1937. Insects and arachnids from Canadian amber. Univ. Toronto Studies, Geol. Ser., 40, 7-62, 12 figs.
Harrington, B.J., 1891. On the so-called amber of Cedar Lake, north Saskatchewan, Canada. Amer. Jour. Sci., Ser. 3, 42, 331-335.
Hoffmann, G.C., 1893. Catalogue of Section One, Museum of the Geological Survey. Geol. Survey Canada, VIII, 150.
McAlpine, J.F. Martin, J.E.H., 1969. Canadian amber – a paleontological treasure chest. Can. Entomol., 101, 819-838.
McKellar, R.C., Wolfe, A.P., Tappert, R., Muehlenbachs, K., 2008. Correlation of Grassy Lake and Cedar Lake ambers using infrared spectroscopy, stable isotopes, and palaeoentomology. Can. J. Earth Sci., 45, 1061-1082.
McKellar, R.C., Chatterton, B.D.E., Wolfe, A. P., Currie, P. J., 2011. A diverse assemblage of Late Cretaceous dinosaur and bird feathers from Canadian amber. Science, 333(6049), 1619-1622. DOI: 10.1126/science.1203344.
Poulin, J., Helwig, K, 2012. Class Id resinite from Canada: A new sub-class containing succinic acid. Organic Geochemistry, 44, 37-44.
Poulin, J., Helwig, K., 2014. Inside Amber: The Structural Role of Succinic Acid in Class Ia and Class Id Resinite. Analytical Chemistry, dx.doi.org/10.1021/ac501073k.
Tyrrell, J.B., 1892. Fossil resin ("amber"), Cedar Lake, Manitoba. Geol. Survey Canada Annual Report, 5, pt. 1, s14-s15.
Walker, T.L., 1934. Chemawinite or Canadian amber. Univ. Toronto Studies, Geol. Ser., 36, 5-12; 2 plates.
Wolfe, A.P., Csank, A.Z., Reyes, A.V., McKellar, R.C., Tappert, R., Muehlenbachs, K., 2012. Pristine early Eocene wood buried deeply in kimberlite from Northern Canada. PLoS ONE, **7**(9): e45537. doi:10.1371/journal.pone.0045537.

Natural green amber from Ethiopia

Lore Kiefert

Gubelin Gem lab Ltd., Maihofstrasse 102, Luzern 6006, Switzerland; lore.kiefert@gubelingemlab.com

Keywords Ethiopia, amber, Cretaceous, green amber

The discovery of Ethiopian amber is relatively new (Schmidt et al., 2010), and previous literature does not give an exact location. Also, the described amber appears to be mostly yellowish brown in colour.

On a recent visit to Ethiopia, the author was presented with several pieces of green amber (Figure 1 left), which sometimes resembled the appearance of green autoclaved amber as seen in the mid- to late 2000's (Abduriyim et al., 2009). However, the colour of some of these was distinctly different, and some of the pieces contained plant matter and even insects (Figure 2).

Figure 1. Natural green amber from Ethiopia.

Figure 2. Insect in green amber from Ethiopia.

The amber deposits are located approximately 150 km north-northwest of Addis Ababa, near the town of Alem Ketema (Figure 3). According to the local geologist, Dr. Begosew Abate, who studied the area where the green amber is found, it occurs within Mesozoic sedimentary rocks just under the contact with the oldest Cenozoic volcanic rocks, in which opal bearing layers are found (Abate, pers. comm. 2014).

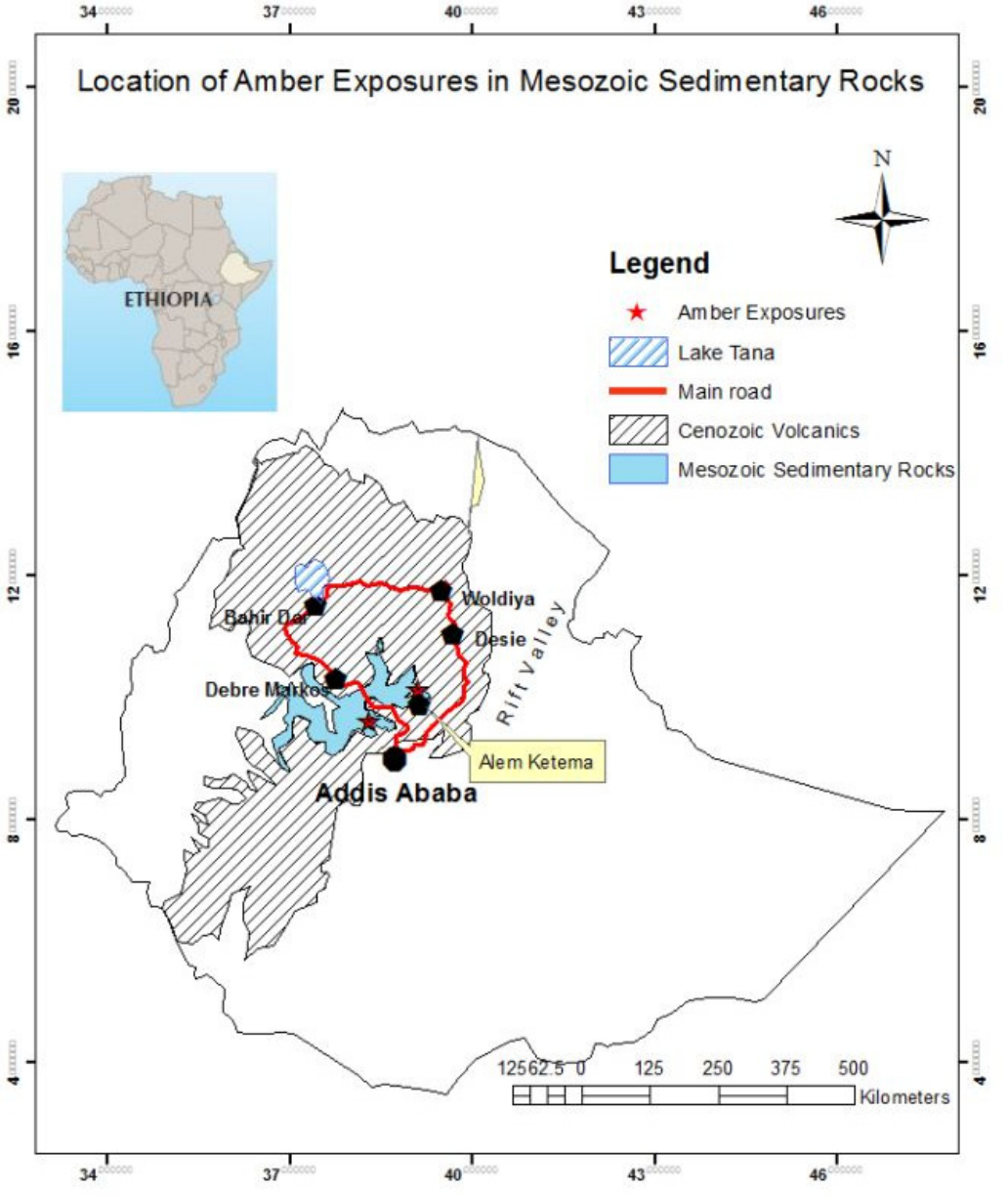

Figure 3. Location of amber deposits in Ethiopia. The green amber is found near Alem Ketema. Map: Begosew Abate.

The amber deposits are hosted within cretaceous age sandy limestones and exposed at different localities within the canyons cut by major tributaries of the Blue Nile river such as Jema, Wonchit and Mugher. Amber occurs in at least three colors, i.e., green, blue green, yellowish and reddish. Ethiopian Amber is new to the market but it is attracting more and more people in recent days. The following photographs show the exposure in the Wonchit river valley close to Zemero (Figures 4 and 5).

The presentation will focus on the properties of green amber from Ethiopia, showing inclusion photos and FTIR spectra that may also be used to distinguish it from its treated counterpart.

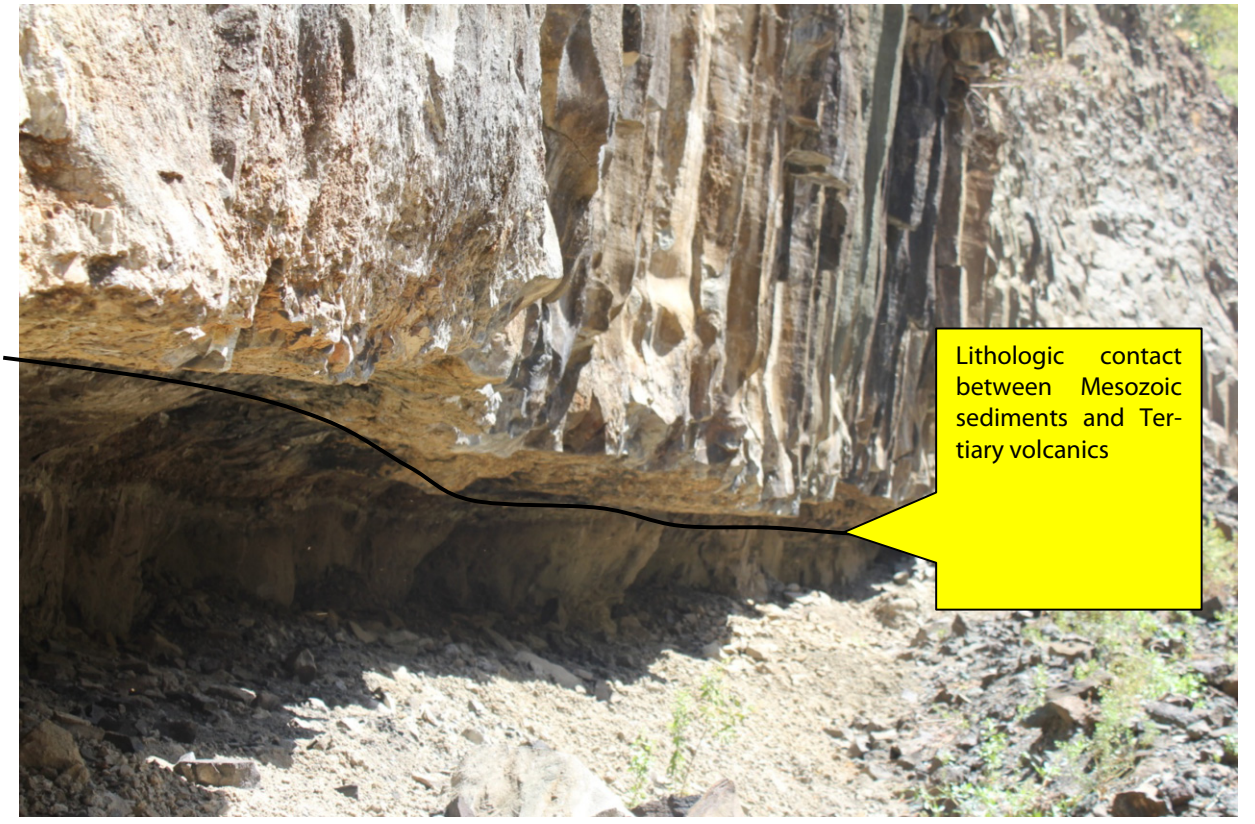

Figure 4. Amber occurs within the sandy limestone just below the contact with Tertiary volcanic represented here by columnar basalts. Photo: Begosew Abate.

Acknowledgements

The author wishes to thank Tewodros Sintayehu of Orbit Ethiopia plc for the supply of the amber pieces, as well as Dr. Begosew Abate of Orbit Ethiopia plc for geological information of this amber.

Figure 5. Horizon of the Amber bearing Mesozoic Sandy Limestone overlaid by basalt. Note the people to the left sitting in the shade. Photo: Begosew Abate.

References

Abduriyim, A., Kimura, H., Yokoyama, Y., Nakazono, H., Wakatsuki, M., Shimizu, T., Tansho, M., Ohki, S., 2009. Characterization of "Green Amber" With Infrared and Nuclear Magnetic Resonance Spectroscopy. - Gems & Gemology, Vol. 45, No. 3, 158-177.

Schmidt, A.R., Perrichot, V., Svojtka, M., Anderson, K.B., Belete, K.H., Bussert, R., Dörfelt, H., Jancke, S., Mohr, B., Mohrmann, E., Nascimbene, P.C., Nel, A., Nel, P., Ragazzi, E., Roghi, G., Saupe, E.E., Schmidt, K., Schneider, H., Selden, P.A., Vavra, N., 2010. Cretaceous African life captured in amber. Proc. Nat. Academy Sci. USA, Vol. 107, No. 16, 7329-7334.

Burmese amber from Hti Lin

Tay Thye Sun[1], Arunas Kleismantas[2], Thet Tin Nyunt[3], Zheng Minrui[4], Murali Krishnaswamy[5], Loke Hui Ying[1]

[1]Far East Gemological Laboratory, 12 Arumugam Road #04-02, Lion building B, Singapore 409958.
[2] University of Vilnius, Department of Geology and Mineralogy, M.K. Ciurlionio 21/27, Vilnius, Lithuania.
[3]University of Yangoon, Department of Geology, Yangon, Myanmar.
[4]National University of Singapore, Physics department, Kent Ridge, Singapore.
[5]NUS High School of Mathematic and Science, Department of Chemistry, 20 Clementi Ave 1, Singapore.

Keywords Amber, Myanmar, infrared spectroscopy

Introduction

Burmese amber or Burmite, more correctly amber from Myanmar, has been commercially exploited for a millennium and its main market is China. The history of the use of Burmite has been reviewed by several authors (Webster & Read, 1994; Zherikhin and Ross, 2000; Grimaldi et al., 2002; Ross et al., 2010). The main amber producing area in Burma has been the Hukawng valley (Hukawng Basin) in the Kachin region, northern Myanmar (Noetling, 1892; Chhibber, 1934; Cruickshank and Ko, 2003; Guanghai Shi et al., 2014).

A new location of amber mining in Burma is at Tilin or Hti Lin township, Gangaw District, Magway Region, Central Myanmar and located at N21˚- 41′ – 44.6″, E94˚-5′ – 47″. The author (TTS) took the opportunity to visit the area in mid-March 2015 with the help of travel guide Mr Nyi Nyi Aung and geologist Mr Kyaw Kyaw and villager of Yaw people Mr Kyaw Min and a few of his colleagues. At Hti Lin, the actual amber location is at Kyakhe (translating to English as tiger bite).

Brief geology & mining of amber at Hti Lin

At the amber mine sites, the geology of Hti Lin area is made up of reddish brown mudstone, shales with coal bearing layers, some greenish, fine to medium grained calcareous sandstone, gritty sandstone with quartz pebble and conglomerate (per comm. Aung Kyi, 2015). At Kyakhe, shales could be found on dump sites, occasionally broken sub-bituminous coal together with ball-like pyrite and broken white calcite blocks. At one of the site, there were two small sulphur vents giving out sulphur fumes, i.e. volcanic activities. This sandstone bed has been named Kabaw Formation, and is from the upper Cretaceous (Than Htut, 2015). The strike of the sandstone bed is nearly NS, dipping east (approximately 330/50NE). Its lithology mainly consists of shale intercalated with occasional fine grained turbiditic sandstones which is unconformably overlain by Paunggyi Formation (Win Swe, 2012; per comm. Mitchell, A.H.G., 2015). Therefore, the geological setting is quite similar to that of Hukawng valley, Tanai, the better known amber locality.

At Kyakhe, about 100 miners (mainly farmers) work in 20-30 pits, covering an area approximately 10 km^2. Based on the miners' observations, amber is found in the shale which is from 30 to 40 cm thick. Miners usually look for traces of thin coal layers and follow them until they find amber in the shale bedding plane. The miners dig a lebin or square pit to a depth of about 15 to 20 m before reaching the shale with amber. Nearly all the rough ambers found are opaque with blackish skin. The samples weigh from a few grams to a few kilograms per piece.

Figure 1. Some of the polished amber from the new Hti Lin deposit in Myanmar – the largest one on the top left hand weighs 27.7 g (6.6x5.9x1.2 cm); and one rough amber sample on the right 45.9 g (8.7x8.8x1.4 cm). Photo by Tay.

Materials and methods

Twenty samples of amber from Hti Lin (Figure 1) were examined using basic gemmological methods. Another five samples from Hti Lin and five samples from Tanai (Hukawng Valley) were examined using Fourier Transform Infrared spectroscopy of Shimadzu model IR Prestige-21 in the range 4000-400 cm^{-1}, with a resolution of 4.1 cm^{-1}, accumulating 45scans. Raman spectroscopy was performed on a Renishaw InVia in the range 1400 cm^{-1} to 1768 cm^{-1}, using a 785 nm laser in the continuous waving mode.

Results

Gemological data

The colour of Hti Lin amber ranges from white, yellow, yellowish-brown to dark brown, and some is reddish-brown. The materials can be transparent to opaque. The refractive index ranges from 1.54 to 1.55, and specific gravity ranges from 1.03 to 1.05. Slightly higher SG was attributed to the presence of pyrite inclusions. Under magnification, there are flattened gas bubbles, flow marks, thin film inclusions that is reflective (Figure 2a) under oblique fibre optic lighting, some unidentifiable probably organic debris but no insects were found. Some pieces show dark brown droplet inclusion and also older flow marks interrupted by a second generation of flow marks. There are also pyrite included crystals (Figure 2b). Under ultraviolet radiation, Hti Lin amber tends to fluoresce very strong chalky blue with white veins under long wave and weak chalky blue under short wave.

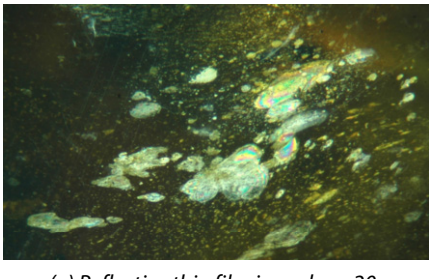

(a) Reflective thin film in amber x20

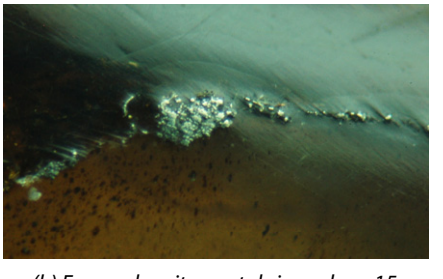

(b) Exposed pyrite crystals in amber x15

Figure 2. Some of the inclusions found in amber from Hti Lin. Photo by Tay.

Infrared and Raman spectrometer data

Infrared spectroscopy in the transmission mode of Hti Lin ambers show significant peaks at 2925 cm^{-1}, 1725 cm^{-1}, 1460 cm^{-1}, 1375 cm^{-1}, also between 1300–1000 cm^{-1} and a weak pair of peaks between 855 cm^{-1}–810 cm^{-1} (Figure 3a).

In a brief comparative analysis of Hti Lin amber versus Tanai amber absorption spectra, it was found that both spectra are similar except that some of the Hti Lin has double peaks at 1724 cm^{-1} and 1699 cm^{-1} whereas Tanai has a peak at 1724 cm^{-1} only. More samples are needed to strengthen this indication.

Using Raman spectroscopy on Hti Lin and Tanai amber, it becomes apparent that both show strong photoluminescence which makes Raman measurement ineffective. Previously, the 1400-1800 cm^{-1} region had been successfully used in the study of Baltic amber (Tay et al., 1998; Thanong et al., 2013) but is unfortunately now not effective due to strong fluorescence of Burmese amber.

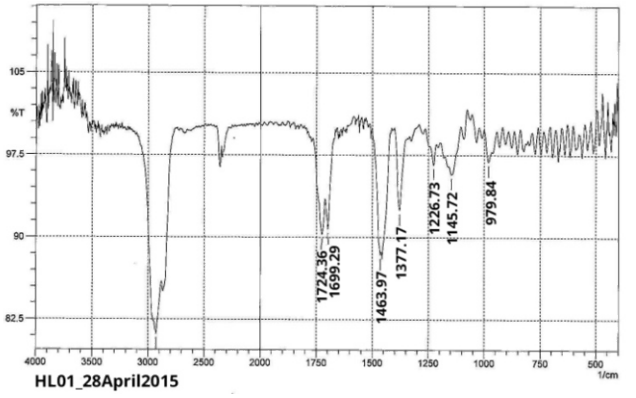

Figure 3a. Infrared spectrum of amber from Hti Lin with a double peak at 1724 and 1699 cm^{-1}.

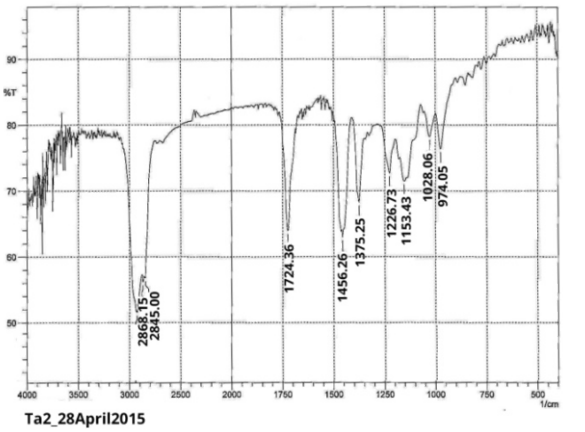

Figure 3b. Infrared spectrum of amber from Tanai shows a single peak at 1724 cm^{-1}.

Discussion & conclusion

Amber from Hti Lin is found in the late Cretaceous sedimentary rock, and quite similar to Hukawng valley of Tanai area. To some geologists, Hti Lin amber area could have overlap into Eocene deposits (per comm. Aung Kyi, 2015).

The gemmological data of amber from Hti Lin is quite similar to that of amber from many areas around the world. For example, the R.I. ranges from 1.54 to 1.55, the S.G. from 1.03 to 1.05, with inclusions such as gas bubbles, flow marks, pyrite included crystals, thin reflective film and some unidentified, probably organic, debris. Burmese amber from Hukawng valley is famous for its abundance of some rare, as well as common insects, whereas in Hti Lin, no insect has been found in the samples we examined.

Based on the mid-IR result, the spectrum of amber from Hti Lin looks quite similar to that from Hukawng Valley, Tanai area, but some of the Hti Lin amber shows double peaks at 1724 cm^{-1} and 1699 cm^{-1}. Looking for the 'Baltic amber shoulder' i.e. 1259-1184 cm^{-1} and associated feature at 1159 cm^{-1} (Beck et al., 1964; Langenheim, 1969), the Hti Lin sample does not show the 'Baltic amber shoulder', but rather broad peaks between 1226 – 1145 cm^{-1}.

References

Aung Kyi – per communication, 2015. Department of Geological Survey and Mineral Exploration, Ministry of Mines, Myanmar.

Beck, C., Wilbur, E., Meret, S., 1964. "Infrared spectra and the origin of amber", Nature, Vol. 201, pp. 256-257.

Bannert, D., Sang Lyen, A., Than Htay, (Hannover 2011) "The Geology of the Indoburman Ranges in Myanmar", Geologisches Jahrbuch, Reihe B Heft 101, 61 pp.

Chhibber, H.L., 1934. "The Mineral Resources of Burma" London, Macmillan & Co.

Cruickshank, R.D., Ko Ko, 2003. "Geology of an amber locality in the Hukawng Valley, Northern Myanmar", Journal of Asian Earth Sciences 21, pp. 441-455.

Grimaldi, D.A., 1996. "Amber: Window of the Past". Harry B. Abrams, Publishers, in association with the American Museum of Natural History, 216 p.

Langenheim J., 1969. "A botanical inquiry" Science, Vol. 163, pp. 1157-1169.

Mitchell, A.H.G., per communication, 2015. In the process of finishing his book on the Geology of Myanmar.

Noetling, F., 1892. "Preliminary report on the economic resources of the amber and jade mines area in Upper Burma" Rec. Geol. Surv. India 25: 130-35.

Ross, A., Mellish, C., York, P., Crighton, B., 2010. "Burmese amber. In: Penney, D. (Ed.), Biodiversity of Fossils in Amber from the Major World Deposits. Siri Scientific Press, Manchester, pp. 192-207.

Pavia, D.L., Lampman, G.M., Kriz, G.S., Vyyan, J.R. 2009. "Introduction to Spectroscopy". 4th ed. Cengage Learning: Belmont.

Shi, G.H., Grimaldi, D.A., Harlow G.E., Wang Jing, Wang Jun, Yang M.C., Lei W.Y., Li Q.L., Li X.H., 2012. "Age Constraints on Burmese amber based on U-Pb dating Zircons", Cretaceous Research, 37, pp. 155-163.

Tay, T.S., Shen, Z.X., Yee, S.I., 1998. "On Identification of Amber and its Imitations using Raman Spectroscopy – Preliminary results" The Australian Gemmologist, Vol. 20, No. 3, pp. 114-123.

Thanong L., Pornsawat W., Sumarni P., Chakkaphan S., Boontawee S., Pimtida B., 2013. "The Characteristics of amber from Indonesia" The Australian Gemmologist, Vol. 25, No. 4, pp. 142-145.

Than Htut, 2015. "The Shale Gas Prospect in Myanmar", Journal of the Myanmar Geosciences Society, Vol. 6, No. 1, 99-130 pp.

Webster, R., 1994. "Gems: Their sources, description and identification". P 573, 5th ed. Revised by P. Read. Butterworth-Heinemann: London 2003.

Win Swe, 2012. "Outline Geology and Economic Mineral Occurrences of the Union of Myanmar", Journal of the Myanmar Geosciences Society, Special Publication No. (1), 215 pp.

Yan Liu, Shi G.H., Shen Wang, "Colour Phenomena of Blue Amber", Gems & Gemology, Summer 2014, Vol. 50, No. 2, Notes & New Techniques pp. 2-8.

Zherikhin, V.V., Ross, A.J., 2000. "A review of the history, geology and age of Burmese amber (Burmite). Bulletin of the Natural History Museum, London (Geology) 56, 3-10.

Acknowledgements

Many thanks to Ma Gjam, Ko Aung Naing, Ko Nyi Nyi Aung, Ko Kyaw Kyaw for directing Tay Thye Sun to the Tilin location. Also thanks to Ms Pek Lay Pheng, Senior Laboratory Technologist, NUS High School of Mathematics and Science for preparation of samples for IR. Prof. Shen Zexiang and Ms.Yin Ting Ting for Raman microscopy work at Centre For Disruptive Photonic Technologies, Nanyang Technology University, Singapore. Also many thanks to Mr. Tin Kyaw Than, Mr. Aung Kyi, Dr Andrew Mitchell and Prof. Dr Khin Zaw (CODES Centre of Excellence in Ore Deposits, University of Tasmania), for discussion on the geology of Myanmar especially Tilin area.

Natural „lonsdaleite and CO_2 rich“ diamonds

Thomas Hainschwang[1], Franck Notari[2], Emmanuel Fritsch[3]

[1] GGTL Laboratories - GEMLAB (Liechtenstein), Gnetsch 42, 9496 Balzers, Liechtenstein; thomas.hainschwang@ggtl-lab.org
[2] GGTL Laboratories - Gemtechlab, 4bis route des Jeunes, 1227 Geneva, Switzerland; franck.notari@ggtl-lab.org
[3] Université de Nantes – CNRS Institut des Matériaux Jean Rouxel (IMN), UMR 6502, 2 rue de la Houssinière, BP32229, F-44000 Nantes, France; emmanuel.fritsch@cnrs-imn.fr

We have studied 20 facetted “lonsdaleite and CO_2 rich” diamonds of unknown origin, purchased from a parcel of naturally coloured black diamonds from the Mumbai market, that are in our laboratory collection since 15 years, plus one rough impact diamond from the Popigai meteorite crater in northern Siberia, Russia. All these diamonds are apparently polycrystalline, all exhibit a large broad one-phonon infrared absorption band at 1220 cm^{-1} which has been attributed to absorption of the diamond lattice distorted by inclusions of lonsdaleite (Bokii et al., 1986), and finally, all their infrared spectra exhibit very strong CO_2 related absorptions at approximately 2460 cm^{-1}, 660 cm^{-1} and at 3611 and 3727 cm^{-1}. These bands correspond with some deviation to the ν_2 (angular bend, 667 cm^{-1}) and ν_3 (asymmetric stretch, 2349 cm^{-1}) as well as the $\nu_3 + 2\nu_2$ (combination/overtone, 3683 cm^{-1}) and $\nu_3 + \nu_1$ (combination, 3686 cm^{-1}) absorptions of molecular CO_2 (Schrauder and Navon, 1993). The broad one phonon absorption has been described in nano-polycrystalline synthetic diamonds (so-called “NPD”) (Sumiya et al., 2009; Skalwold, 2012; Skalwold et al., 2012), but the CO_2 absorptions have not been published for such synthetic diamonds. The CO_2 absorptions but have been described as very common features in natural impact diamonds (Yelisseyev et al., 2013) and as relatively rare spectral features in some - mostly brown - natural diamonds (Wang et al., 2005; Hainschwang et al., 2006; Hainschwang et al., 2008). The 1220 cm^{-1} band has been attributed to absorption of the diamond lattice distorted by inclusions of lonsdaleite; EPR spectroscopy has identified a very high concentration of broken C-C bonds due to interconnected textures of diamond (111) and lonsdaleite (1010) (Bokii et al., 1986). Lonsdaleite is known since the early 1960’s (Ergun and Alexander, 1962), but its existence as a discrete material has been questioned recently (Németh et al., 2014) and instead faulted and twinned cubic diamond has been suggested as being responsible for the unusual properties of so-called “lonsdaleite-rich diamonds”. Since there is clearly additional research required on this topic, to confirm or deny the existence of lonsdaleite, we will continue to call these diamonds “lonsdaleite-rich” for simplicity’s sake. The 21 analysed diamonds all contain distinct amounts of graphite inclusions and are heavily strained due to their polycrystalline structure. We have several samples which show naturals on their surface that are unambiguously remnants of the surface of natural crystals and not of synthetic diamonds. Additionally some of these facetted diamonds contain iron oxide lined fissures plus unidentified solid inclusion other than graphite. All these features are unambiguous proof for their natural origin. The photoluminescence spectra of the natural samples excited by 405nm, 473 nm, 532 nm and 635 nm lasers are characterized by very broad bands with always three broad bands superimposed at 701.8, 720.8 and 732.0 nm (Fig. 1), a signature very different from the broad band with relatively sharp bands at 612 and 667 nm described by Skalwold et al. (2012). While impact diamonds have been published before, these are the first cut diamonds ever described. With up to 1.05 ct cut and more than 6.5 mm diameter, they strongly surpass the average impact diamond, which measures maybe 1.5 mm in the rough state (Yelisseyev et al., 2013).

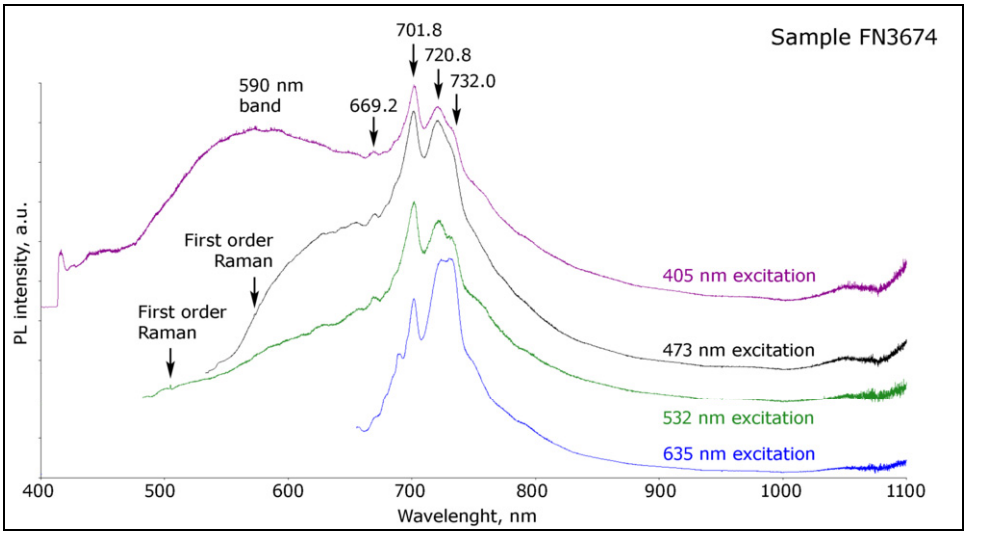

Figure 1. The photoluminescence spectra of a natural impact diamond rich in CO_2 and lonsdaleite, excited by 4 lasers of different wavelengths, show that the orange to red PL of such diamonds is caused by rather broad emission bands. It is also noticeable that the Raman line is barely detectable, which clearly point to very distinct disorder in the structure of these diamonds.

References

Bokii, G. B., Bezrukov, G. N., Klyuev, Y. A., Naletov, A. M., Nepsha, V. I., 1986. Natural and synthetic diamonds. Science.

Ergun, S., Alexander, L. E., 1962. Crystalline forms of carbon: a possible hexagonal polymorph of diamond. Nature 195, 765–767.

Hainschwang T., Notari F., Fritsch E., Massi L., Breeding C.M., Rondeau B., 2006. Natural « CO_2-rich » colored diamonds. Gems & Gemology, Vol. 42, No. 3, pp. 97.

Hainschwang T., Notari F., Fritsch E., Massi L., Rondeau B., Breeding C.M., Vollstaedt H., 2008. HPHT treatment of CO_2 containing and CO_2-related brown diamonds. Diamond and Related Materials, vol. 17, pp. 340-351.

Németh, P., Garvie, L. A., Aoki, T., Dubrovinskaia, N., Dubrovinsky, L., Buseck, P. R., 2014. Lonsdaleite is faulted and twinned cubic diamond and does not exist as a discrete material. Nature communications, 5.

Schrauder, M., Navon, O., 1993. Solid carbon dioxide in a natural diamond. Nature, 365(6441), 42-44.

Skalwold, E. A., 2012. Nano-polycrystalline diamond sphere: a gemologist's perspective. Gems & Gemology, Vol. 48, No. 2.

Skalwold, E. A., Renfro, N., Shigley, J. E., Breeding, C. M., 2012. Characterization of a synthetic nano-polycrystalline diamond gemstone. Gems & Gemology, Vol. 48, No. 3, pp. 188-192.

Wang, W. Y., Moe, T. M. K. S., Shen, A. H. T., 2005. Large diamond with microinclusions of carbonates and solid CO_2. Gems & Gemology, Vol. 41, No. 2, pp. 165-167.

Yelisseyev, A., Meng, G. S., Afanasyev, V., Pokhilenko, N., Pustovarov, V., Isakova, A., Lin, Z. S., Lin, H. Q., 2013. Optical properties of impact diamonds from the Popigai astrobleme. Diamond and Related Materials, 37, 8-16.

Sumiya, H., Harano, K., Arimoto, K., Kagi, H., Odake, S., Irifune, T., 2009. Optical characteristics of nano-polycrystalline diamond synthesized directly from graphite under high pressure and high temperature. Japanese Journal of Applied Physics, 48(12R), 120206.

Type Ib yellow to brownish yellow CVD synthetic diamond

Hiroshi Kitawaki, Mio Hisanaga, Masahiro Yamamoto, Kentaro Emori

Central Gem Laboratory, Tokyo; kitawaki@cgl.co.jp

Keywords synthetic, CVD-grown, yellow diamond, type Ib

Introduction

In mid-2012, one of the international diamond grading laboratories in Antwerp reported undisclosed CVD synthetic diamonds, causing a stir in the diamond industry (Even-Zohar, 2012). Since then, reports of undisclosed CVD synthetics have also emerged from gem testing laboratories in India and China (D' Haenens-Johanson et al., 2013; Song et al., 2014). Central Gem Laboratory (CGL) also reported on undisclosed over 1 ct size CVD synthetic diamonds (Kitawaki et al., 2013). Gem quality CVD products have been improved in their size and quality year after year, and a variety of colours have appeared. Most of the CVD synthetic diamonds reported previously are type II, however, recently some yellow CVD synthetic diamonds containing isolated substitutional nitrogen have been supplied to the gem market (Moe et al., 2014; Hainschwang, 2014).

This report describes the gemmological features of fifteen yellow to brownish yellow type Ib CVD synthetic diamonds submitted to CGL without disclosure.

Materials and methods

The fifteen diamonds submitted to CGL for standard grading as natural diamonds were subjected to this study. All the samples were loose, round brilliant cut, weighing between 0.18 and 0.40 ct, with an average of 0.25 ct.

Figure 1. Fifteen type Ib yellow-brownish yellow CVD-grown synthetic diamonds(0.18-0.40ct). Photo by H. Kitawaki.

In addition to standard gemmological tests, the samples were analysed with laboratory techniques. Infrared spectral analysis was carried out using JASCO FT/IR4200 in the range between 7000-400 cm^{-1}, resolution 4.0 cm^{-1} and 20 scans. Photoluminescence analysis was performed with all samples being immersed in liquid nitrogen using a Renishaw inVia Raman Microscope and a Renishaw Raman System-model 1000 with lasers at 633, 514, 488 and 325 nm. Also UV luminescence images were observed using a DiamondView™.

Results and discussion

◆Colour and clarity

Most of the samples fell in the colour range from Very Light yellow to Light yellow, and three of them were Light brownish yellow. Two of them were graded as VS2 clarity, nine were SI1 and four were SI2.

◆Microscopic examination

Each sample contained a few pinpoint inclusions under 10X loupe, which kept the clarity grades below VVS. The dark, irregularly shaped inclusions were presumably non-diamond carbon. Some samples showed dark graphitization on the girdle. A similar feature is seen in HPHT-treated diamond, which strongly suggests that these samples underwent post-growth treatment.

◆Birefringence

Under microscopic imaging with crossed polarizers, the characteristic streak pattern of anomalous double refraction due to strain (low-order black and white interference colours) was observed in all the samples. The streaks run parallel with the growth direction of the crystal, which is perpendicular to seed face. The patterns were elongated along the crystal's growth direction and presumably caused by growth along a screw dislocation.

◆Infrared spectroscopy

Absorption peaks due to isolated substitutional nitrogen were detected at 1130, 1344 and 1332 cm^{-1} in all samples. The peaks at 1130 and 1344 cm^{-1} are due to a neutral charged state, N_s^0 (Collins et al., 1987) and the 1332 cm^{-1} line is associated with a positive charge state, N_s^+ (Lawson et al., 1998). From these peak intensities, the concentration of isolated nitrogen can be estimated from 1.1 to 7.2 ppm with an average of 3.6 ppm. Also, peaks at 2875, 2908, 2948, 3032 and 3107 cm^{-1} were detected, which are considered to originate from absorptions due to C-H related defects that was formed by HPHT treatment after the growth (Charles et al., 2004). The peaks at 2875 and 2908 cm^{-1} in the three Light brownish yellow stones shifted towards lower wavelength at 2871 and 2902 cm^{-1} respectively, presumably due to the annealing temperature slightly lower than the temperature for creation of the yellow colour.

◆Photoluminescence analysis

Photoluminescence spectra (PL) using a 633 nm laser, Si-related peak at 737 nm (736.4/736.8 nm doublet) was detected in 13 out of the 15 samples. Five of them showed very weak peaks. Most of the samples showed small, non-attributed peaks at 908.9, 876.7, 853.4, 851.6, 850.2, 824.6, 819.1 and 795.8 nm.

In the PL spectra obtained with a 514 nm laser, very strong peaks at 637 nm (NV^-) and 575 nm (NV^0) were detected in all the samples. A pair of peaks at 630.4 and 628.6 nm was detected in 9 samples out of 15. Most of the samples showed small, non-attributed peaks at 565.6, 555.6, 554.4, 536.5, 534.9, 533.0, 532.0, 529.1, 528, 524.1 and 521.4 nm.

In the PL spectra obtained with a 488 nm laser, strong peaks at 637 nm (NV^-), 575 nm (NV^0) and 503.2 nm (H3) were detected in all the samples. The intensity ratio of H3/NV^- was 1.43 on average for the 12 yellow stones, but 0.82 on average for the 3 brownish stones. It is known that the H3 centre is not detected in as-grown CVD synthetic diamonds and the H3/NV^- ratio becomes larger by high temperature heat treatment (Charles et al., 2004; Meng et al., 2008), and this also helps to assume that the temperature of annealing performed on the three brownish diamonds was rather low.

In the PL spectra using a 325 nm laser, a peak at 415.2 nm (N3) was detected in all samples. It is known that the N3 peak is not detected in as-grown CVD synthetic diamonds but it is formed by HPHT treatment after the growth (Charles et al., 2004; Martineau et al., 2004). Other than the N3 series, peaks were detected at 425, 428, 439, 441, 451, 453, 457, 462, 486, 492 and 499 nm.

◆DiamondView™ observations

The high-intensity UV wavelength of the DiamondView™ revealed that all the samples have an essentially green luminescence, presumably due to H3, together with alternating pattern of striations characteristic of CVD synthetic diamonds. Phosphorescence in similar colour was also observed in all samples.

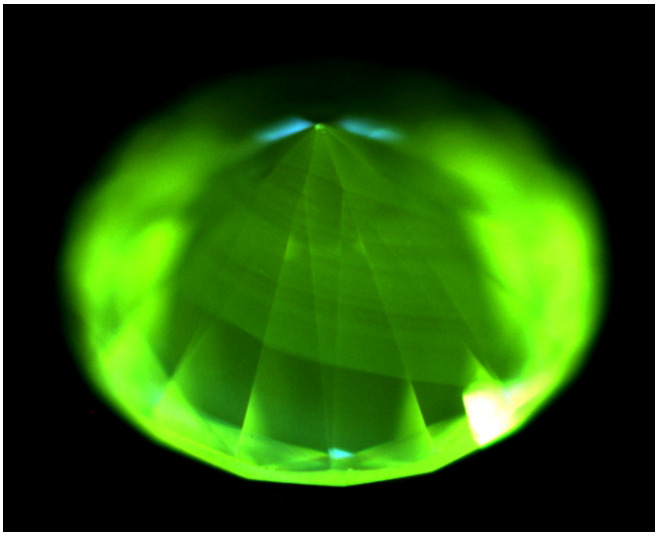

Figure 2. DiamondView™ image: All the samples with dominantly green luminescence together with alternating pattern of striations characteristic to CVD synthetic diamonds. Photo by M. Yamamoto.

Concluding remarks

Fifteen CVD synthetic diamonds in yellow hues submitted for grading without disclosure were tested in this study. They were proved to be of type Ib, containing on average 3.6 ppm of isolated substitutional nitrogen . From the presence of H3 and N3, the H3/NV^- intensity ratio and the infrared absorption peaks due to C-H related defects , these stones can be assumed to have undergone annealing at about 1900-2200°C (supposedly HPHT treatment) after the growth.

Acknowledgement

We express our gratitude to Dr. Kenji WATANABE of the National Institute for Materials Science for his cooperation on the PL analyses with UV lasers, and to Dr. Hisao KANDA of the TSUKUBA Expo Center for his discussion with us on the optic centres.

References

Charles S.J., Butler J.E., Feygelson B.N., Newton M.E., Carroll D.L., Steeds J.W., Darwish H., Yan C.-S., Mao H.K., Hemley R.J., 2004. Characterization of nitrogen doped chemical vapour deposited single crystal diamond before and after high pressure, high temperature annealing. Physica Status Solidi (a), 201(11), 2473-2485.

Collins A.T., 1978. Migration of nitrogen in electron-irradiated type Ib diamond. Journal of Physics C: Solid State Physics, 11(10), L417-L422.

D' Haenens-Johansson U., Eaton-Magaňa S., Bhoir M., Shinde Y., 2013. Three CVD Synthetic Diamonds Submitted to Mumbai Laboratory. G&G, vol.49, No.1, 49-50.

Eaton-Magaňa S., D' Haenens-Johansson U.F.S., 2012. Resent Advances in CVD synthetic diamond quality. Gems & Gemology, 48 (2), 124-127.

Even-Zohar C., 2012. Synthetic specifically "made to defraud". Diamond Intelligence Briefs, 27(709), 7281-7290.

Hainschwang T., 2014. First CVD Synthetic Diamond Discovered in a parcel of Natural Melee-sized Diamonds. Journal of Gemmology, 34(4), 300-302.

Kitawaki H., Y amamoto M., Hisanaga M., Okano M., Emori K., 2013. Undisclosed sample of large CVD synthetic diamond.Gems & Gemology,49 (1), 60-61.

Lawson S.C., Fisher D., Hunt D.C., Newton M.E., 1998. On the existence of positiv.ely charged single-substitutional nitrogen in diamond. Journal of Physics: Condensed Matter, 10 (27), 6171-6180.

Meng Y.F., Yan C.S., Lai J., Krasnicki S., Shu H., Yu T., Ling Q., Mao H.K., Hemley R.J., 2008. Enhanced optical properties of chemical vapour deposited single crystal diamond by low-pressure/ high-temperature annealing. Proceedings of the National Academy of Sciences, 105(46), 17620-17625.

Moe K.S., Wang W., D' Haenens-Johansson U.F.S., 2014. Yellow CVD synthetic diamond. Gems & Gemology, 50(2), 154-155.

Song Z., Lu T., Lan Y., Shen M., Ke J., Liu J., Zhang Y., 2012. The identification features of undisclosed loose and mounted CVD synthetic diamonds which have appeared recently in the NGTC laboratory, Journal of Gemmology, 33(1-4), 5-48.

Identification and influence to the future market of synthetic diamond

Dr. Joe C. C. Yuan[1,2,3]

[1] Taiwan Gemmological Institute, Taipei, Taiwan
[2] Zhengzhou Solstar Diamond Co., Ltd., Zhengzhou, China
[3] Taidiam Technology (Zhengzhou) Co., Ltd., Zhengzhou, China
yuanjoechihchun@gmail.com

Keywords Synthetic diamond, HPHT, CVD, identification

Introduction

The total reserve of diamonds on Earth is about 2.5 billion carats, of which about one-fifth is gem quality. Diamonds are now mined at the rhythm of about 100 million carats each year, so in a few decades, natural diamond reserves should be exhausted. Low-cost, high-quality near-colorless synthetic diamonds produced by chemical vapor deposition (CVD) appeared on the market starting in early 2012. Their price is about 2/3 to 1/2 that of the natural diamond, causing a shock. In the next few years, the price will gradually drop down to 1/3 to 1/5 the price of the equivalent natural gem diamond. Lower price, medium-quality, near-colorless synthetic small (200-50 pieces/carat) diamonds grown by HPHT method appeared on the market in mid-2014. Those small diamonds are polished in India. Colored synthetic diamonds have also been introduced in earlier years (by Gemesis for example), but there is little demand for them, and sales are very limited. As synthetic diamond growth technology improves, the market for synthetic diamond is maturing, and synthetic diamonds of better quality will gradually fill the vacancy left by the lack of natural diamonds in the future.

The author has the equipment to grow small HPHT colorless diamonds and large CVD colored or near-colorless diamonds, as well as conduct research to identify them efficiently from natural diamonds.

Enhancement of CVD diamond color after growth

After growth, CVD diamonds show a light brown color because of lattice distortion. To enhance such synthetic diamonds, we can use HPHT or LPHT treatment apparatus (Meng et al., 2008), which eliminates or weakens the brown color and produces thus a colorless or near-colorless transparent crystal.

Identification of CVD-grown synthetic colorless/near colorless diamonds

A. Observations with magnification under the microscope

1. Feather: Because of the carbon deposition in "columns", along a growth dislocation, the surface of the feather shows a "zigzag" pattern (Figure 1).

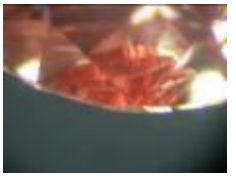

Figure 1. Zigzag aspect of feather.

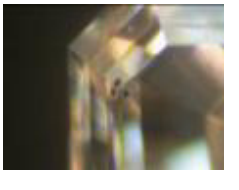

Figure 2. Black "cotton balls".

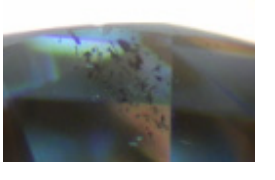

Figure 3. Near-surface black spots.

2. Black points: The individual black spots inside show a hairy appearance as cotton balls (Figure 2).

3. Near-surface multiple black spots: When a CVD single crystal diamond is grown, polycrystalline diamond formed around the crystal surface, and are not completely eliminated during polishing. Thus they are seen near the girdle or under the surface, producing irregular black spots, as shown in Figure 3.

Between crossed polarizers, a typical pattern can be seen, due to the hair or column like growth pattern (figure 4 to 7, Table 1).

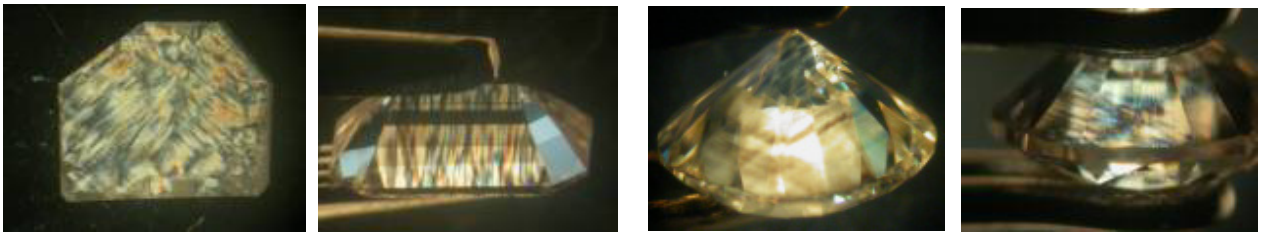

Figure 4. A type IIa brown CVD diamond plate shows spots and a striped or cross-hatched pattern.

Figure 5. CVD diamond grows from the substrate upwards in parallel, thicker "columns".

Figure 6. CVD diamond with different direction of birefringence pattern, with thicker "columns".

Figure 7. Natural type IIa brown diamond, HPHT enhanced to colorless, show a finer (tatami) cross hatched pattern.

Table 1. Results of magnification between crossed polarizers

	Type of Diamonds	Character of Observation
a	CVD Synthetic Diamonds	Full of parallel anomalous birefringence "columns"(Thicker than in natural brown Type IIa HPHT enhanced diamonds)
b	Natural Brown IIa Type HPHT Enhanced Colorless Diamonds	"Tatami" cross-hatched slip-planes with extremely micromesh parallel lines, seen in some directions.
c	Natural / HPHT Synthetic Diamonds	None or with sectorial anomalous birefringence

B. Luminescence imaging: Shell-like curved lines from flow step growth (Martineau et al., 2004) are the only evidence of synthetic CVD origin seen in the DiamondView, as seen in figures 8. In cathodoluminescence (CL), orange to purple colors, as well as green are seen related to various classic defects and hydrogen content. The blue color is obtained through ultra annealing, and is reminiscent of natural diamonds (see Figure 9).

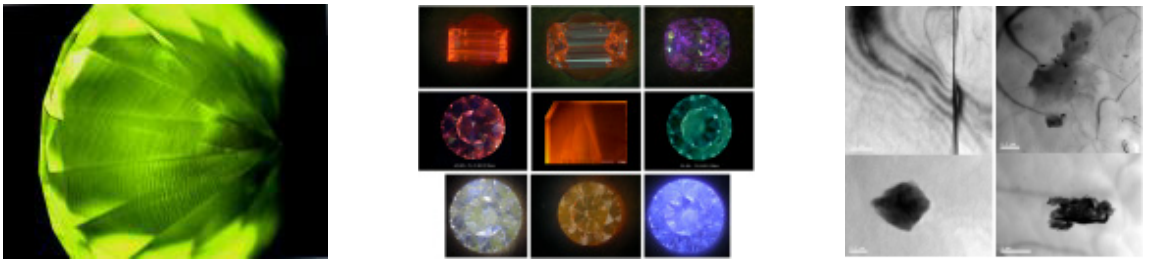

Figure 8. DiamondView: Shell-like curved lines provide evidence of CVD origin.

Figure 9. CL color of CVD synthetic diamond: from classic orange to blue obtained by ultra-annealing.

Figure 10. TEM: graphite and carbon-like inclusions (the scales on figure 10 are respectively 0.2, 0.5, 0.2 and 1 micron, from left to right and top to bottom).

C. Transmission electron microscope (TEM): Very small inclusions of graphite or "carbon" can be seen (Figure 10). They presumably correspond to the black spots seen in the gemological microscope.

D. Spectroscopy: In UV-Visible-NIR spectroscopy, the 415 nm peak caused by the N3 color center is found only in natural type Ia diamonds. Using an FTIR infrared microscope, it becomes apparent that CVD diamond contains a lot of hydrogen, creating C-H peaks in the range 6400 to 7400 cm^{-1}. Those will disappear gradually according to the degree of annealing (Courtesy Qi Li-Jian; Figure 11).

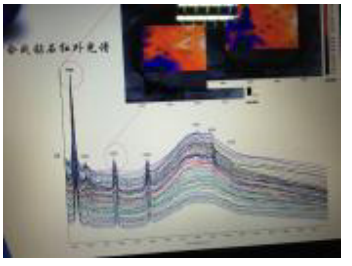

Figure 11. FTIR CH peaks around 6400 to 7400 cm-1.

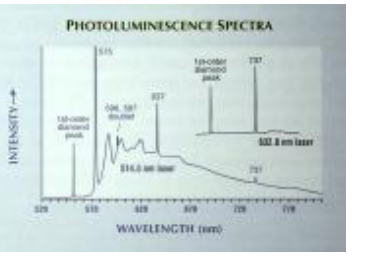

Figure 12. 737nm Si-V color center (after Wang et al., 2003).

In photoluminescence (PL) spectroscopy at liquid nitrogen temperature, we found anneal peaks at 596 and 597 nm and the Si-V peak at 737 nm (Wang et al., 2003; Figure 12). CVD diamonds produced inside a quartz bell emit the silicon-related 737 nm peak; if they are produced inside a stainless steel tank they emit little or no 737 peak.

Current market of synthetic diamonds

Table 2. Classification and comparison of synthetic diamonds on current market

Growing Method	HPHT Seed-Temp. Gradient	HPHT without Seed-Temp. Gradient /Even Temp*.	CVD
Size	Large Diamonds	Small Diamonds	Large Diamonds
Color	Colorless/ Near Colorless	Colorless/ Near Colorless	Colorless/ Near Colorless
Clarity	Fair	Fair	Good
Growing cost compared to natural diamonds	Higher	Lower	Much Lower
Prospect	No Good	Acceptable	Very Good

***** Without seed, diamond nuclei grow automatically inside the whole experimental volume.

Identification of HPHT-grown synthetic colorless/near colorless small diamonds

HPHT Seed-Temperature gradient grow small colorless to near colorless rough diamonds, with poor shape and thus lower recovery (figure 13). The HPHT even temperature method produces colorless to near colorless small rough diamonds of good shape and allowing higher recovery (figure 14).

Figure 13. HPHT Seed and Temp. gradient grown rough diamonds.

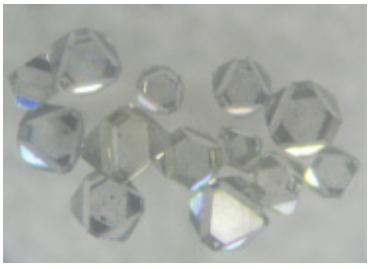

Figure 14. HPHT even temp. grown rough diamonds.

To quickly identify a large number of small colorless / near colorless diamonds is not so easy, the practical methods are the following in our experience:

- Using a **strong magnet** near the diamonds, natural diamonds are almost non magnetic, if a significant proportion of stones is attracted to the magnet, we can believe that the parcel was mixed with some synthetic diamonds.

- **UV-Vis-NIR spectroscopy** can measure one small diamond within a few seconds, when checking natural diamonds parcel. One should find about 98% of type Ia with the N_3 color center at 415 nm. However, when checking big parcels, if the quantity of non-type Ia diamonds is much more than 2 %, we can reasonably suspect that the parcel of diamond was mixed with some synthetic diamonds.

Conclusion

Natural diamond mining destroys the Earth's environment, wastes a lot of resources, creates the "blood diamond" ethical issue, and is overall expensive. Synthetic diamond grown in the laboratory is comparatively "greener", does not damage the environment, represents a lesser use of energy, with no "blood diamond" issue, and is overall less expensive. The future price of CVD diamonds will represent only a small fraction of that for natural diamonds of equivalent quality. HPHT-grown colorless small diamonds will sell for less than natural diamonds, and will supply the market for quantity of smaller stones.

In the future, natural diamond will be scarce and expensive. Synthesis technology as well as identification equipment and methods will improve. It will be easy to separate natural from synthetic diamonds, both large and small. We believe that soon, a number of diamond stores claiming "lab-grown real diamonds" will occupy a segment of the diamond markets. We predict synthetic diamonds will eventually exceed the quantity of natural diamond in the market.

References

Martineau P.M., Lawson S.C., Taylor A.T., Quinn S.J., Evans D.J.F., Crowder M.J., 2004. Identification of synthetic diamond grown using chemical vapor deposition (CVD). Gems & Gemology, 40 (1), 2-25.

Meng Y.-F., Yan C.-S., Lai J., Krasnicki S., Shu H., Yu T., Liang Q., Mao H.-K., Hemley R.J., 2008. Enhanced optical properties of chemical vapor deposited single crystal diamond by low-pressure/high-temperature annealing. Proceedings of the National Academy of Sciences, 105(46), 17620-17625.

Wang W., Moses T., Linares R.C., Shigley J.E., Hall M., Butler J., 2003. Gem-quality synthetic diamond grown by a chemical vapor deposition (CVD) method. Gems & Gemology, 39(4), 268-283.

Small scale mining of rubies and pink sapphires at Fiskenaesset, Greenland

Anette Juul-Nielsen

Geology Department, Ministry of Mineral Resources, Government of Greenland, Imaneq 1A – 201, P. O. Box 930, 3900 Nuuk, Greenland; anjn@nanoq.gl

Keywords Ruby, sapphire, small scale mining, Greenland, Fiskenaesset Anorthosite Complex

Introduction

In the last couple of years, Greenland (Figure 1) and more specifically the Fiskenaesset Anorthosite Complex in South West Greenland (Figure 2) has received attention due to the True North Gems Greenland A/S Aappaluttoq ruby and pink sapphire deposit, which is to start production in summer 2015. The granting of the exploitation license at Aappaluttoq in 2014 has resulted in a huge public interest in starting up small scale mining activities on rubies and sapphires.

Greenland Fact box	
Location:	Northernmost point is 740 km south of the North Pole
Area:	2,166,086 km²
Ice-free area:	410,499 km²
Terrain:	Ice cap covers all but a narrow, mountainous, rocky coast
Climate:	Arctic to subarctic, mean temperature does not exceed 10° C
Population:	56,282
Languages:	Greenlandic, Danish
Religion:	Evangelican Lutheran
Currency:	Danish Kroner (DKK)
Government type:	Parlimentary democracy within a constitutional monarchy
Dependency status:	Part of the Kingdom of Denmark, Self-government
Legal system:	Danish
Primary industry:	Fishing
Average income:	DKK 420,236
Unemployment:	9.8 % (age 18-64)

Figure 1. Map of Greenland with the major cities and a fact box on Greenland. Statistical data is from Statistics Greenland (2014).

Geological setting

The Fiskenaesset Anorthosite Complex is a deformed and metamorphosed layered intrusion set within a region dominated by Late Archean basement gneisses (Herd et al., 1969; Myers, 1985). Metamorphism in the region reached amphibolite facies conditions, locally up to granulite facies (Herd et al., 1969). The intrusive complex has a total length of more than 200 km and comprises anorthosites, leuco-gabbros, gabbros and ultramafic rocks infolded with amphibolites and orthogneisses (Figure 2).

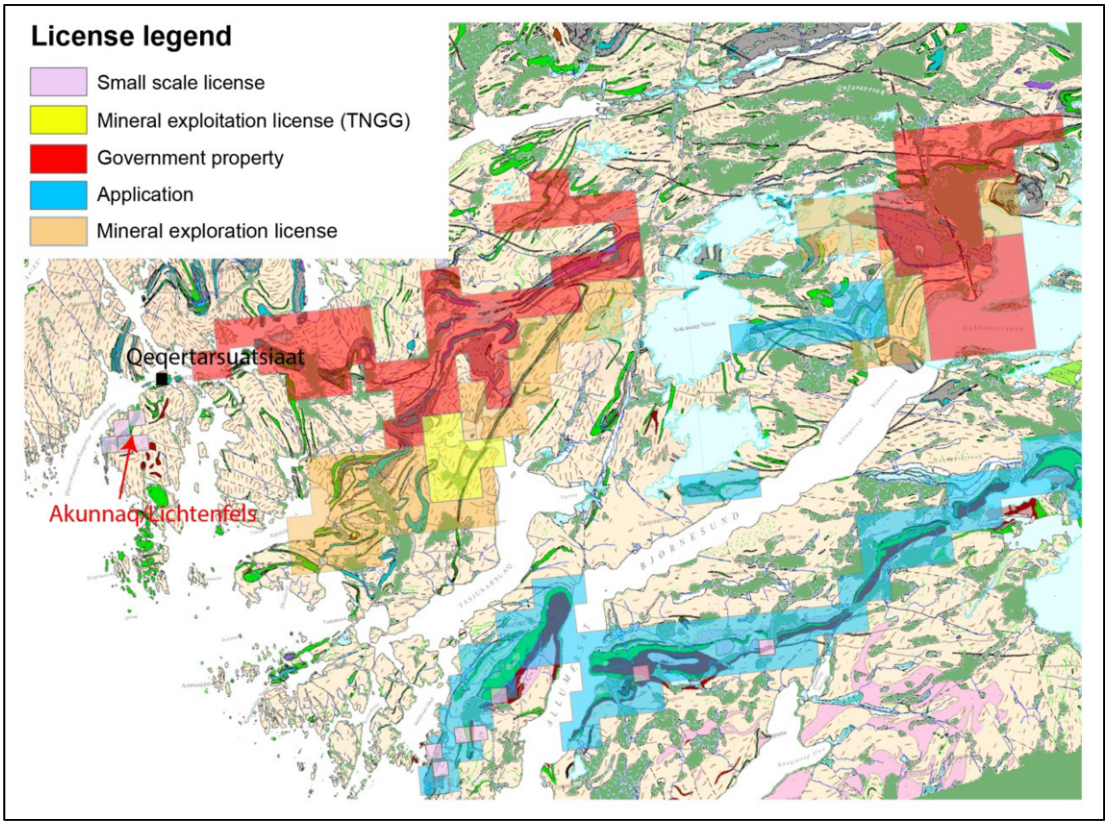

Figure 2. Geological map of the Fiskenaesset area: Pale orangy pink: Orthogneiss. Grey: Fiskenaeset Complex Anorthosite and upper leucogabbro units. Purple: Fiskenaesset Complex upper gabbro unit with net-veins of gneiss. Greenish blue: Fiskenaesset Complex middle gabbro and lower leucogabbro units. Green: Amphibolite. Dark grey: Dolerite dyke. Brown: Diorite and tonalite. Pink: Granite. Light green: Undifferentiated deposits including moraine older than 4000 BC. The map also shows the license areas with focus on rubies and pink sapphires as well as the location of the Akunnaq/Lichtenfels occurrence.

The rubies and pink sapphires are most commonly found at the amphibolite-anorthosite contact zone and are usually related to the following mineral assemblages (Appel, W. U., Ghisler, M., 2014):

- Corundum, sapphirine, pargasite, spinel, phlogopite ±plagioclase ±cordierite.
- Corundum, sapphirine, gedrite, phlogopite ±cordierite ±spinel ±plagioclase ±pargasite.
- Corundum, sapphirine, phlogopite ±plagioclase ±cordierite ±spinel.
- Corundum, pargasite, plagioclase, cordierite.
- Corundum, gedrite, plagioclase ±cordierite ±phlogopite.
- Corundum, phlogopite, plagioclase, cordierite.

The ruby and pink sapphire occurrences vary in size from just a few square meters to outcrops with lengths of up 1.6 km and varying widths.

Small scale mining of rubies and pink sapphires

In 2014 Greenland experienced a marked increase in the number of small scale mining licenses from 13 licenses in 2013 to 40 licenses by the end of 2014, most probably due to the granting of the exploitation license for rubies and pink sapphire to True North Gems Greenland A/S in 2014. Two thirds of the small scale licenses focus on rubies and pink sapphires and 13 of these licenses lie within the Fiskenaesset area (Figure 2).

Since most of the small scale licenses were granted in 2014 and 2015, limited mining has been done so far. The small scale projects which have progressed the furthest are located approximately 1 km south of Qeqertarsuatsiaat (Figure 1). The properties lie on or within the vicinity of a known ruby/pink sapphire occurrence called Akunnaq/Lichtenfels, which actually constitutes two small localities situated 450 m apart (Figure 2). The southernmost occurrence is a 20 m wide and 4 m thick lens with a mineral assemblage comprising corundum, sapphirine, pargasite, biotite, tremolite and plagioclase. The rubies and pink sapphires occur in a 1 m thick zone within the lens (Appel, W. U., Ghisler, M., 2014).

One of these small scale licenses is owned by the company Ice Cold Gems A/S and covers part of the Akunneq/Lichtenfels occurrence. The sample material from the property consists of corundum, sapphirine, pargasite, biotite and plagioclase. Pink sapphires dominate the occurrence. The company has collected approximately 50 kg of rock material during their first field season in summer 2014 and expects to start production on rubies, fancy colored sapphires and sapphirine in summer 2015. The gemstones will be cut and polished locally. At present, only a few rubies and pink sapphires have been faceted while the main part of the processed material has been fashioned into cabochons and beads (Figure 3).

Figure 3. Faceted 0.72 ct ruby (upper left) and cabochons (lower left) from the southernmost occurrence at Akunnaq/Lichtenfels. Examples of the different rock types found in the Fiskenaesset area: Corundum-sapphirine-phlogopite schist (upper right) and a 7 cm long rock sample consisting primarily of corundum-pargasite and plagioclase (lower right).

The adjoining licenses to the Akunneq/Lichtenfels occurrence have ruby- and sapphire-bearing rocks that are very similar to the rocks at the Akunneq/Lichtenfels occurrence (Figure 3). The mineral assemblage of the occurrences is directly linked to the mining and processing methods used by the small scale miners. The lack of or low amount of biotite in some of the rocks is a challenge to small scale miners in regard to gemstone processing as a higher amount of biotite or other micas in the host rock facilitates corundum extraction. Difficulties in extracting the rubies and pink sapphires often results in poorly processed material or ruby/pink sapphire rock slabs as an end product (Figure 3). In order to facilitate a small scale gemstone industry in Greenland, other than export of low commercial value gemstones, some initiatives need to be taken.

Small scale mining initiatives

With an increasing interest from the public in obtaining small scale licenses for extraction of rubies and pink sapphires, the Ministry of Mineral Resources has initiated a preliminary assessment of the Greenland gemstone potential and in 2016 will start mapping the gemstone occurrences. A special focus is on occurrences with easy access and easy gemstone extraction. Some of the areas within government property ruby/pink sapphire occurrences in the Fiskenaesset region suitable for small scale mining (e.g. ruby/pink sapphire in schist), will be designated as reserved areas for small scale mining in summer 2015.

Other small scale mining initiatives include setting up a gemstone conference for small scale miners, investigating the possibilities of establishing a certification system for Greenlandic gemstones and increasing the knowledge of the small scale miners through an increased level of public gemstone information and courses related to small scale mining.

References

Appel, P. W., Ghisler, M., 2014. Ruby- and sapphirine-bearing mineral occurrences in the Fiskenaesset, Nuuk and Maniitsoq Regions, West Greenland. Danmarks og Grønlands Geologiske Undersøgelse, Rapport 2014/72, 71 pp.

Heard, R. K., Windley, B. F, Ghisler, M., 1969. The mode of occurrence and petrogenesis of the sapphirine-bearing and associated rocks of West Greenland. Grønlands Geologiske Undersøgelse, Rapport 24, 44 pp.

Myers, J. S., 1985. Stratigraphy and structure of the Fiskenæsset Complex, southern West Greenland. Grønlands Geologiske Undersøgelse, Bulletin 150, 72 pp.

Statistics Greenland, 2014. Greenland in Figures, 11th revised edition, 40 pp.

Acknowledgements

The author would like to thank Ice Cold Gems A/S and Suulut Simonsen for supplying sample material from the Akunneq/Lichtenfels area as well as Julie Hollis (Ministry of Industry and Mineral Resources, Greenland) for helpful suggestions and Jan Schulz Adolfssen (Ministry of Industry and Mineral Resources, Greenland) for ArcGIS-assistance.

Investigation into the asterism observed in the star ruby from Neriya, Karnataka, India

Jayshree Panjikar[1], Aatish Panjikar[2]

[1]Pangem Testing Laboratory, Pune, India
[2]PANGEMTECH – Panjikar Gem Research & Tech Institute, Pune, India; jayshreepanjikar@gmail.com

Keywords Karnataka, Neriya, star ruby, inclusions, tialite, analyses

Introduction

Star ruby found in the village of Neriya (**12° 58' 40":77° 34' 7"**) in the Belthangady taluk, Dakshina Kannada district of Karnataka state have been studied. Karnataka was formerly known as Mysore state and has been known for deposits of star corundum and the classic locales produce mainly opaque, low-grade star rubies. In Neriya, the area is largely composed of lateritic soil forming a blanket over Precambrian rocks composed of granitic gneiss, mica schists and mafic to ultramafic schistose rocks. Extensive formation of corundum especially of semi-transparent star ruby with deep red colour has been found in bands of schistose ultramafic rocks intruded by pegmatitic veins. Gemmological properties, values for refractive indices, specific gravity, as well as FTIR and UV-Vis data have been determined. Semi-quantitative analyses were carried out using EDXRF show considerable presence of titanium and iron oxides. Inclusions studies along with Raman spectroscopy identified mineral inclusions as rutile, tialite, ilmenite, zircon, and spinel. Asterism may be due to tialite and rutile.

Figure 1. Nine star rubies from Neriya ranging from 3.57ct to 18.21cts.

Materials and methods

Nine cabochon star rubies (Figure1.) ranging from 3.57carats to 18.21carats with inclusions were selected and with gemmological methods their optical properties, specific gravity, UV fluorescence etc were determined. In depth study of the internal features was done using gemmological microscopes. Laser Raman Spectroscopy was used to determine the identity of the microscopic inclusions crystallizing near the surface. Non-polarized UV-Vis spectra for all samples were collected using JASCO F660 spectrophotometer over the 350nm - 800nm range. Mid Infrared spectra of 5 star ruby samples were collected in transmission mode by JASCO FT/IR-6600 with a resolution of $4cm^{-1}$. Semi-quantitative analyses were carried out using EDXRF.

Results

Visual appearance

The star rubies from Neriya village have a deep red colour with plenty of black needles visible to unaided eye. Most of material was semi transparent and all the pieces examined exhibited a very clear sharp asterism displayed by 6 fine thin rays.

Gemmological Properties

Specific Gravity was found to be in the range of 3.92 to 4.01, refractive indices fell in the range n_o1.766 to 1.772 and n_e1.758-1.764 determined on the polished base of the cabochon with a negative birefringence of 0.008. All samples showed strong fluorescence under LWUV and moderate to weak fluorescence under SWUV.

Microscopic observations

As expected in a star ruby, the crystalline form of titanium oxide (TiO_2) was the most common inclusion. But in the case of Neriya star rubies titanium oxide had crystallized in different time periods, in different mineral types as well as in different crystal sizes. Titanium oxide, in the form of fine rutile needles, was observed oriented parallel to the first order prism of the host. The silk occurred in the growth zones thus reflecting a varying supply of Ti and Fe during the ruby formation as can be observed from the growth in-homogeneities observed using dark field and reflected light for microscopic techniques.

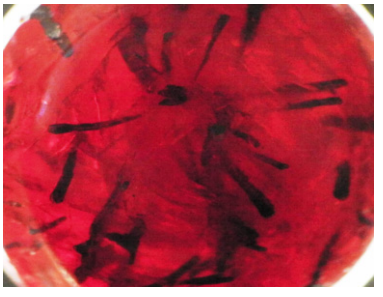

Figure 2. Needles of rutile and ilmenite radiating.

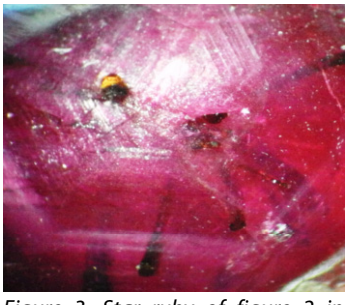

Figure 3. Star ruby of figure 2 in reflected light.

Figure 4. Milky haziness with crystals of tialite.

When observed under dark field illumination one could observe the long needles of rutile and ilmenite literally spurting out in a radial manner (Figure 2) and when observed under reflected light source the same stone showed clouds of fine rutile silk arranged in a hexagonal pattern which is due to ex-solution of titanium oxide that occurred as the host cooled (Figure 3). The titanium oxide in some regions had crystallized in the form of tialite Al_2TiO_5 along with aluminum oxide which was responsible for some of the asterism especially where there was milky haziness (Figure 4). This was confirmed by Raman spectroscopy. At the same time due to temperature variations during crystallization, had led to the short stubby needles of rutile crisscrossing at 120/60 degrees with reflecting spectral colours (Figure 5).

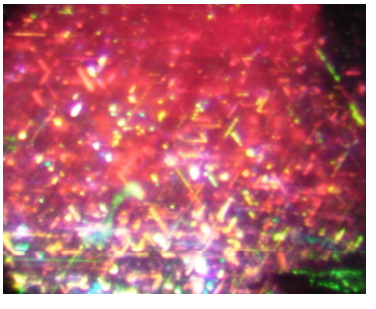

Figure 5. Rutile needles crossing at 120/60 degrees.

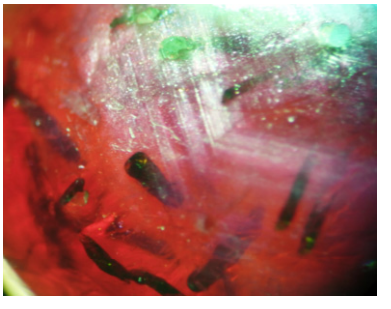

Figure 6. Zircon, ilmenite and rutile crystals.

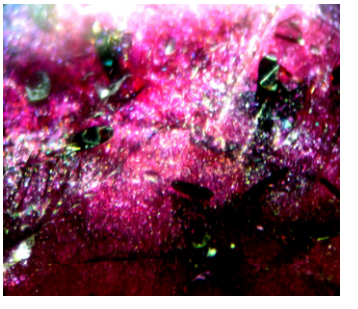

Figure 7. Octahedral crystal of spinel.

Besides titanium oxide, the star rubies in this study had a wide variety of internal features indicative of their metamorphic origin, crystals of zircon (Figure 6), ilmenite (Figure 6) and mica flakes. In one of the star rubies an octahedral crystal (Figure 7) was clearly visible and was further verified by Raman spectra as spinel. Tiny rounded oval and irregular crystal clusters of zircon were along with lamellar twinning.

UV-Vis spectra

The unpolarized UV-Vis spectroscopy of Neriya rubies revealed the typical Cr^{3+} absorption peaks at 695nm, 665nm and 603nm (Figure 10). In addition the spectra generally exhibited a strong background absorption starting from 600nm decreasing toward the UV edge. Other peaks 753nm and 547nm have not been assigned to any particular element. Minor peaks at 388 which may have been due to Fe^{3+} have not been labelled.

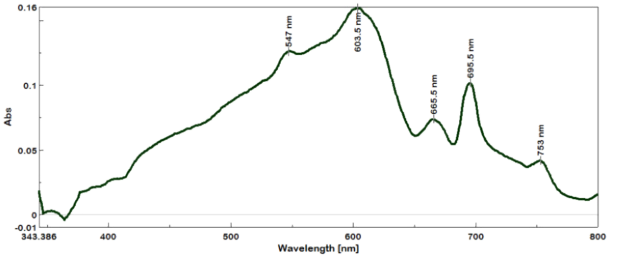

Figure 8. UV-Vis spectrum of Neriya star ruby.

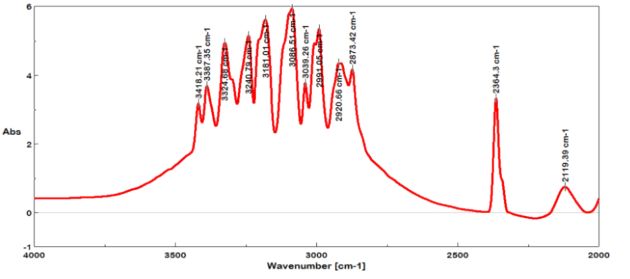

Figure 9. FTIR spectrum of Neriya star ruby shows TiO_2 contamination.

FTIR spectra

The FTIR spectra in the mid infrared region between 4000 and 2000cm^{-1} region for the Neriya star ruby showed certain distinct features of contamination by titanium oxide (Figure 9). The absorption peaks at 3086, 3240, 3324 and 3418 may be assigned to ruby whereas the peaks at 3387, 3181, 3039, 2991, 2920 and 2364 are probably due to titanium oxide as well as due to tialite (Al_2TiO_5).

Chemical analyses

Semi-quantitative chemical analyses by EDXRF for star rubies from Neriya gave the oxide wt % for Al_2O_3 = 91.93 to 98.36 the concentration of Al_2O_3 in some samples was reduced by the presence of mineral inclusions located at or just below the surface of the area measured. The oxide wt % for Cr_2O_3= 0.260-1.955, for TiO_2= 0.065-2.765, for Fe_2O_3= 0.016-0.145, for V_2O_5= 0.13-0.055 and for Ga_2O_3=0.003-0.041.

Discussion

In 1878, Gustav von Tschermak was the first researcher to identify rutile in corundum. Thereafter it has been generally accepted that asterism in star rubies is caused by needles of rutile (TiO_2) aligned along crystallographic planes of the corundum (Tait, 1955,). According to Nassau (1968): "the evidence given by Tait (1955) was: (1) the presence of titanium, (2) the needle like habit, and (3) the square cross-section of the needles. Based on the analogy with rutilated quartz, and by eliminating octahedrite and brookite by the morphology, rutile was accordingly identified. This type of evidence, however, is explained equally well by either TiO_2 or the compound aluminium titanate Al_2TiO_5". Nassau (1968) had felt that on the basis of the phase diagrams he studied [Bunting (1933) and by Lang, Fillmore and Maxwell (1952)], Al_2TiO_5 is the phase that should separate out from the corundum when the solubility is exceeded at temperatures near the melting point of corundum. Hence there was a strong possibility of the formation of tialite or fine needles of Al_2TiO_5 instead of rutile needles responsible for the formation of asterism in certain cases of natural star corundum.

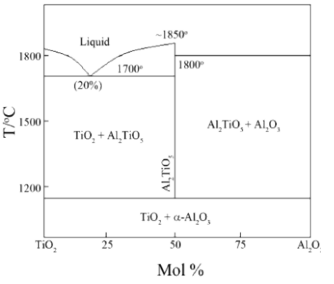

Figure 10. Phase diagram of TiO2:Al2O3 after Goldberg (1968) in Abali (2011).

Neriya ruby are a characteristic case where the rutile has crystallized in several forms; needle like crystals, sometimes as thin, long and slender acicular needles and sometimes as thick almost flat plate-like form. The crystallization of the acicular crystals has a specific pattern in three directions crossing at $120/60^0$ horizontally arranged parallel to the basal plane. One can also observe very fine thin, crisscross arrangement of silk which when illuminated with strong reflected light source, iridescent colours can be observed due the interaction of these short thin needle-like crystals with light. Changes and fluctuations in temperature are said to be responsible for the different morphologies of TiO_2 crystals. There is a thick whitish haze of fine needle like inclusions in certain places in the hexagonal arrangement which is generally attributed to rutile. Experiments carried out by Abali (2011) have reiterated Goldberg's theory proved in 1968 that Al_2TiO_5 and Al_2O_3 can co-exist according to phase diagram shown in Figure 10. During the present study the Raman spectra of the inclusions in this region showing the milky haziness formed by the titanium oxide gave a strong peak at $748cm^{-1}$ which is actually assigned to tialite (Abali, 2011). Further it has been proved by Camaratta et al. (2011) that although tialite is generally said to dissociate into rutile and corundum, if the dwell time is sufficient then tialite can retain its identity at lower temperatures when there are co-precipitations. Hence there is a strong possibility that some of these tiny crystals are indeed tialite. The authors therefore believe that the asterism in Neriya star rubies is also due to the presence of tialite.

Conclusion

Neriya star ruby display a wide range of inclusions especially with titanium oxide. Crystalline inclusions observed and identified were zircon, spinel, mica, ilmenite and rutile. These star rubies from Neriya, crystallized at a high temperature and with fluctuations in temperature. The melt had large quantity of titanium which initially formed tialite Al_2TiO_5 some of which may have got converted to corundum and rutile. On studying the phase diagram one can see that the formation of tialite is possible. It has been proved that if the dwell time is optimum then tialite can retain its structure (Camaratta et al., 2011). Therefore the asterism in Neriya star rubies is not only due to titanium oxide in the form of rutile but also due to the presence of tialite (Al_2TiO_5).

Acknowledgements

Authors thank Mr. K. Bharat for his invaluable help to visit the location and collect samples. Authors express their gratitude to National Chemical Laboratory, Dept. of Geology, University of Pune and their scientists for carrying out the analyses.

References

Abali, S., 2011. Effect of TiO_2 doping on micro structural properties of Al_2O_3 based single crystal ceramics. Journal of Ceramic Processing Research Vol. 12, No. 1, pp 21-25.

Camaratta, R., Acchar W. and Bergmann, C.P., 2011. Phase transformations in the Al2O3/TiO2 system and metastable phase formation at low temperatures. Rev. Adv. Mater. Sci., Vol. 27.pp64-68.

Nassau, K., 1968. On the cause of asterism in star corundum. The American Mineralogist, Vol.53 Jan-Feb.

Tait, A. S., 1955. Asterism in corundum. Journal of Gemmology, Vol. 5 pp 65-72.

Tschermak, G., 1878. Optisches Verhalten von Korund-Krystallen. - Tshermaks Min. Petr. Mitt. N.F.1:362-364.

Geographic origin determination of ruby and blue sapphire based on trace element analysis using LA-ICP-MS and 3D-plot

Kentaro Emori, Hiroshi Kitawaki

Central Gem Laboratory, Tokyo; emori@cgl.co.jp

Keywords LA-ICP-MS, corundum, 3D-plot, origin determination, trace element

Introduction

Gem minerals have information about their geological environment of the host crystal and occurrence. Analyzing the component of gem minerals leads to identify geological environment of the host crystal and occurrence and is important in determination of location where the mineral is produced.

X-ray fluorescence analysis is commonly used for chemical analysis in gemological testing laboratories, but its sensitivity is not always satisfactory and it has disadvantage that it cannot detect light element such as Li, Be and B in particular.

LA-ICP-MS (laser ablation inductively coupled plasma mass spectrometer) is a tool to detect impurities of ppb to ppm level with simultaneous multi-element analysis including light elements in high-sensitivity performance. It has been applied in the gemological field as a new analytical technique that is essential for the identification of Be-diffused corundum, although the laser ablation gives a little damage, i.e. formation of tiny holes of 10 micro meters from several points on surface of samples (Abduriyim, 2006).

In this study, we describe successful analysis using 3D-plot of LA-ICP-MS data to determine geographic origin of ruby and sapphires. This analysis has given difference of the origin more clearly than 2D-plot.

Material and method

Ruby from Cambodia (Pailin), Madagascar, Myanmar (Mo-gok, Mong-Hsu, Nam-Ya), Tanzania (Morogoro, Tanga, Winza), Vietnam (Luc-Yen) and blue sapphires from Cambodia, China, Laos, Madagascar, Myanmer, Nigeria, Sri Lanka, Tanzania, Thailand (Kanchanaburi, Chanthaburi) were analyzed.

In this study, LA-ICP-MS system was used, consisting of NEW WAVE UP-213 for laser ablation and Agilent 7500a ICP-MS. Analysis conditions were as follows: Laser ablation setting: laser wavelength 213nm, crater size 30μm and 80μm, laser power 0.025mJ, laser frequency 20Hz, ICP-setting: ICP 27.15MHz, RF Power 1200W, Plasma gas(Ar) 14.93 l/min, Auxiliary gas (Ar) 0.89l/min, Carrier gas(Ar) 1.44 l/min.

For 3D-plot graph, we used a software, 'gnuplot'. This software is a command line application software which can make 2D and 3D graphs. This is a free software and is distributed available in various operating systems, Linux, UNIX, Windows and MAC OS X.

Results

Ruby: Rubies from Myanmar show higher content of vanadium (above 120ppm) than those from other locations. The magnesium content of rubies from Cambodia tends to be higher than others and is at least 180ppm. The numeral range of analyzed elements is very close in rubies from Madagascar, Tanzania, and Vietnam but the 3D-plot

graph in Mg-V-Fe shows their difference (Figure 1). It has also been found that the 3D-plot graph in V-Fe-Ga shows a difference in marble origin rubies from Vietnam, Myanmar and Tanzania (Morogoro).

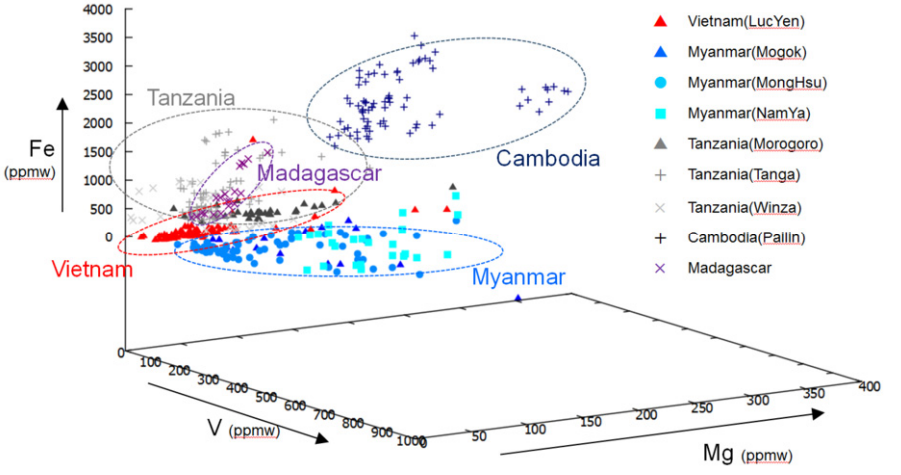

Figure 1. The 3D plot graph in Mg-V-Fe of rubies in this study.

Blue Sapphire: It has been found that the ratio of Mg to Ti of the non-basaltic blue sapphire is a good indicator of locality; Madagascar, Myanmer or Sri Lanka, which are difficult in origin determination form observation of inclusions and optical spectrometry. Peucat et al. (2007) describe that 2D-plot graph in Ga/Mg and Fe is useful to determine basaltic origin blue sapphire. In this study, 3D-plot graph in Mg-Fe-Ga shows a clear difference in basaltic origin blue sapphire from Cambodia, China, Laos, Nigeria, Tanzania and Thailand (Kanchanaburi, Chanthaburi) (Figure 2). It has also been found that the presence of trace element (Li, Be, B, Sc, Zn, Zr, Nb, Zr, In, Sn, Sb, La, Ce, Hf, Ta, W, Pb, Bi, Th) varies between locations.

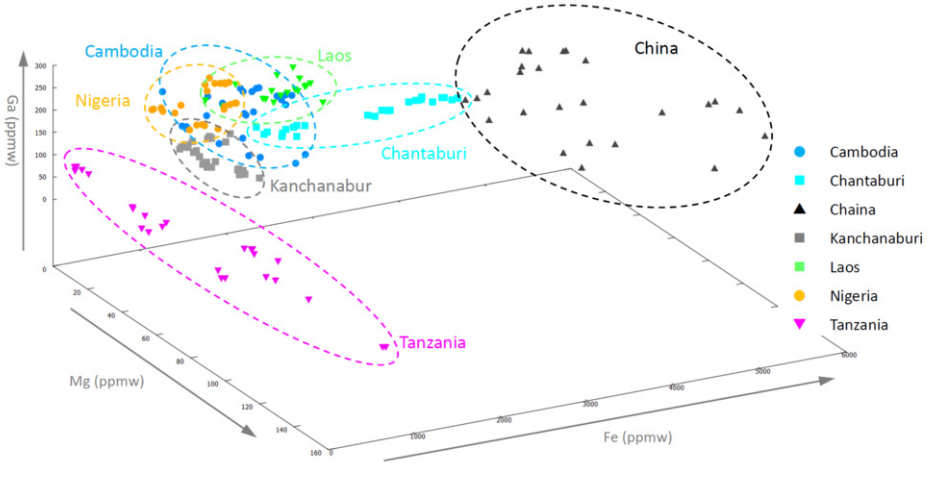

Figure 2. The 3D plot graph in Mg-Fe-Ga of basaltic blue sapphires in this study.

Conclusion

Trace element analysis of LA-ICP-MS shows information about geological environment of the host crystal and occurrence and leads to geographic origin determination of ruby and blue sapphire. But origin determination in trace element analysis by LA-ICP-MS does not always bring reliable information because the data obtained from different locations are sometimes the same. It must be used complementary with an observation of inclusions and gemological characteristics. For increase accuracy, it is necessary to collect samples with secure origin information and their chemical database.

Acknowledgement

We thank Yoichi Horikawa (Central Gem Laboratory, Japan) for supplying the corundum samples obtained the origin determination and discussing the data for this article. Dr. Hisao Kanda (Tsukuba Expo Center, Japan) kindly provided a critical reading of this manuscript.

References

Abduriyim A., Kitawaki H., 2006. Applications of Laser Ablation-Inductively Coupled Plasma-Mass Spectrometry (LA-ICP-MS) to Gemology. Gems & Gemology, 42(2), 98-118.

J.J. Peucat, P. Ruffault, E.Fritsh, M. Bouhnik-Le Coz, C.Simonet, B. Lasnier, 2007. Ga/Mg ratio as a new geochemical tool to differentiate magmatic from metamorphic blue sapphires. Lithos, 98, 261-274.

Zircon inclusions in blue sapphires

Emilie Elmaleh[1], Stefanos Karampelas[2*], Susanne Theodora Schmidt[1], Federico Galster[3]

[1]Section of Earth and Environment Sciences, University of Geneva, Switzerland
[2]Gübelin Gem Lab, Lucerne, Switzerland; Stefanos.Karampelas@gubelingemlab.com
[3]Faculty of Geosciences and Environment, University of Lausanne, Switzerland

Keywords blue sapphires, zircon inclusions, U/Pb dating

Zircons are present as inclusions in gem quality corundum, including blue sapphires. An important characteristic of zircon is its thermodynamic stability over long periods of geological time and its use as the best geochronometer with the radioactive decay of uranium and lead (for summary see Harley and Kelly, 2007). For the present study 103 unheated faceted and rough samples from different mines in Madagascar (Andilamena, Ilakaka), Sri Lanka (Ratnapura, Balangoda) and Burma (Mogok) were carefully examined under the microscope in order to find "zircon-like" inclusions (see some examples in Figures 1 and 2). In parallel, they were studied using EDXRF, FTIR and UV-VIS-NIR. The samples presented similar spectroscopic and chemical characteristics.

All inclusions were characterized using Raman spectroscopy equipped with a microscope. Only 17 samples were found to have indeed zircon inclusions showing a size of <150 microns (see again some examples in Figures 1 and 2); large enough for U/Pb dating with a LA-ICP-MS method. The trace elements of these samples were analyzed also by LA-ICP-MS and found also to be similar.

Figure 1. An apatite inclusion (bigger crystal; around 300 microns long) and a roundish zircon inclusion (smaller crystal; around 100 microns), identified by Raman spectroscopy, in a blue sapphire from Andilamena, Madagascar.

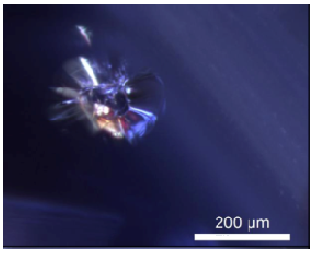

Figure 2. Zircon inclusion (identified by Raman spectroscopy) in a blue sapphire from Ilakaka, Madagascar.

The blue sapphires with zircon inclusions were cut so that the zircons were at the surface with a maximal surface area and were polished. All zircon inclusions were examined using cathodoluminescence (CL) attached to a SEM in order to make chemical zoning/structural damage visible. All zircons presented zoning; the most pronounced was observed in the samples from Ilakaka (Figure 3). Studied samples from Sri Lanka presented faint zoning but pro-

nounced halos (Figure 4) and these from Burma present a zoning different from that in samples from the other areas (Figure 5). Before dating, different parts of the dated zircons were measured again using Raman microspectrometry.

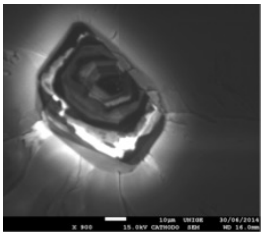

Figure 3. CL image of a zircon inclusion (around 30 microns wide) in a blue sapphire from Ilakaka (Madagascar) with a pronounced zoning.

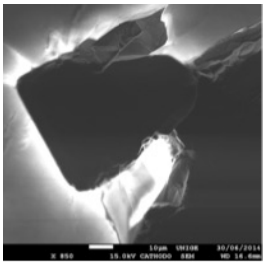

Figure 4. CL image of a zircon inclusion (around 50 microns wide) in a blue sapphire from Ratnapura (Sri Lanka) with a pronounced halo.

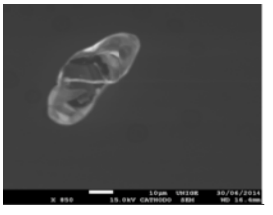

Figure 5. CL image of a zircon inclusion (around 10 microns wide) in a blue sapphire from Mogok (Burma).

Zircons from Mogok (Burma) show an age of 67±5 Ma, the youngest in this study. This age though is older than expected as the host rock is 30 Ma old. However, the morphology of these zircons is possibly of detrital origin, and they were likely to be incorporated during the crystallisation of the sapphire. The samples from Andilamena and Ilakaka (Madagascar) show the oldest age with an age of 1580±300 Ma and 1470±550 Ma respectively; also older than expected (<600 Ma). These ages are probably mixed of a detrital core and latter overgrowths. Samples from Ratnapura and Balangoda (Sri Lanka) were dated at 560±8 Ma and 550±7 Ma, in accordance with the expected mother rock ages. The first results of Raman spectra on the dated zircons vary from sample to sample but it looks that the origin/age did not play an important role in the exact position and shape of the zircon related bands.

Although only few zircons have been analysed, these first results show that morphologies and ages of the zircons from different deposits are promising for geographical origin determination. More zircon inclusions in more samples from these as well as other mines should be studied in order to confirm the dating and spectroscopic results. Additionally, dating methods with smaller beam (e.g., SIMS) should be used to date individual growth zones in zircon order to see if different ages are observed within the same zircon. Other non-destructive methods (e.g. Raman mapping) in should be applied as well to characterize faceted gemstones and help with the sometimes challenging origin determination of blue sapphires.

References

Harley, L.S., Kelly, N.M., 2007. Zircon: Timely but tiny. Elements, (3)1, 13-18.

Alluvial sapphires from Montana – Inclusions, geochemistry and indications for a metasomatic origin

J.C. (Hanco) Zwaan[1], Eric Buter[1], Regina Mertz-Kraus[2], Robert E. Kane[3]

[1]Netherlands Gemmological Laboratory - Naturalis Biodiversity Center, Darwinweg 2, 2333 CR Leiden, the Netherlands; Hanco.Zwaan@naturalis.nl
[2]Johannes Gutenberg-Universität Mainz, Institut für Geowissenschaften, Johann-Joachim-Becher-Weg 21, D-55128 Mainz, Germany
[3]Fine Gems International, P.O. Box 1710, Helena, Montana 59624, USA

Keywords Montana, Rock Creek, sapphire, mineral inclusions, geochemistry, metasomatic

Mineral inclusions and provenance

Source rocks of alluvial sapphires in Montana have never been discovered. However, inclusions and geochemistry may give clues on their original source. A parcel of faceted sapphires (total weight of 702.63 carats), has been studied. These sapphires had been previously removed from the faceted gem-sapphire inventory of the American Gem Corporation (AGC) because of their (relatively) many inclusions. The parcel mainly contained sapphires from Rock Creek, but also a few stones from Dry Cottonwood Creek and from the Eldorado Bar deposit on the Missouri River could be included, due to mixing of small quantities from those deposits, by the AGC, in the mid 1990s.

Mineral inclusions in Montana alluvial sapphires, such as topaz, barite, apatite, monazite, pyrochlore, anatase, allanite, and K-feldspar, suggest the involvement of pegmatites and related veins during formation, and/or an environment rich in incompatible elements and volatiles (such as in alkali magmas, Giuliani et al., 2007, and carbonatites, Guo et al., 1996). On the contrary, the presence of chromite-spinel and Ca-rich plagioclase would indicate an ultramafic to mafic igneous source. Phlogopite is often present associated with ultramafic intrusions, as a result of metasomatism. Together these inclusions may reflect a metasomatic origin of the alluvial sapphires from Montana. The mineral inclusions that might be indicative of a particular growth environment were all found in different sapphires. This leaves the option open that the alluvial sapphires might have two (or more) different sources, as advocated by Berger & Berg (2006).

Chemistry

However, the sapphires that contained inclusions suggesting different growth environments (as indicated above), do not show supporting evidence for a bimodal origin. The 52 secondary Montana sapphires chemically analysed, show completely overlapping compositions.

They are characterised by mean values of Fe 4686 µg/g, Ca 577 µg/g, Ti 58 µg/g, Ga 51 µg/g, Mg 35 µg/g and Cr 21 µg/g. Comparing the chemical compositions with the large dataset of many sapphire occurrences published by Peucat et al. (2007), and with data of Australian sapphires (Sutherland and Abduriyim, 2009), Montana alluvial sapphires can be separated clearly from primary sapphires found at Yogo Gulch, Montana (that are thought to be of mantle origin), and showed most overlap with plumasitic/metasomatic and metamorphic sapphires, with a slight overlap into the magmatic sapphires field (Fig.1). A factor that clearly separates alluvial Montana sapphires from magmatic blue sapphires from alkali basalts and syenitic blue sapphires, is the 10,000 Ga/Al ratio, being between 0.7 and 1.2, which is in agreement with values of the continental crust (1 – 1.5), much lower than the ratios of magmatic sapphires that vary between 2.5 and 3.7 (cf. Peucat et al., 2007).

Involvement of F-rich fluids is supported by the presence of topaz, apatite and pyrochlore inclusions, and by these low Ga/Al ratios in the sapphires, which may be caused by extraction of GaF_6^{-3} ions, during F-rich fluid circulation (cf., Whalen et al. 1987).

Concentrations and ratios of Fe, Ga, Mg, Ti, Cr and V, help to distinguish alluvial Montana sapphires further from most other metasomatic sapphires with overlapping properties.

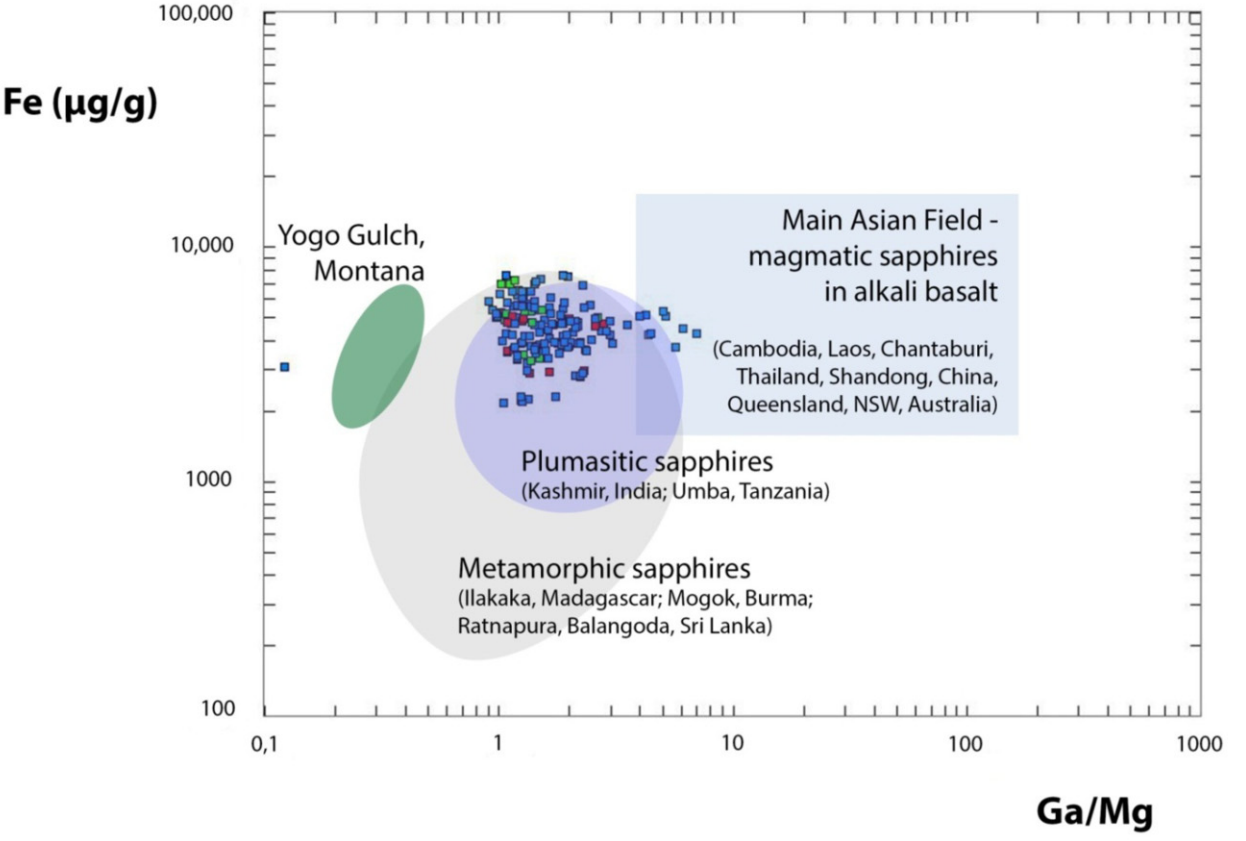

Figure 1. Compositions of alluvial Montana sapphires in relation to compositional fields for metamorphic, magmatic and plumasitic (blue) sapphires, as shown by Peucat et al., 2007. Red symbols indicate sapphires that contained inclusions suggesting a volatile-rich formation environment and green symbols indicate sapphires that contained inclusions of possible ultramafic/mafic origin.

References

Berger A.L., Berg R.B., 2006. The Silver Bow Sapphire Occurrence, Montana: Evidence for a Volcanic Bedrock Source for Montana's Alluvial Sapphire Deposits. Economic Geology, Vol. 101, pp. 679-684.

Giuliani G., Ohnenstetter, D., Garnier, V., Fallick, A.E., Rakotondrazafy, M., Schwarz, D., 2007. The Geology and Genesis of Gem Corundum Deposits. Mineralogical Association of Canada, Short Course Series, Vol. 37: 23-78.

Guo J., O'Reilly S.Y., Griffin W.L., 1996. Corundum from basaltic terrains: a mineral inclusion approach to the enigma. Contributions to Mineralogy and Petrology, Vol.122: 368-386.

Peucat J.J., Ruffault P., Fritsch E., Bouhnick-le Coz M., Simonet C., Lasnier B., 2007. Ga/Mg ratio as a new geochemical tool to differentiate magmatic from metamorphic blue sapphires. Lithos, 98: 261–274.

Sutherland, F.L., Abduriyim, A., 2009. Geographic typing of gem corundum: a test case from Australia. Journal of Gemmology, Vol. 31, No. 5-6, pp. 203-210.

Whalen J.B., Currie K.L., Chappell B.W., 1987. A-type granites: geochemical characteristics, discrimination and petrogenesis. Contributions to Mineralogy and Petrology, Vol. 95, pp. 407-419.

Sapphire deposits of Sri Lanka

E. Gamini G. Zoysa

Institute of Gemmological Sciences, Colombo, Sri Lanka; gaminigz@hotmail.com

Abstract

Sri Lanka has long been known for its unique sapphires. The most desirable colours are shades of blue, yellow and pink.

The production of the corundum variety known as "Geuda" - milky or transparent to translucent - has been shown a greater interest in the recent past.

Geologically Precambrian metamorphic rocks covers over 75% - of Sri Lanka's land mass. Those have been divided into 4 major divisions according to their lithology and age (figure 1).

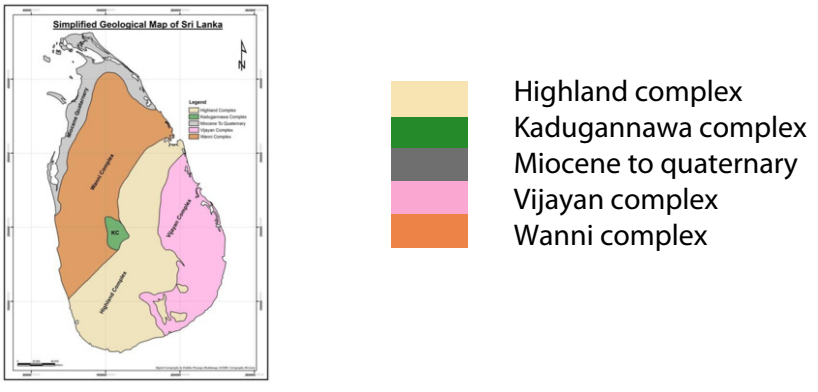

Figure 1. Simplified geology map of Sri Lanka (GSMB).

It is a fact that most of the gems are mined from alluvial gem fields. The large number of these mines are located within the Highland series (figure 2).

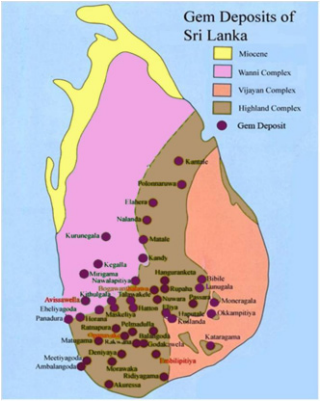

Figure 2. Distribution of Gem deposits in Sri Lanka.

Primary in-situ sapphire deposits are scattered within the Highland and Vijayan series.

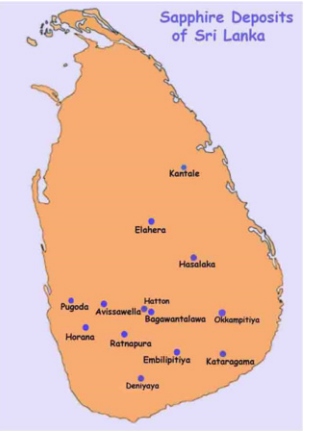

Figure 3. Sapphire deposits of Sri Lanka.

Geuda is a milky variety, transparent to translucent, found in the gem gravels .This material is enhanced to various shades of blue, yellow and pink depending on its chemical nature. Butane gas mixed with oxygen is used for its treatment. A desirable blue colour may be obtained by using reducing conditions at a higher temperature around 1800°C, while the yellow colour requires oxidizing conditions at about 1500°C. It is classified into six categories (see Table 1 and figure 4).

Table 1. Classification of Geuda corundum

1. Diesel Geuda	2. Milky Geuda
3. Silky Geuda	4. Ottu Geuda
5. Dhun Geuda	6. Kowangu Pushparaga

Figure 4. Assorted types of Geuda sapphire.

FTIR is helpful in the identification of heated blue and yellow sapphires. The spectra for both will not show the peak for OH in the heated stones while it is obvious in the unheated types.

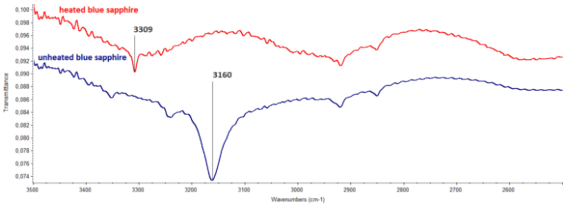

Figure 5. FTIR Spectra of unheated (blue trace) – and heated (red trace) blue Sapphire.

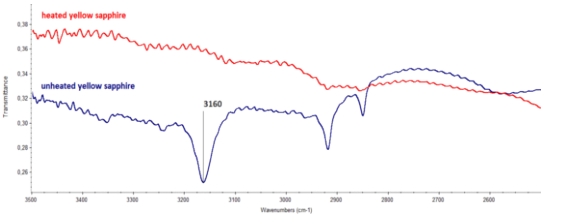

Figure 6. FTIR Spectra of unheated heated (blue trace) – and heated (red trace) yellow Sapphire.

Hydroxyl (OH-) bond stretching peaks were used for the determination of heat treatment of Sri Lankan sapphires. These peaks are situated from 3100 to 3600 cm^{-1}. Sri Lankan unheated sapphires (blue as well as yellow) displayed OH stretching IR absorption peak at 3160 cm^{-1} (Figures 5 and 6), while heat treated blue sapphire showed a peak at 3309 cm^{-1} (Figure 5). Heat treated yellow sapphire does not display any peak in the region from 3100 to 3600 cm^{-1}, which could be caused by treatment at lower temperatures.

The number of sapphire mines according to the National Gem & Jewellery Authority was around 6000 in 2014 (table 2). Out of these 3300 gem mines are located in the Ratnapura district.

Table 2. No of gem licenses in Sri Lanka

Year	No of Licenses
2000	3634
2001	3712
2002	3827
2003	3702
2004	3988
2005	4471
2006	4734
2007	5024
2008	4204
2009	3970
2010	4061
2011	4687
2012	5956
2013	6565
2014	5928

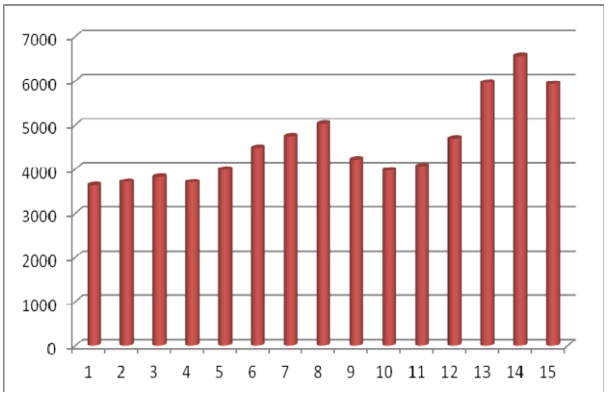

An unusual occurrence of sapphires in a geode - like form is encountered in a village called Getahetta in Awissawella. Inside this geode over 200 pieces of sapphire may be found .Their sizes vary from 1 to 2 cts and the mainly blue & yellow coloured sapphires are found. Most of the stones are transparent to translucent and of very good gem quality.

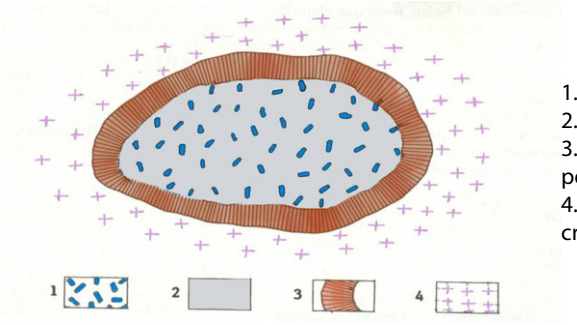

1. Cross-section of a Sapphire bearing pocket
2. Feldspar
3. Crust composed of phlogopite mica plates oriented nearly perpendicular to interior kaolin surface
4. Quartz- 60%, phlogopite mica 39%, Spinel microscopic crystals-1

Figure 7. Cross section of a geode like sapphire bearing body.

Another new deposit is Hasalaka in the north central part of Sri Lanka. In this relatively recent gem producing area sapphires up to - 50 cts have been discovered. Larger crystals of non - gem quality up to 15 Kg have also been discovered in the vicinity of Hasalaka.

Results 2.56ct_BK

Element	Concentration		Peak (cps)	Background (cps)
MgO	0.00 ppm	0.00000	40.275	
SiO2	0.00 ppm	0.00000	24.245	
TiO2	2064 ppm	5.9560	2.0240	
V2O3	73 ppm	0.37450	1.1255	
Cr2O3	0.00 ppm	0.00000	0.26000	
MnO	0.00 ppm	0.00000	0.56500	
Fe2O3	1169 ppm	5.2927	0.74726	
Ga2O3	102.5 ppm	2.4994	0.62557	
ZrO2	[4.3] ppm	0.34014	3.2899	
Nb2O5	15.4 ppm	1.3254	13.825	
SnO2	[2.3] ppm	0.048937	0.52106	
Ta2O5	0.00 ppm	0.00000	0.37500	
WO3	0.00 ppm	0.00000	1.9650	
PbO	0.00 ppm	0.00000	0.22500	
Al2O3	99.657 %	Diff		

Sample Ref. No	Be (ppm)	Mg (ppm)	Ti (ppm)	V (ppm)	Cr (ppm)	Mn (ppm)	Fe (ppm)
GM 4	0.28	33.4	786	3.2	1.66	< .099	982
GM 4	0.34	32.7	841	3.22	2	< .099	915
GM 4	0.22	54.3	668	6.89	2.06	< .099	1710
GM 8	< .051	173	237	9.04	4.02	< .099	826
GM 8	< .051	147	200	7.85	3.22	< .099	780
GM 14	< .051	104	112	6.87	2.51	< .099	890
GM 14	< .051	86.4	98.6	5.66	2.78	< .099	733
GM 24		83.2	94.1	9.05	2.56	< .099	1170
GM 24	0.17	81.7	98	9.56	3.3	< .099	1170
GM 35	< .051	182	234	11.1	3.41	< .099	835
GM 35	< .051	127	151	9.88	3.24	< .099	804
GM 35	< .051	119	144	10	3.48	< .099	837
	0.107	0.538	0.026	0.378	0.099	7.785	0.011

Figures 8 & 9. Chemical analyses of sapphire from Hasalaka.

References

Cooray P.G., 1967. The Geology of Ceylon P 1-300.

Herath, J.W., 1984. Geology & Occurrence of Gems in Sri Lanka, Journal of National Science Commission Sri Lanka 12 (2), 257-271.

Prame, W.K.B.N, 1991. Metamorphism Nature of Granulite facies in south west of Sri Lanka, Geological Survey Department of Sri Lanka, Professional paper 5, 188-200.

Zwaan, J.C. and Zoysa, E.G., 2007. New primary gem occurrences in Sri Lanka. Zeitschrift der Deutschen Gemmologischen Gesellschaft, 57, 23-32.

Liu, S. E., Zoysa, E.G ., 2011. The Miriswatta primary sapphire deposit in Sri Lanka, In Color, 18, 34-39.

Dual-color double stars in corundum and quartz

K. Schmetzer[1], M.P. Steinbach[2], H.A. Gilg[3], A.R. Blake[4]

[1]Petershausen, Germany; SchmetzerKarl@hotmail.com
[2]Idar-Oberstein, Germany; Gstargems@aol. com
[3]Technische Universität München, Munich, Germany; agilg@tum.de
[4]Chevy Chase, MD, USA; andreablake02@gmail.com

Asterism involving a single white six-rayed star, due to the presence of three series of oriented needle-like inclusions, is frequently observed in natural and synthetic rubies and sapphires and in natural quartz cabochons. Twelve-rayed stars as well as "double" or "multiple" star patterns of several stars with identical whitish colour have also been seen in corundum and quartz and can be attributed to additional series of inclusions (in quartz and corundum) or twinning (in ruby and sapphire).

To separate the different phenomena, the following short overview might be helpful:

	Ruby and sapphire	Quartz and rose quartz
Single six-rayed star	Three series of needles in planes parallel to the basal face	Three series of needles in planes parallel to the basal face
Single twelve-rayed star	Six (2 x 3) series of needles in planes parallel to the basal face	Six (2 x 3) series of needles in planes parallel to the basal face
Two displaced stars with identical colour	Twinned individual, each part of the twin with a single six-rayed star	
Multiple stars with identical colour* (or different additional light spots)		Several series of needles parallel and inclined to the basal face (or additional flat inclusions)
Double stars with a silvery white first star and a body-colored second star	To be described here	To be described here

*also observed in garnets and spinels due to the cubic symmetry of the host

Corundum and quartz samples showing a further type of double star, consisting of two differently coloured six-rayed stars, have occasionally been noted or depicted as well (Killingback, 2006; Schmetzer & Hainschwang, 2012). However, in absence of any comprehensive study of the mode of formation for this latter type of dual-colour double stars, the instant project was undertaken to elucidate the optical phenomenon.

Diffusion-treated synthetic rubies and sapphires

Synthetic corundum cabochons that had undergone diffusion treatment exhibit the three intersecting light bands of an ordinary white six-rayed star such as is commonly seen in asteriated natural and synthetic rubies and sapphires. In addition, three intersecting light bands producing a second, variously coloured six-rayed star could be observed under fibre optic illumination or in direct sunlight (Figure 1).

When these cabochons were illuminated through the center of the dome more or less perpendicularly to the slightly curved or flat base and viewed parallel to the incident light, both stars showed the same orientation and overlapped each other. In contrast, when illuminated and/or viewed obliquely, both stars were clearly separated from each other, and the second body-coloured star seemed to emanate from the curved or almost flat, slightly polished base of the cabochons. The ordinary white star was confined to the dome of the cabochons. The arms of both stars appeared to intersect and meet at the transition between dome and base of the cabochons (Figure 2). In all samples, the second six-rayed star showed the body colour of the host corundum crystals, e.g. red, orange, yellow or green.

After grinding and re-polishing the base of certain of these cabochons, all such samples showed only one remaining white six-rayed star (Figure 3). The second star having the body colour of the cabochon was no longer observed. Upon grinding and re-polishing the curved dome of others of these synthetic corundum cabochons, the samples so tested showed only the second six-rayed star with the body colour of the sapphire, but the ordinary white star had disappeared.

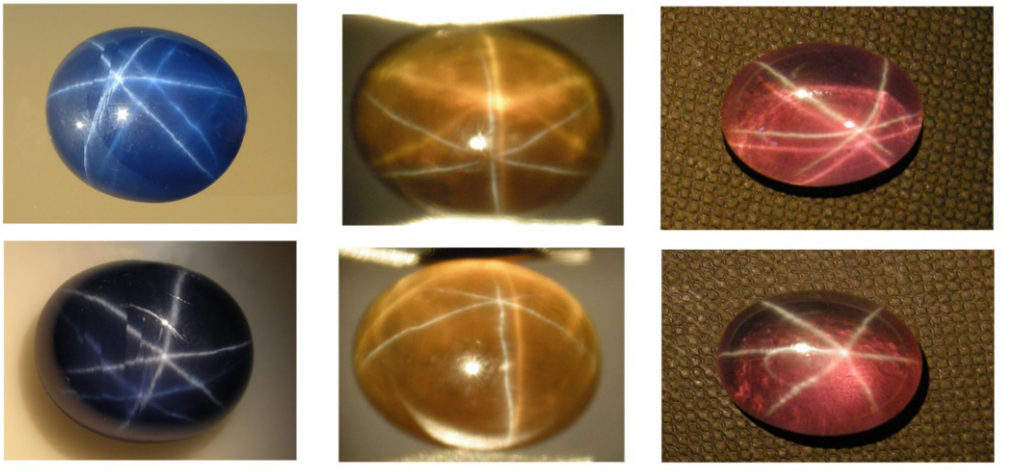

Figure 1 (left). Large diffusion treated sapphire grown by the Verneuil method; the sample of 91.41 ct in weight measures 27.7 x 23.5 mm and reveals, due its high transparency, a typical double star pattern. The photos show the different visual appearance of the sample in direct sunlight (above) and under fiber optic illumination (below). Photos by K. Schmetzer.

Figure 2 (center). This light yellow orange cabochon shows a six-rayed white and a second yellow orange star; two different orientations of the sample are depicted, the arms of the two stars seem to intersect each other and meet at the transition between dome and base of the cabochon. The sample measures 11.5 x 8.7 mm and weighs 6.94 ct. Photos by K. Schmetzer.

Figure 3 (right). This pink sapphire shows a white six-rayed star and a second pink star (above); after grinding and re-polishing the base of the cabochon, the pink star is removed and only the remaining white star is observed (below). The sample measures 14.1 x 11.2 mm and weighs 12.37 ct. Photos by K. Schmetzer.

Non-diffusion-treated natural and synthetic rubies and sapphires

A similar double star pattern was observed in a natural transparent purplish pink sapphire. The sample reportedly originated from Mogok, Myanmar. The gemstone showed two clearly separated six-rayed stars: one white star reflected from the dome of the cabochon and one purplish pink star confined to the curved base of the sample (Figure 4).

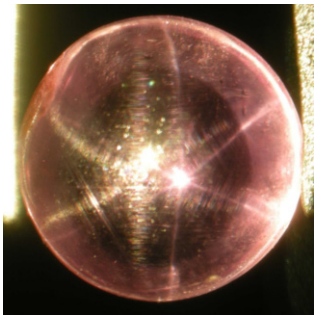

Figure 4. This purplish pink sapphire from Myanmar shows a first white star reflected from the dome of the cabochon and a second body-coloured star reflected from the curved base of the sample. The sapphire measures 7.0 mm in diameter and weighs 1.62 ct. Photo by K. Schmetzer.

Transparent synthetic sapphires produced by Linde in the early 1970s also showed a similar dual-colour double star pattern (Figure 5). For most of these samples, neither the white star confined to the dome nor the body-coloured second star confined to the base was removed or altered by the grinding and re-polishing process.

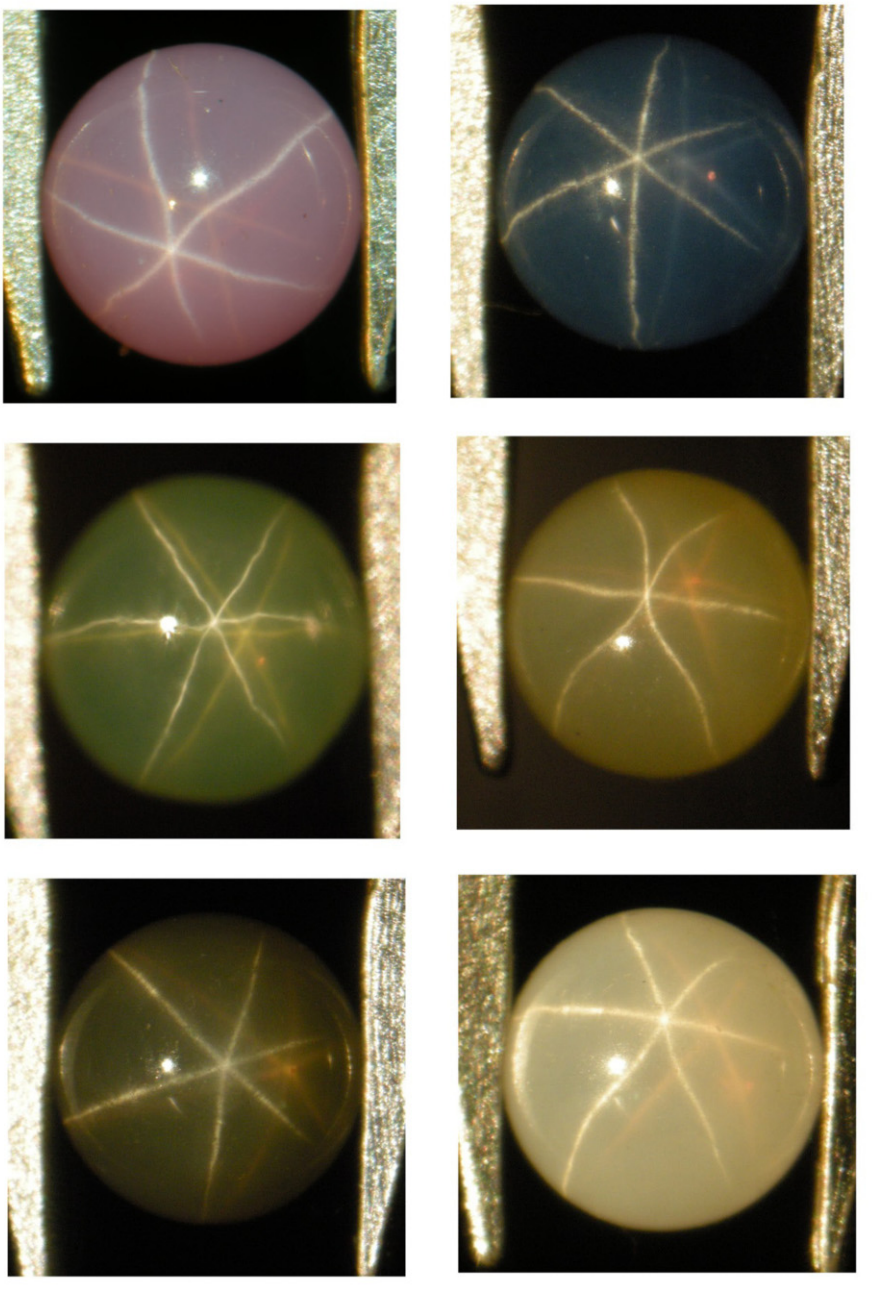

Figure 5. Six transparent to translucent Linde synthetic sapphires from a collection purchased in the 1970s; the samples show a six-rayed white star and a second body-coloured star. Diameter of the samples from 5.2 to 5.0 mm, weights from 0.75 to 0.63 ct, thickness from 2.7 to 2.5 mm; A. Hodgkinson collection. Photos by K. Schmetzer.

Diffusion treatment of ruby and sapphire

According to information from former employees of Union Carbide (Linde) and from the directors of Wiede's Carbidwerk, Freyung, Germany, diffusion treatment to create or improve asterism and to improve colour has been performed commercially for various types of corundum since the early 1970s, at least for part of the production.

Summary of observations for rubies and sapphires

The observations for the different groups of asteriated sapphires and rubies clearly indicate the mechanism set forth below for the formation of double stars in transparent or at least highly translucent samples from various sources. Such double stars were observed in two groups of samples:

a) In one group of samples, with rutile needles only at relatively thin layers confined to the dome and the base of the cabochons, both stars are likewise confined to surface layers of variable thickness of the ruby and sapphire cabochons. If no rutile precipitates are present in the outermost layers at the dome or at the base, e.g. after grinding and re-polishing of the sample, no corresponding star is visible. This means that the body-coloured star is removed after grinding and re-polishing of the base, and the white star is removed after grinding and re-polishing of the dome.

b) In a second group of samples with rutile needles or rutile precipitates distributed throughout the body of the complete sample, similar appearing dual-colour double stars are observed. No change of asterism is apparent after several grinding and re-polishing steps.

Natural quartz and rose quartz

Quartzes from two sources revealed an analogous double star pattern. Specifically, examinations of two almost colourless, very slightly pink rose quartz cabochons from Brazil and two slightly brownish pink quartz cabochons from India were performed. These transparent asteriated quartzes showed, in addition to the normal white six-rayed star, a second star confined to the base of the cabochons (Figure 6).

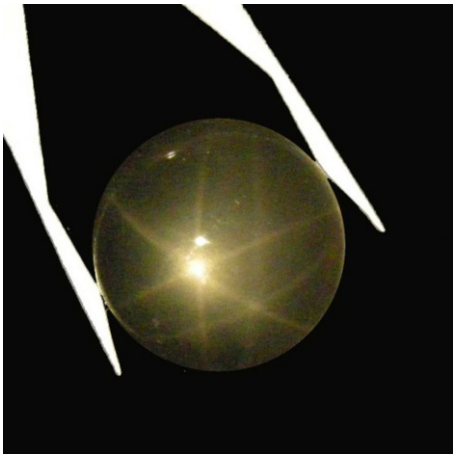

Figure 6. Very light rose quartz cabochon from Brazil showing double stars in reflected light. The cabochon measures 21.0 mm in diameter and weighs 26.18 ct. Photo by K. Schmetzer.

Mode of formation of a dual-colour double star pattern in corundum and quartz

Through comparison of commonalities between the different types of materials studied, it was determined that the following mechanism could be applied to explain the phenomenon in all groups of samples examined:

a) The ordinary silvery white star is formed by reflection and scattering of light at a layer confined to the curved dome of the cabochons consisting of a matrix of corundum or quartz containing minute needle-like inclusions.

b) The body-coloured second star is formed by reflection and scattering of light at a layer confined to the base of the cabochons consisting of a matrix of corundum or quartz containing minute needle-like inclusions.

c) The light forming the second star travels twice through the body of the cabochons and is absorbed by trace elements or other features, e.g. lattice defects, that are responsible for the body colour of the corundum or quartz crystals. Thus, the colour of the second star is identical to the body colour of the host.

In diffusion-treated corundum samples, it is possible to remove the white or the body-coloured star by grinding and re-polishing the outermost (upper or lower) surface, thus removing the diffusion-treated layer.

References

Killingback, H., 2006. Diasterism in rose quartz. Gems & Jewellery, 16**(**2), 64.

Schmetzer, K., Hainschwang, T., 2012. Star ruby. Gems & Jewellery, 20(4), 14-17.

Role of Be in reduction and oxidation heating of sapphire

Visut Pisutha-Arnond, Chaniya Rochd, Wilawan Atichat, Pornsawat Wathanakul, Nalin Narudeesombat

The Gem and Jewelry Institute of Thailand (Pub. Org.), Bangkok 10500, Thailand; pvisut@gmail.com

Keywords role of Be, sapphire, reduction and oxidation heating

Introduction

Even though beryllium (Be) treated corundum has been extensively investigated (e.g., Atichat et al., 2004; Emmett et al., 2003, Fritsch et al., 2003; Hänni and Pettke, 2002, McClure et al., 2002, Peretti and Günther, 2002, Peretti et al., 2003; Pisutha-Arnond et al., 2004a,b, 2006, 2009; Schmetzer and Schwarz, 2004; Themelis, 2003), the role of Be, Mg, Ti and Fe in causing color of natural sapphire under reducing conditions has not yet been fully understood. In this study, therefore, reduction heating followed by oxidation heating and trace element analysis were performed systematically on Be-treated natural sapphire to evaluate the effect of such treatment and trace element concentrations on the stone's coloration.

Sample and procedures

In this investigation, a reduction and oxidation heating experiment was systematically carried out on a 7.35 ct oval-cabochon cut yellow-greenish blue sapphire that was subjected to a prolonged Be-diffusion treatment by a Thai gem heating specialist. The selected stone was firstly cut and polished as a 2 mm-thick oval wafer disc

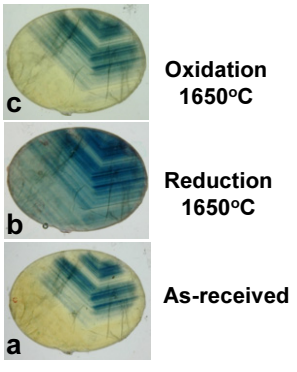

Figure 1. Photos of the as-received stone (a), reduction heating (b), and oxidation heating (c), by C. Rochd, in methylene iodide immersion.

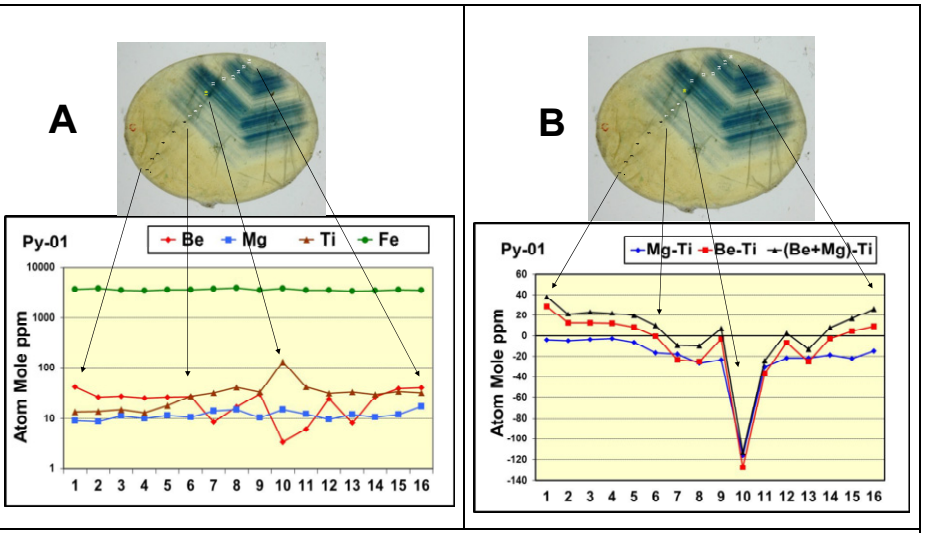

Figure 2. a 16-points traverse analysis by LA-ICP-MS across the yellow-blue zones of the as-received stone. The contents of Be, Mg, Ti and Fe are shown on the left diagram (A) and the subtraction values of Mg-Ti, Be-Ti and (Be+Mg)-Ti contents are plotted on the right diagram (B).

perpendicular to the c crystallographic axis (Figure 1a). On the sample surface, a 16-points traverse analysis across the yellow and greenish blue zones for trace element contents (Be, Mg, Ti, Fe, Cr, V, Ga etc.; Figure 2) was performed by Laser Ablation Inductively-Coupled-Plasma Mass Spectrometry (LA-ICP-MS). The stone was then simply heated at 1650°C for 3 hours under pure N_2 atmosphere (reducing condition) (Figure1b) and again at 1650°C for 3 hours in air (oxidizing condition) (Figure1c), to see whether the stone color was reversible without addition of beryllium. In each of those steps, the sample was photographed and ultraviolet-visible–near infrared (UV-Vis-NIR) absorption spectra were recorded at exactly the same positions on both yellow and greenish blue zones. After reduction and oxidation heating, another traverse analysis run near the 16-points was also carried out to verify the earlier chemical data.

Results and discussion

Gemological properties of the as-received sample are consistent with those of natural corundum that was subjected to high temperature Be-diffusion heating (i.e., R.I. 1.763-1.770, S.G. 3.96, inert under both SW-UV and LW-UV, with internal features, including a yellow color rim surrounding greenish blue zones, a blue halo around Ti-bearing minerals, blue color bleeding, healed fissures with a thin film, black inclusions, negative crystals, and straight and angular color bands).

LA-ICP-MS analysis

The 16-points traverse analysis across the yellow and blue zones of the as-received sample (Figure 2) reveals that the stone contains rather high iron content (Fe ~ 3400-3800 atom mole ppm or ppma), some Beryllium (Be ~ 3-40 ppma), Titanium (Ti ~ 13-130 ppma) and Magnesium (Mg ~ 9-17 ppma).

All points in the broad yellow zone (spots 1-6) give (Be+Mg)>Ti [(Be+Mg) -Ti ~ 10 to 38 ppma] and the points in the yellow rim (spots 15-16) also give (Be+Mg)>Ti [(Be+Mg) -Ti ~ 17 to 26 ppma], whereas all the points in the blue zones (spots 7-14), reveal (Be+Mg)< or close to Ti [(Be+Mg) -Ti ~ 8 to -113 ppma]. These chemical data are consistent with the assumption that the excess Be and/or Mg together with Fe, after the formation of colorless $BeTiO_3$ and/or $MgTiO_3$ clusters, could form stable yellow color centers (i.e., Be and/or Mg trapped hole color centers) under oxidizing conditions (see Pisutha-Arnond et al., 2004a, 2006). Notably, all analyzed points give Mg<Ti [(Mg–Ti) ~ -3 to -117 ppma] suggesting that the original raw material before Be-treatment might have been a completely blue stone (see Häger,1996, 2001).

The result of another traverse analysis run near the 16-points after reduction plus oxidation heating gave similar trace element contents. Such outcome suggests that our heating experiment has not significantly changed the trace element contents of the stone (e.g., by a 'reverse' Be diffusion, out of the stone) as it was performed at relatively low temperature (1650°C) and a short period of time (3 hours for each treatment).

Heating experiment

The reduction heating was able to turn the as-received yellow-greenish blue sapphire (Figure 1a) to almost completely greenish blue throughout the whole stone (Figure 1b). By contrast, after oxidation heating the stone appeared quite similar to the as-received condition, except that the yellow and blue hues are slightly less intense and the yellow color rim was not as clearly seen (Figure 1c). Our heating experiment result has also suggested that the as-received stone has likely been heat-treated in oxidizing conditions.

UV-Vis-NIR absorption spectra

The UV-Vis-NIR spectra of the as-received stone versus those after reduction and subsequently, oxidation heating (Figures 3-4), confirm that the yellow coloration under oxidizing condition is caused by absorption peaks related to Fe^{3+} (Lehman and Harder, 1970; Krebs and Maisch, 1971; Ferguson and Fielding, 1972; Nassau and Valente, 1987), as well as to Be and/or Mg trapped hole color centers or yellow color centers as shown by the residue spectrum in figure 3A&C, by which the absorption pattern increases continuously from ~500 nm. towards the UV region [those centers only occur after heating in oxidation conditions where (Be+Mg)>Ti in the presence of Fe] (Pisutha-Arnond et al., 2004a, 2006; Häger,1996, 2001).

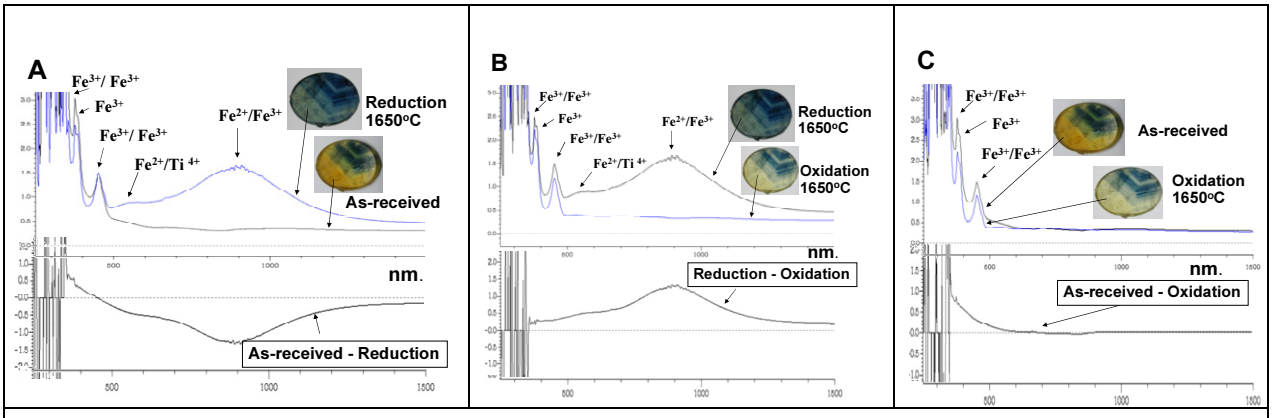

*Figure 3. comparison of UV-Vis-NIR absorption spectra (O-ray) recorded at the **yellow zone** of (A) the as-received (black line) and after reduction heating (blue line) with the residue spectrum after subtraction shown below, (B) the after reduction heating (black line) spectrum and after oxidation heating spectrum (blue line) with the residue spectrum after subtraction below, (C) the as-received (black line) and after oxidation heating (blue line) with the residue spectrum after subtraction below.*

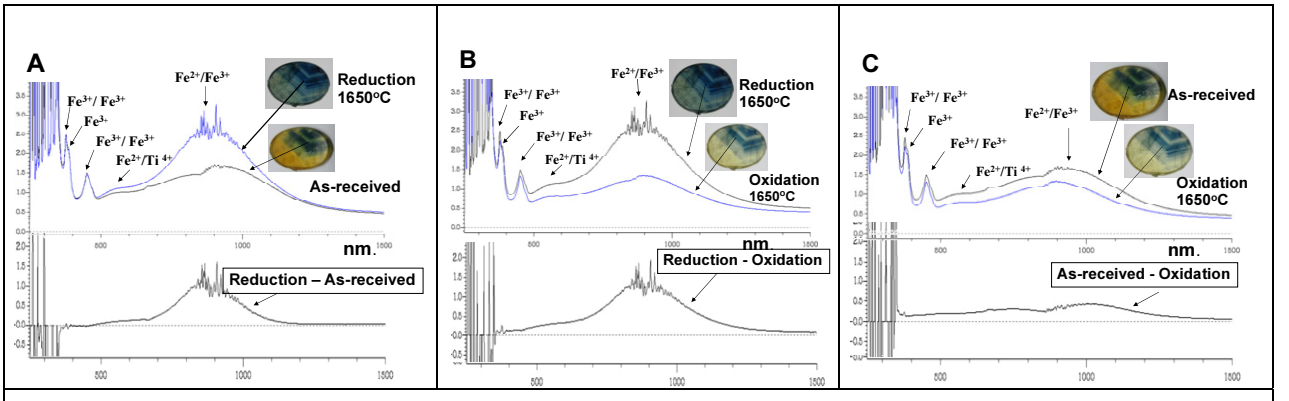

*Figure 4. comparison of UV-Vis-NIR absorption spectra (O-ray) recorded at the **blue zone** of (A) the as-received (black line) and after reduction heating spectrum (blue line) with the residue spectrum after subtraction shown below, (B)) the after reduction heating spectrum (black line) and after oxidation heating spectrum (blue line), with the residue spectrum after subtraction below, (C) the as-received (black line) and after oxidation heating spectrum (blue line) with the residue spectrum after subtraction below.*

The blue coloration is mainly caused by strong broad absorption bands of Fe^{2+}/Ti^{4+} inter-valence charge transfer mechanism (IVCT) and Fe^{2+}/Fe^{3+} IVCT (Townsen 1968; Ferguson and Fielding, 1972; Häger, 1996, 2001). The prominent Fe^{3+} related peaks at 450, 377, and 388 nm are in agreement with the high iron content of this stone (~ 3400-3800 ppma) and the presence of the Fe^{2+}/Fe^{3+} IVCT absorption band strongly indicates basaltic origin of this sapphire. The absorption peaks related to the presence of Fe^{3+}, causing the pale yellow color, are always present after both reduction and oxidation heating, and turn the stone to somewhat greenish blue (pale yellow plus blue gives a greenish blue), which is commonly found in blue sapphire from basaltic-type origin.

Combining the color appearance and absorption spectra recorded after reduction and oxidation heating with the chemical data does suggest that Be has become inactive during the reduction heating [if (Be+Mg)>Ti and both Be and Ti were active, the stone should turn colorless instead of blue under reducing conditions, as seen in Figure 1b]. As a result, the blue coloration during reduction heating is likely to be controlled by Mg/Ti < 1, whereby excess Ti, after the formation of colorless $MgTiO_3$ clusters, can create Fe^{2+}/Ti^{4+} IVCT (Häger,1996, 2001).

Conclusion

The result of these reduction and oxidation heating experiments clearly demonstrates that the active Be-trapped hole yellow color centers that are created during oxidation heating and Be-diffusion, can be made inactive after reduction heating. As such, the resulting color after reduction heating is solely controlled by the Mg/Ti ratio, without any influence of Be (i.e., the stone will turn blue when Mg/Ti<1 or colorless when Mg/Ti>1). However after re-heating in oxidation conditions, the role of Be becomes active once again. Thus the Be-diffusion treatment (such as that of the as-received stone) can be effective only when heating occurs in oxidizing conditions.

References

Atichat, W., Sriprasert, B**.,** Wathanakul, P**.,** Pisutha-Arnond, V., Sun, T.T., Puttarat, T., Leelawatanasuk, T., 2004. Characteristics of "Beryllium" Heat-treated Yellow Sapphires. Proceedings of the 29th IGC, 207-214, Wuhan, China.

Emmett, J.L., Scarratt, K., McClure, S.F., Moses, T., Douthit, T.R., Hughes, R.W., Novak, S., Shigley, J.E., Wang, W., Bordelon, O., Kane, R.E., 2003. Beryllium diffusion of ruby and sapphire. Gems & Gemology, **39**(2), 84-135.

Ferguson, J., Fielding, P.E., 1972. The origins of the colours of natural yellow, green and blue sapphires, Aust. J. Chem.,25, 1372-85.

Fritsch, E., Chalain, J.-P., Hänni, H.A., Devouard, B., Chazot, G., Giuliani, G., Schwarz, D., Rollion-Bard, C., Garnier, V., Barda, S., Ohnenstetter, D., Notari, F., Maitrallet, P., 2003. Le nouveau traitement produisant des couleurs orange à jaune dans les saphirs. Revue de Gemmologie A.F.G., 147, 11-23.

Häger, T., 1996. Farbrelevante Wechselwirkungen von Spurenelementen in Korund. Ph.D. Thesis, University of Mainz, 170 pp.

Häger, T., 2001. High temperature treatment of natural corundum. In: Hofmeister, E., Dao, N.Q., and Quang V.X. (eds), Proceedings of the International Workshop on Material Characterization by Solid State Spectroscopy: The Minerals of Vietnam, Hanoi, April 4-10, 2001, 24-37.

Hänni, H.A., Pettke, T., 2002. Eine neue Diffusions behandlung liefert orangefarbene und gelbe Saphire. Gemmologie. Zeitschrift der Deutsche Gemmologischen Gesellschaft, 51(4), 137-52.

McClure, S.F., Moses, T., Wang, W., Hall, M., Koivula, J.I., 2002. A new corundum treatment from Thailand. Gems & Gemology, 38(1), 86-90.

Krebs, J.J., Maisch, W.G., 1971. Exchange effects in optical absorption spectrum of Fe^{3+} in Al_2O_3, Physical Review B, 4, 757-69.

Lehmann, G., Harder, H., 1970. Optical spectra of di-and trivalent iron in corundum, American Mineralogist, 55, 98-105.

Nassau, K., Valente, G.K., 1987. The seven types of yellow sapphire and their stability to light, Gems & Gemology, 23 (4), 222-31.

Peretti, A., Günther, D., 2002. Colour enhancement of natural fancy sapphires with a new heat-treatment technique (part A). Contribution to Gemology, 1, 1-48.

Peretti, A., Günther, D., Graber, A.-L., 2003. The beryllium treatment of fancy sapphires with a new heat-treatment technique (part B). Contributions to Gemology, 2, 21-33.

Pisutha-Arnond, V., Häger, T., Wathanakul, P., Atichat, W., 2004a. Yellow and brown coloration in beryllium treated sapphires. Journal of Gemmology, 29(2), 77-103.

Pisutha-Arnond, V., Haeger, T., Wathanakul, P., Atichat, W., Win, T.T., Leelawatanasuk, T., Somboon, C., Sutthirat, C., 2004b. Chemical Characteristic of "Classical" versus "Beryllium" Heat-Treated Ruby and Sapphire. Proceedings of the 29th IGC, 92-94, Wuhan, China.

Pisutha-Arnond, V., Häger, T., Atichat, W., Wathanakul, P., 2006. The role of Be, Mg, Fe and Ti in causing colour in corundum. Jour. Gemmology, 30(3/4), 131-143.

Pisutha-Arnond, Somboon, C., Atichat, W., Leelawathanasuk, T., Sutthirat, C., Wathanakul, P., Sriprasert,B., Häger, T., Boonchai, A., 2009. Towards a better understanding of the orange coloration in beryllium treated sapphires**.** 31th International Gemmological Conference (31th IGC), Arucha, Tanzania, 8-14 October 2009, Extended Abstract, 41-42.

Schmetzer, K., Schwarz, D., 2004. The causes of colour in untreated,heat treated and diffusion treated orange and pinkish orange sapphires – a review. Journal of Gemmology, 29(3), 129-162.

Themelis, T., 2003. Beryllium-treated rubies and sapphires. 48 p., printed in Thailand.

Townsend, M.G., 1968. Visible charge transfer band in blue sapphire. Solid State Commun., 6, 81-83.

Be-detection by FTIR on corundum: A preliminary report

Walter A. Balmer[1,2], Michael S. Krzemnicki[1]

[1]SSEF Swiss Gemmological Institute, Aeschengraben 26, 4051 Basel, Switzerland; w.balmer@quicknet.ch
[2]Department of Geology, Faculty of Science, Chulalongkorn University, Bangkok 10330 University, Bangkok 10330, Thailand

Keywords Be-diffusion, FTIR, corundum

Introduction

In mid-2001 Be-diffusion for corundum was first reported, when suddenly an unusually large number of Padparadscha coloured sapphires appeared in the market (Hänni & Pettke, 2002). Ever since, gemmological laboratories were confronted with the challenging task of detecting Be in corundum. Be however is a very light element and therefore not detectable by conventional ED-XRF trace-element analysis. New analytical methods had to be found in order to detect Be in gemstones, which potentially had been diffusion treated. Soon LA-ICP-MS (Guillong & Günther, 2002; Abduriyim & Kitawaki, 2006) and LIBS (Krzemnicki et al., 2004; Krzemnicki et al., 2007) where introduced to the field of gemmology.

Although these methods are highly sensitive and Be can be detected efficiently, they were also very sophisticated and costly. Many laboratories with smaller budgets and less specialised personnel were therefore left with no solution in the detection of Be-treatments in general and corundum in particular.

The aim of this research was to investigate the possibility to use FTIR as an alternative method and to offer an analytical option to those labs which had not been in the position to test gemstones for potential Be-diffusion treatments other than by microscopy so far.

Sample description and experimental methods

In order to investigate the potential of FTIR as a possible analytical method for Be-detection in gemmology, three samples of colourless sapphires created by three different producers of synthetic corundum were investigated. Sample 69142_A is a 4.43ct octagonal/ step cut colourless sapphire cut from rough by Thairus Gems, Russia 69142_B is a 3.15ct slab sawn and polished from rough produced by Rusgem, Russia, whereas 69142_C is a 0.71ct round/ brilliant cut colourless sapphire cut from synthetic corundum rough produced by Jeva, Switzerland (see Fig. 1).

The Be-diffusion treatment was carried out by local burners in Chantaburi, Thailand, along with a batch of commercially treated corundum, processed at the same time.

The three samples were measured by FTIR spectrometry both before and after Be-diffusion treatment. The FTIR spectra were taken in condensed-beam mode by a Thermo Scientific, Nicolet 6700 unit. For each measurement 124 scans at resolution 2 were accumulated. The spectra were taken in the range between 1500 and 5000cm^{-1}.

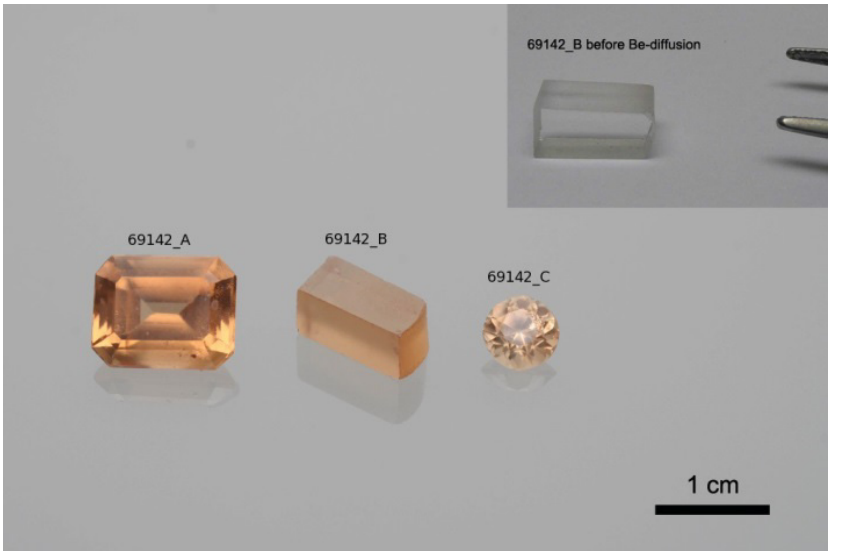

Figure 1. The photograph shows the three investigated samples after Be-diffusion treatment. As a comparison, sample 69142_B is shown before treatment in the upper right corner.

Results and discussion

Besides known artefacts related to CO_2, H_2O and grease no other signals were recorded for the examined synthetic corundum samples before treatment. Subsequent to Be-diffusion treatment two new features were observed in all three samples instead. A clear band at 3053 cm^{-1} and a less pronounced band at 2490 cm^{-1} were observed (see Fig. 2).

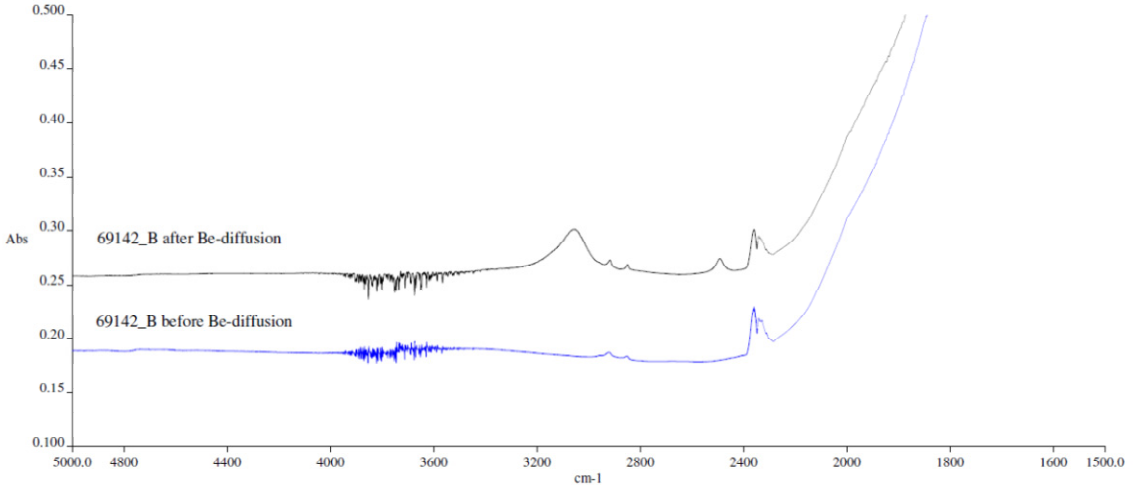

Figure 2. The samples tested in this study showed distinct differences in their FTIR signature before and after Be-diffusion treatment. Especially a clear band at 3053cm^{-1} and a less pronounced band at 2490cm^{-1} were identified as typical characteristics for Be-diffusion treated corundum.

The band at 3053 cm^{-1} seems to be the same band as observed by Kitawaki & Abduriyim (2008) at 3068cm^{-1} and is located in an IR-range where bands related to diaspore (Farmer, 1974; Downs, 2006), dolomite (Downs, 2006), and an "unknown" band (Smith & van der Bogert, 2006) had been described before. The band at 2490cm^{-1} however lays in an IR-range where no common artefacts or signals of inclusions in corundum are known so far (Balmer, 2011).

Conclusion

All three samples showed the same distinct changes in their FTIR signature compared to the FTIR spectra taken before the Be-diffusion treatment was carried out. Due to the fact that the same effect was observed in three individual samples and that the band at 2490cm^{-1} in particular was never described in gemmology before, it is assumed that it is possible to positively link the latter to Be-diffusion treatments in corundum when detected.

However, the cause of the distinctive spectra characteristics is not yet understood. It further has to be investigated how frequent the introduced criterion occurs in Be-diffusion treated natural corundum. In order to verify whether quantification of Be-contents in corundum by FTIR is possible, trace-element analyses by LA-ICP-MS have to be carried out first. And finally, whether the analytical criteria presented in this study can be applied to all types of corundum still has to be examined however. This implies that further information still has to be collected.

Nevertheless, it had been possible to demonstrate that FTIR has the potential to be used as an alternative analytical method for Be-detection in corundum in the future.

References

Abduriyim, A., Kitawaki, H., 2006. Application of laser ablation – inductively coupled plasma – mass spectrometry (LA-ICP-MS) to gemology, Gems & Gemology, 42(2), 98-118.

Balmer, W.A., 2011. Petrology, Geochemistry, and Gemmological Characteristics of Marble-Hosted Ruby Deposits of the Morogoro Region, Tanzania, unpublished Ph.D. thesis, Department of Geology, Faculty of Science, Chulalongkorn University, Bangkok, Thailand, 185pp.

Farmer, V.C., 1974. The infrared spectra of minerals, Mineralogical Society Monograph, 4, Mineral Society, London, 539pp.

Guillong, M., Günther, D., 2001. Quasi 'non-destrictive' laser ablation-inductively coupled plasma-mass spectrometry fingerprinting of sapphires, Spectrochimica Acta Part B, 56, 1219-1231.

Hänni, H.A., Pettke, T., 2002. Eine neue Diffusionsbehandlung liefert orangefarbene und gelbe Sapphire, Zeitschrift Deutsche Gemmologische Gesellschaft, 51(4), 137-512.

Kitawaki, H., Abduriyim, A., 2008. Identification of Be-diffusion Treated Corundum, Gemmology, 9, 24-27.

Krzemnicki, M.S., Hänni, H.A., Walters, R.A., 2004. A new method for detecting Be diffusion-treated sapphires: Laser induced breakdown spectroscopy (LIBS), Gems & Gemology, 40(4), 314-322.

Krzemnicki, M.S., Pettke, T., Hänni, H.A., 2007. Perspectives of LIBS in gemstone testing .Analysis of light elements such as beryllium, boron, lithium, Poster Publication, GIT2007, Bangkok, Thailand.

Downs, R.T., 2006. The RRUFF Project: an integrated study of the chemistry, crystallography, Raman and infrared spectroscopy of minerals. Program and Abstracts of the 19th General Meeting of the International Mineralogical Association in Kobe, Japan. www.rruff.info

Smith, C.P., van der Bogert, C., 2006. Infrared Spectra of Gem Corundum, Proceedings of the GIA Gemological Research Conference, Gems & Gemology, 42(3), 92-93.

"Surface de-leaded" ruby

Thanong Leelawatanasuk, Nalin Naruedeesombat, Namrawee Susawee, Pantaree Lomthong, Pornsawat Wathanakul

The Gem and Jewelry Institute of Thailand (Public Organization), Bangkok 10500, Thailand; wpornsawat@git.or.th

Keywords SDL ruby, fracture-filled ruby, Pb-glass ruby

Introduction

Lead glass-filled corundum manufactured by Thai gemstone-heating specialists was firstly marketed in 2004 (Rockwell and Breeding, 2004; Smith et al., 2005; McClure et al., 2006; Milisenda et al., 2006). Such treated stones may pose durability problems; i.e., during jewelry manufacturing/repair and cleaning, the glass filler could be etched by certain acidic or basic solutions, and heat from a jeweler's torch may easily melt the glass (McClure et al., 2006; LMHC, 2012; Leelawatanasuk et al., 2013). Nonetheless, because of their affordability, mass availability and wide range of quality, these products are still circulating in the market after almost a decade. With continuing development by Thai gemstone-heating experts, blue cobalt-doped lead glass-filled corundum was invented and entered the market in 2012 (GIT, 2012; Leelawatanasuk et al., 2013) and was followed by green glass-filled sapphires in 2014 (Henn et al., 2014; Leelawatanasuk et al., 2015).

The most recent improvement was encountered during the 55th Bangkok Gems and Jewelry Fair in February 2015. In the fair, an article from the "Leader Jewel" magazine, vol. 01, no. 02 (Figure 1) got much attention: It refers to a newly treated ruby that is claimed to be a toxic-free gem material, and is marketed under the name "Organic Ruby", by Spa Gems Company in Chanthaburi.


Kwanmuang Bumrungpanichtarworn
and the emerging market of
Organic Ruby
"Toxic-free Gemstone"
Story/Images: Aekasit Jaingam
When talking about gems in Thailand, one cannot avoid talking about Chantaburi, a hub of gem trading of the country, where raw gemstones would go through heat treatment and turn into vivid coloured gems that contribute to the economies of Chantaburi and Thailand. That said, nowadays, raw materials in the area are diminishing and cannot respond to high demands of the gemstone market as it used to be. Besides, Chinese and Indian merchants are looking for opportunities to create new trading hubs in their home countries in place of Thailand.

Figure 1. Article from the "Leader Jewel" magazine, vol. 1, no. 2, page 30.

The article further explained that this new product actually was a lead-glass-filled ruby that had been treated using a new technique, one that was able to remove a significant amount of lead (Pb) from the glass filler of the stone. As a result, this newly treated gem material purportedly appeared to contain much less or an almost insignificant amount of lead, as shown by the EDXRF analysis of the surface of the stone that was shown in the article.

Nevertheless, after the launch of this new product, the trade name "Organic Ruby" has created much doubt and controversy among traders who fear that it could be misleading to consumers. To avoid further confusion and misunderstanding of this new gem material in the market, GIT is providing some facts about the "Organic Ruby" based

on our analyses of samples provided directly by the owner of the Spa Gem company. We prefer to call this new product "Surface De-Leaded (SDL) Ruby" in this communication.

Samples and procedures

In total thirteen SDL ruby samples have been received from the Spa Gems Company. Three samples were selected for detailed study. Standard gemological equipment was used to obtain refractive indices, hydrostatic specific gravity, pleochroism, and fluorescence to long- and short-wave UV radiation for all of the faceted samples; they were also examined with a gemological microscope. Chemical analysis by energy-dispersive X-ray fluorescence (EDXRF) spectroscopy was performed on all samples with an Eagle III instrument using an Rh X-ray tube, an accelerating voltage of 30 kV and a beam current of 200 mA. The diameter of the X-ray beam was 2,000 µm, and diffraction artefacts were avoided by sample rotation. Ultraviolet-visible–near infrared (UV-Vis-NIR) spectra of all samples were recorded in the range 250–800 nm using a PerkinElmer Lambda 950 spectrophotometer with a sampling interval of 3.0 nm, scan speed of 441 nm per minute and slit width of 2**.** X-radiography of all samples was performed using a Softex SFX-100 instrument. Samples were also visually inspected with the DiamondView**™** luminescence imagery system.

Results and discussion

Gemological properties
The standard gemological properties of SDL ruby product (e.g., RI, SG) are consistent with those of normal lead-glass fracture-filled ruby, such as the presence of color flash effects, flattened gas bubbles (Figure 2).

Figure 2. Flash effect (left, 40x magnification) and flattened bubbles (right, 50x magnification) usually present in SDL ruby samples. Photos: N. Susawee.

Inspection under the DiamondView™
Inspection of SDL ruby samples under the DiamondView™ proved to be useful; the samples display bright red glowing fractures that were filled with lead glass, having darker rims where lead has been removed (Figure 3).

Figure 3. DiamondView™ images of 1.45 ct. SDL ruby sample (left: table view, right: pavilion view). Photos: N. Susawee.

Lead content analysis

The X-ray images of the stones reveal the presence of heavy elements, i.e., lead (Pb), in the glass filler in fissures and cavities (Figure 4). Chemical analysis by EDXRF on the surface of the stone shows minor Pb content as compared to those of the former (normal) lead-glass fracture-filled stones (Table 1).

Normal heated ruby (no Pb-glass filler) *Pb-glass filled ruby* *Surface de-leaded ruby*

Figure 4. Photos of ruby samples (top row from left to right; 2.55, 4.11 and 2.32 cts., respectively) and their X-Ray images (bottom row). Photos: N. Naruedeesombat and N. Susawee.

Table 1. Examples of chemical analysis on sample surfaces by EDXRF

Oxide (Wt%)	Al_2O_3	TiO_2	V_2O_5	Cr_2O_5	Fe_2O_3	Ga_2O_3	PbO_2
Newly treated (SDL) ruby	99.13	0.01	0.00	0.10	0.39	0.01	0.35
Normal Pb-glass filled ruby	98.01	0.02	0.01	0.16	0.29	0.02	1.47

It should be emphasized here that, due to the instrument capability, the EDXRF technique can analyze the chemical content of the stone's surface only. The stability test, however, has not been performed on this product at this stage, yet. However it is expected that the stability of SDL ruby should be similar to that found in the previous lead-glass filled corundum (McClure et al., 2006; LMHC, 2012; GIT, 2012; Leelawatanasuk et al., 2013). Thus, at this point, we

would recommend jewelers to handle this newly treated stones with the same special care as those provided for previous lead glass filled materials.

Concluding remarks

Our preliminary testing reveals that these SDL stones still contain significant lead in the glass filler found inside the stone's fissures and cavities, as seen in the X-ray images (Figure 4). As such, it is yet uncertain to be able to distinguish this newly treated product from the normal lead glass-filled ruby based on the detection of a lesser lead signal on the surface alone. Hence, more experimental results on before and after treatment are necessary to identify this product

It appears that the trade name "Organic Ruby" is being used as a marketing strategy to imply a (surface only) lead-free product, and has nothing to do with any organic gem material derived from living plants or animals.

A special meeting of academics and traders, called by the GIT on Thursday 5th March 2015, resulted in the suggestion that, for proper disclosure of the product, a more appropriate trade name should be chosen other than the locution "Organic Ruby." Nonetheless, this remains to be discussed.

Acknowledgements

The authors would like to express their thanks to Dr. Visut Pisutha-Anond, Ms. Wilawan Atichat, Mr. Surapon Chaiamnuay, Ms. Cynthia Unninayar for help improving this manuscript.

References

GIT, 2012. Blue dyed and clarity modified sapphire with cobalt+lead-glass filler in fractures and cavities. Gem and Jewelry Institute of Thailand online report, www.git.or.th/2014/eng/testing_center_en/lab_notes_en/glab_en/2012/Cobalt_Lead_Glass_FF_Sapphire_ Final.pdf.

Henn, U., Schollenbruch, K., Koch, S., 2014. Gem Notes: Corundum with coloured lead-glass fillings. Journal of Gemmology, 34(2), 111–112.

Leelawatanasuk, T., Atichat, W., Pisutha-Arnond, V., Wattanakul, P., Ounorn, P., Manorotkul, W., Hughes, R.W., 2013. Cobalt-doped glass-filled sapphires: An update. Australian Gemmologist, 25(1), 14–20, www.git.or.th/2014/eng/testing_center_en/lab_notes_en/glab_en/2013/cobalt_doped_glass_filled_sapphires.pdf.

Leelawatanasuk, T., Susawee, N., Promwongnan, S., Atsawatanapirom, N., 2015. Green Lead Glass-filled Sapphires, The Journal of Gemmology, 34(5), 2015, 420-427.

LMHC, 2012. Information Sheet #3—Corundum. Laboratory Manual Harmonization Committee, Version 9, December, 3 pp., www.lmhc-gemology.org/pdfs/IS3_20121209.pdf.

McClure, S.F., Smith, C.P., Wang, W., Hall, M., 2006. Identification and durability of lead glass-filled rubies. Gems & Gemology, 42(1), 22–34, http://dx.doi.org/10.5741/gems.42.1.22.

Milisenda, C.C., Horikawa, Y., Manaka, Y., Henn, U., 2006. Rubies with lead glass fracture fillings. Journal of Gemmology, 30(1–2), 37–42, http://dx.doi.org/10.15506/jog.2006.30.1.37.

Rockwell, K.M., Breeding, C.M., 2004. Lab Notes: Rubies, clarity enhanced with a lead glass filler. Gems & Gemology, 40(3), 247–249.

Smith, C.P., McClure, S.F., Wang, W., Hall, M., 2005. Some characteristics of lead-glass-filled corundum. Jewellery News Asia, 255.

The application of VPSEM-Raman coupled system in studying Fei Cui

S.I. Liu[1], C.M. Ouyang[1,2], F.Y. Ng[2]

[1]The Gemmological Association of Hong Kong; edwardliu@gahk.org
[2]The Hong Kong Institute of Gemmology

Keywords Raman-spectroscopy, Variable Pressure Scanning Electron Microscopy, Backscattered electron imaging, heterogeneity, microminerals

Introduction

The discovery of bright green omphacite jade raised many questions in gemmology, not only regarding its identification but also concerning the very definition of jade (Liu et al, 2010, 2011; McClure, 2012). Although micro-Raman spectroscopy is widely used in characterizing "Burmese jade" (Fei Cui), the complex and heterogeneous nature of Fei Cui makes mineral recognition difficult when the constituents or isomorphous submicroscopic minerals show similar appearance under the optical microscope. The repeatability and traceability of test results of random point sampling are under question. This study demonstrates the use of VPSEM-EDS Variable Pressure Scanning Electron Microscopy- Energy Dispersive Spectroscopy, backscattered electron (BSE) imaging coupled with a Raman spectroscopy system for *in situ* non-destructive Fei Cui micromineral elemental, chemical and structural analyses (Wille et al., 2014).

Samples and experimental methods

68 green Fei Cui samples (cabochons and slabs) were collected in jade markets in Myanmar, Hong Kong and Mainland China. They are semi-transparent to near opaque. Colours ranged from light green to dark green.

All samples were studied using conventional gemmological instruments. All features and colour distribution were examined under the microscope. FTIR specular reflectance spectra were obtained on a Nicolet 670 FTIR spectrometer, using a spectral resolution of 4 cm^{-1} and 64 scans in the range of 4000 cm^{-1} to 400 cm^{-1}.

All characterizing tests of this study were mainly performed on a Hitachi S-3400N variable pressure scanning electron microscope (VP-SEM) under low vacuum mode. The innovative Quad Bias system allows sharp and brilliant images to be obtained even below an accelerating voltage of 3 kV. Thus, Fei Cui samples could be protected from radiation damage and no metal coating or sample preparation is needed. Chemical analyses were obtained by SEM-EDS (INCA, Oxford). Element maps were acquired to show the spatial distribution of chemical zoning and to better evaluate the minerals present in samples. Compositional images were obtained by the high-sensitivity, 4-segments backscattered electron (BSE) detector in low vacuum VP-mode (4.0 nm resolution at 30 kV). In order to understand the whole picture of the spatial distribution of different minerals in a sample, nine to fourteen BSE images at low magnification of different parts of each distinct sample were merged together using Photoshop layer mask.

Micro-Raman measurements were performed on a Renishaw InVIA Reflex micro-spectroscopy combined with the VPSEM — a SEM-Raman coupling system which is developed by Renishaw under the name SEM-SCA (Structure & Chemical Analyzer; http://www.usif.arizona.edu/equipment/s3400.html). The Raman laser beam and scattered radiation detector were placed inside the chamber. (The large analytical chamber is designed to handle specimen of a size up to 200 mm in diameter and 80 mm in height at an analytical working distance of 10 mm and to provide a total of ten ports for other optional analyses e.g. FTIR, Full Focusing WDS, EBSD, and XRF.) Spectra were recorded using λ_0=514.5nm argon ion laser excitation with an acquisition time of 30 s in the range of 200 to 2000 cm^{-1}, with a

spot size of 2 µm and a repeatability <0.5 µm. Spot measurements were only practiced on those minerals that had been previously analyzed by backscattered electron imaging and element mapping. Mineral identification was performed using the RRUFF database (The RRUFF™ Project: http://rruff.info).

Results and discussion

The backscattered electron (BSE) imaging can help to visualize the mineral composition and its spatial distribution on the surface of Fei Cui samples according to the atomic weight of elements. Minerals containing atoms of higher atomic number appear brighter in the BSE image. Using this technique, the size of mineral grains of Fei Cui can be measured, the textural relationships among minerals can be examined (even when they show similar appearance), and the amount of jadeite, omphacite and kosmochlor and other constituents such as chromite, feldspar and clinoamphibole within Fei Cui samples can be estimated.

BSE overlay images allow us to build the picture of minerals distribution on the surface layer of the samples. SEM-EDS provides a qualitative and semi-quantitative chemical analysis of each individual mineral in complex intergrowths and mineral zoning within the sample. The presence of jadeite, omphacite, kosmochlor, chromite and amphibole, and their spatial distribution in the sample can be easily estimated combining the two approaches. For example, the BSE overlay images (top and bottom) of a fine quality bright green Fei Cui sample - J03 (Figure 1) mainly consists of omphacite as the background, with little veins and patches of jadeite. Omphacite appears light grey while jadeite appears relatively dark grey (Fan et al., 2014). In such a sample, interpretation of insufficient data from random testing may lead to incorrect results. Previously, this sample was suspected to have a layer of jadeite on top and omphacite at the bottom because of FTIR spectroscopy results, but there is no major visual difference between top and bottom.

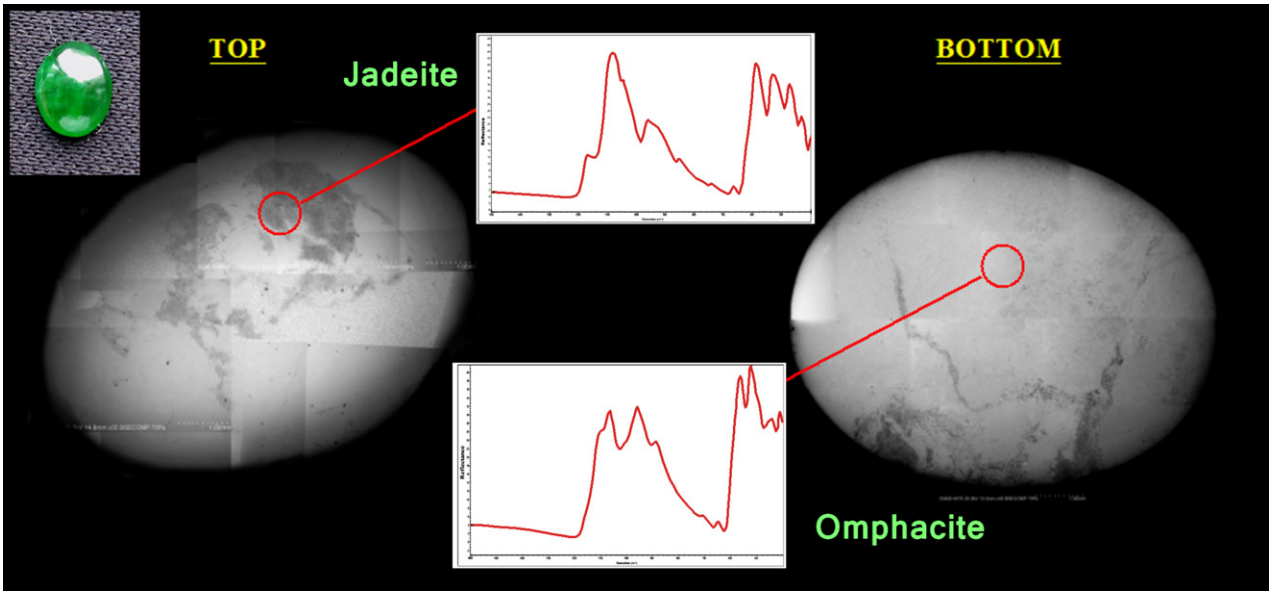

Figure 1. BSE overlay images of low magnification of a fine-quality bright green Fei Cui sample (J03) (top-left corner). Top view (left) and bottom view (right) of a double cabochon. This sample was being tested by conventional FTIR spectroscopy before using the VPSEM-Raman couple system.

Chemical analyses revealed that this type of bright green Fei Cui variety contains more Cr (Cr_2O_3=0.588 wt%) but less Fe (FeO =0.99 wt%) compared to the dark "inky green" (omphacite) variety. X-ray diffraction analysis (author's previous study: Liu et al., 2011) revealed that the space group of this bright green omphacite belongs to P2/n (not C2/c). The regular arrangement of cations in the crystal structure revealed that it formed in a relatively low temperature geological environment.

Mixture of jadeite, omphacite and kosmochlor

3 of our samples mainly consist of both jadeite and omphacite. 2 of them mainly consist of both kosmochlor and omphacite (with little jadeite). 8 of them are essentially a mixture of both jadeite and kosmochlor. 2 contain mainly kosmochlor, clinoamphibole and chromite. Radiating kosmochlor (rim) were formed around chromite grains (core) (Figure 2). Dark green to black clinoamphibole were commonly found in the outer rings and filling fractures around kosmochlor. BSE images of some samples revealed that the three components of Fei Cui form many complex intergrowth textures/structure (Shi, 2009; Franz *et* al., 2014; Kan-Nyunt, 2015). This explains the inconsistent test results using separately conventional FTIR and Raman micro-spectroscopy from random sampling. Although the beam size or excitation spot of Raman micro-spectroscopy is small enough to identify individual micromineral within a sample, the repeatability of test results are under question when minerals show almost no visual differentiation (or very little) under the microscope (Figure 3). Using random spot testing is inappropriate to reconstruct the real picture of mineral composition and spatial distribution of complex inhomogeneous aggregate of Fei Cui.

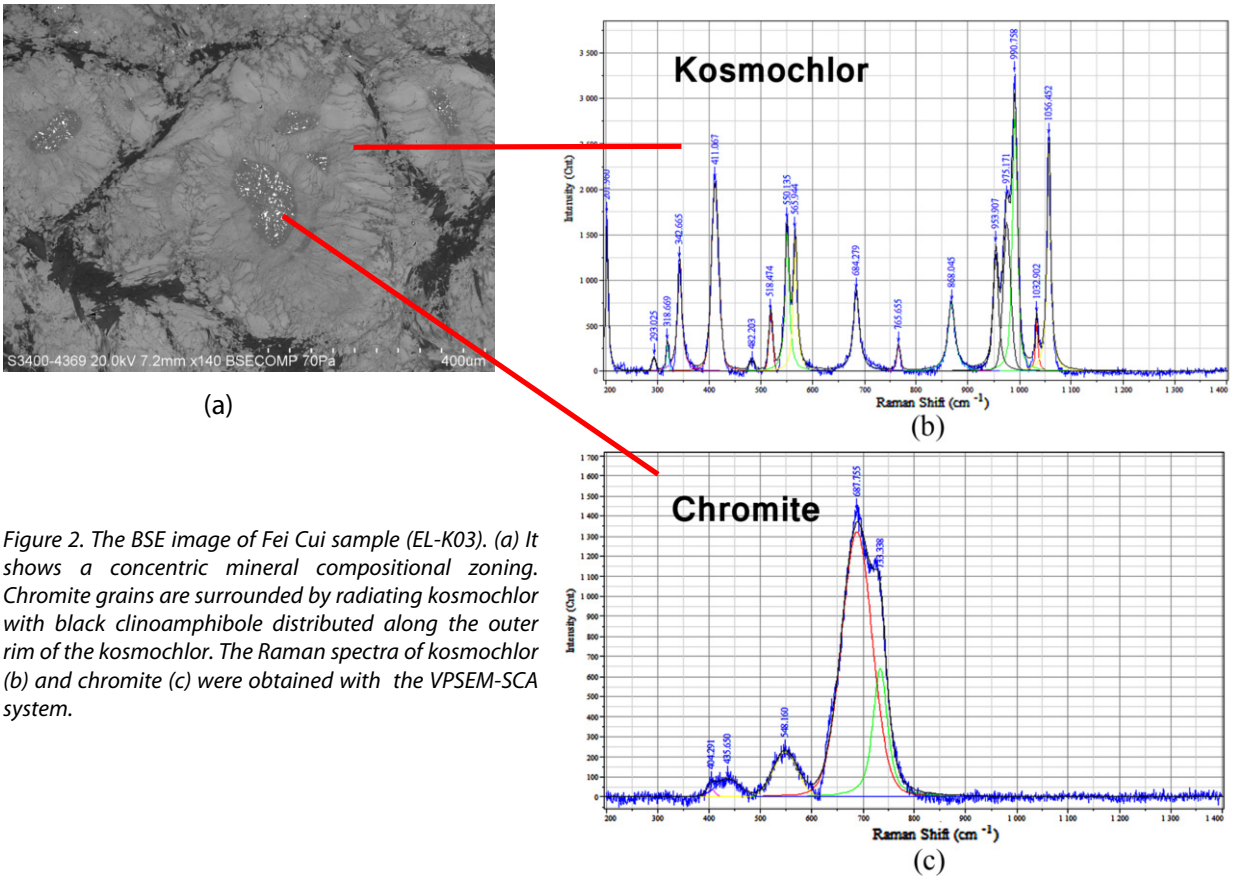

Figure 2. The BSE image of Fei Cui sample (EL-K03). (a) It shows a concentric mineral compositional zoning. Chromite grains are surrounded by radiating kosmochlor with black clinoamphibole distributed along the outer rim of the kosmochlor. The Raman spectra of kosmochlor (b) and chromite (c) were obtained with the VPSEM-SCA system.

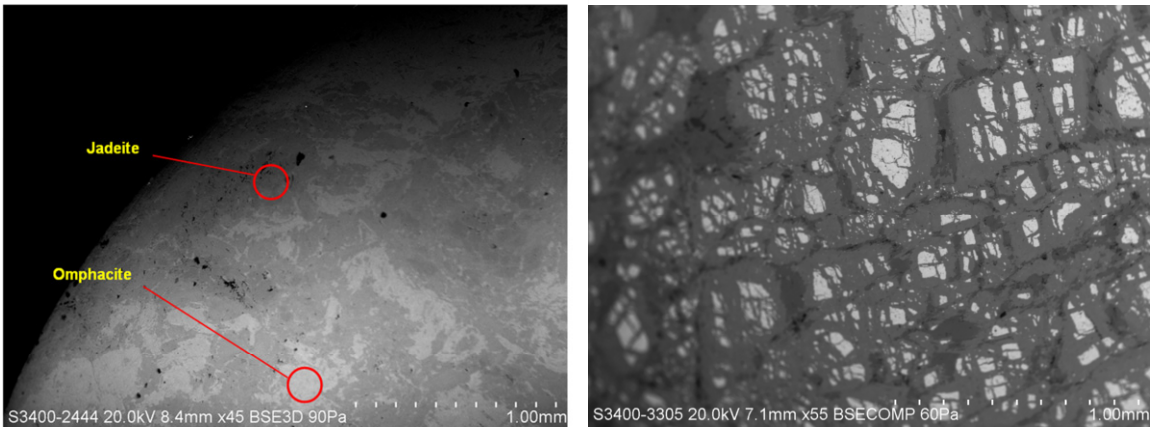

(a) (b)

Figure 3. The BSE images of J09 (a) and ESX-10 (b) show the complex (interlocking or concentrate) texture and inhomogeneous micromineral composition of the samples. ESX-10 consists of large amounts of chromite grains (45%, light grey due to Cr) which bring the physical properties e.g. SG and RI over the upper limit of Fei Cui.

Conclusion

The identification of homogeneous Fei Cui is sometimes possible by basic gemmological tests with the use of Raman or infrared spectroscopy. However, the complex and heterogeneous nature of Fei Cui makes mineral identification difficult. We propose the use of VPSEM-Raman coupled system for *in situ* Fei Cui analyses. The term Fei Cui is suggested as a family name for jade and includes 3 members: jadeite jade, omphacite jade and kosmochlor jade (Ou Yang, 2012). It should also be applied to name those heterogeneous "Burmese jade" for identification.

References

Fan E., Liu E.(Liu S.I.), Tsui T., 2014. New Findings in Fei Cui bring New Opportunities, The Journal of the Gemmological Association of Hong Kong, 35, 14-19.

Kan-Nyunt, H.P., Kwok B., Chan S.L., 2014. The use of FTIR and Raman Spectroscopy in the testing of Fei Cui: Jadeite, Omphacite and Kosmochlor. The Journal of the Gemmological Association of Hong Kong, 35, 29-38.

Liu S.I., Peng M.S., 2010. A Study of a New Emerald Green (Old Mine Variety) Omphacite Fei Cui. Acta Mineralogica Sinica, (Proceedings of the National Conference of Mineral Science and Engineering, Fujian (2010), China, 30 (suppl.), 26-28 (in Chinese).

Liu S.I., Peng M.S., Chan W.C., 2011. Gemmological and mineralogical studies of Omphacite. Proceedings of the Annual Conference of the Chinese Society for Mineralogy, Petrology and Geochemistry (2011), Guangzhou: 28-29 (in Chinese).

Ou Yang C.M., Ng F.Y., 2012. Nomenclature and classification of Fei Cui (Pyroxene jade) Proceedings of the 3rd International Gem and Jewelry Conference (GIT 2012), 12-16 December, Bangkok, Thailand, 240-243.

Shi G., Wang X., Chu B. and Cui W., 2009. Jadeite jade from Myanmar: Its texture and gemmological implications. Journal of Gemmology, 31 (5-8), 185-195.

Wille G. et al., 2014. Raman-in-SEM, a multimodal and multiscale analytical tool: Performance for materials and expertise, Micron, 67, 50-64.

Brazilian emeralds from the Belmont mine

Shane F. McClure

Director of West Coast Identification Services
GIA Laboratory, Carlsbad, California, USA; smcclure@gia.edu

Keywords Emerald, Brazil, Belmont

Introduction

Last year a team from GIA had the opportunity to visit nine different mines in Brazil. This presentation will discuss just one of them – the Belmont emerald mine. The Belmont mine is the largest and most technologically advanced emerald mine in Brazil. With the kind permission of the owners we were able to witness every aspect of the mine operation. We even were able to document a large stone from the rough all the way to the final product set in jewelry and sold to an end buyer. A good group of emerald samples were also acquired for research purposes, for which the information gathering process is still in progress.

Location

The Belmont mine is located near the town of Itabira in the state of Minas Gerais, Brazil. Itabira lies northeast of the city of Belo Horizonte, the capital of Minas Gerais. The mine itself is located 13 km southeast of Itabira, but the main offices of the company, along with the sorting, grading and cutting facilities are located in Itabira.

The mine

The mine started as an open pit operation in 1978 which is still operating today and is now approximately 150 meters by 100 meters in size, although it is now reaching the end of its productive life (Figure 1). Belmont estimates they will be working it for another two years. However, there are two other open pits being developed.

In 1994 the decision was made to go underground, so over the next several years exploratory shafts were cut and numerous core samples were collected. In time the mine owners felt confident enough to make the considerable investment to develop a ramp style underground mine. This means that instead of vertical shafts they cut sloping ramps down into the deposit to retrieve the ore and carry it out of the mine. They built the ramps big enough so that front loaders and trucks can enter the mine and therefore move large volumes of material. When in full production they can remove 30 to 40 truckloads of material per day, which equals approximately 400 to 500 tons of ore.

Figure 1. The old open pit mine and mine buildings of Belmont.

Once the ore is brought out of the mine, it is taken to the processing plant and dumped onto the first grating. Pieces smaller than 500 millimeters fall through the grating and the larger pieces are broken up by a hydraulic hammer until they too fall through. This starts the process of the ore moving through a series of crushers, screens and conveyor belts until all the ore is 40 millimeters or less in size. It is run through a series of high pressure nozzles to clean it, sorted by size and run through one of two optical sorters. Cleaning as much of the dirt from the ore as possible is very important to the efficient operation of the optical sorters.

The sorters separate out the emerald bearing ore with an estimated 95% accuracy rate. This ore is then fed by conveyor belts into a "safe room", after which it is transported in locked boxes to the final sorting facility in Itabira. Here, in a process referred to as "cobbing", the phlogopite mica and quartz matrix is removed by hand with pliers leaving just the emerald crystals. The highly included areas of the emeralds are also removed during this process.

Figure 2. Sorting processed emeralds into different qualities.

The samples

The end result is gem quality material that is ready to be sorted into final categories based on size, color, shape and clarity, which is then put into parcels (Figure 2). Marcelo Ribiero, the mine manager, allowed us to pick a significant group of samples directly from the stones that had just been sorted which we then purchased for our research efforts. In this way we were able to acquire 77 rough samples of good gem quality material (Figure 3). They mostly came from a parcel of smaller moderately included material with good color that averaged 1.75 carats each in size, but we also included a few stones from a parcel that averaged almost 4 carats and four small stones from the category considered to be their top quality.

Initial examination of the samples revealed that most had at least one or two crystal faces. The faces were usually etched and irregular but there often was at least one hexagonal angle present. Complete prisms were rare and there were no crystals with terminations in our samples. Observation of inclusions was difficult because of the etched faces and lack of polished surfaces. What could be seen were mica crystals, blocky two phase inclusions and parallel growth tubes. Obviously once we have polished windows on the samples we will be able to see much more. These stones are currently being cataloged, windowed and readied for data collection, inclusions studies and evaluation.

Figure 3. Emerald samples purchased by GIA at the Belmont mine.

From mine to market

While we were there we had the opportunity to see a high quality piece of rough weighing 29.8 grams that had been discovered shortly before we arrived. Marcelo held the stone until we got there so we would be able to witness and document it being processed and finished.

Figure 4. A 29.8 gram high quality crystal being examined before cutting.

The process began with careful examination of the rough by Belmont's master cutter named Donizete, after which he discussed the cutting strategy with Marcelo at length (Figure 4). Decisions were made and the next day the first cut was made on the diamond saw with Donizete holding the stone in his fingers. More examination, more discussion and then comes the second cut. So it proceeds, all the while focusing on ending up with the largest stone with the best quality possible. When he is finished, the original stone is cut into 39 pieces with the largest weighing 40.66 carats (Figure 5).

Figure 5. The crystal ended up being cut into 39 pieces.

While all the pieces would eventually be faceted into gems, the focus was on the large stone. Another period of examination and discussion decided where the table facet would be placed, after which the stone was preformed. When this step was finished the stone weighed 26.95 carats. Faceting and polishing the stone resulted in a finished stone weighing 19.70 carats.

As with almost all emeralds, all of the fissures present in the rough could not be removed without unacceptable weight loss. Therefore the stone needed to be clarity enhanced. The areas where they hoped appearance would be improved were pointed out and the stone was treated in a very simple fashion – cleaning in a solvent and then

soaking in a beaker of cedarwood oil with some gentle heating. The next day the stone was examined again to see if the results were satisfactory. In this case Marcelo was not happy with the result and the decision was made to slightly recut the stone to remove part of a feather.

Any time a stone is put back on the wheel chances are being taken that some unintended damage may occur. In this case a chip occurred on the pavilion while the stone was being repolished that had to be repaired, resulting in a reduction of weight from 19.70 to 18.17 carats. This was the final weight of the stone (Figure 6).

Figure 6. The largest finished stone weighed 18.17 carats.

We were even able to follow the stone on its journey to the market. It left Brazil for New York where it received a laboratory report. It was then taken to the June Gem and Jewellery show in Hong Kong where it was sold to a jewelry manufacturer and retailer from Thailand. The Thai jeweler took it back home and designed a custom ring to fit the stone (Figure 7). When the ring was finished, its journey ended when it was purchased by a regular client of the jeweler.

The opportunity to document an important stone from just after it came out of the ground to the final client was truly a unique one.

Figure 7. The large emerald set in a custom diamond ring.

Gemological features of pallasitic peridot of six different meteorites

Masaki Furuya[1], Scott Davies[2]

[1]Japan Germany Gemmological Laboratory, Kofu, Japan; jggl@sapphire.co.jp
[2]American Thai Trading, Bangkok, Thailand; scott@americanthai.com

Keywords pallasite, meteorite, peridot, Admire, Brahin, Esquel, Fukang, Jepara, Seymchan

There has been a recent influx in the market of faceted peridot gems cut from olivine found in pallasite meteorites. Gemmological laboratories have done research on the stones in order to differentiate these 'pallasitic peridots' from terrestrial peridot (Henn et al., 1992, Leelawathanasuk et al., 2011 and Shen et al., 2011).

Polished slices of each pallasite meteorite show unique structures. For example, Fukang pallasite shows a rounded Widmanstätten pattern and relatively large olivine while Seymchan pallasite shows more blurred patterns and small but connected olivine (Figure 1). As these features are characteristic to confirm their origins, when slices are offered for sale, the pallasite of origin is always labeled.

Just as peridot from each terrestrial source has characteristic gemmological properties, this research shows that peridot from each major pallasite is also unique. For this research, we used gemmological techniques to compare the properties of faceted pallasitic peridot from 6 origins. The origins of these gems include the following pallasite meteorites: Admire (found in Kansas, United states in 1881, 21pcs), Brahin (found in Gomel, Belarus in 1810, 39pcs), Esquel (found at Chubut, Argentina in 1951, 18pcs), Fukang (found in Xinjiang, China in 2000, 21pcs), Jepara (found in Jawa Tengah, Indonesia in 2008, 12pcs) and Seymchan (found in Magadanskaya oblast, Russia in 1967, 22pcs)(The Meteoritical Society and Graham et al 2000). For Brahin, we separated gems cut from the interior of the pallasite (Brahin) from gems cut from the burned edges of the meteorite, known as the 'fusion crust' (BrahinFC).

The inclusions observed under the microscope are quite characteristic for each pallasite. The reddish brown platy inclusions are seen in almost all pallasitic peridots except Jepara and Seymchan. Also, a cross pattern of intersecting needle inclusion (dislocation) is often seen in pallasitic peridots from Admire, Esquel and Fukang (Figure 2 and 3). The fine needles of dislocation are also seen in stones from Brahin, BrahinFC and Seymchan pallasites, but they do not intersect and are most often parallel. Jepara peridot usually contains thicker tubular inclusion not seen in peridot from other pallasites (Figure 4 and 5).

In FT-IR spectra, more than half of the samples from Seymchan have the transmission peaks around 1000-400cm^{-1} (1062, 983, 943, 632, 528 and 432cm^{-1}) as shown in Figure 6. As these transmissions are only seen in Seymchan samples which contain many fine needles and no liquid inclusions, interference from these needles may be the cause. Roughly half the samples from Brahin and BrahinFC have wide absorption at around 3352cm^{-1}. This absorption is seen in a few others samples as well. Overall, the features of FT-IR are not always found in each pallasitic peridot, but if they are found, they can be helpful in identifying the origin.

In UV-Vis spectra, all samples from Jepara show a strong absorption at 453nm caused by Fe^{2+} (Henn et al, 1992). Also, in all Jepara samples, the transmission at 560nm is stronger than that of 670nm. This coincides with the greener tone seen in Jepara stones when compared with a generally more yellowish or brownish tone seen in gems from other pallasites (Figure 7).

Trace element analysis was conducted using LA-ICP-MS for 10 samples from each group. Previous research has shown that all pallasitic peridot consistently shows lower Ni, lower Cr, and higher Mn, when compared with terres-

trial peridot. (Leelawathanasuk et al., 2011 and Shen et al., 2011) Our research confirms this result. In addition, our comparison of peridot from each of the 6 pallasites shows that peridots from Esquel and Fukang consistently show higher Mn, Al and Cr content than the others (Figure 8).

Previous research clearly enabled separation of pallasitic peridot from terrestrial peridot using various gemmological testing. This additional research on gems from six pallasites, Admire, Brahin, Esquel, Fukang, Jepara and Seymchan, confirms results from previous research. We have also shown that gems from each pallasite have unique properties as well, and that origin determination of pallasitic peridot is possible in some cases.

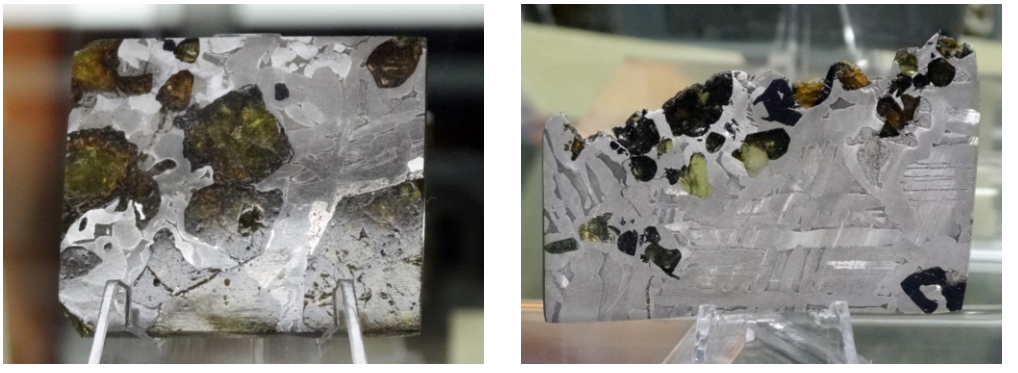

Figure 1. Pallasite slices of Fukang (left) and Seymchan (right).

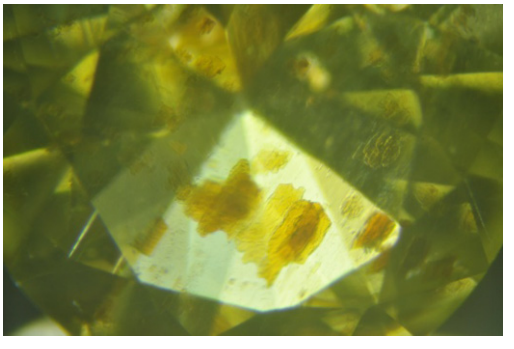

Figure 2. Reddish brown platy inclusions in Admire pallasitic peridot (X40).

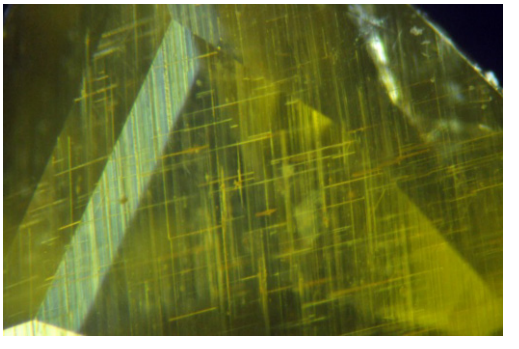

Figure 3. Cross section of needle inclusion in Fukang pallasitic peridot (X40).

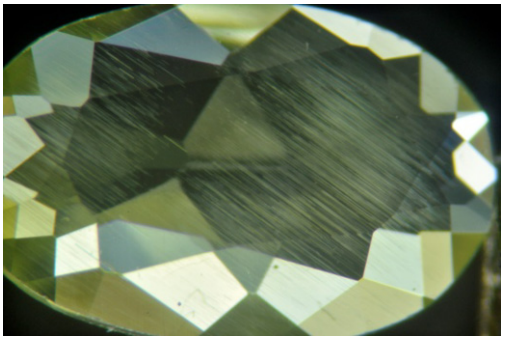

Figure 4. Fine needle inclusions in Seymchan pallasitic peridot (X20).

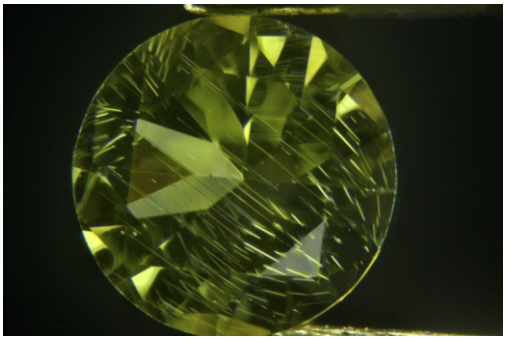

Figure 5. Thick tube inclusion in Jepara pallasitic peridot(X10).

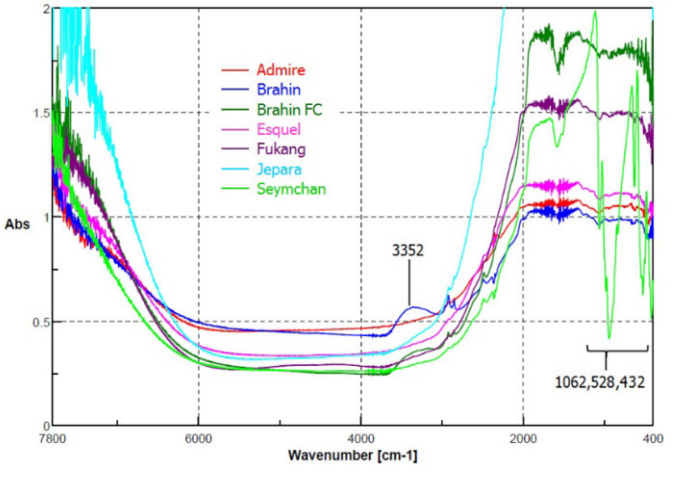

Figure 6. FT-IR spectra of each pallasitic peridot.

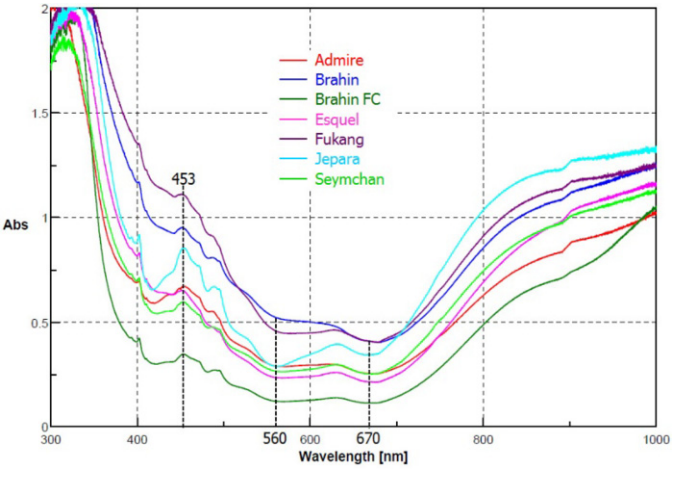

Figure 7. UV-Visible spectra of each pallasitic peridot (not polarized).

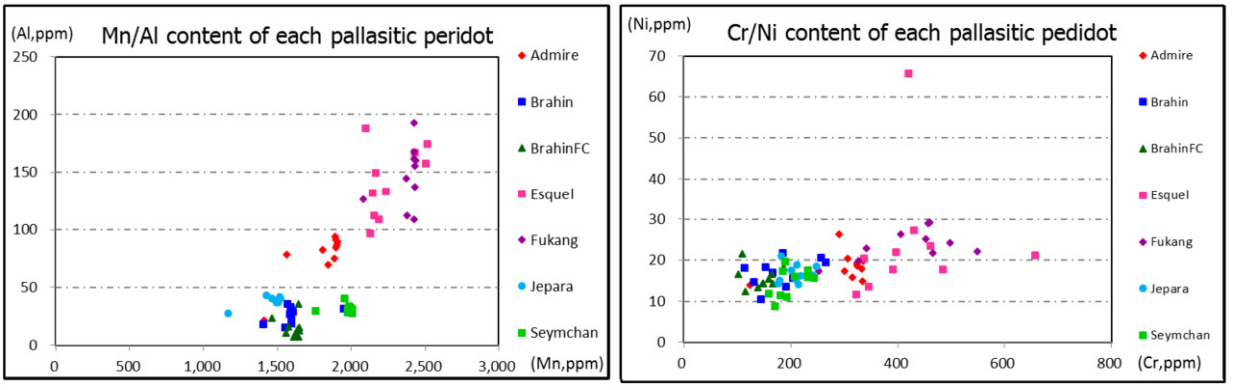

Figure 8. Comparison of trace elements of each pallasitic peridot.

Acknowledgments

Aerolite Meteorites, LLC
Mr. Steve Arnold, Meteorite Men
Yamanashi Prefectural Industrial Technology Center

References

Graham, A.L., Grady, M.M., 2000. Catalogue of Meteorites Reference Book with CD-ROM, Cambridge University Press, London, ISBN 0-5216-6303-2, 58, 113, 195.

Henn, U., Becker, A.F.A., 1992. On the properties of meteoritic gem olivine from a pallasite from Esquel, Patagonia, Argentina, Journal of Gemmology, 23(2), 86-88.

Leelawathanasuk. T., Atichat, W., Suthirat, C., Wathanakul, P., Sriprasert, B., Naruedeesombat, N.,, Srithunayothin, P., Davies, S., 2011. Pallasitic peridot: The gemstone from outer space, 32nd IGC 2011 Abstracts, 110-113.

The Meteoritical Society website: Meteoritical Bulletin Database http://www.lpi.usra. edu/meteor/.

Shen, A.H., Koivula, J.I., Shigley J.E., 2011. Identification of extraterrestrial peridot by trace elements. Gems & gemology, 47(3), 208-213.

Stevens, M.R., Bell, D.R.,Buseck, P.R., 2010. Tubular symplectic inclusions in olivine from the Fukang pallasite, Meteoritics & Planetary Science 45(5), 899–910.

Russian demantoid color origin

R. Serov, Y. Shelementiev, A. Serova

Gemological Center, Lomonosov Moscow State University, Moscow, Russia; potom_skajy@mail.ru

Keywords Demantoid, Heat Treatment, Color, Spectroscopy

Introduction

Demantoid is famous for its vivid green color and high dispersion. The heat treatment usually applies to improve the color and reduce the brown tint of demantoids mined in Russia. Despite numerous studies the causes of demantoid color modification during the heat treatment process remain controversial (Pezzotta et al., 2011, Chatagnier, 2012).

Samples and methods

A set of untreated brown and green rough demantoid crystals from Karkodino, Urals, Russia was investigated. UV-VIS-NIR spectra were recorded on Ocean Optics QE65000 spectrometer in the range of 400-1100 nm, accumulating 30 scans at 1 nm resolution.

Mössbauer spectra were measured on MS 1104 Em Mössbauer spectrometer using a ^{57}Co radioactive source with activity of 50 microcurie.

Samples were heated at 650° C. The heating rate to the required temperature was carried out at 300°/hour. The cooling rate of the sample was about 150°/hour. Regular atmosphere (air) was used for heat treatment in oxidizing conditions. Samples were sealed in crucible with charcoal powder for heat treatment in reducing conditions.

Results

All samples were heat treated at 4 successive stages (see Fig. 1) with different red-ox conditions and heat treatment duration.

The first stage was performed in reducing atmosphere for 1 hour. All samples showed the reduction of brown tint. Initially brown samples became green.

The second stage was performed in oxidizing atmosphere for 2 hours. All samples became brown to orange-brown.

Stages three and four were performed in reducing atmosphere for 2 and 6 hours, respectively, and showed gradual decreasing of brown coloration in all samples.

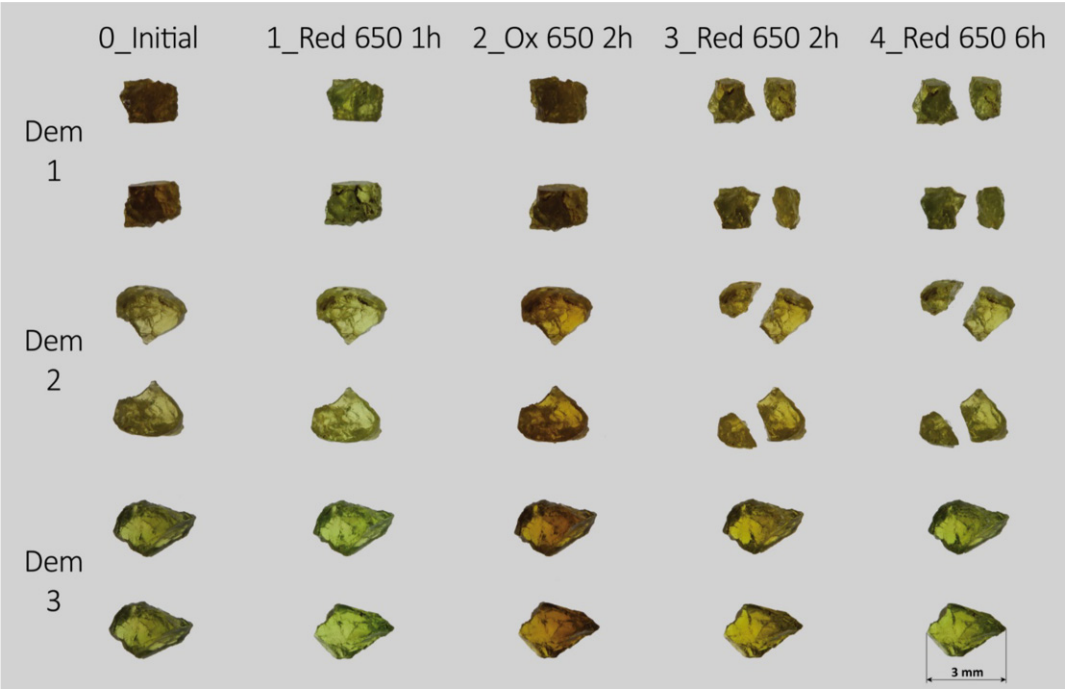

Figure 1. Demantoid crystals color modifications during the successive heat treatment processes.

The VIS-NIR spectra of initial brown samples or samples with brown tint (see Fig. 2a) always show the edge of very broad absorption band with the center presumably about 430 nm that determines the brown color of the sample. The absorption of that band is very high in blue area of the spectrum, so we could not establish the precise position of the absorption band.

The character of that band resembles the absorption bands found in other garnets:

1) in melanite-schorlomite garnets (Locock et al., 1995) or pyralspite garnets (Platonov et al., 1991) where it was assigned to Fe^{2+}-Ti^{4+} charge-transfer.

2) in almandine-skiagite garnets (Taran et al., 2007) where it was assigned to Fe^{2+}-Fe^{3+} charge-transfer.

Together with the broad 430 nm band, the spectra show Fe^{3+}-related features at 855, 617 and 575 nm (see Fig. 2b). Some samples also exhibit Cr^{3+}-related absorption band at 621 nm (see Fig. 2c).

Heat treatment in oxidizing atmosphere results in the very effective formation of 430 nm band and changing the color of all samples to brown (see Fig. 1, the second and third column). There is no evidence that heat treatment in oxidizing atmosphere alters other Fe- and Cr-related absorption bands.

On the contrary, heat treatment in reducing conditions decreases the intensity of 430 nm band. In Fig. 2d, the subtraction spectra between stage 1 and stages 2, 3, 4 are shown. It is clear that heat treatment in oxidizing atmosphere on stage 2 produces 430 nm band only, while the absorption of Fe- and Cr-related bands remains exactly the same. The heat treatment at stages 3 and 4 in reducing conditions can progressively decrease the intensity of 430 nm band.

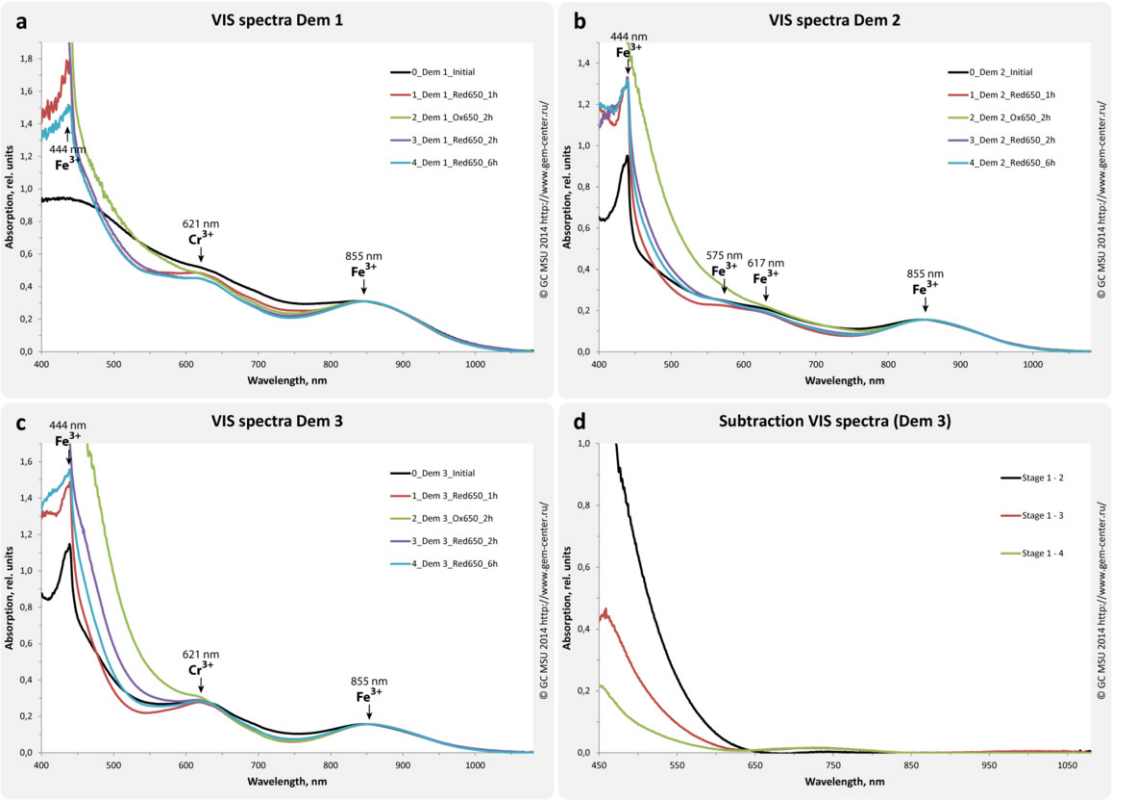

Figure 2. VIS-NIR spectra of demantoid samples during heat treatment processes.

All studied demantoids before and after annealing displayed significant absorption bands in the OH-stretching region of their IR spectra (Fig .3). Thermal re-ordering of hydrogen occurs during heat treatment. We observe that position of 3605.5 cm^{-1} absorption band shifts to 3603-3604 cm^{-1} and its intensity increases at least twice. Also we see the formation of the 3582 cm^{-1} band and formation of the 3630 cm^{-1} band (in some samples, predominantly after heating in OX conditions).

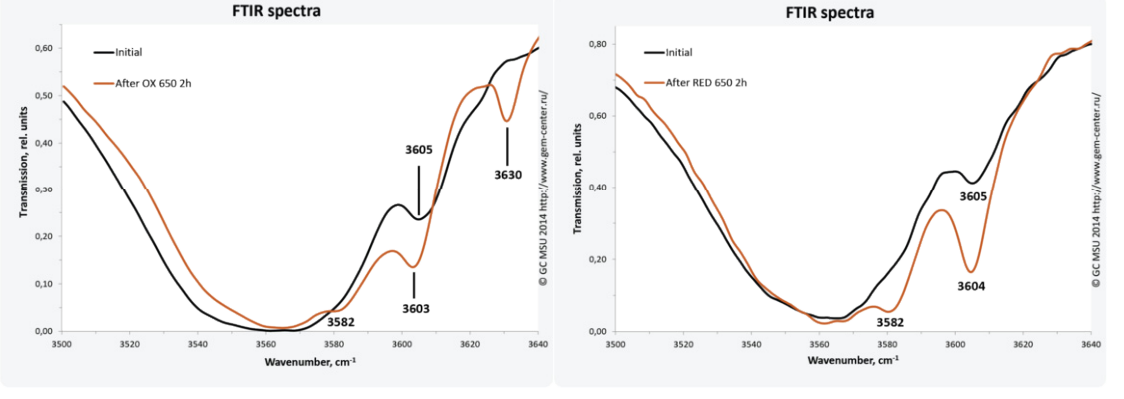

Figure 3. FTIR spectra of demantoid samples before and after heat treatment processes in oxidizing (left) and reducing (right) atmosphere.

Garnets with "horse-tail" inclusions before annealing showed bands in the IR spectra assigned to the OH mode of "byssolite". The subtraction spectrum between initial and heat treated garnet is shown on Fig. 4. After annealing process "byssolite" underwent dehydroxylation and its OH bands were completely removed.

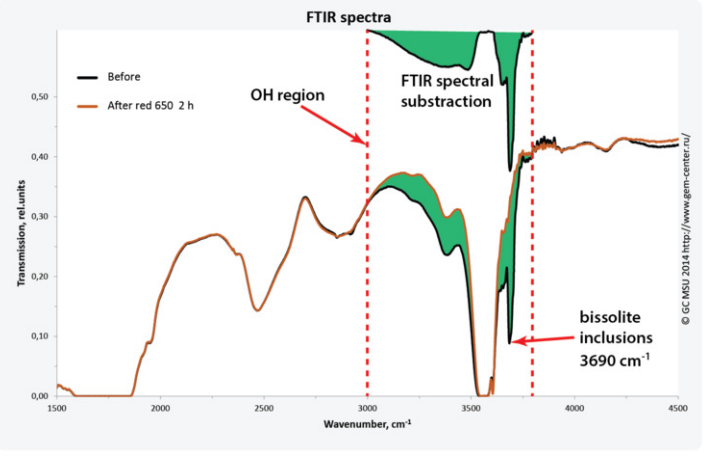

Figure 4. FTIR spectra of demantoid sample with "byssolite" inclusions before and after heat treatment processes in reducing atmosphere.

Conclusion

Color modification in demantoid is reversible and takes place at as low as 400° C temperatures. The phenomenon can be explained by: changes of valence state of iron or destruction of unknown defects under reducing conditions and its re-formation under oxidizing conditions of annealing.

Heat treatment does not affect Fe^{3+} and Cr^{3+} optical absorption and valence state (according to optical and Mössbauer spectroscopy). The cause of brown coloration of demantoid seems to be different from brown coloration in other garnets.

Thermal re-ordering of hydrogen takes place irrelevant to the heat treatment atmosphere. No extraction/incorporation of hydrogen has been noted (according to FTIR spectroscopy). Thus redox reaction

$Fe^{3+} + O^{2-} + ½H_2 = Fe^{2+} + OH^-$ is not active.

References

Chatagnier, Pierre-Yves, 2012. Le traitement thermique de l'andradite, DUG, university of Nantes, France

Locock, A., Luth, R.W., Cavell, R.G., Smith, D.G.W., and Duke. M.J.M., 1995. Spectroscopy of the cation distribution in the schorlomite species of garnet, Am. Miner., 80, pp. 27-38.

Pezzotta, F., Adamo, I., and Diella, V., 2011. Demantoid and topazolite from Antetezambato, northern Madagascar: review and new data, Gems and Gemology, 47 (1), pp. 2-14.

Platonov, A., Langer, K., Matsuk, S., Taran, M. and Hu, X., 1991. Fe^{2+}-Ti^{4+} charge-transfer in garnets from mantle eclogites, European Journal of Mineralogy, 3, pp. 19-26.

Taran, M., Dyar, M., and Matsyuk, S., 2007. Optical absorption study of natural garnets of almandine-skiagite composition showing intervalence $Fe^{2+} + Fe^{3+} \rightarrow Fe^{3+} + Fe^{2+}$ charge-transfer transition, American Mineralogist, 92, pp. 753–760.

Country of origin determinations of nephrite jades from East Asia Regions

Andy H Shen*, Zemin Luo, Mingxing Yang

Center for Innovative Gem Testing Technologies (CIGT), Institute of Gems and Jewelry Studies,
China University of Geosciences (Wuhan), Wuhan, CHINA; *ahshen@foxmail.com

Keywords country of origin determination, provenance, nephrite jade, LA-ICPMS, linear discriminant analysis (LDA)

Introduction

Nephrite jade is the most important jade species in ancient Chinese history and there are a lot of nephrite jade ceremonial artifacts discovered in many ancients Chinese tomb burial sites. Therefore, there is a very strong interest in the archeological community to study the provenance of these artifacts. Additionally, modern jadeite jade/nephrite jade market in China is very large, second only to the gold market. Among all nephrite jade production areas, only the jade coming from the Hetian area in Xinjiang Province have enjoyed higher market price and popularity. There is a real need to study the country of origin of these nephrite jades.

Methods and instrumentation

We analyzed samples directly collected from the following eight locations (figure 1): western Xinjiang (this area includes the famous Hetian area), eastern Xinjiang (Xinjiang province, China), Geermu (Qinghai province, China), Xiuyan (Liaoning province, China), Luodian (Guizhou province, China), Liyang (Jiangsu province, China), Baikal (Russia), Chuncheon (South Korea).

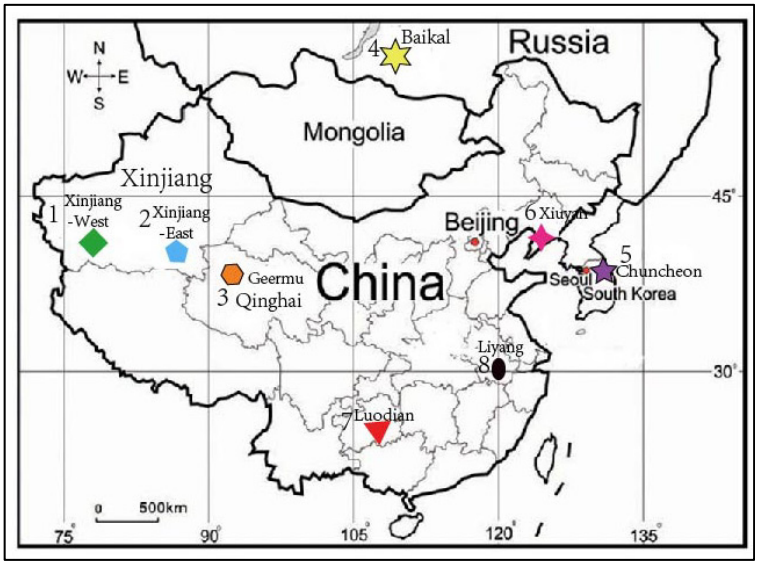

Figure 1. Geographical map of the locations of the eight major production area in East Asian region. Among them: (1) western Xinjiang (this area includes the famous Hetian area), (2) eastern Xinjiang (Xinjiang province, China), (3) Geermu (Qinghai province, China), (4) Baikal (Russia), (5) Chuncheon (South Korea); (6) Xiuyan (Liaoning province, China), (7) Luodian (Guizhou province, China), (8) Liyang (Jiangsu province, China).

In total 138 nephrite samples were selected for this study. All samples were cut into the size of 30x15x5 mm (length x width x height). The main color of samples ranged from white to light greenish, with mottled yellow area (figure 2).

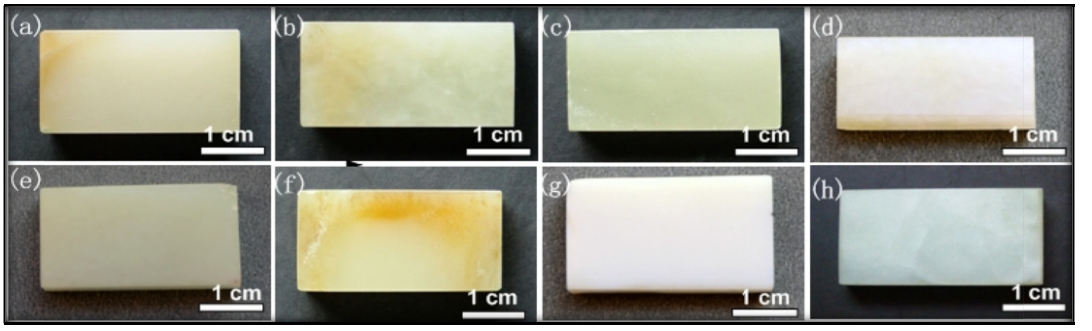

Figure 2. Nephrite samples from the above 8 geographic locations. (a) Xinjiang-West; (b) Xinjiang-East; (c) Geermu; (d) Baikal; (e) Chuncheon; (f) Xiuyan; (g) Luodian; (h) Liyang. Only one representative sample was selected for display. Photos by Zemin Luo.

Trace elements concentrations of these 138 nephrite samples were measured by using a LA-ICPMS system at the State Key Laboratory of Geological Processes and Mineral Resources, China University of Geosciences, Wuhan. The LA-ICPMS system consists of a GeoLas 193nm laser and an Agilent 7500 ICP-MS. The laser fluence was set as 10 J/cm^2 and the ablation spot size was 32 μm. The widely used quantitative calibration standards of NIST synthetic glasses SRM610, U.S. Geological Survey (USGS) synthetic glasses of BCR-2G, BHVO-2G and BIR-1G (Jochum et al., 2005) were used as reference materials. Two to three spots on each sample were collected for analysis. ^{29}Si was used as internal standard. Detailed operating conditions for the laser ablation system and the ICP-MS instrument and data reduction were the same as description by Liu *et al.* (2008, 2010). Total 45 elements were collected during the LA-ICPMS runs.

Among these 8 localities, Liyang samples can be easily separated by its very high Sr and Na+K values. The other 7 localities require further procedure to separate them. We used a well established statistical procedure to maximize the separation among locations ("groups"). This procedure is known as Linear Discriminant Analysis (LDA) (Fisher, 1936). We used the GNU licensed free software of R-3.1.2 for this analysis. Among the 138 nephrite samples, we randomly selected 108 from 7 locations (excluding Liyang samples) as the "training set". Sixteen additional samples (2 from each location, including Liyang samples) are used as "testing set". LDA procedure performs linear combinations of a number of variables of samples in the training set so that it maximizes the separations of different groups while minimizes the variations within the same group. The results are seven discriminant functions, each represents one group (one location). The value of such function can be viewed as a merit score: the higher the score, the better fit into the group it represents. An alternative way to visually observe such separation is by plotting one discriminant function against the other.

Results

The elements selected for our LDA analysis are Li, Be, Na, Al, K, Sc, Rb, Sr, Zr, Nb, Eu, Th, and U. The following are two discriminant functions obtained from the 108 training set samples in our analysis (all in ppm):

$$Y_{xinjiang\text{-}West} = 0.431*[Li]+0.89*[Be]+0.001*[Na]+0.004*[Al]+0.012*[K]+0.817*[Sc]-0.674*[Rb]-0.073*[Sr]+0.818*[Zr]+5.924*[Nb]+14.269*[Eu]-17.241*[Th]+8.057*[U]-27.392$$

$$Y_{xinjiang\text{-}East} = 0.755*[Li]+0.108*[Be]+0.012*[Na]+0.003*[Al]+0.019*[K]+2.989*[Sc]-0.546*[Rb]+0.125*[Sr]-0.408*[Zr]-3.453*[Nb]+8.352*[Eu]-2.736*[Th]+5.632*[U]-16.46$$

Two of the discriminant function plots are shown in figure 3 and 4. In Figure 3, the separation of Xinjiang-East (turquoise pentagons) and Xinjiang-West (green diamonds) is very good; whereas in figure 4 the separation of Geermu, Qinghai (brown hexagons) and the neighboring Xinjiang-East (turquoise pentagons) is clearly defined. Further details will be discussed in the presentation.

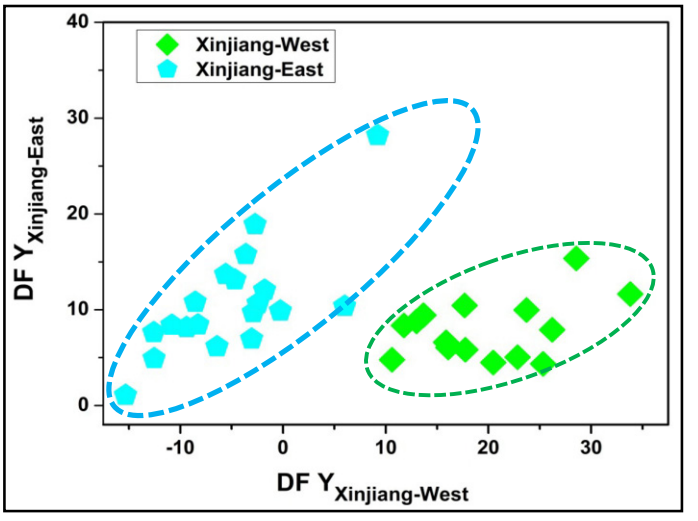

Figure 3. Discriminant function plot of Xinjiang-West vs. Xinjiang-East.

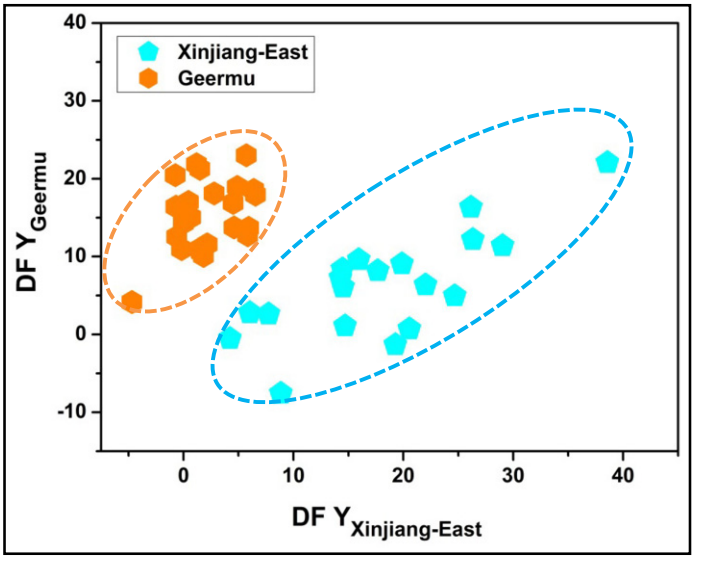

Figure 4. Discriminant function plot of Geermu, Qinghai vs. Xinjiang-East.

References

Fisher R.A., 1936. The use of multiple measurements in taxonomic problems. Annals of Eugenics, Vol. 7, pp. 179-188, doi:10.1111/j.1469-1809.1936.tb02137.x.

Liu, Y., Hu, Z., Gao S., Günther, D., Xu, J., Gao, C., Chen, H., 2008. In situ analysis of major and trace elements of anhydrous minerals by LA-ICP-MS without applying an internal standard. Chemical Geology, 257, 34-43.

Liu Y.S., Hu Z.C., Zong K.Q., Gao C.G., Gao S., Xu J., Chen H.H., 2010. Reappraisement and refinement of zircon U-Pb isotope and trace element analyses by LA-ICP-MS. Chinese Science Bulletin, 55(15), 1535-1546.

Jochum K.P., Willbold M., Raczek I., Stoll B., Herwig K., 2005. Chemical characterization of the USGS reference glasses GSA-1G, GSC-1G, GSD-1G, GSE-1G, BCR-2G,BHVO-2G and BIR-1G using EPMA, ID-TIMS, ID-ICP-MS and LA-ICP-MS. Geostandards and Geoanalytical Research, 29(3), 285-302.

Opal Adventures in the Land of Never Never

Karen E. Fox

Waterloo, ON, Canada; k_e_fox@yahoo.com

Keywords opal, opal-A, opal-CT, Lightning Ridge, Coober Pedy, Quilpe, Yowah, Australia

Introduction

In his book *Opal, The Gem of the Never Never*, Tully Wollaston, reputed father of the Australian opal industry, describes his arduous trek into Queensland during the scorching summer of 1888, enduring "miles of fierce sun, sandhill and shadeless plain" and "heat almost unbearable" in search of a rumoured opal claim (Leechman, 1969). Today the land is little changed, but many intrepid souls have devoted their lives to proving that Australia's Great Artesian Basin (GAB) holds the most productive opal ground in the world. On a quest to develop a basic understanding of this phenomenal material, a journey through three of Australia's prime opal producing regions provides a view of the geological environment in which opal is found and the extraction techniques employed, and sparks vigorous discussion about opal's structure, behaviour and deposition.

The Nature of Opal

The play of colour in precious opal (Figure 1) arises from the diffraction of light from a regular three-dimensional arrangement of hydrous silica spheres of uniform diameter ranging from about 150 nm to 400 nm (Sanders, 1964; Sanders and Darragh, 1971). *Common* or *potch* opal lacks play of colour because the spheres are not of the appropriate diameter, or lack the uniformity in size, shape or arrangement requisite for diffraction of visible wavelengths of light.

Figure 1. Crystal opal displaying vivid play of colour. Specimens from the Umoona Opal Mine and Museum, Coober Pedy, South Australia. Photo: K. Fox.

The term *silica* encompasses materials with the SiO_2 chemical composition, whereas *opal* constitutes a hydrous $SiO_2 \cdot nH_2O$ phase that lacks the long range crystal structure required to produce distinct sharp X-ray powder diffraction patterns (Flörke et al., 1991). Two forms of opal are of greatest relevance to the gemmologist: amorphous opal-A, which forms spheres of concentric shell structure that make up opal most often associated with sedimentary environments, as found over much of Australia; and opal-CT, which is an intergrowth of disordered cristobalite with tridymite that makes up bladed *lepispheres* or fibrous structure in opal typically associated with volcanic environments, as in Mexico or Ethiopia (Elzea & Rice, 1996; Gaillou et al., 2008).

The polymerization of silica into colloids, sols and gels is understood and used in industrial processes (Iler, 1979; Bergna & Roberts, 2006), and plays a role in the development of new nanomaterials (Ozin et al., 2009). Diagenetic processes that convert opal-A to opal-CT to microcrystalline quartz have also received considerable attention (Williams et al., 1985). Still under debate, however, are a multitude of topics, including the source of silica for the opal deposits in the GAB, the factors governing stability of opal from different localities, and how to prospect for opal. A trip to the opal fields of Australia serves to establish a framework for understanding the nature of opal and the roots of these conflicting opinions.

In the Field

Three significant opal-producing regions were visited — Lightning Ridge in New South Wales, the Queensland boulder opal fields, and Coober Pedy in South Australia.

Precious opal in these fields is found in weathered Lower Cretaceous sedimentary rocks. During the early Cretaceous, up to 60% of the continent was flooded as subsidence led to marine transgression and formation of the Eromanga Sea. Sediments from an andesitic volcanic arc on the east coast of the continent were carried into the basin and formed the strata that are currently mined for opal at Coober Pedy and Lightning Ridge. The late Cretaceous saw a switch from marine to freshwater deposition that gave rise to the Winton formation in which the Queensland boulder opal deposits are found. A protracted period of uplift produced extensive erosion, followed by deposition of the Cenozoic rocks of the Eyre Basin. Where these rocks remain today, they are capped with silcretes made of silicified sandstone and conglomerate (Rey, 2013).

Queensland

The areas in the vicinity of Quilpe and Yowah provide a representative picture of boulder opal country, and display a vibrant red colouration that bears witness to extensive oxidation. The durable Cenozoic silcrete cap has protected the opal-bearing weathered sandstone and mudstone of the Winton formation in some areas, while the land has been eroded to a flat plain in the surround (Figure 2). Opal has selectively filled cavities in ironstone concretions (Figure 3) and Yowah nuts (Figure 4). Open-cut mining is common, as at the property depicted in Figure 2, while underground mining is undertaken at other sites.

Coober Pedy

The approach to Coober Pedy from the air reveals a red plain speckled with conical mounds of white claystone extracted from innumerable drill holes and underground excavations. The region lies on the edge of the Stuart Ranges which form a high plateau capped by silcrete that protects the softer claystone below. This is best visualized at the Breakaways Reserve 32 km north of town where erosion has left remnants of cap protecting a picturesque display of mesas and buttes (Figure 5). The marine environment in which the opal-bearing Bulldog shale was deposited has provided fine examples of opalized bivalves (Figure 6), belemnites and marine vertebrates (Smallwood, 2014).

Figure 2. Boulder opal is extracted from Eric Stelzer's mine on the Alaric property in south Queensland. Note flat top preserved by the protective silcrete cap. Photo: K. Fox.

Figure 3. The curved meniscus indicates the horizontal when silica gel was settling in the cavity in this concretion to deposit precious opal. Specimen courtesy of Sam Manis. Photo: K. Fox.

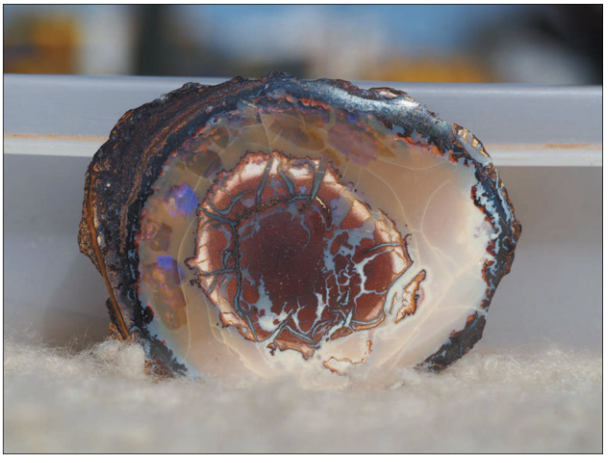

Figure 4. Yowah nut from Queensland exhibiting secondary infilling of dessication cracks with potch. Photo: K. Fox.

Figure 5. The Breakaways outside Coober Pedy retain remnants of a silcrete cap protecting friable claystone. Photo: K. Fox.

Noodling machines are used to recover opal from old mine dumps by inspecting the refuse rock (*mullock)* under long wave ultraviolet (UV) light. UV excites the characteristic luminescence of Australian white opal, reported to be associated with silica surface defects (Fritsch, 2001).

Lightning Ridge

The "Ridge" produces distinctive black opal that shows a vibrant play of colour against a dark backing of potch. Seam opal and nodules (*nobbies*) are found at 6-30 m below ground in the claystone of the Griman Creek formation. Mining involves sinking a shaft through sandstone and conglomerate to the claystone, and then excavating *levels* using tools such as hydraulic digging machines (Figure 7). Opal dirt is trucked to *puddling* operations to be agitated with water in a modified cement mixer to grind away the claystone leaving the tailings to be sorted (Figure 8).

Figure 6. Opalized marine bivalves from Coober Pedy. Photo: K. Fox.

Conclusion

In general terms, the fundamental requirements for the formation of opal are evident: there must be a source of silica, perhaps released by weathering processes, biogenic activity or hydrothermal waters; pathways must exist for the transport of silica-bearing solutions; depositional sites must enable the accumulation of solutions, yet still allow for slow evaporation of water as colloidal particles compact; and a stable geologic environment is essential, free of processes that could lead to destabilization or dissolution of the opal.

Most discussions to date have focused on the details pertaining to particular Australian opal fields, while the challenge of providing an integrated understanding of opal deposition across opal-producing environments worldwide provides ample opportunity for further investigation.

Figure 7. A hydraulic digging machine is used to excavate a level at an underground mine near Sheepyards in the vicinity of Lightning Ridge, NSW. Photo: K. Fox.

Figure 8. Wet puddling operation for processing opal dirt at Lightning Ridge. Photo: K. Fox.

References

Bergna, H.E., Roberts, W.O., 2006. Colloidal Silica, Fundamentals and Applications. CRC Press, Boca Raton, 912 pp.

Elzea, J.M., Rice, S.B., 1996. TEM and X-ray diffraction evidence for cristobalite and tridymite stacking sequences in opal. Clays and Clay Minerals, 44(4), 492-500.

Flörke, O.W., Graetsch, H., Martin, B., Röller, K., Wirth, R., 1991. Nomenclature of micro- and non-crystalline silica minerals, based on structure and microstructure. Neues Jahrbuch für Mineralogie—Abhandlungen, 163(1), 19-42.

Fritsch, E., Mihut, L., Baibarac, M., Baltog, I., Ostrooumov, M., Lefrant, S., Wery, J., 2001. Luminescence of oxidized porous silicon: Surface-induced emissions from disordered silica micro- to nanotextures. Journal of Applied Physics, 90(9), 4777-4782.

Gaillou, E., Fritsch, E., Aguilar-Reyes, B., Rondeau, B., Post, J., Barreau, A., Ostroumov, M., 2008. Common gem opal: An investigation of micro- to nano-structure. American Mineralogist, 93, 1865-1873.

Iler, R.K., 1979. The Chemistry of Silica. John Wiley & Sons, Inc., New York, 866 pp.

Leechman, F., 1961. The Opal Book. Ure Smith, Publishers, North Sydney, 263 pp.

Ozin, G.A., Arsenault, A.C., Cademartiri, L., 2009. Nanochemistry. RSC Publishing, Cambridge, 820 pp.

Rey, P.F., 2013. Opalisation of the Great Artesian Basin (central Australia): an Australian story with a Martian twist. Australian Journal of Earth Sciences, 60(3), 291-314.

Sanders, J.V., 1964. Colour of precious opal. Nature, December 19, 1151-1153.

Sanders, J.V., Darragh, P.J., 1971. The microstructure of precious opal. Mineralogical Record, 2(6), 261-268.

Smallwood, A., 2014. The unique attributes of Australian precious opal. The Australian Gemmologist, 25(6/7), 207-230.

Smith, E., 1999. Black opal fossils of Lightning Ridge. Kangaroo Press, Sydney, 112 pp.

Williams, L.A., Parks, G.A., Crerar, D.A., 1985. Silica diagenesis, I. Solubility controls. Journal of Sedimentary Petrology, 55(3), 301-311.

Green-luminescing, gem hyalite opal from Zacatecas, Mexico

Emmanuel Fritsch[1], Peter Megaw[2], Tyler L. Spano-Franco[3]

[1]Institut des Matériaux Jean Rouxel CNRS (UMR 6502) & University of Nantes, BP 32229, F-44322 Nantes cedex 3, France; emmanuel.fritsch@cnrs-imn.fr
[2]IMDEX Inc., Tucson, Arizona, USA
[3]Department of Civil and Environmental Engineering and Earth Sciences, University of Notre Dame, Notre Dame, IN, USA

Keywords opal, hyalite, luminescence, uranium, PL, Raman

Introduction

At the Tucson 2014 show, interesting specimens of yellow hyalite from the state of Zacatecas, Mexico, attracted the attention because they gained a green color when put under direct daylight (Moore, 2014; see figure 1). At first perceived as a mineralogical curiosity, it became quickly apparent that gems could be faceted from this material. At Tucson 2015, faceted gems of this material were available from several rare stones cutters or dealers, the largest reaching a little under 4 ct. This is mostly due to the fascinating color change with lighting due to the green luminescence, hence its trade name of "Electric opal".

Figure 1. This 20ct+ rough piece of hyalite opal from Mexico was mounted as a pendant. Its color changes with lighting from yellow, left, with incandescent lighting, to green, center, in indirect Arizona sunlight. Many amateurs like to use a 405 nm violet laser to excite this spectacular green luminescence. All pictures taken in short sequence with an iPhone5. Photos E. Fritsch.

Occurrence, mining and production

The opal forms crusts and botryoidal deposits on a rust-colored matrix, which appears to be a devitrified rhyolitic welded tuff. These are found in small veins and cracks. The occurrence is located in the Sierra Madre Occidental Volcanic Province, in a series of mid Tertiary rhyolitic rocks, not unlike the many fire opal deposits of central Mexico. The digging area is quite remote, and is located on a high mesa in a cactus-infected arid zone, which makes access quite difficult. The material is extracted with basic hand tools, and mining is not in any way mechanized.

The silica forming the opal probably originates from weathering and dissolution of the glass chards in the tuff. There are actually a series of uranium-containing minerals found as well in the veins, under the opal. Meta-autunite ($Ca(UO_2)_2(PO_4)_2{\cdot}6\text{-}8H_2O$), haiweeite ($Ca(UO_2)_2[Si_5O_{12}(OH)_2]{\cdot}6H_2O$), uranophane ($Ca(UO_2)_2(HSiO_4){\cdot}5H_2O$), and meta-uranospinite ($Ca(UO_2)_2(AsO_4)_2{\cdot}8H_2O$) are the most prominent uranyl species located in proximity to botryoidal masses of hyalite (Spano-Franco et al., 2015). The lateral and depth extensions of the find seem to be limited, and production is not expected to be large or continue much longer.

Materials and methods

All specimens were provided by the second author. They are mostly hand specimens and small fragments of gem materials broken from their matrix. Three stones were fashioned for this study, ranging in final size from 0.83 to 1.81 ct, in order to measure gemological properties.

We used standard gemological testing equipment, including a binocular Leica MZ6 microscope with a Nossigem gemological lighting system, a GIA Gem Instruments refractometer, a Mettler Toledo XS104 electronic scale for mass and specify gravity (automatic) hydrostatic measurements. UV luminescence observations were done under a VL-215-LC Vilber-Lourmat filtered UV Lamp with a total power of 30W, We used a 405 nm, 0.5 mW pointer laser to estimate emission in the violet: such a device is often incorrectly referred to as a "blue" laser. Raman spectra were obtained on a Bruker MULTIRAM Fourier-Transform spectrometer. The excitation is a 2 Watts Nd:YAG laser, and the opal data were collected at the standard resolution of 4 cm^{-1}, accumulating 1000 scans. Photoluminescence emission and excitation spectra as well as « 3D » blocks were obtained on FluoroLog-3 from Horiba Jobin-Yvon via the FluorEssence software. Two detectors are available, a classical photomultiplier, and a CCD Synapse detector coupled to a iHR320 spectrometer. UV-Visible absorption spectra were recorded on a Cary5G UV-Vis-NIR spectrometer at a resolution of about 1 nm (sampling: 1 nm, spectral band width: 1 nm) in the visible range. Each point was collected for 1s.

Gemological properties

The RI was measured at about 1.45, although spot RI readings are quite difficult. There was no problem with RI liquid getting into the opal, as often feared for gem opals. The SG was measured between 2.12 and 2.16 on inclusion-free, massive gem specimens. The yellow body color of the specimen is absorption related. It is generally homogeneous, but some specimens may show quite light to near-colorless . It is best observed inside in various types of mixed lighting. When put under direct daylight, however, all selected specimens show a green component to their color due to luminescence excited by visible light (see again figure 1). Some of the opal crusts observed go continuously from yellow to actually milky white. The white zones do not show either the yellow or green component of the color. The pure green luminescence of the gems is extremely intense under ultraviolet radiation. The emission in SW is sometimes superior but often visually equal in intensity to that in LW. This emission is much stronger than our "very strong" SW intensity reference stone. This emission shows no milkiness. There is no eye-visible phosphorescence. Remarkably, all colors of opal, from medium yellow, to near-colorless to milky, fluoresce with exactly the same intensity. The level of radioactivity was checked and found to be within background even for a long (half hour) dose measurement. So there is no danger in wearing such gems on the skin for example.

Scattering spectroscopies: Raman and luminescence

Raman scattering spectroscopy has been established as a reliable method to characterize opal (Smallwood et al., 1997; Ostrooumov et l., 1999, Rondeau et al., 2004). The hyalite specimens show spectra typical for opal A (figure 2) with in particular a broad band with an approximate maximum at about 435 cm^{-1}, and a brutal drop at about 500 cm^{-1}. This is a little different from typical opal A, that is opal AG (Rondeau et al., 2004) which shows a more Gaussian-like band centered around 420 cm^{-1} (Rondeau et al;, 2004). Subsequently broad bands are observed at about 790, 970 and 1075 cm^{-1} as in above cited publications. A relatively broad band finishing in a sharp peak at 1550 to 1595 cm^{-1}, depending on the specimen, is rather unique to this series of samples. Then a broad band with an apparent maximum at 3110 to 3120 cm^{-1} is related to water, but perhaps modified by an artifact.

Besides small differences in Raman scattering, this gem material has a very different appearance from typical opal-A from Australia, and its botryoidal morphology and transparency, without any play-of-color, indicates that it is most likely opal-AN (i.e., amorphous with a network-like or glass-like structure). Often called *hyalite* in gemmology, this is probably the rarest gem opal variety (Fritsch et al., 2014).

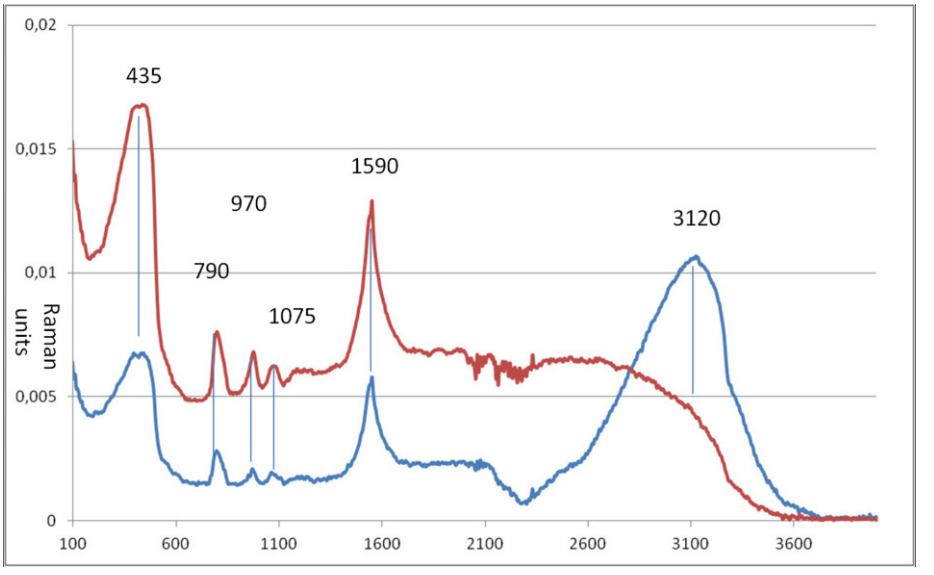

Figure 2. Typical Raman spectra of green-fluorescing hyalite opals from Mexico, identifying them as opal A. The abscissa is in wavenumbers. Note the strong peak around 1590 cm-1. The water region, 3000-3500 cm-1 appears unreliable.

Finally, photoluminescence (PL) properties have been carefully documented, to understand the origin of the visible-light excited green emission. Green ultraviolet luminescence is common in opal. It is well-known to be related to uranium in the form of the uranyl group (Gaillou et al., 2011). Without surprise, the emission spectrum of all samples investigated revealed a very typical emission spectrum of the uranyl group, with four maxima, the strongest at about 524 nm (figure 3), which is in the green, explaining the color of the emission. Less obvious is the reason why this opal also luminesces green in daylight, not just in UV, which is unusual. The excitation spectrum records all wavelengths that will excite a given emission. When this is done on our specimens, there is a broad excitation region in the UV, commonly seen in opal; In addition, there is a smaller one at the beginning of the visible, extending from roughly 400 to 440 nm with a maximum at about 420 nm. This is all in the violet, which explains why daylight, which contains much violet excites this luminescence, and why it is so spectacular with a 405 nm violet laser (again see figure 1). The detailed shape of this excitation spectrum duplicates the absorption spectrum of the yellow specimen, due to the uranyl group. So that means that daylight luminescence occurs strictly within the uranyl molecular ion, without interaction with UV absorbing centers, as is usually the case.

Conclusion

This new gem material is a rare example of hyalite opal, opal AN, which is rarely encountered fashioned in jewelry. Its intense uranium-related, daylight-excited green luminescence gives it an extremely bright and saturated color. It is one of the very few gems for which color is dominated by luminescence.

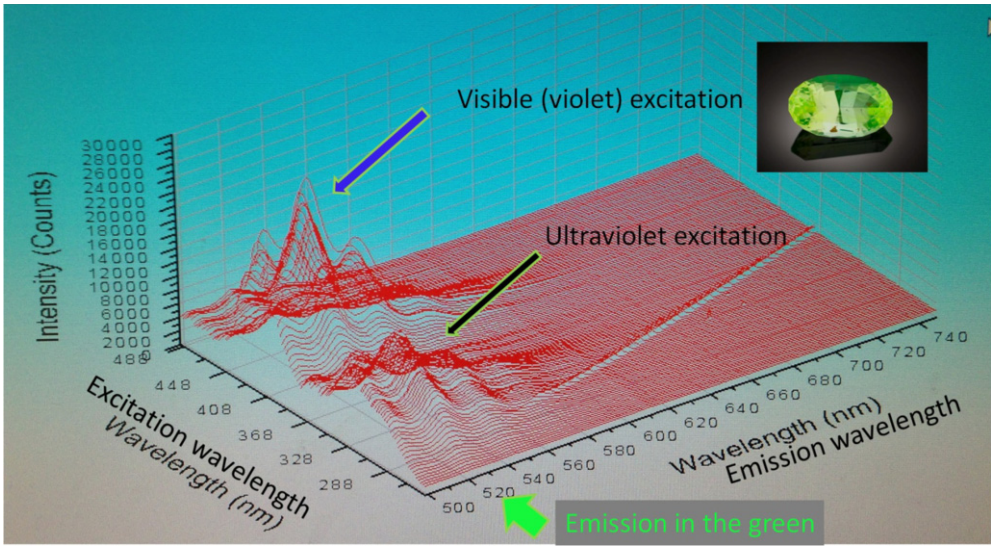

Figure 3. "3D block" of the hyalite photoluminescence. Traced in red are emission spectra from 500 to 740 nm, obtained by increasing the excitation wavelength by 3 nm, from 260 to 490 nm. The broad green arrow points to the main uranyl emission in the green, at 524 nm, four uranyl emission peaks being visible on this block, from 500 to 600 nm. The excitation, red on the left scale, is maximum in two spectral domains, in the UV and in the violet. Picture by Tino Hammid.

References

Fritsch E., Spano-Franco T., Megaw P., 2014. Green daylight-fluorescent hyalite opal from Mexico. The Journal of Gemmology, 34-4, 294-296.

Gaillou E., Fritsch E., Massuyeau F., 2011. Luminescence of gem opals: a review of intrinsic and extrinsic emission. The Australian Gemmologist, 24- 8, 200-201.

Moore T.P., 2014. What's new: Tucson show 2014. Mineralogical Record, 45(3), 345–375.

Ostrooumov M., Fritsch E., Lasnier B., Lefrant S.,1999. Spectres Raman des opales: aspect diagnostique et aide à la classification, European Journal of Mineralogy, 11, 899-908.

Rondeau B., Fritsch E., Guiraud M., Renac C., 2004. Opals from Slovakia: a re-assessment of the conditions of formation. European Journal of Mineralogy, 16, 789-799.

Smallwood A., Thomas P.S., Ray A.S., 1997. Characterization of sedimentary opals by Fourier transform Raman spectroscopy. Spectrochimica Acta A, 53, 2341-2345.

Spano T.L., Burd A.M., Kovacks J.D., Burns P., 2015. Distribution of uranium and uranyl minerals near and within hyalite opal. 249th ACS national Meeting & Exposition, Denver,Colorado, USA. Abstract in proceedings book, p. 160.

Observations on some rare gem materials

Ulrich Henn

German Gemological Association; ulihenn@dgemg.com

Keywords Wurtzite, Tanzania, afghanite, Afghanistan, mosandrite, Russia, buchite, Germany, physical and chemical characteristics, inclusions

Introduction

Popular occurrences of commercially important gemstones consistently produce accessory minerals which may possess gem quality and often represent interesting collector stones. Two particular examples are represented: wurtzite from the tanzanite mining area Merelani Hills in Tanzania and afghanite from the lapis lazuli mines of Sar-e-Sang in Afghanistan.

Another source of rare gem materials are the world-renowned mineral localities. Even of such materials two samples are described, mosandrite from Kola Peninsula in Russia and buchite from the Eifel in Germany.

Wurtzite from Merelani, Tanzania

Transparent to translucent orange-red wurtzite (Figure 1) was found in the Merelani Hills Tanzanite mining area, Tanzania in 2012.

Wurtzite is the hexagonal polymorph of zinc sulfide and generally termed β-ZnS. Reference data indicate a hardness of 3½ to 4, refractive indices of n_o = 2.356 and n_e = 2.378 with a birefringence of 0.022 and a density of 3.98-4.09 g/cm^3 (Phillips & Griffen, 1981). The Merelani Hills material of gem wurtzite possesses a density of 3.81 g/cm^3. The high refractive indices cannot be determined by using a gemmological standard refractometer. Testing with a so-called digital refractometer (reflectometer) yields an approx. value of 2.36. The chemical composition analyzed by electron microprobe shows distinct contents of 9.19-9.26 % manganese as well as 0.41-0.43 % Cd which characterize the material as a member of the wurtzite-rambergite-greenockite (ZnS-MnS-CdS) series. The lower density compared to reference data of wurtzite is due to the distinct manganese content, consequently the rambergite content. The orange-brown colour is caused by Mn^{2+} electron transition.

Fluid inclusions including two-phase film-like cavities were observed by microscopic studies.

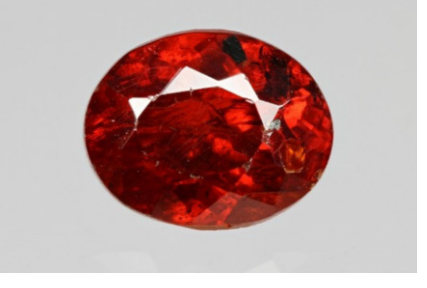

Figure 1. 0.91 ct. faceted orange-red wurtzite from Merelani Hills, Tanzania (Foto: S. Koch, DSEF).

Figure 2. 0.34 ct. blue afghanite from Sar-e-Sang, Afghanistan (Foto: S. Koch, DSEF).

Afghanite from Sar-e-Sang, Afghanistan

Gem quality afghanite (Figure 2) is found on the market since 2003. The deep blue mineral belongs to the cancrinite group, has a complex chemical formula $(Na,K,Ca)_6Ca_2[(SO_4,CO_3)_2/(Cl,OH)_2/(Al,SiO_4)_6]\cdot nH_2O$ and crystallizes in the

trigonal crystal system. The Mohs hardness is attributed to 5½ to 6. The translucent gem material which is found in the famous lapis lazuli occurrence of Sar-e-Sang in Afghanistan possesses refractive indices of n_o=1.523 and n_e=1.529 with a birefringence of 0.006. The density is 2.48 g/cm^3. An orange fluorescence can be observed under both longwave and shortwave UV. The deep blue colour is due to SO_3^- electron centers which cause a broad absorption band with a maximum at 600 nm comparable to the colour cause of hauyne (Platonov, 1976).

Mosandrite from Kola Peninsula, Russia

The famous Kirovsky Apatite Mine in the Khibiny syenite Massif of the Russian Kola Peninsula bears gem quality mosandrite besides a wide spectrum of interesting rare minerals. The rare transparent to translucent species shows a yellowish-brown colour and includes numerous fine crystals already visible by the naked eye (Figure 3). Mosandrite is a REE mineral with the chemical formula $(Na,Ca)_3(Ca,Ce)_4(Ti,Nb)[F_2/(O,F)_2/(Si_2O_7)_2]$, crystallizes in the monoclinic system and has a Mohs hardness of 5. The faceted specimen investigated shows refractive indices, birefringence and density of n_x=1.650, n_y=1.653, n_z=1.658, Δn=0.008 and D=3.28 g/cm^3 which correspond to reference data given by Phillips & Griffen (1981). The absorption spectrum is characterized by sharp lines caused by Nd^{3+}: 877, 805, 749, 684, 585, 527 and 512 nm (Wybourne, 1960). The octahedral shaped crystal inclusions were determined as pyrochlore by SEM analyses.

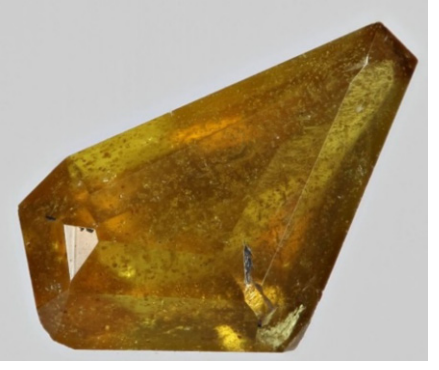

Figure 3. 0.38 ct faceted yellowish-brown Mosandrite from Kola Peninsula, Russia (Foto: S. Koch, DSEF).

Figure 4. 0.25 ct. green buchite from the Eifel, Germany (Foto: S. Koch, DSEF).

Buchite from the Eifel, Germany

The term buchite is generally used for pyrometamorphic volcanic glassy rocks. An occurrence in the Eifel volcanic area in Germany provides transparent material (Figure 4) of gem quality. The material was formed by contact of volcanic melts with a sandstone and therefore represents a glassy sandstone. This fact is reasoned by the chemical analyses with a dominant SiO_2 content of 73.47 wt.%. Further components are 3.72 wt.% Al_2O_3, 6.68 wt.% Na_2O, 8.59 wt.% K_2O, 3.40 wt.% FeO, 1.72 wt.% CaO, 0.64 wt.% MgO and 0.06 wt.% MnO. The refractive index is 1.510, the density 2.40 g/cm^3. Microscopic studies yielded distinct tabby extinction as well as solid inclusions as a result of recrystallization processes.

References

Phillips, W.R., Griffen, D.T., 1981. Optical Mineralogy. Freeman, San Francisco.

Platonov, A.N., 1976. The nature of colour in minerals. Naukova dumka, Kiev (in Russian).

Wybourne, B.G., 1960. Analysis of the Solid-State Spectra of Trivalent Neodymium and Erbium. J. Chem. Phys. 32(3), 639-642.

Gemstones with photochromism

Claudio C. Milisenda[1], Stefan Koch[1], Stefan Müller[1,2],Tom Stephan[1,2] , Michael Wild[3]

[1] DSEF German Gem Lab
Prof.-Schlossmacher-Str.1, D-55743 Idar-Oberstein, Germany; gemlab@dgemg.com
[2] DGemG German Gemmological Association
Prof.-Schlossmacher-Str.1, D-55743 Idar-Oberstein, Germany; info@dgemg.com
[3] Hauptstr. 474, D-55743 Idar-Oberstein

Keywords photochromism, hackmanite, tugtupite, scapolite, absorption spectra

Photochromism can be simply defined by an electromagnetic radiation induced reversible change of colour. During the transformation, the change in the absorption spectra is also accompanied by a change in other physicochemical properties (Irie, 2000). Photochromism, also known as tenebrescence, may occur in both organic and inorganic compounds. The most known application of photochromism is colour-changing lenses for sunglasses. In this study, we report on the photochromic behaviour of hackmanite, tugtupite and scapolite from various occurrences.

At the end of the 2000's an increasing amount of gem-quality sodalites from sources in Afghanistan and Myanmar appeared in the trade (e.g. Wehr et al., 2009; Kondo & Beaton, 2009). Many of them showed a photochromism that is characteristic for the sodalite variety hackmanite. They commonly showed a violetish or purplish colour of very low to medium saturation and changed to a medium to intensive saturated colour when exposed to ultraviolet light for several seconds to a few minutes. The colour faded reversibly within several hours to about a day when the stones were exposed to incandescent light or a daylight-equivalent fluorescent lamp.

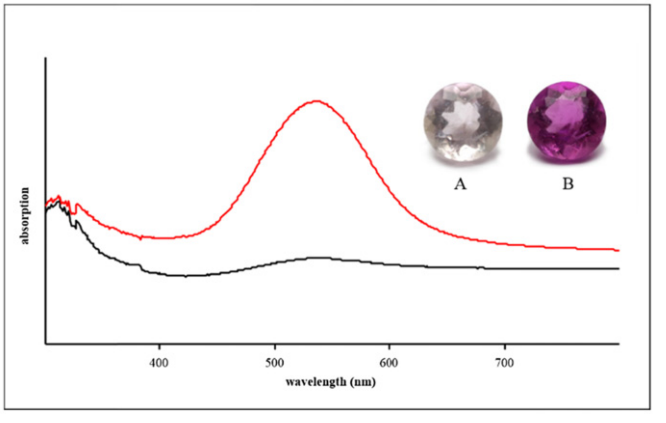

Figure 1. Hackmanite before (A) and after (B) exposure to UV light and corresponding absorption spectra (for explanation see text).

Recently we had the opportunity to study some specimens from Greenland, where hackmanite was first discovered. The brilliant cut stone shown in Figure 1 weighs 0.10 ct. and measures 3.03 - 3.05 x 2.22 mm. It was nearly colourless with a very light tinge of violet when submitted to the laboratory (Figure 1 A). This tinge was still observable after the stone was exposed to daylight for several days. When exposed to short wave UV the stone changed to an intensive violet-pink (Figure 1 B) within seconds. After several days, the stone faded to a moderate violetish-pink, which would last for months. The absorption spectra of the specimen examined in its desaturated and excited state show that UV radiation intensify an absorption band with a maximum at around 535 nm. This is also observed in hackmanites from other occurrences (e.g. Hainschwang, 2007; Kondo & Beaton, 2009, Wehr et al., 2009).

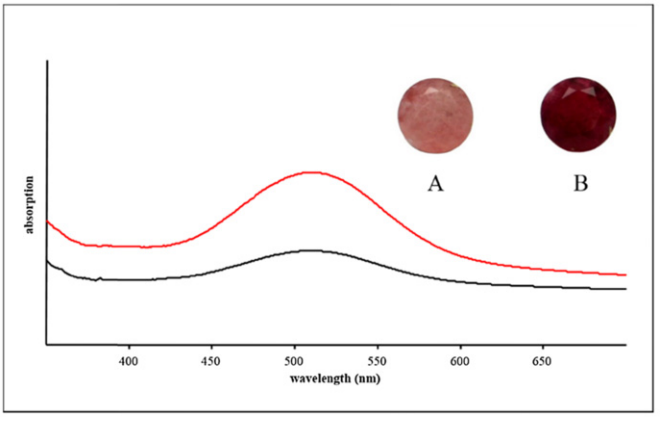

Figure 2. Tugtupite before (A) and after (B) exposure to UV light and corresponding absorption spectra (for explanation see text).

Another stone, which is known to originate from Greenland, is tugtupite, a rare beryllium bearing silicate that occurs in high alkali intrusive rocks. The strength in photochromism is controversially described in the literature ranging from almost absent (Tunzi & Pearson, 2008) to distinct (Jensen & Peterson, 1982). We studied both rough and cut specimens and they consistently showed a strong photochromic effect. Figure 2 (A) shows a translucent, faceted specimen of 0.45 ct. There was no obvious fading observed when the stone was illuminated by incandescent light. Exposure to short wave UV induced a dark crimson-red (Figure 2 B) accompanied by an increasing absorption band centered at around 512 nm. The stone was excited in 2013 and the saturation is still stronger than it was before exposure.

Photochromic scapolite from Afghanistan was first described by McClure & Rossman in 2005. The transparent, colourless samples investigated were also reportedly from the Badakhshan Province of Afghanistan. One representative specimen is shown in Figure 3 (A). When charged with a UV light the stones turned blue. The saturation was much stronger under SUV (Figure 3 C) than under LUV (Figure 3 B). Also observed was a light yellow fluorescence to short wave and a bright orange fluorescence to long wave UV. When the stones were exposed to daylight, the colour faded completely within seconds. UV exposure induces an absorption band centred at around 615 nm and a transmission maximum in the blue part of the visible spectrum. Comparable absorption spectra have been observed in both natural and reportedly irradiated scapolites from Afghanistan (Allen et al. 2014). Chemical analyses showed that the samples represent marialite-rich scapolites with both elevated sodium and chlorine as well as minor sulfur contents. The photochemistry of sulfide is commonly postulated as the cause of photochromism in hackmanite and tugtupite (e.g. Warner & Andersen, 2012).

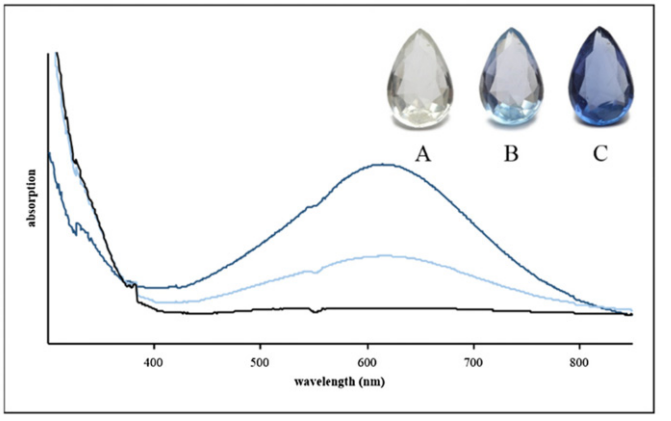

Figure 3. Scapolite before (A) and after (B and C) exposure to UV light and corresponding absorption spectra (for explanation see text).

References

Allen, T., Renfro, N., Nelson, D., 2014. Tenebrescent irradiated scapolite. Gems & Gemology, 50(1), 91-92.

Hainschwang, T., 2007. A study of an unusual hackmanite from Myanmar. Gemlab online publications. Research Newsletter (www.gemlab.net).

Irie, M., 2000. Photochromism: Memories and Switches – Introduction. Chemical Reviews, 100(5), 1683–1684.

Jensen, A., Peterson, O.V., 1982. Tugtupite: a gemstone from Greenland. Gems & Gemology, 18(2), 90-94.

Kondo, D., Beaton, D., 2009. Hackmanite/Sodalite from Myanmar and Afghanistan. Gems & Gemology, 45(1), 38-43.

McClure, S., Rossmann, G. R., 2005. Tenebrescent scapolite from Afghanistan. Gems & Gemology, 41(3), 269-271.

Tunzi, J., Pearson, G., 2008. Hackmanite, tugtupite and afghanite tenebrescence and fluorescence of some sodalite related minerals. Austr. Gemmol. 23, 329-372.

Warner, T.E., Hutzen Andersen, J., 2012. The effects of sulfur intercalation on the optical properties of artificial 'hackmanite', $Na_8[Al_6Si_6O_{24}]Cl_{1.8}S_{0.1}$; 'sulfosodalite', $Na_8[Al_6Si_6O_{24}]S$; and natural tugtupite, $Na_8[Be_2Al_2Si_8O_{24}](Cl,S)_{2-\delta}$.

Wehr, K., Milisenda, C.C., Wild, M., 2009. Photochromism in hackmanites from Afghanistan and Myanmar. Z. Dt. Gemmol. Ges. 58(3-4), 115-126.

Colored gemstones – Mines and markets

Dietmar Schwarz

AIGS - Bangkok; drdietmarschwarz@hotmail.com

Keywords Mining strategies, marketing concepts

Introduction

The general mining/market situation in South America, Africa, the SE-Asian Ruby Belt, and the SE-Asian basalt-related ruby/sapphire deposits is presented. Besides this, new mining/marketing concepts are discussed.

General mining/marketing situation

The most important 'gemstone countries' in South America are Colombia and Brazil. Colombia has been the top emerald producer for many years, but problems in the form of market decline, guerilla activities, and conflicts with drug cartels led to a precipitous drop in official exports (Shor & Weldon, 2010). The government has realized that this sector had different problems which hindered the sector's proper growth and development. Such problems (that are present in a similar way also in other gemstone-producing countries) are: mining rights held by speculators; high levels of informal mining and lack of regulation; poor safety relating to work conditions; widespread artisanal mining with very poor extraction methods; little information about the supply chain in the country; low direct foreign investment; poor investment in social responsibility (Angarita, 2014).

For a long time, Brazil was one of the most important producers of colored gemstones in the world. Brazil distinguished itself by of a large variety of colored gemstones: different "pegmatite minerals (tourmalines, aquamarine and other beryl varieties, spodumene, …), imperial topaz, emerald. Today, the production of colored gemstones in Brazil is relatively low. The main reasons are high mining costs and a strict legislation regarding environmental aspects. Some traditional deposits (e.g. the alexandrite occurrence near Hematita/Minas Gerais) seem to be nearly exhausted.

The most important 'gemstone continent' in our days is Africa. The arrival of high-quality blue sapphire from a new source in Africa in 2014 has caused considerable excitement in the Bangkok marketplace. These gems, reportedly from the Mambilla Plateau in Nigeria's Taraba State, are available in large rough sizes, some as big as 100–300 ct. The Nigerian sapphires are mined from basalt-related secondary deposits. The quality of the sapphires is significantly better than any seen to date from those sources (GIA, 2014). In fact, basalt-related blue sapphires from the Nigeria-Cameroon border region are known already in the market since the 1990's. Right now, the "East African Gemstone Belt" (hosting countries like Kenya, Tanzania, Mozambique, Zambia, Malawi, and Madagascar) is probably the most promising gemstone area in the world. In 2008/2009 several ruby deposits were discovered in N-Mozambique (M'sawize area in Niassa Province and Montepuez in Cabo Delgado Province). The so-called "Mozambique", "Lichinga" or "Niassa" rubies represent an enormous contribution to the international gemstone market. Another spectacular find was made in Ethiopia. Noble opal has been mined since March 2008 in several deposits near Wegel Tena in the province of Wollo (also written as Welo or Wello) in Ethiopia (Opalinda, 2010). Madagascar is still one of the main producers of colored gemstones. However, the overall production has declined. This goes back mainly to the unstable political situation in the country and to the fact that the so-called "easy mining" (i.e. mining with simple methods at the surface) had to be replaced by more sophisticated and more expensive large-scale min-

ing methods. Sri Lanka is one of the most traditional colored gemstone producers. The island is still a considerable and steady contributor to the international market.

The so-called "SE-Asian Ruby Belt" extends from Afghanistan in the north-west to Vietnam in the south-east. The ruby deposits of this belt are all hosted by marble rocks. Potential ruby-producing countries in the belt are (from NW to SE): Afghanistan (Jegdalek), Pakistan (Hunza Valley), Azad Kashmir (Nangimali; Batakundi), Tajikistan (Pamir), Nepal (Ganesh Himal), Myanmar [Burma] (Mogok; Mong Hsu; Namya Seik), Vietnam (Luc Yen – Yen Bai; Qui Chau), and China (Yunnan). All these deposits have a potential to produce good-quality "marble-type rubies". Rubies from Afghanistan, Vietnam, Azad Kashmir and Tajikistan are seen from time to time in the Bangkok/Chanthaburi markets; however, their production is rather sporadic. The Mogok area in Myanmar (Burma) is still one of the most important mining regions in the world. Rubies, sapphires (blue and other colors), spinels (red and other colors) and a large variety of other colored gemstones are still mined in primary and secondary deposits using different types of mining techniques.

The south-east Asian basalt-related ruby/sapphire deposits are situated in the Thai/Cambodian border region, in Laos, SW-China, and southern Vietnam. Production in all these countries has declined significantly. Especially in the Thai/Cambodian border region, mining activities take place only in a few restricted areas; mostly in the form of small-scale mining.

New mining/marketing concepts

New philosophies and policies in the mining sector are 'environmental-sensitive mining', 'sustainable mining', 'fair mining', and 'ethical mining' (ethical and social/socio-economic aspects). There was a strong impact of large mining companies on colored gemstone mining. So-called 'vertically integrated' colored gemstone companies try to cover all gemstone-related activities: exploration/exploitation; mining; beneficiation and marketing. The 'vertical integration model' is not really new. It was already applied in the 1990's by the Gemstone Corporation of Pakistan for the emerald deposits of the Swat Valley, and later by companies like AFGEM/TanzaniteOne (Tanzanite deposits in the Merelani Hills), and TSAR/Selen Kamen (emerald deposits in the Ural mountains). The most advanced versions of this model were developed by Muzo International (Muzo emerald mine in the Cordillera Oriental/Colombia) and by Gemfields (Kagem emerald mine in Zambia).

New mining/marketing concepts address topics like: 'Mine-to-market'; 'Traceability'; 'Branding'; 'Monopolization policy'; 'Fair trade practices'/'Fair trade gemstones'; 'Conflict-free gemstones'; 'Authenticity certificates'. Since 2009, the trade company *Muzo International* is trying to apply a *'monopolization policy'* for the emerald production of the Muzo mine. Muzo International considered itself as unique in the emerald business since it has complete control from the Muzo Mine to the international market (Muzo Emerald, 2009). This controlled trail ensures that both the stones themselves and the methods by which they have been processed are of the highest quality. This 'mine-to-market strategy' is -according to Muzo International-, the guarantee that a stone is from a particular mine. By issuing "authenticity certificates" the provenance from the Muzo mine is confirmed. The certificate details the carat weight, Muzo origin, down to the exact mining locality, and the absence of any resin treatment; the certificate guarantees origin, quality, and ethical production (→ *"branding")*.

In June 2008, Gemfields acquired the renowned Kagem Emerald Mine in Zambia, the largest emerald mine in Africa and one of the most sophisticated gemstone mining operations in the world. Gemfields Company is also applying a 'Mine-to-market model' for the production of their Zambian mines (mainly the Kagem mine). Each "Gemfields Emerald" is supposed to come with a certificate of authenticity, an encoded mark and the assurance that you can trace its origins from source to stores. 'Certificates of authenticity' confirm the origin from the Gemfield mines (→ *"branding")*. "Certificates of authenticity" are issued by mining companies (e.g. Gemfields or Muzo International) to guaranty the authenticity of a gemstone originating from a specific geographic location (mining region or even mines). On the other hand, "geographic origin reports" are issued by gemological laboratories. The geographic origin given in such reports represents the opinion of the issuing laboratory regarding the provenance of the exam-

ined gemstone. The given result is based on the know how and the experience of the gem lab, it is not a guaranty for the indicated geographic origin.

References

Angarita, L.G., 2014. Colombia strengthens emerald mine to market regulations. InColor, Summer 2014, 25-26.

GIA, 2014. http://www.gia.edu/gia-news-research-nigerian-source-blue-sapphire.

Muzo emerald. (www.muzoemerald.com).

Opalinda, 2010. http://www.opalinda.com/index.php?option=com_content&view=article&id=77:wegel-tenanovember2010&catid=18:activefilesopalinda.

Shor, R., Weldon, R., 2010. An era of sweeping change in diamond and colored stone production and markets. Gems & Gemology, 46(3), 166-185.

The present situation of freshwater pearls from Wisconsin

Elisabeth Strack

Gemmologisches Institut Hamburg, Hamburg, Germany; info@strack-gih.de

Keywords American freshwater pearls, pearl rush, Wisconsin, Sugar River, Albany

Introduction

In 1857, the discovery of pearls in mussels from Notch Brook in New Jersey started a frenetic search for pearls that was later called the first American pearl rush.It concentrated on Pennsylvania, New York and the New England States. From 1878 onwards, a second pearl rush followed in Ohio, Kentucky, Tennessee and Alabama (Kunz & Stevenson, 1908).

In August 1889, Wisconsin entered the scene when a pearl was found in the Sugar River that flows through the middle of Albany, a small town with about 800 inhabitants south of Madison.It created the Wisconsin pearl rush that was in the same year followed by findings in the Pecatonica and the Rock River and had by 1890 spread over to 23 communities. They included places like La Crosse and Prairie du Chien on the Mississippi River and places in bordering states like Minnesosta, Iowa and Illinois. Buyers came from Chicago,New York and Paris.Within a year of the discovery, pearls worth $ 300.000 had been sold in Albany alone. Inspite of this figure, the success rate of about ten thousand mussels yielding one pearl of marketable quality was in reality low (Johnson, 2012). The sole criterium for evaluation was if and in how far the pearls resembled oriental pearls.

The mother-of-pearl industry that emerged in the decades after 1891 led to the search of mussel shells by the ton and did severe damage to mussel populations. After 1900 pearls had become a bye-product of „clamming" as the search for shells was locally called or they were found by hobby fishers or villagers using the mussels for fish bait. Since 1996 all collecting of shells is forbidden, with the exception of a quota regulation for supply to the cultured pearl industry.

The present situation

Wisconsin pearls and pieces of pearl jewellery are kept in collections of the Wisconsin Historical Museum in Madison and in the Zoological department of the Milwaukee Public Museum in Milwaukee that houses also a collection of local shells.

A number of families in rural areas still owns jewellery with pearls that were found in the time of the pearl rush, a few of them are on loan at the museums just mentioned and also at the museum of the Albany Historical Society. Today, there is not more than a handful of people involved in selling local freshwater pearls or using them for making jewellery. They include two wholesale dealers, two jewellery stores and a designer-goldsmith. All pearls originate from before 1996. Dealers usually bought the pearls directly from the so-called clammers who would call on them. The word clammer" is derived from the word „clam" that is used in local slang for mussels. Dealers might also have visited clammers in their tents along the rivers and jewellery stores would also have bought from clammers or their family descendants. Most pearls available today originate thus from the decades after World War II, but going as far back as the 1930s (Swan, 2008).Occasionally,pearls are offered for sale by hobby fishermen who collected them when a quota of 50 mus- sels per day was still allowed before fishing was banned in 1996 (Johnson, 2012).

The pearl-producing mussels

There are no production figures or records available and it cannot be said when and where most pearls have been found. It can also not be said from which species of musssels they came from as no records were kept. From about 300 species of freshwater mussels occuring in the United States, about 50 were regarded producing pearls regularly but in Wisconsin and neighbouring states the number may have been limited to under 20 species (Strack, 2006 and information made available at the pearl exhibition of the Milwaukee Public Museum that the author visited in 2008). A few species excelled. In Lake Pepin in the Mississippi area (situated in Minnesota, bordering on Wisconsin), the so - called Three Ridge (*Amblema plicata*) and the Washboard (*Megalonaias gigantea*) dominated (Swan, 2008)while in the Sugar River it was the Mucket (*Lampsilis carinata*)and in the Wisconsin River the Black Sandshell (*Ligumia recta*), (Pluth, 2014).

The pearls

It can probably be estimated that the total number of pearls available in Wisconsin today does not go above ca. 2000 pieces of which about 60 - 70 per cent are of poor quality. The remaining 30 – 40 per cent are made up of commercial qualities and probably not more than 5 per cent are of good qualities while only a few select pearls are of fine quality. Quality distribution reflects the overall sitution on the natural pearl market.

Sizes vary from a few millimeters (comparable to seed pearls)and go up to 15mm,some pearls may attain a length of up to 20mm. Round or near round shapes are extremely rare . The good qualities usually have off-round but symmetrical shapes with smooth surfaces and few blemishes. The majority of pearls have baroque shapes with irregular surfaces that can attain a rosebud or strawberry pattern. Wing shapes are also to be found (Figures 1-4).

Most pearls encountered are white but colours occur. The pre-dominant colour is pink, it varies in hue from light pink to deep purplish pink. Pink is followed by so-called metallic colours that show a combination of pink,blue and green overtones, combined with a pronounced, rather metallic lustre (Figure 1 and 3).

Figure 1

Figure 2

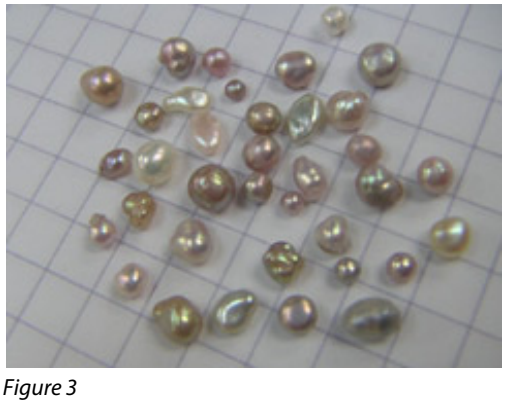

Figure 3

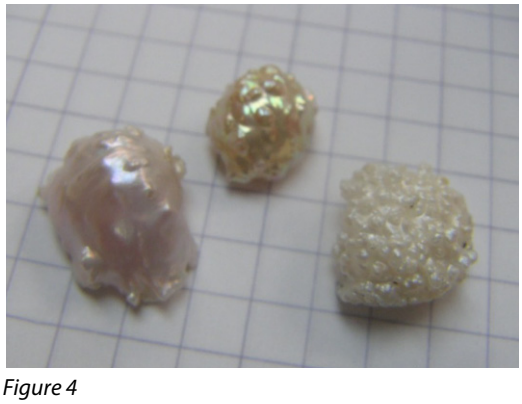

Figure 4

Figures 1-4. Wisconsin pearls in sizes of up to 15mm in length, showing characteristic shapes, colours and surfaces. Courtesy: Hanna Cook Wallace, Madison.

Testing results for a Wisconsin pearl necklace

At present, there are only two necklaces of Wisconsin pearls available of which one was tested by standard gemmological methods, Raman spectroscopy and by using micro-focus radiography. The necklace is shown in Figure 5. Microscopic examination revealed a pattern of elevated surface irregularities. Fluorescence under long wave ultra violet light (366nm) is light blue and it is weaker under 254nm.The presence of manganese, an indication of freshwater origin, was tested by using the Merck manganese test for random checking. Raman spectroscopy, by applying the Gem Ram/Gem Expert system, was used to confirmed that the outer layers of the pearls are made up of aragonite. Further, the necklace was submitted to micro-focus radiography. The radiogram revealed a remarkable uniform picture with few indications of organic matter that appear dark on the radiogram (Figure 6).

Figure 5. Necklace with 59 Wisconsin freshwater pearls, 4.4 – 10mm. Private ownership.

Figure 6. Radiogram (micro-focus radiography) of the necklace shown in Fig. 5. YXLON, Hamburg.

Conclusion

Wisconsin freshwater pearls, apart of being exhibited at local museums, are still available with a few local dealers and jewellers. Stocks originate from the decades before 1996 (the year in which fishing was banned), going back as far as the 1930s. Quality distribution equals other pearl sources, with only about 5 per cent being of good and a few select pearls being of fine qualities. Sizes can go above 15mm, baroque shapes dominate over rounded or symmetrical shapes and white colours dominate over fancy colours with pronounced pink, purple, blue and green hues. The latter often show a metallic lustre. Only two necklaces of Wisconsin origin have become known so far, of which one was tested by both standard gemmological methods and micro-focus radiography, allowing to determine a natural freshwater origin.

References

Johnson, G., 2012. The American Pearl Rush - Its Wisconsin Beginnings. Wisconsin Magazine of History, Spring 2012, Wisconsin Historical Society, Madison, 2-15.

Kunz, G.F., Stevenson, C.H., 1908. The Book of the Pearl. The Century Co., New York.

Pluth, C., 2014. Personal Communication, Madison, July 2014.

Strack, E., 2006. Pearls. Rühle-Diebener-Verlag GmbH, Stuttgart, 696 pp.

Swan, S., 2008. Personal Communication, Lake City, July 2008.

X-ray phase contrast and X-ray scattering images of pearls

Michael S. Krzemnicki[1], Vincent Revol[2], Carina Hanser[3], Laurent Cartier[1], Henry A. Hänni[1]

[1]Swiss Gemmological Institute SSEF; michael.krzemnicki@ssef.ch
[2]CSEM Centre Suisse d'Electronique et Microtechnique, SA, Alpnach, Switzerland
[3]Institute of Earth and Environmental Sciences, University of Freiburg, Germany

Keywords X-ray radiography, X-ray phase contrast, X-ray scattering, tomography, pearl structures

Introduction

The separation of natural pearls from cultured pearls is mainly based on the analysis and observation of their internal structures. Due to their value and their importance as a cultural and even archaeological heritage, it is absolutely mandatory that such testing is non-destructive. Traditionally, pearl testing is mainly based on X-ray radiography (Anderson 1931, Strack 2006, Sturman 2009), visualizing slight variations in X-ray absorption within a pearl. These variations are linked to the presence, concentration, and orientation of organic matter or voids within the calcium carbonate pearl matrix. In recent years, X-ray microtomography (Xray-µCT) has strongly contributed to a better understanding of the spatial distribution of such internal features (Wehrmeister et al. 2008, Krzemnicki et al. 2010). In the present study, we have investigated the potential of X-ray phase contrast and X-ray scattering as new and promising complementary methods for pearl analysis.

Instrumentation and samples

Conventional X-ray imaging (radiography, CT scans) relies on the absorption of X-rays (attenuation) when transmitted through a sample material but does not take into account the phase shift of the X-ray beam caused by the sample. One of the main drawbacks in conventional X-ray imaging is the limited possibility to increase the absorption contrast, especially for materials of similar absorption properties (e.g. biological samples) (Zhu et al. 2010).

Although widely used in gemmological laboratories, X-ray radiography has a number of limiting factors due to instrument parameters (e.g. focal size of the X-ray tube), analytical geometry (X-ray exposure is cone-shaped, resulting in lateral geometrical distortions of any 3D-object on the detector) and dynamic range and resolution of detectors (or X-ray films). But the most limiting factors are intrinsic properties of the pearl, such as its spherical geometry and thus variable path length (and attenuation) of the transmitted X-rays, and the tiny dimension and geometric orientation of internal structures (e.g. organic matter in the centre of the pearl).

By using a combination of gratings it is possible to build an X-ray interferometer and obtain X-ray phase contrast images, for which the beam phase shift is transformed into intensity variations, which are then recorded by a detector. Phase contrast X-ray imaging substantially improves contrast information compared to conventional attenuation-based methods. Especially for biological samples (e.g. tissues) made up of low-Z elements, the phase contrast effect is much more pronounced than the X-ray attenuation (Zhu et al. 2010).

Based on ground-breaking research on synchrotron X-ray interferometry by research groups at the Paul Scherrer Institute (PSI) in Switzerland and the University of Tokyo (David et al. 2002**,** Momose et al. 2003), Pfeiffer et al. (2006) were able to transfer the grating-based method to conventional laboratory X-ray tubes. The same research group developed an additional imaging method, using the X-ray signal scattered at microstructures of the sample (Pfeiffer et al. 2008).

By using an experiment setup at the Centre Suisse d'Electronique et Microtechnique (CSEM) (Revol et al., 2011) we were able to simultaneously register conventional X-ray absorption, X-ray phase contrast, and X-ray scattering images of numerous natural and cultured pearl samples. Not only was it possible to analyse with our setup single loose pearls, but also pearls strung on a strand and to display such a strand in one image. For our study, we used the following samples: natural pearls from *Pinctada radiata* and *Pinctada maxima*, beaded cultured pearls from *Pinctada margaritifera* and *Pinctada fucata,* Tokki cultured pearls (Krzemnicki et al. 2011) from *Pinctada margaritifera*, beadless cultured pearls from *Hyriopsis cumingii*, and Keshi cultured pearls (beadless) from *Pinctada maxima* and *margaritifera*.

Furthermore, a natural pearl from *Pinctada maxima* from Australia was selected to register absorption, phase contrast and scattering CT scans (microtomography).

Results and discussion

Our preliminary results show that both, X-ray phase contrast and X-ray scattering are adding valuable information to conventional X-ray absorption when analysing the internal structures of pearls.

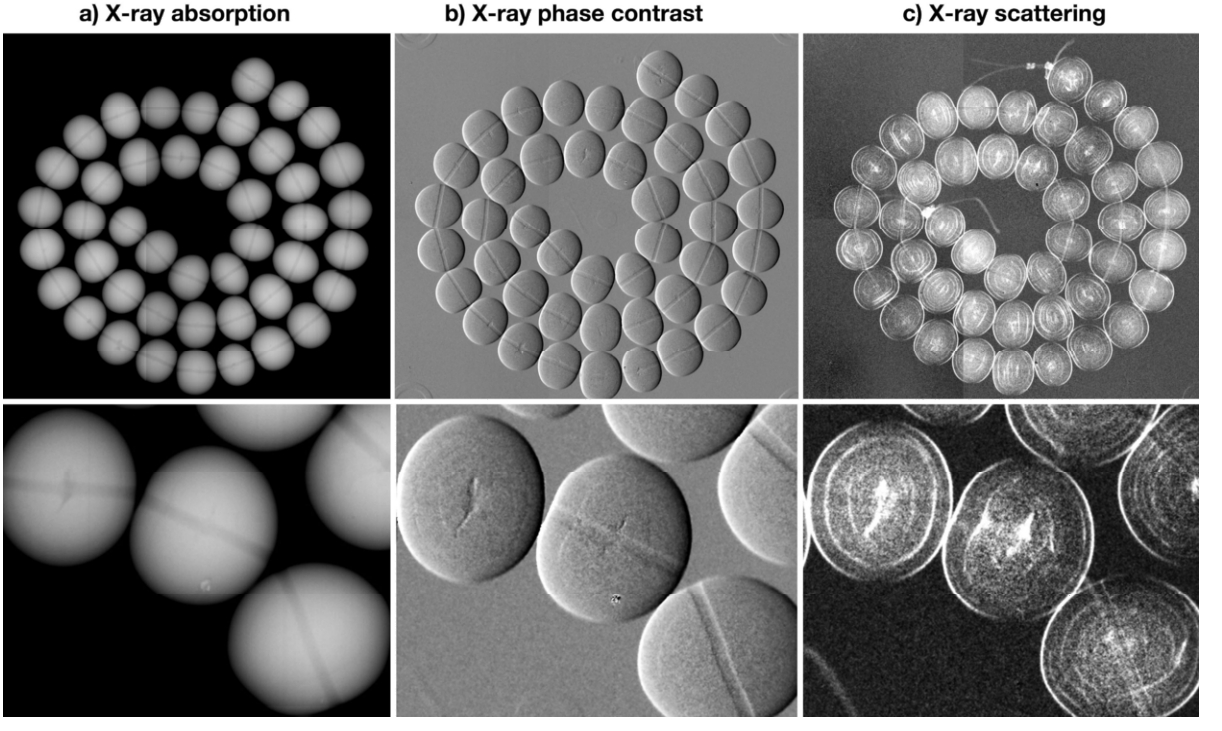

Figure 1. Comparison of a) X-ray absorption (attenuation), b) X-ray phase contrast, and c) X-ray scattering images of a strand of 44 beadless freshwater cultured pearls from China (Hyriopsis cumingii) as the whole necklace and magnified.

With our setup with a large focal spot size (1x1 mm^2), the absorption radiographies showed a rather low contrast, compared to conventional digital radiography using a microfocus X-ray tube. So when testing a strand of beadless Chinese freshwater cultured pearls from *Hyriopsis cumingii*, their characteristic comma-shaped central structure rich in organic matter (Strack 2006) was hardly visible (Figure 1a). Even though the absorption gradient between the organic matter (conchiolin) in this central structure and the surrounding calcium carbonate is very pronounced. Apart from the instrumental limitations with our setup, this is also due to the nearly two-dimensional geometry of this structure and to its random orientation within the centre of these cultured pearls in respect to the X-ray beam.

The phase contrast image of the same strand reveals a virtual morphological pattern of these pearls superposed by a relief-shading effect at the outline of the pearls and along the drill hole (Figure 1b). The very fine onion-like growth layers of these beadless cultured pearls are hardly discernible, in contrast to the partly marked visibility of their characteristic central feature.

However, the most detailed information is gained from the X-ray scattering image (Figure 1c), which in fact reveals not only the multi-layered onion-like growth structure of these cultured pearls, but also in great detail the complex geometry of the characteristic central structure of these beadless cultured pearls. Although a number of image processing software is available, superposing the different X-ray images and adding colour conversions, already a simple greyscale inversion is very helpful (Figure 2). It readily enables a laboratory gemmologist to compare an X-ray scattering image with a conventional absorption radiograph, in which less dense and organic rich zones are darker compared to nacre.

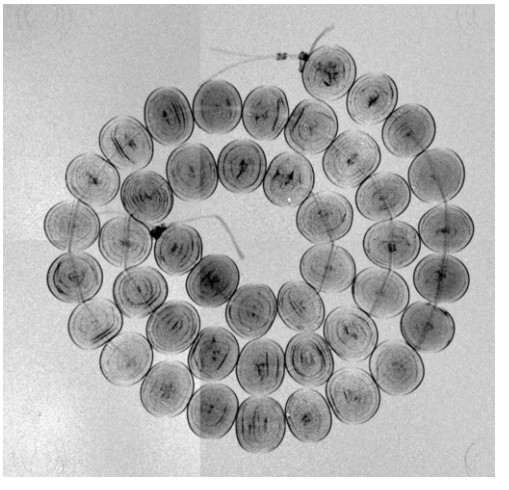

Figure 2. Simple inversion of the X-ray scattering image results makes comparison with conventional X-ray absorption images more easy.

In analogy to the above stated observations, the X-ray images of the other tested pearls (natural and cultured) revealed very similar results. Again, the X-ray scattering images were by far the most promising in terms of visualisation of internal structures of the studied pearls.

Finally, a natural pearl from *Pinctada maxima* (7.58 ct) was chosen for CT scans, using X-ray absorption, phase contrast and scattering. Compared to a conventional CT scan using a microfocus X-ray tube, this first attempt is still rather unsatisfactory due to its low resolution and rather high noise signal. Nevertheless the obtained X-ray scattering CT data was rendered into a three-dimensional virtual model of this natural pearl, enabling us to see its internal structures during rotation.

Conclusions

Preliminary results of our study on the application of new X-ray imaging methods using phase contrast and X-ray scattering show that both methods, but particularly X-ray scattering, add valuable information to conventional absorption radiography.

Despite the current drawbacks at this level of research, we presume that these new X-ray imaging techniques - including CT scans based on X-ray scattering – will become important for pearl analysis in the near future when commercial instruments become available.

Acknowledgements

The authors would like to thank the following individuals for supplying pearl samples for this study: Andy Muller, Hinata Trading Ltd., Kobe, Japan, and Michael and Peter Bracher, Paspaley, Darwin and Sydney, Australia, Thomas Frieden, Frieden AG, Thun, Switzerland, and Ronny Totah, Horowitz & Totah, Geneva, Switzerland.

References

Anderson, B. W., 1931. The use of X-rays in the study of pearls. British Journal of Radiology, 5, 57-64.

David, C., Nöhammer, B., Solak, H.H., Ziegler, E., 2002. Differential X-ray phase contrast imaging using a shear interferometer. Applied Phys. Letter, 81, 3287. http://dx.doi.org/10.1063/1.1516611.

Krzemnicki, M.S., Friess, S.D., Chalus, P., Hänni, H.A., Karampelas, S., 2010. X-ray computed microtomography: Distinguishing natural pearls from beaded and non-beaded cultured pearls. Gems & Gemology, 46 (2), 128–134.

Krzemnicki, M.S., Mueller, A. , Hänni, H.A., Gut, H-P., Düggelin, M. 2011. Tokki pearls: additional cultured pearls forming during pearl cultivation: external and internal structures. Abstract volume of the 32nd IGC Conference, 56-58. http://www.igc-gemmology.org/#/abstract-proceedings/4540447685.

Momose, A., Kawamoto, S., Koyama, I., Hamaishi, Y., Takai, K., Suzuki, Y., 2003 Demonstration of X-ray Talbot interferometry. Japanese Journal of Applied Physics. 42 (part 2, No. 7B), L866 – L868. http://dx.doi.org/10.1143/JJAP.42.L866.

Pfeiffer, F., Weitkamp, T., Bunk, O., David, C., 2006. Phase retrieval and differential phase contrast imaging with low-brilliance X-ray sources. Nature Physics, 2, 258 - 261. doi:10.1038/nphys265.

Pfeiffer, F., Bech, M., Bunk, O., Kraft, P., Eikenberry, E.F., Brönnimann, C., Grünzweig, C., David, C., 2008. Hard-X-ray dark-field imaging using a grating interferometer. Nature Materials, 7, 134-137. doi:10.1038/nmat2096.

Revol, V., Jerjen, I., Kottler, C., Schütz, P., Kaufmann, R., Lüthi, T., Sennhauser, U., Straumann, U., Urban, C.. Sub-pixel porosity revealed by X-ray scatter dark field imaging. Journal of Applied Physics, 110, 44912, 1-5. doi:10.1063/1.3624592.

Strack, E., 2006. Pearls. Rühle-Diebener Verlag, 707 pp. ISBN: 978-3981084801.

Sturman, N., 2009. The microradiographic structures of non-bead cultured pearls. www.giathai.net/pdf/The_ Microradiographic_structures_in_ NBCP.pdf (accessed: April 2015).

Wehrmeister, U., Goetz, H., Jacob, D.E., Soldati, A.L., Xu, W., Duschner, H., Hofmeister, W., 2008. Visualization of the internal structure of freshwater cultured pearls by computerized X-ray microtomography. Journal of Gemmology, 32 (1–2), 15–21.

Zhu, P., Zhang, K., Wang, Z., Liu, Y., Liu, X., Wu, Z., McDonald, S.A., Marone, F., Stampanoni, M., 2010. Low dose, simple and fast grating-based X-ray phase-contrast imaging. Proceedings of the National Academy of Scicene (USA) PNAS, 107(31), 13576-13581.

X-ray computed microtomography (μ-CT) structures of known natural and non-bead cultured *Pinctada maxima* pearls

Nick Sturman, Artitaya Homkrajae, Areeya Manustrong, Nanthaporn Somsa-ard

GIA Laboratory, Bangkok, Thailand; nsturman@gia.edu

Keywords Identification, μ-CT, Natural pearls, Non-bead cultured pearls, GIA, *Pinctada maxima,* Structure

Introduction

In the past pearl identification focused on the experience of the people undertaking the work together with the analysis of some known samples to gain an idea of what structures were to be expected in pearls of different types. However, the vast majority of opinions on client's pearls was, and to a certain extent continues to be, based on the experience of those undertaking the work and their recollection of what they consider to be natural or non-bead cultured, amongst other, structures. We are in the process of building a database of known pearl structures from specific sources to use as references for direct comparison during the examination of pearls submitted for identification, therefore eliminating the "subjectivity" and moving to a more fact driven form of analysis. Some of the structures encountered in these known pearls, if examined "blind" in laboratory conditions, would quite likely lead to incorrect identification calls. Locations visited to source samples include Broome & Darwin (Australia; Scarratt et al., 2012), Lombok (Indonesia) and The Mergui Archipelago (Myanmar).

Sample details

All the samples studied, or being studied, were obtained directly from molluscs by GIA staff members who recorded their recovery using digital images and/or video. The largest group of pearls collected was on a ten-day trip off the coast of Broome when 776 pearls of various sizes were recovered from 20,488 wild *Pinctada maxima* shell being fished for their mother-of-pearl only. The pearls were simply a by-product of the main purpose of the trip, however their analysis and the data recorded for them have proved invaluable. The work in Darwin, Lombok and The Mergui Archipelago has proved revealing on the non-bead cultured pearl front.

μ-CT results

While most pearl testers use microradiography (film or real-time) to reach their conclusions the use of μCT units is becoming more and more prevalent as time passes owing to the need to interpret more challenging structures (Wehrmeister et al., 2008; Karampelas et al., 2010; Krzemnicki et al., 2010). It is also particularly helpful when conducting research work due to the more detailed results obtained. The results of the μ-CT analysis for the natural pearls recovered from the wild shell in this study revealed a wide range of structures as would be expected for a completely random sampling made in the field. The majority showed "tight" structure (no clear structure to just a weak arc or two), while others exhibited more obvious arcs or concentric features (figure 1); small dark "nuclei/cores"; larger "meaty" conchiolin rich features; or a range of unusual features (figure 2) that could be interpreted in different ways by different gemologist/experts. The non-bead cultured pearls in contrast either showed characteristic void-like features (figure 3) or more linear and/or conchiolin like structures. Some of the latter also, like their natural counterparts, revealed uncharacteristic structures that could, and no doubt would, be challenging to correctly identify. Some of the non-bead cultured pearls examined were removed from wild shells

that had been recovered from the sea-bed and transported to farms for later operation. These wild shells therefore produced cultured pearls from their gonads post operation.

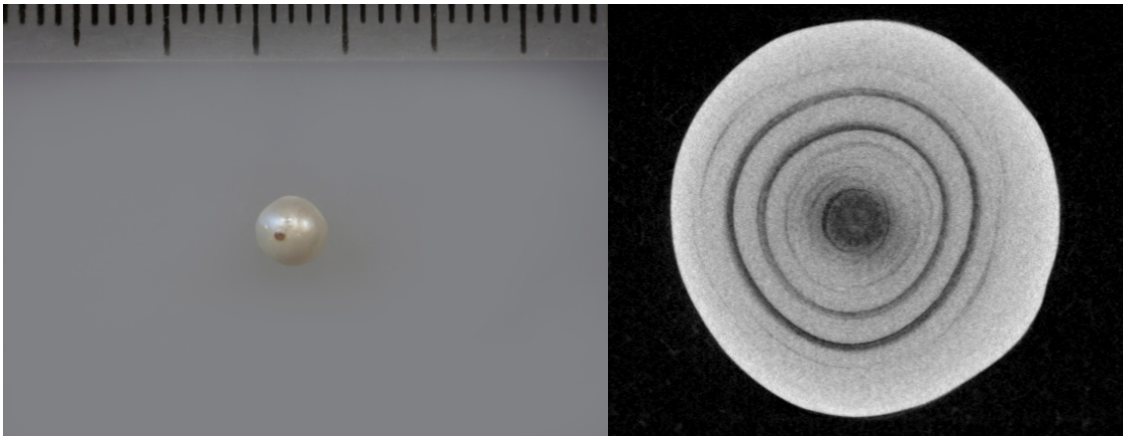

Figure 1. A natural pearl weighing 0.37 carat recovered directly from a wild Pinctada maxima shell (left) and a μ-CT slice of its straightforward internal structure (right). Photomacrography: Sasithorn Engniwat.

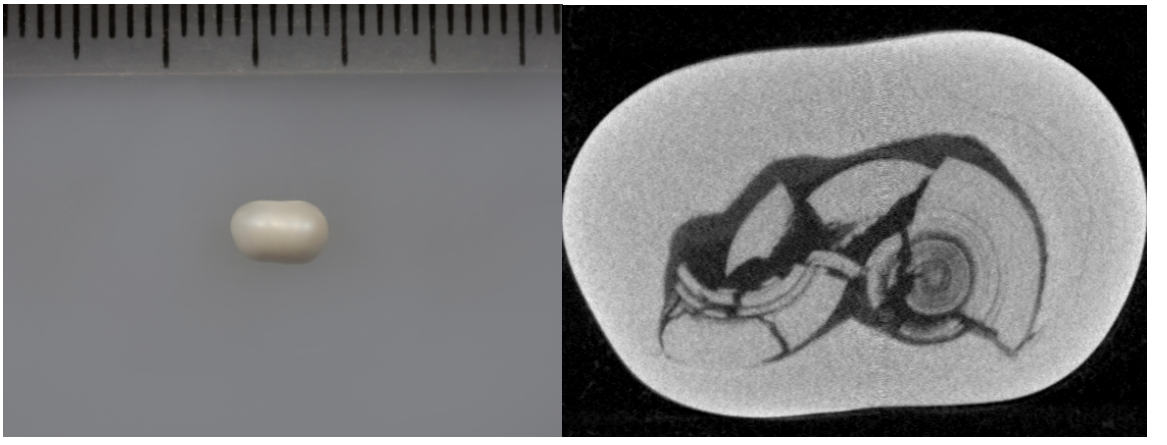

Figure 2. A natural pearl weighing 0.57 carat recovered directly from a wild Pinctada maxima shell (left) and a μ-CT slice of its unusual internal structure (right). Photomacrography: Sasithorn Engniwat.

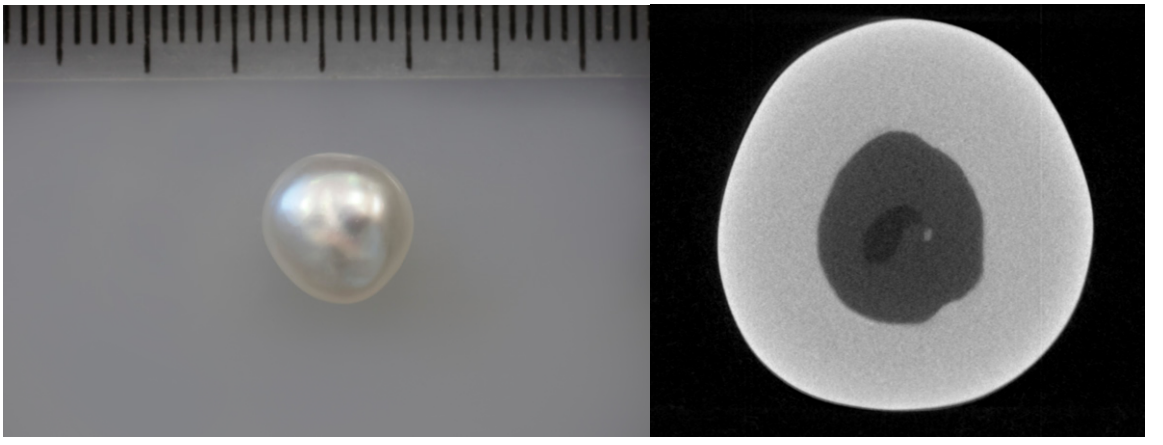

Figure 3. A non-bead cultured pearl weighing 3.35 carats (left) recovered directly from a wild but operated Pinctada maxima shell and a µ-CT slice of its internal structure (right). Photomacrography: Sasithorn Engniwat.

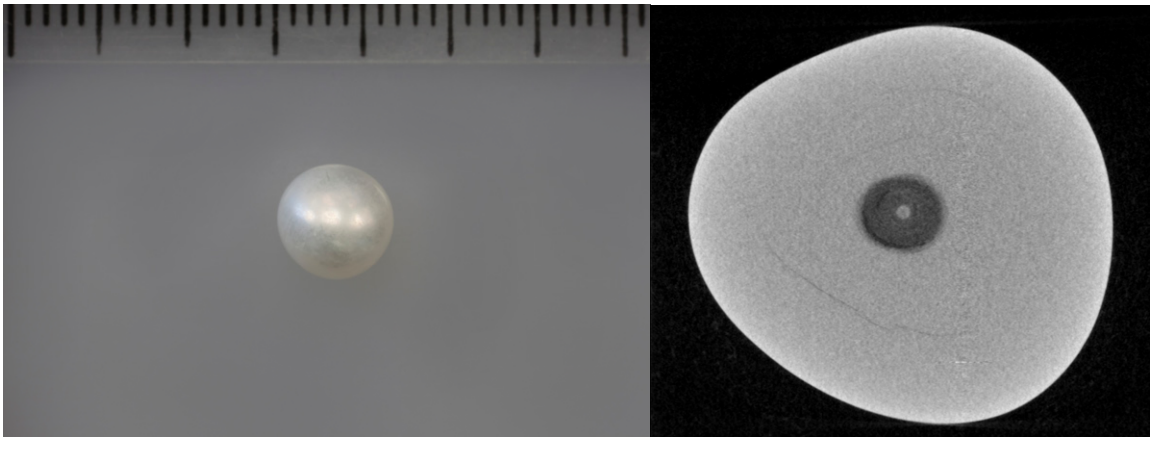

Figure 4. A non-bead cultured pearl weighing 1.80 carats (left) recovered directly from a wild but operated Pinctada maxima shell and a µ-CT slice of its unusual internal structure (right). Photomacrography: Sasithorn Engniwat.

Conclusion

Pearl identification can be an unquestionably challenging field of gemology (Sturman, 2009), even to those experienced practitioners with multiple years of hands-on practical skill. While most pearl testers would reach the same conclusions on the identification of pearls, providing the same equipment was used to obtain the results, there are still numerous examples in the market where the interpretation of their internal structures leads to differences of opinion. By collecting samples in the "field", recording the exact locations of the majority of pearls within their hosts at the time of removal, and subsequently obtaining both real-time and µ-CT X-ray data on their structures, we are in the process of building a comprehensive database of known structures to use when determining the identification of the more unusual/challenging pearls submitted.

References

Karampelas, S., Michel, J., Zheng-Cui, M., Schwarz J-O., Enzmann, F., Fritsch, E., Leu, L., Krzemnicki, M. 2010. X-ray computed microtomography applied to pearls: Methodology, advantages, and limitations. Gems & Gemology, 46 (2), pp. 122-127.

Krzemnicki, M., Friess, S., Chalus, P., Hänni, H., Karampelas, S. 2010. X-ray computed microtomography: Distinguishing natural pearls from beaded and non-beaded cultured pearls. Gems & Gemology, 46 (2), pp. 128-134.

Scarratt, K., Bracher, P., Bracher, M., Attawi, A., Safar, A., Saeseaw, S., Homkrajae, A., Sturman., N. 2012. Natural pearls from Australian Pinctada maxima. Gems & Gemology, 48 (4), pp. 236-261.

Sturman, N. 2009. The microradiographic structures of non-bead cultured pearls. GIA Thailand, Bangkok, November 21, www.giathai.net/pdf/The_microradiographic_structures_of_NBCP.pdf

Wehrmeister, U., Goetz, H., Jacob, D., Soldati, A., Xu, W., Duschner, H., Hofmeister, W. 2008. Visualization of the internal structures of cultured pearls by computerized X-ray microtomography. The Journal of Gemmology, 31 (1/2), pp. 15-21.

Observations on natural non-nacreous pearls reportedly from Tridacna (clam) species

Sutas Singbamroong, Nazar Ahmed, Ayesha Rashid Ahmed, Mohamed Karam, Ghaliah Hassan, Sameera Mohammed, Nahla Al Muhairi

Gemstone and Precious Metal Laboratory Unit, Dubai Central Laboratory Department, Dubai, United Arab Emirates; sutas.singbamroong@gmail.com

Keywords Natural pearl, Non-nacreous, Tridacna, clam

Natural non-nacreous pearls from various clam species are more available in the market nowadays. Natural non-nacreous pearls from Tridacna species are among them. Bonhams's auctioned recently many pieces of white Tridacna pearls with fine flame structure for a price above US$ 1000 per carat (Bonhams, 2014).

Recently, The Gemstone Laboratory of Dubai Central Laboratory (DCL) received over 300 pearls submitted as natural non-nacreous pearls from Tridacna species (figure 1) such as Tridacna gigas, Tridacna derasa, Tridacna crocea, Tridacna Squamoma, Tridacna maxima. Mr. Umit Koruturk, director of Australian Pure Pearls Trading EST, who is the owner, stated that he has been collecting over 5,000 pieces of this type of pearls from Indonesia and Philippines during the past 6 years.

Figure 1. Natural non-nacreous pearls reportedly from Tridacna (giant clam) species. The longest pearl shown approximately 4 cm. Photo by Sutas Singbamroong.

Tridacna is a genus of large saltwater clams, marine bivalve mollusks in the subfamily Tridacninae. They inhabit shallow waters of coral reefs in warm seas of the Indo-Pacific region. They commonly live in symbiosis with photosynthetic algae, which cause their mantle lips to exhibit an attractive bright, colored pattern (Huelsken et al., 2013).

The Tridacna pearl samples exhibited an interesting variety of shapes: near-round, oval, drop, button, elongated or tooth-like, circled, twinned, aggregated and baroque with white, off-white, grey and uneven light yellow coloration

of semi-translucent to opaque (see again figure 1). The surfaces exhibited porcelaneous appearance with fine flame-like structure, which is finer than the structure of conch and Melo pearls (Hänni, 2010 and Strack, 2006). Many of the flames had distinct shimmering iridescent colors (figure 2). The flame structure varies from a tiny or classic flame type to the patchy or "leopard" flame (figure 3).

Figure 2. Tridacna pearls exhibit distinct shimmering iridescent colors. Photo by Sutas Singbamroong.

The size of the pearls ranges from a few millimeters to approximately five centimeters. The specific gravity of most samples was determined between 2.81 and 2.85, although a few lower values between 2.63 and 2.67 had been recorded, which can be attributed to organic matter contained in those pearls. Long-wave UV produced a very weak to moderate chalky blue emission, weaker in short-wave UV, even inert.

Figure 3. The patchy "leopard" flame structure (left) and the tiny classic flame structure (right). Photo by Sutas Singbamroong.

Microradiography revealed opaque internal structure in most of the samples. However, some showed prominent void-like structure of organic matter, which correlates with a lower SG (figure 4).

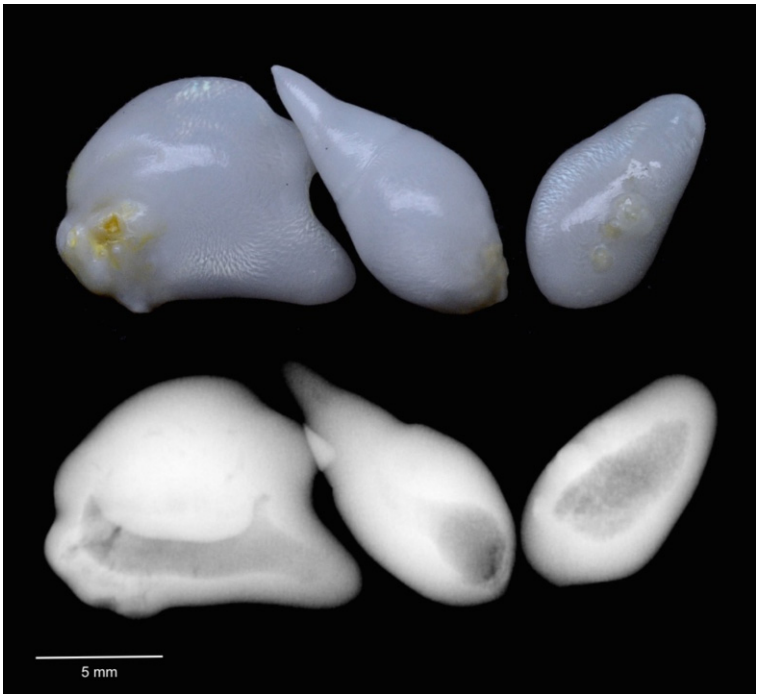

Figure 4. Natural non-nacreous pearls (upper) showed void-like structure in X-ray microradiographs (lower). Composite photo by Sutas Singbamroong.

Raman spectra showed that the pearls were composed of aragonite. The EDXRF results revealed low levels of Mn, consistent with pearls from a saltwater environment, which is also confirmed by the absence of X-ray luminescence.

These examples were noteworthy for their shapes, distinct shimmering iridescent flame structure, interesting different flame types, and their internal structure when observed with microradiography.

References

Bonhams, 2014. Non-nacreous natural pearl-"A Giant Clam Pearl", http://www.bonhams.com/auctions/21819/lot/1222 (date accessed: 04/05/15).

Hänni, H.A., 2010. Explaining the flame structure of non-nacreous pearls. Australian Gemmologist, 24(4), 85-88.

Huelsken, T., Keyse, J., Liggins, L., Penny, S., Treml, E.A., Riginos, C., 2013. A Novel Widespread Cryptic Species and Phylogeographic Patterns within Several Giant Clam Species (Cardiidae:Tridacna) from the Indo-Pacific Ocean. Plos One, DOI: 10.1371/journal.pone.0080858.

Strack, E., 2006. Pearls. Rühle-Diebener Verlag GmbH, Stuttgart, 696 pp.

The scientific importance of gem zircon as analytical reference materials

Lutz Nasdala[1], Chutimun Chanmuang[2], Tobias Häger[3], Wolfgang Hofmeister[3], Allen K. Kennedy[4], Peter W. Reiners[5], Tamás Váczi[6], John W. Valley[7], Bhuwadol Wanthanachaisaeng[2], Wu Fuyuan[8], Manuela Zeug[1], E. Gamini Zoysa[9]

[1] Institut für Mineralogie und Kristallographie, University of Vienna, 1090 Wien, Austria; lutz.nasdala@univie.ac.at
[2] Faculty of Gems, Burapha University, Chanthaburi Campus, Chanthaburi, 22170, Thailand
[3] Institut für Geowissenschaften, Johannes Gutenberg-Universität, 55099 Mainz, Germany
[4] Department of Imaging and Applied Physics, Curtin University of Technology, Bentley, 6102, Australia
[5] Department of Geosciences, University of Arizona, Tucson, AZ 85721, U.S.A.
[6] Department of Mineralogy, Eötvös Loránd University, H-1117 Budapest, Hungary
[7] Department of Geoscience, University of Wisconsin, Madison, WI 53706, U.S.A.
[8] Institute of Geology and Geophysics, Chinese Academy of Sciences, Beijing, 100029, PR China
[9] Mincraft Company, Mount Lavinia, Sri Lanka

Keywords Reference materials, Zircon, U–Pb geochronology, Ion microprobe, SIMS, Oxygen isotopes

Besides being objects of beauty, attractiveness and commercial value, gemstones have also become increasingly valuable in a different field: Tiny fractions of the highest-quality gems are used as reference materials in the microprobe analysis of geological materials. This is particularly the case for gem zircon, a tetragonal orthosilicate with chemical formula $ZrSiO_4$. This mineral can incorporate minute amounts of uranium and thorium (and other elements) within its lattice. Over geological periods of time, the radionuclides, and their unstable daughter nuclei, decay to form radiogenic lead and helium. However, unlike many other U-bearing minerals, zircon mostly excludes the element lead during primary growth. As a consequence, the vast majority of Pb detected in a zircon is radiogenic in nature. This, and the remarkable ability of zircon to store the radiogenic Pb, makes it possible to determine with high accuracy a zircon's age from the observed ratios of radiogenic Pb and U isotopes. Analogously, (U–Th)/He gives a zircon's thermal history (Reiners et al., 2005) whereas stable-isotope analysis may provide valuable information on the formation milieu (Valley et al., 2005; Scherer et al., 2007; Liu et al., 2009).

Gem-quality zircon is used as reference material especially for micro-analysis techniques with particularly low demand of material, such as SIMS (secondary ion mass spectrometry). In SIMS analysis, a tiny amount of sample material (typically a shallow, round pit at the sample surface ca. $15 \times 15 \times 1$ μm^3 in size; see Fig. 1) is sputtered by a focused beam of oxygen ions, and secondary ions are focused and counted in a large-radius mass spectrometer. The determination of isotopic ratios in unknowns needs to be calibrated against results of analogous measurements of a calibrant (which can either be a natural reference or a synthetic standard). Tiny chips of well-characterized calibrants, typically 100 μm in size, are therefore included in epoxy mounts produced from unknowns for ion microprobe analysis. It is obvious that the reliability of any micro-scale analysis of U–Pb isotopic ratios of unknown zircon is controlled by the precision of alternating co-measurements of the calibrant material(s). Any calibrant therefore needs to be extremely well characterized, and it needs to be homogeneous (Pidgeon, 1997). The latter requirement arises from the necessity that each tiny particle of the reference must represent the chemical, physical and isotopic properties of the entire, pre-characterized bulk material. If, in contrast, references are used that show extensive internal variations in their chemical and structural composition, unwanted effects such as non-uniform ablation or sputter rates and matrix/charge effects need to be considered (for laser-ablation analysis discussed by Sláma et al., 2008). A homogeneous reference (such as M257 shown in Fig. 2; Nasdala et al., 2008) may also be used as elemental calibrant.

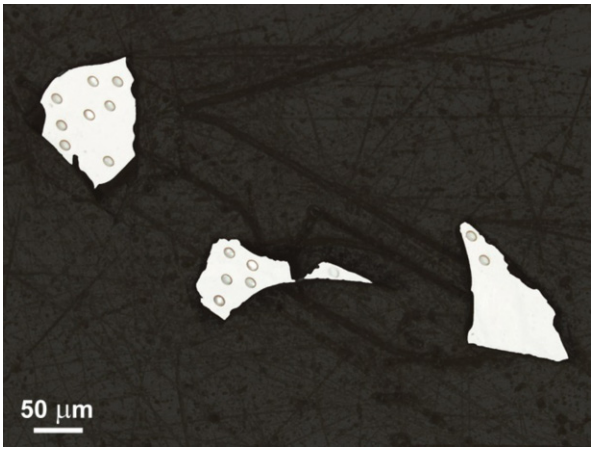

Figure 1. Photomicrograph of chips of reference CZ3 in a SHRIMP mount after analysis. The shallow, rounded pits are points of analysis done to calibrate results for unknowns in the same epoxy mount.

Finally, homogeneity of stable isotopes is needed if a particular reference is to be used in multi-technique analysis (i.e. U–Pb geochronology combined with oxygen or hafnium isotope analysis; Valley et al., 2005; Liu et al., 2009).

The worldwide need for highest-quality gem-zircon references as U–Pb calibrants has increased appreciably. Several new SIMS systems and laboratories – in particular SHRIMP (Australia Scientific Instruments Pty. Ltd.) and IMS 1270/1280 (Cameca SAS) – have been established in recent years. This generally positive development has however led to the situation that the current availability of calibrants hardly meets the needs. Their shortage is caused by the facts that (i) no synthesis technique is currently available that allows one to produce homogeneous U- and Pb-bearing zircon crystals, and (ii) glass standards cannot be used because of their different sputter behaviour under the oxygen-ion beam, compared to that of the unknowns to be analysed. For these reasons, well-performing synthetic standards for the U–Pb analysis of zircon are not readily available.

Figure 2. Zircon reference M257 (width 19 mm), a 25.7 ct stone from the Ratnapura, Sri Lanka, gem gravels.

Figure 3. A high-quality, cut zircon from Madagascar (127.5 ct) that appeared recently in the Sri Lankan market.

Consequently, high-quality natural references must be sought for. Besides the requirement for homogeneity discussed above, quality features needed include an undisturbed (i.e. concordant) U–Pb system. Only if no post-growth alteration or weathering has occurred, leaching of isotopes (especially Pb) and hence bias of analytical results is excluded. Also, any gem enhancement or other heat treatment must be excluded, because otherwise the U–Pb isotope system may be affected, and the radiogenic helium is likely to be lost (Reiners et al., 2005).

All of the arguments discussed above underline the need to seek homogeneous, concordant, untreated, large zircon gems, in order to find a suitable ion microprobe reference. The importance of a fairly large size is underlined by the consideration that calibration analyses to characterize the zircon reference, and intended distribution of multitudes of tiny chips to several laboratories, are possible only if a sufficient quantity of material is available. To give an example, reference CZ3, a 4.5 ct stone (Pidgeon, 1997), has been consumed after being used for more than ten years. The much larger reference M257 (Fig. 2) is currently used in the SHRIMP labs in Perth, Canberra, Beijing and St. Petersburg and at the NordSIM facility, Stockholm; it is expected to last several more years.

Also, a well-performing reference zircon should be relatively high in U and radiogenic Pb (whereas the concentration of common – i.e. non-radiogenic – Pb being should be close to zero). High concentrations of radiogenic Pb are advantageous because they result in high count rates and hence good counting statistics. The lead concentration of a given stone is of course difficult to ascertain in the sale; however a helpful parameter is its degree of radiation damage. This is because the formation of the radiogenic Pb correlates with the creation of damage. The structural state – that can be recognised from changes in optical parameters and decreased specific gravity – therefore provides a first estimate of a stone's chemical and isotopic composition (only if no heat treatment has been done). To provide an example, the high-quality stone shown in Fig. 3 is not of interest as potential SIMS reference in spite of its large size and homogeneity, because it is nearly perfectly crystalline (and hence it must be either low in U and Pb, or heated, or both). Too elevated levels of radiation damage, in contrast, affect negatively the performance of a zircon as SIMS reference: Matrix effects may occur under the ion beam and hence result in biased SIMS U–Pb results, and potential exchange of oxygen isotopes may result in a non-equilibrated state. The challenge is, consequently, to find large untreated, gem-quality stones that are neither too much nor too mildly radiation-damaged.

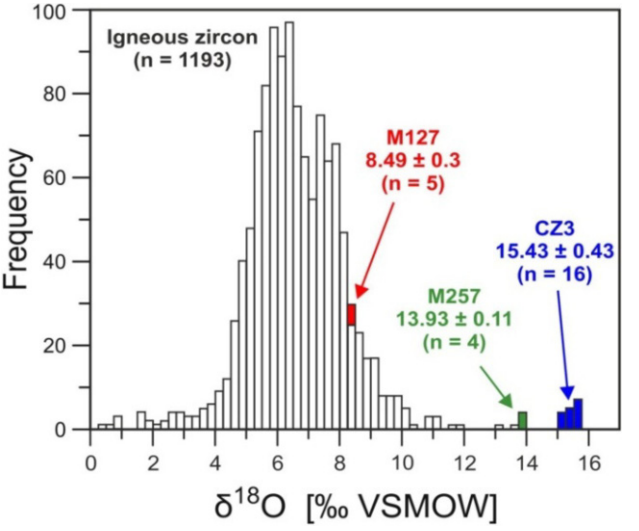

Figure 4. Plot of $\delta^{18}O$ data for the Sri Lankan gem-quality zircon references M127 (unpublished), M257 (Nasdala et al., 2008), and CZ3 (Cavosie et al., 2011) in comparison with those for igneous zircon from localities worldwide (Valley et al., 2005).

The essential requirements for SIMS references are often met by highest-quality zircon derived from gem gravels in the Ratnapura district (Dahanayake and Ranasinghe, 1985). This material is mostly unaltered and yields concordant Late-Precambrian to Cambrian U–Pb ages (570–520 Ma; Nasdala et al., 2004). Large, perfectly homogeneous stones (i.e. no internal variations in chemical, structural, and isotopic composition; no fractures and notable inclusions) are derived quite frequently. However, the primary source of these high-quality stones still remains unknown. The Ratnapura zircon typically shows igneous zoning (Chakoumakos et al., 1987). Some of the unzoned references were found to have $\delta^{18}O$ values that are clearly higher than what is typical of igneous zircon (Fig. 4). This suggests that such gems might be metamorphic, presumably originating from a marble or Ca-silicate skarn (Cavosie et al., 2011). It may be a worthwhile effort to search for their source rocks, if they should still exist.

Acknowledgments

This research project was partially funded by the European Commission through contract no. MEXC–CT–2005–024878, and the Austrian Science Fund (FWF) through grants P20028–N10 and P24448–N19 to L.N. Financial support by the Faculty of Geosciences, Geography and Astronomy, University of Vienna, is gratefully acknowledged.

References

Cavosie, A.J., Valley, J.W., Kita, N.T., Spicuzza, M.J., Ushikubo, T., Wilde, S.A., 2011. The origin of high $\delta^{18}O$ zircons: marbles, megacrysts, and metamorphism. Contributions to Mineralogy and Petrology, 162, 961–974.

Dahanayake, K., Ranasinghe, A.P., 1985. Geology and mineralogy of gemming terrains of Sri Lanka. Bulletin of the Geological Society of Finland, 57, 139–149.

Liu, D., Wilde, S.A., Wan, Y., Wang, S., Valley, J.W., Kita, N., Dong, C., Xie, H., Yang, C., Zhang, Y., Gao, L., 2009. Combined U–Pb, hafnium and oxygen isotope analysis of zircons from meta-igneous rocks in the southern North China Craton reveal multiple events in the Late Mesoarchean–Early Neoarchean. Chemical Geology, 261, 140–154.

Nasdala L., Reiners P.W., Garver J.I., Kennedy A.K., Stern R.A., Balan E., Wirth R. (2004). Incomplete retention of radiation damage in zircon from Sri Lanka. American Mineralogist, 89, 219–231.

Nasdala, L., Hofmeister, W., Norberg, N., Mattinson, J.M., Corfu, F., Dörr, W., Kamo, S.L., Kennedy, A.K., Kronz, A., Reiners, P.W., Frei, D., Košler, J., Wan, Y., Götze, J., Häger, T., Kröner, A., Valley, J.W., 2008. Zircon M257 – a homogeneous natural reference material for the ion microprobe U–Pb analysis of zircon. Geostandards and Geoanalytical Research, 32, 247–265.

Pidgeon, R.T., 1997. Gem zircon: a new role a standard for the measurement of geological time using ion microprobes (in German). Zeitschrift der Deutschen Gemmologischen Gesellschaft, 46/1, 21–28.

Reiners, P.W., 2005. Zircon (U-Th)/He thermochronometry. In P.W. Reiners, T.A. Ehlers, Eds., Thermochronology. Reviews in Mineralogy and Geochemistry, 58. Mineralogical Society of America, Washington, D.C., pp. 151–176.

Scherer, E.E., Whitehouse, M.J., Münker, C., 2007. Zircon as a monitor of crustal growth. Elements, 3, 19–27.

Sláma, J., Košler, J, Condon, D.J., Crowley, J.L., Gerdes, A., Hanchar, J.M., Horstwood, M.S.A., Morris, G.A., Nasdala, L., Norberg, N., Schaltegger, U., Tubrett, M.N., Whitehouse, M.J., 2008. Plešovice zircon – a new natural reference material for U-Pb and Hf isotopic microanalysis. Chemical Geology, 249, 1–35.

Valley, J.W., Lackey, J.S., Cavosie, A.J., Clechenko, C.C., Spicuzza, M.J., Basei, M.A.S., Bindeman, I.N., Ferreira, V.P., Sial, A.N., King, E.M., Peck, W.H., Sinha, A.K., Wei, C.S., 2005. 4.4 billion years of crustal maturation: oxygen isotope ratios of magmatic zircon. Contributions to Mineralogy and Petrology, 150, 561–580.

Modern mining methods for primary and secondary gem deposits in Mogok, Myanmar

Brendan M. Laurs

Editor-in-Chief, The Journal of Gemmology, Gem-A, Encinitas, CA 92024 USA; brendan@gem-a.com

Keywords Mogok, Myanmar, ruby, spinel, primary deposits, secondary deposits, mining

Introduction

The Mogok Stone Tract of central Myanmar has a long tradition of gem mining, exploiting both primary and secondary deposits. The main gems produced are ruby, sapphire, spinel, peridot, tourmaline and topaz, and the area is famous for producing some of the world's finest examples of many of these gem varieties—especially ruby. In December 2014, a team from Gem-A visited the Mogok area (for a general description of the trip, see Laurs, 2015). Guided by Federico Bärlocher, a gem dealer and collector from Switzerland, the group consisted of Gem-A CEO James Riley, trustee Jason Williams, and this author.

Mogok was closed to foreigners for decades until it was reopened in 2012; a special permit from the Burmese government is needed to visit there. The town revolves entirely around gem mining, and according to Bärlocher there are about half a million people directly affected by the area's 1,200 mines, which are situated in an area measuring 900 square miles (nearly 2,500 square kilometers).

To learn about the mining techniques that are currently used in the Mogok area, our team visited well-organized operations at both primary and secondary deposits that are mined for ruby, spinel, and other gems.

Mogok pride primary ruby mine, Bapawdan

Numerous hard-rock (primary) ruby mines explore the 'marble ark' in the mountainous terrain of the Mogok area (Themelis, 2008). We visited the Mogok Pride mine in the Bapawdan area, located approximately 5 km northwest of Mogok. Our host owned the mine since 2007 in a joint venture with the Myanmar government; the property was initially worked in 2000.

Figure 1. The entrance to the Mogok Pride ruby mine, Bapawdan, Mogok. Photo by B. M. Laurs.

Figure 2. The main adit is fitted with track for ore cars and also a water drain. Photo by B. M. Laurs.

Geologic mapping of the mining area by a Burmese geologist showed the presence of two main marble units that are locally separated by a lens of garnet-sillimanite gneiss, leucogneiss, and schistose gneiss. The marble units are themselves contained within garnet-biotite±sillimanite gneiss. One of the marble layers is mostly fine-grained and contains spinel mineralization, while the other is coarse-grained and hosts ruby. Leucogranite is locally present along the contact between the ruby-bearing marble and the host gneiss. The marble layers dip steeply to the south, and the mineralization locally occurs along specific horizons in the marble that follow the general trend of a natural karst (cave) system.

Figure 3. This winze connects the main adit to the mine workings. Photo by B. M. Laurs.

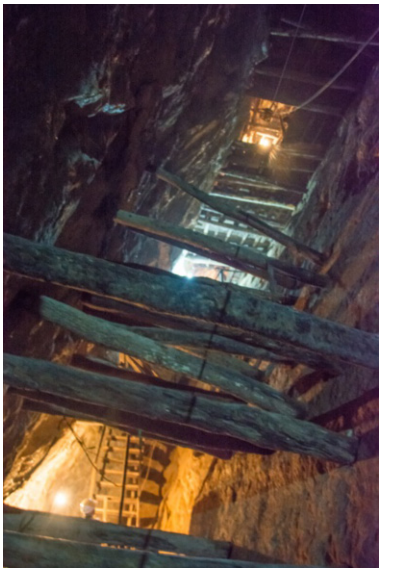

Figure 4. Ladders and platforms provide access to the working face. Photo by B. M. Laurs.

The deposit is worked nearly 24 hours/day in two shifts. Access to the mine is provided by a 100-m-long adit (fitted with track for ore carts; Figures 1 and 2) and several shafts. A winze (Figure 3) then leads to another adit that penetrates the ore zone and also is the starting point for two additional shafts. The active workings consist of a series of inclines and declines that follow the ruby-bearing horizon. A complex network of ladders and platforms (e.g. Figure 4) provide access to the workings. The miners use pneumatic drills (e.g. Figure 5) to make a series of holes in the marble for explosives. Ruby mineralization is encountered only occasionally in the marble, and it is very rare to see gems in the mine exposures, either before or after blasting. The marble pieces that are broken up by the explosives are immediately placed into heavy-duty bags and secured with a theft-resistant tie. The bags are placed into rubber buckets that are hung from a cable (Figure 6), and a pulley system brings the buckets to the closest adit, where the bags are loaded into ore cars. The miners also collect gravels that have weathered from the marble and deposited on the floor of the cave system. These gravels are likewise placed into bags for transport to the surface.

At the mine's processing facility, the marble is passed into a small jaw crusher that reduces it to <2 cm pieces, which are then washed into a jig using water from a nearby stream. All material that washes over the riffles is hand-sorted for pieces of ruby-bearing marble. In addition, at the end of the day, the gravel and rocks trapped in the riffles above the jig are placed into sieves (~2 mm mesh size) for further washing, followed by hand picking. The rubies recovered during this process are placed into a locked steel receptacle. The secondary gravels that are brought up from the mine are washed in the stream using the same sieves.

Figure 5. A miner uses a pneumatic drill to prepare the marble for blasting. Photo by B. M. Laurs.

Figure 6. Buckets full of marble are transported to the ore cars using a cable system. Photo by B. M. Laurs.

In the brief time that we witnessed the processing of the ore, only one small ruby specimen was recovered, as well as one minute grain each of ruby and red-orange spinel that were sieved from the karst gravels. The secondary deposits reportedly also produce moonstone, apatite, and other minerals.

The Mogok Pride mine is a well-organized operation that employs modern equipment and also uses traditional methods of extraction such as sieving the gem gravels by hand. While most of the ruby production is not of high quality, only a few good stones per month are needed to make the operation viable.

Secondary gem deposit near Bernardmyo

We also visited a secondary gem deposit located 7.6 km northwest of Mogok, near the village of Ingyauk (or Injauk) in the Bernardmyo area. At the time of our visit, the mine owner had just completed the first year of his three-year lease. He works the mine for six months of the year, during the dry season. Mining is not done during the wet season because the pit fills with water.

The large open pit (Figure 7) is situated in a valley that contains material weathered from a variety of metamorphic and igneous rocks in the area (e.g. marble, gneiss, and pegmatites). At the time of our visit, mining was taking place approximately 15–20 m below the surface. Water cannons were used to wash material from the pit into a sump, and the slurry was then pumped out of the pit to a washing plant (Figure 8). Larger stones (+1 inch or 2.5 cm) were screened off, and the remainder of the material flowed into a jig. The heavier stones (including gems) were caught in riffles above the jig, and at the end of each day the miners removed the concentrate by hand. Material from the top half of the riffles was discarded, and the heavier gravels from the bottom were put into sacks for hand picking off-site. Any gems seen during this process were placed into a metal bowl.

During our visit a rather small amount of gems were extracted from the jig. Most of the material consisted of low-quality ruby, sapphire and spinel with some small pieces of pale brown topaz, smoky quartz and black tourmaline (e.g. Figure 9). The sapphires were mostly colorless to yellow or blue, while the spinel was pink-to-red, purple-grey, yellow, blue or black. The corundum and spinel produced from this mine are only rarely of gem quality, and typically consists of waterworn broken pieces or less commonly as somewhat rounded tabular pseudohexagonal crystals. By contrast, the topaz is mostly transparent and shows extremely variable degrees of rounding from alluvial transport. Some of the smoky quartz crystals recovered from the operation have sharp crystal faces and attain relatively large sizes (20+ cm long), suggesting that their original source rock was not far away.

According to the mine owner, after a few months of the mining season have passed, it is common to see local families (especially children) picking tiny grains of gem material from the tailings of the mine. These are cut into melee-sized stones or (mostly) used in gem 'paintings' that are commonly seen in Mogok and in tourist centers throughout Myanmar.

Figure 7. A secondary deposit in the Bernardmyo area is mined in this large open pit. Photo by B. M. Laurs.

Figure 8. Stones >2.5 cm are screened off and the rest of the material passes into a jig. Photo by B. M. Laurs.

Figure 9. Most of the production consists of low-quality material. Photo by B. M. Laurs.

Conclusions

Visiting these mines provided a much deeper appreciation for the extreme rarity of good-quality gems, even within such a famous area for producing world-class stones. It is the possibility of finding these high-quality gems that keeps the miners digging. As time goes on, and the easier-mined gem deposits are exhausted, the likelihood of success declines. More effort, equipment, and money (for laborers, fuel, explosives, maintenance, etc.) are necessary, making gem mining an increasingly risky proposition. However, by utilizing current technology and the expertise obtained through years of experience, some enterprising miners continue to succeed in finding Mogok's gems.

References

Laurs B., 2015. Journey to Mogok, Myanmar. Gems & Jewellery, 24(1), 10–13.

Themelis T., 2008. Gems & Mines of Mogok. Self-published, 352 pp.

Technical progress report on LED, gemmology and sustainability

Manfred Eickhorst, M Sc Physics

SYSTEM EICKHORST, Borsteler Chaussee 85-99, 22453 Hamburg / Germany
www.eickhorst.com

Today LED technology is available in a variety of options that allows us the selection of the perfect type for gemmological applications with regard to design, lighting power, colour of light and efficiency by Lumen per Watt.

LEDs for professional applications became a lot more reliable than in their beginning, which has less to do with the manufacturer of the LED chip, but with the quality of the LED arrangement on basis material and the associated cooling. The guarantee of heat exhaust from the chip-area is the striking point for the life-time of an LED. Whereas in the consumer section this problem is still leading to failures of LED, for the professional applications there was kind of a learning process by LED manufacturers and assemblers.

The traditional darkfield microscope is the best example to present the challenges and advantages of LED to the user. It is considered as the LED "ABC" for Gem Microscopy

The LED powered darkfield illumination has meanwhile become state-of-the-art since the introduction (Eickhorst 2011). More brightness, more contrast and as a result a "darker" background (SSEF, 2013) make gem microscopy easier. A noticeable feature of the retrofitted microscope (Figure 1) is: The LED stage stays cool even after long periods of work while the generated heat of traditional incandescent darkfield illuminators is quite annoying and uncomfortable.

Figure 1. GEMMASTER darkfield microscope with triple LED lighting.

Good news for the experienced gemmologist is the new choice of LED colours of light (Figure 2). If preferred the yellowish incandescent colour, the 3.200K LED is available. Also available is the daylight colour of 5.500K, or the most highly accepted 4.000K. All can easily be changed by the user.

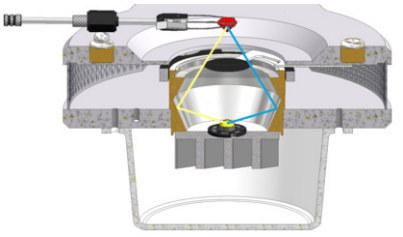

Figure 2. LED darkfield illumination with a choice of colours of light between 3.200 and 5.500 Kelvin.

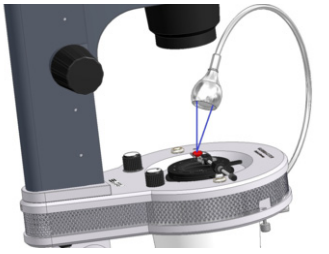

Figure 3. LED poin-point illumination.

Figure 4. LED daylight for overhead illumination.

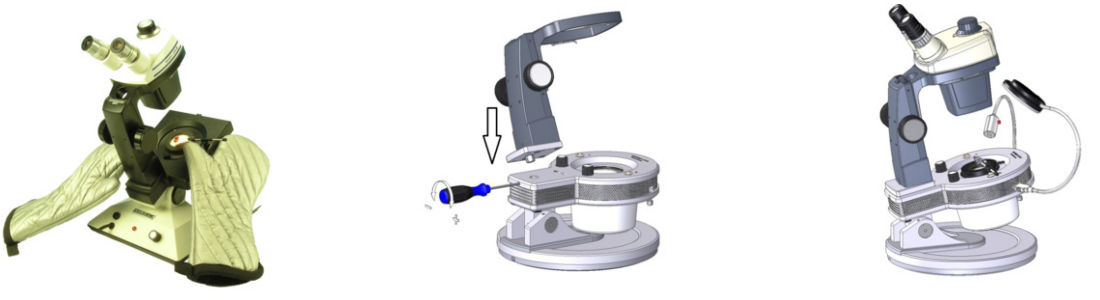

Figure 5. Sustainable LED update of a GemoLite microscope by replacing the darkfield illuminator base and keep the optical system.

The next lightsource of the microscope to be replaced by LED is the fibre optic light guide for spot light illumination (Figure 3). The perfect successor is again LED as a spot light at a gooseneck. Connected by USB or specific connectors to the microscope stage, this new light tool is versatile in its application and easily exchangeable to different beam spreads and also colours of light.

The overhead fluorescent daylight is succeeded as well by LED (Figure 4). Mounted at a flexible gooseneck the new device illuminates the working area of the stage by diffused daylight of 6.500K.

An aim of sustainabilty is the LED update of an old incandescent darkfield microscope (Figure 5). By simply exchanging the technically outdated base, the gemmologist can still use the valuable optical system he/she has been accustomed to for years.

Even when it is preferred to only update the incident lighting of the microscope stage, the external illumination stand with two LEDs at goosenecks is a new choice (Figure 6). Apart from various kinds of focus a UV-LED is also available for longwave 366nm.

Following this new kind of LED illumination a compact, reduced set-up for the gemmologist bag is to be introduced. A selection of useful USB connected LED lights and comfort items is available (Figure 7). This line of products is called USB-Boutique

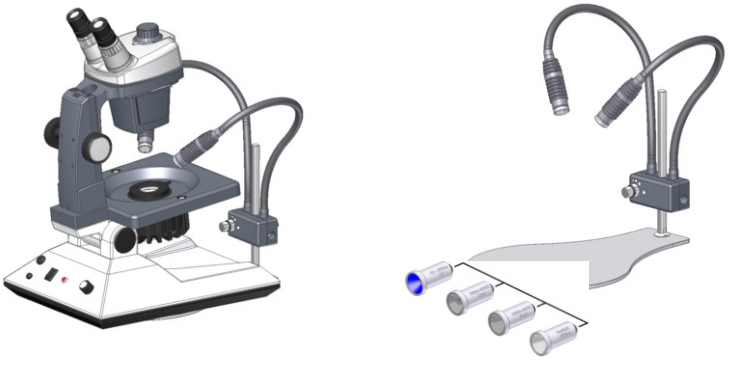

Figure 6. Update of incident lighting only; the use of a UV-LED is also possible.

Figure 7. USB connectable LED for spot or daylight illumination for the gemmologist to go.

Reference

SSEF, 2013. "New Eickhorst GEMMASTER microscopes at SSEF", Facette International Issue No. 20, January 2013, page 32.

Eickhorst, M., 2011. "Putting LED to work for Gemmology", 32nd International Gemmological Conference ICG, Interlaken, July 2011, page 72.

Emeralds from Jharkhand, India: An update

Gagan Choudhary

Gem Testing Laboratory, Jaipur, India; gagan@gjepcindia.com

Keywords Emerald, Jharkhand, properties, inclusions

Introduction

Since December 2012 a new find of emerald occurrence in the state of Jharkhand became quite popular in the local market. The occurrence initially attracted attention because of the reports in local media about arrests for illegal mining and smuggling (Anonymous, 2012; Jenamani, 2012), but within few months, large quantities of these emeralds have already been mined and reached the markets. Initially, only smaller crystals of up to 2g were seen, however, recently crystals as large as 5g have been encountered.

Location and geology

The occurrence is located in the Ghorabandha hills in the Ghatshila sub-division of the East Singhbhum district, which are a part of the Singhbhum Shear Zone (Sengupta et al, 2005). Major mineralized rocks of the shear zone are brecciated quartzite and quartz-chlorite-biotite-magnetite schists which have undergone varying grade of metamorphism (Sarangi, 2003). Study suggests the deposit to be short- distance eluvial / alluvial, while the primary occurrence as mica-rich rocks formed by metamorphic processes.

Figure 1. Range of faceted emeralds (~ 0.10 – 0.40 ct) used for this study. Photo by Gagan Choudhary.

Figure 2. Emerald rough from Jharkhand, India in a range of colour, transparency and size. Photo by Gagan Choudhary.

Results and discussion

Visual observation and crystal morphology

The studied emeralds from Jharkhand displayed a range of colours from bluish green to yellowish green of medium to strong saturation (Figures 1 and 2). However, most of these emeralds are characterized by haziness (Figure 3) which is more prominent in cut stones as compared to rough. Majority of rough crystals appear blackish due to the presence of some mineralic substance, such as mica, making the stones appear opaque. Although, these can be removed during cutting and polishing, some still make their way into the cut stones, making them appear too dark or blackish. Most of the rough samples displayed a typical hexagonal crystal profile with slightly abraded edges, suggesting alluvial / eluvial type deposit. No crystal was found in-situ. One crystal displayed an intergrowth with mica (biotite) with alternating sections of beryl and mica, which suggested that these emeralds were formed in mica-rich rocks.

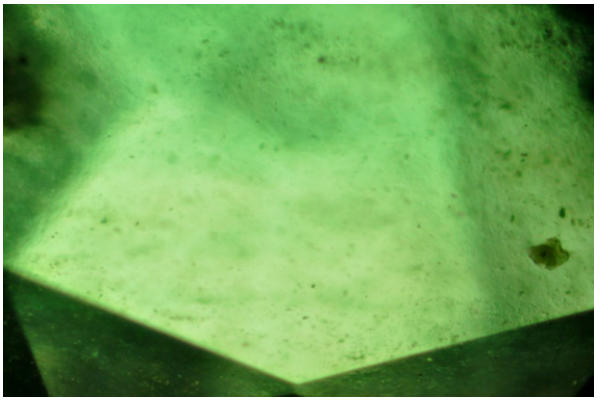

Figure 3. Most of the Jharkhand emeralds appeared hazy due to presence of minute mineral inclusions. Photomicrograph by Gagan Choudhary; magnified 32x.

Properties

The properties of Jharkhand emerald are summarised in Table 1.

Microscopic features

As mentioned above, most of these emeralds are characterized by haziness, caused by minute inclusions, which could not be resolved under a standard gemmological microscope. However, some appeared to be colourless minerals. Further, Raman analysis identified a range of mineral inclusions (Figure 4), such as, actinolite (acicular blades), allanite-La (black - brown, euhedral, sub-metallic), apatite (colourless, euhedral to subhedral), beta-fergusonite (brownish - clusters), epidote (euhedral), chromite / magnetite / picotite (black grains), mica (annite / phlogopite / chamosite / biotite - brown to colourless, elongated and platy), phenakite (colourless, clusters, sub-hedral), quartz (euhedral to anhedral), rutile (dark brown, sub-hedral), sphene (yellow, elongated crystals), zircon (rounded and with stress cracks), etc. In addition, wavy colour and growth zoning was present in almost all samples. However, interestingly, no fluid, phase or fingerprint inclusions were seen in any of the samples.

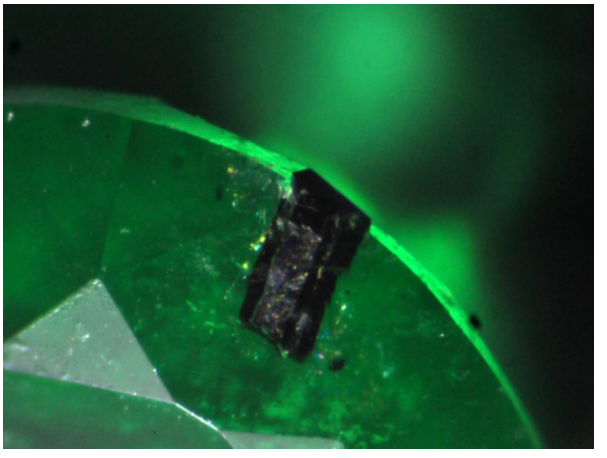

Figure 4.a. This euhedral black crystal was identified as allanite-La by Raman spectroscopy. Photomicrograph by Gagan Choudhary; magnified 80x.

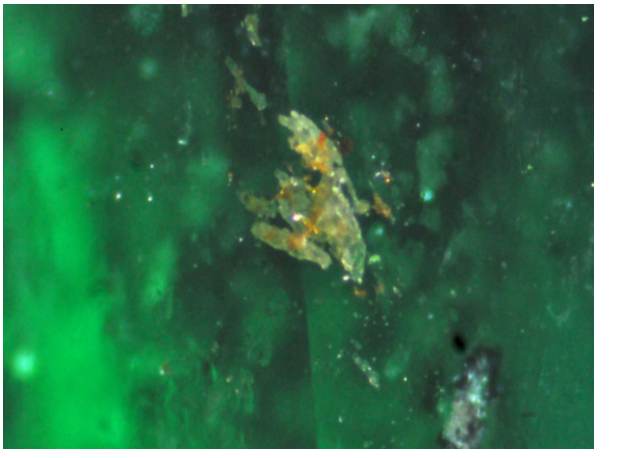

Figure 4.b. Cluster of yellow elongated crystals of sphene in emeralds from Jharkhand. Photomicrograph by Gagan Choudhary; magnified 80x.

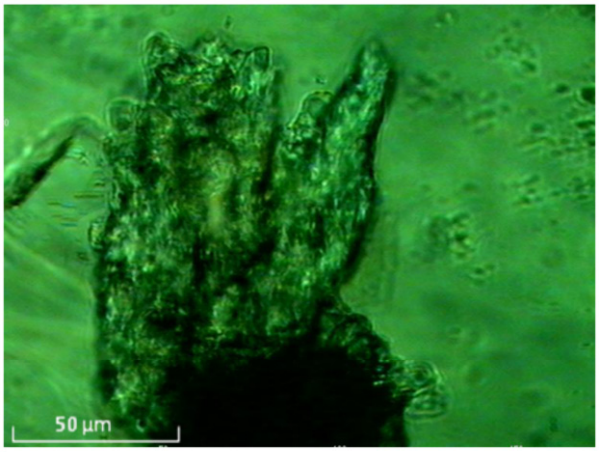

Figure 4.c. These abundant elongated crystals present Jharkhand emeralds were identified as Beta-fergusonite (Y) by Raman spectroscopy. Photomicrograph by Gagan Choudhary.

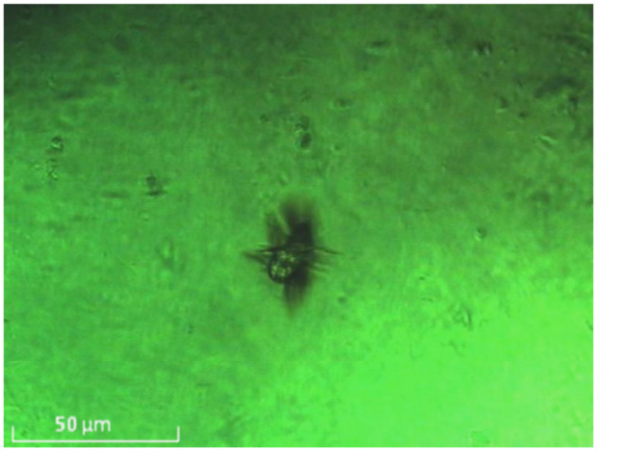

Figure 4.d. Zircon crystal with stress cracks is not usually seen in emeralds from other deposits. Photomicrograph by Gagan Choudhary.

Table 1. Properties of Jharkhand emerald

Property	Description
Colour Range	Bluish green to yellowish green; medium to strong saturation
Transparency	Transparent to translucent (haziness, similar to 'roiled-effect')
Pleochroism	Medium to weak dichroism; yellow green and bluish green

Table 1. Continued.

Refractive index	1.578 - 1.590 (range)
Birefringence	0.008
Specific gravity	2.70 - 2.73 (range)
UV fluorescence	None
Chelsea filter	Inert
Absorption spectrum (desk model)	Typical emerald spectrum; strong Cr-absorptions
Raman spectra	Typical beryl peaks at ~324, 397, 519, 616, 687, 1010, 1068 and 1125 cm^{-1}
Absorption spectra (UV-Vis-NIR)	Consistent with emerald. Broad absorption bands at ~ 440 (Cr^{3+}), 605 (Cr^{3+}) and 835 nm (Fe^{2+}); peaks at ~ 372 (Fe^{3+}), 637 (Cr^{3+}) and 683 nm (Cr^{3+})
FTIR spectra	Consistent with beryl. Features associated with CO_2 at ~ 2357 cm^{-1}; water molecules at ~ 3200 – 4100 cm^{-1} (type I), and ~ 5275 cm^{-1} (type II)

Conclusion

This relatively new find of emeralds from the East Singhbhum district of the state of Jharkhand has produced a lot of interest in the local market. Currently the occurrences are being excavated through illegal mining, but the state government is in the process of acquiring mining rights and clearances, which will help to regulate the supply of these emeralds. As per preliminary observations, these emeralds appear to be of decent colour and transparency. Although, initially smaller sizes lower than 10 ct (for rough) were discovered, but in recent times, larger sizes of up to 20 ct are also seen. It is quite rare for an emerald to be free from fluid inclusions, which was the case with all these studied emeralds from Jharkhand.

References

Anonymous, 2012. Man arrested with emeralds. The Telegraph. (http://www.telegraphindia.com/1121109/jsp/jharkhand/story_16174344.jsp; last accessed 09-04-2015).

Anonymous, 2012. Patrol plea for emerald hills. The Telegraph. (http://www.telegraphindia.com/1130107/jsp/jharkhand/story_16408985.jsp; last accessed 09-04-2015).

Jenamani K., 2012. Emerald hills eye state geology seal. The Telegraph. (http://www.telegraphindia.com/1121221/jsp/jharkhand/story_16342540.jsp; last accessed 09-04-2015).

Sarangi A.K., 2003. Grade control in Jaduguda uranium mine, Jharkhand. Transactions of the Mining, Geological and Metallurgical Institute of India (MGMI), 99(1-2). (http://www.ucil.gov.in/web/pdf/myth/Grade%20control%20in%20Jaduguda,%20Jharkhand.pdf; last accessed 09-04-2015).

Sengupta N., Mukhopadhyay D., Sengupta P., Hoffbauer R., 2005. Tourmaline-bearing rocks in the Singhbhum shear zone, eastern India: Evidence of boron infiltration during regional metamorphism. American Mineralogist, 90, 1241-1255.

A review of synthetic turquoise

Helmut Pristacz[1,2], Toshihiro Kogure[2], Vera M.F. Hammer[3], Gerald Giester[1], Manfred Wildner[1], Eugen Libowitzky[1], Lutz Nasdala[1]

[1] Institut für Mineralogie und Kristallographie, University of Vienna, Austria; helmut.pristacz@univie.ac.at
[2] Department of Earth and Planetary Science, Graduate School of Science, The University of Tokyo, Japan
[3] Department of Mineralogy and Petrography, Natural History Museum Vienna, Austria

Keywords Turquoise, Gilson synthesis, TEM

The triclinic hydrated copper-phosphate mineral turquoise [$X_{0-1}Y_6(PO_4)_{4-z}(PO_3OH)_z(OH)_8 \cdot 4H_2O$; with X = □, Cu, Zn, Fe^{2+}; Y = Al, Fe^{3+}, and z = 0–2] continues to be a well-debated material on the gem market. As described by Elwell (1979), turquoise was one of the first gem materials to be simulated by synthetics like glass, plastic or pressed turquoise powder bonded with resin. Up to now, the so-called "Gilson-created turquoise" is the only genuine synthetic turquoise – that is a material whose chemical composition and structure corresponds to that of natural turquoise – to appear on the market (Williams & Nassau 1976; Eppler 1984; Lind et al., 1985; O´Donoghue 1997).

Analyses by means of non-destructive techniques such as infrared absorption (IR) spectroscopy using an attenuated total reflection (ATR) unit, Raman micro-spectroscopy and handheld energy dispersive X-ray fluorescence (EDXRF) spectrometry are valuable and powerful tools for the identification and characterization of gemmological turquoise-type materials. For a better understanding of synthetic turquoise, however, additional investigations with destructive techniques need to be done. Here we present results of a detailed comparative study that included a historic specimen from the collection of the Natural History Museum Vienna, Austria, labelled "synthetic turquoise" (sample #L8368; Figure 1) and natural turquoise from Gunheath, St. Austell, Cornwall, United Kingdom (Figure 2). The polycrystalline turquoise samples have been studied by ATR–IR, Raman micro-spectroscopy, optical absorption spectroscopy, EDXRF, transmission electron microscopy (TEM), scanning electron microscopy with energy-dispersive X-ray analysis (SEM–EDS) and powder X-ray diffraction (PXRD). The purpose of this study was to characterize the synthetic material and in particular additional crystalline and non-crystalline phases within this product.

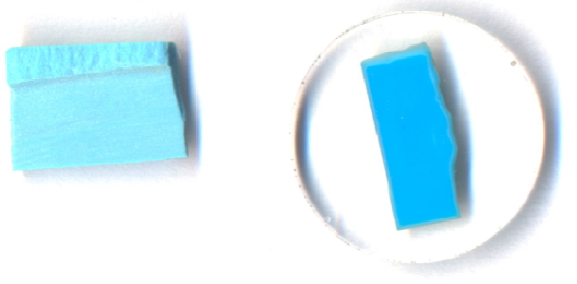

Figure 1. Synthetic turquoise – unprepared (left) and embedded in epoxy resin and polished (right) – from the Natural History Museum, Vienna, Austria, collection. Specimen 20 mm in size.

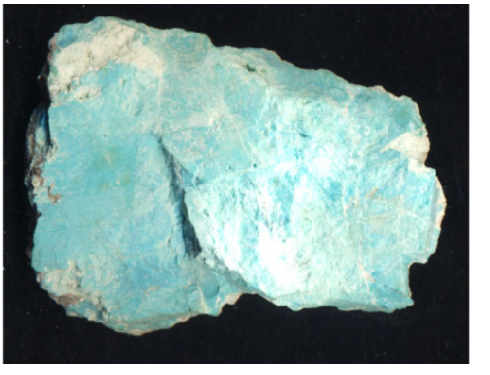

Figure 2. Natural turquoise from the Gunheath pit, St. Austell, Cornwall, England, UK, from a private collection. With of image 8 cm.

When compared with the natural sample, wide concurrence in ATR–IR spectra, optical absorption spectra and PXRD patterns of the supposed synthetic specimen #L8368 support the identity of the former as synthetic turquoise rather than a replacement material. In contrast to natural turquoise, the synthetic sample yielded a PXRD pattern with somewhat broader peaks; an additional Bragg peak at d = 3.227 Å was observed (Pristacz et al., 2013). This is in apparent accordance with results of Lind et al., (1985) who found that samples of Gilson´s synthetic products show additional X-ray diffraction lines caused by one or more additional crystalline phases present. In two out of five samples studied by these authors, diffraction lines of berlinite (PDF 10-0423, strongest line d = 3.369 Å) were detected (Lind et al., 1985). In addition to the characteristic IR spectral pattern of natural turquoise an IR absorption band near 3180 cm^{-1} was found in the spectrum of sample #L8368 (Pristacz et al., 2013).

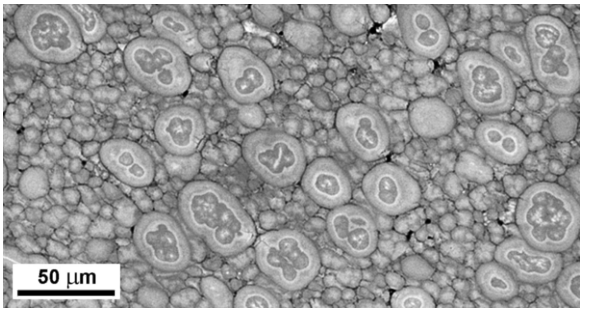

Figure 3. Backscattered electrons image (scanning electron microscope) of synthetic turquoise, showing a multitude of oolithic grains several ten micrometers in size.

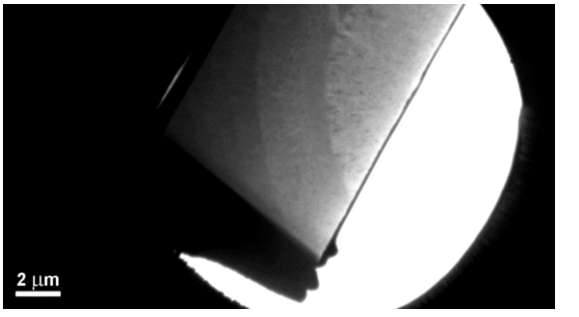

Figure 4. Dark-field image (transmission electron microscope) of an oolithic grain of the synthetic turquoise. Sample prepared by the focused ion beam technique.

Images obtained in the SEM (Figure 3) revealed that sample #L8368 has a somewhat porous, oolithic micro-texture. Transmission electron microscopy images produced from foils prepared using the focus ion beam (FIB) technique, unraveled the presence of a fairly high amount of a fibrous, amorphous phase (Figure 4). It appears that in the core of ooliths the content of this amorphous phase is higher than in the rims. The crystalline phase present was identified as turquoise. Consequently, the "synthetic turquoise" sample #L8368 is composed of three crystalline phases, i.e. natural turquoise, which presumably was used as a precursor material, and a synthetic phase which also has the chemical composition and the crystal structure of turquoise. The third (yet unknown) phase is related to the high-pressure berlinite structure.

References

Elwell, D., 1979. Man-made gemstones. John Wiley & Sons, New York, 121 pp.

Eppler, W.F., 1984. Praktische Gemmologie. Rühle-Diebener-Verlag, Stuttgart, 180 pp.

Lind, T., Schmetzer, K., Bank, H., 1983. The identification of turquoise by infrared spectroscopy and X-ray powder diffraction. Gems & Gemology, 19, 164–168.

Pristacz, H., Wildner, M., Hammer, V.M.F., Libowitzky, E., 2013. Detailed mineralogical investigation of a synthetic turquoise. CORALS–2013, Wien, Austria, July, 2013. Book of Abstracts, pp. 81–82.

O´Donoghue, M. 1997. Synthetic, imitation & treated gemstones. Butterworth-Heinemann, Oxford, 155 pp.

Williams, J.D., Nassau, D. 1976. A critical examination of synthetic turquoise. Gems & Gemology, 15, 226–232.

Unusual and curious gemological materials in the laboratory

Antonello Donini, Elena Gambini, Emanuela Castaman, Giuliano Radice

CISGEM Laboratory - Fondazione Gemmologica Italiana; info@cisgem.com

Keywords rhinoceros horn; ambergris, grey amber, imitation, assembled product, ornamental material

Introduction

The CISGEM Laboratory–FGI, had the opportunity to analyze, among others, a number of unusual gem materials: in some cases it came across curious items, rarely used as ornamental materials or personal ornamentation. The two cases presented here are typical examples; preliminary testing results are presented.

Case 1 - Rhinoceros horn

Several ornamental objects, declared as coming from antique collections, have been submitted to the CISGEM Lab. The items, typically for this kind of material, were shaped mainly as cups and libation cups.

Figure 1. Some of the analyzed items.

Figure 2. Typical texture of rhinoceros horn.

Figure 3. Resinous reddish layer covering the rhino horn.

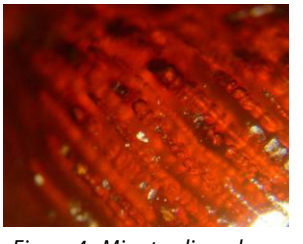

Figure 4. Minute aligned gas bubbles in resin to emulating the structure of the rhino horn.

Figure 5. Texture of imitation.

Some cases are described here below:

Item A : The typical tubular structure of rhinoceros horn (fig. 2), composed of tightly packed hair, could easily be observed. As markedly different orientations of the hair were observed, obviously this item (like 3 other samples we

could look at) was made of two (or more) assembled rhinoceros horn parts glued together. The hot point test revealed that the samples begin to soften slightly at 170°C, with the typical smell of a keratinous substance.

Item B : Different orientations of the hair were observed in this case (1 sample) as well. In addition, several small resinous parts (fig. 3) covering the rhino horn, show minute aligned gas bubbles (fig. 4), resembling the rhinoceros horn structure. These samples soften at around 170°C, with the typical smell of keratinous substances on some parts of the sample, whereas in other portions of the item give a sweet smell. These samples are made of various assembled rhinoceros horn parts and artificial substance portions.

Items C, D and E: These samples show a tightly packed sub-parallel hair structure, at first glance analogue to the rhinoceros horn hair. The hairs of these samples look like thin tubes immersed in a homogeneous yellow-brown or dark red brown matrix (fig. 5). In one sample isolated gas bubbles were observed in the matrix. The hot point test allowed to record the softening temperature at around 200-230°C, giving off an acrid smell. These samples were classified as manufactured products, imitating rhinoceros horn.

All samples were subjected to FTIR analysis (DRIFTS with SiC disks and beam condenser) and further advanced tests. Results will be presented.

Case 2 – "Grey amber" or "ambergris"

Ambergris is produced by the sperm whale (Physeter catodon) as an intestinal secretion product, frequently correlated to the sperm whale's diet: cuttlefish.

Figure 6. Necklace made of "ambergris".

Figure 7. Aspect of the material.

Figure 8. Aspect of the material.

Figure 9. Texture of "ambergris".

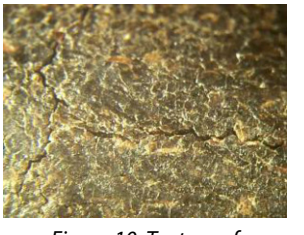

Figure 10. Texture of "ambergris".

Ambergris is expelled naturally by the sperm whale through feces, or, in the case of accumulating too large to be expelled through the stretch fecal, is occasionally regurgitated. In both cases solid masses are formed in the shape of blocks that, once expelled, may float, driven by the currents, to be found on the coasts. This typically happens in the Indian Ocean (in India or East Africa).

This material has outspoken fixative properties for flavours and fragrances and for this reason it has been used in the past for the production of perfumes.

It is unusual to find this material used as an ornamental material. At CISGEM we had the opportunity to analyse a necklace (Figures 6-10) made of black carved spheres, cylinders and drops, dark grey in colour, completely opaque, grainy and waxy.

The material had a granular with sometimes layered organic structure. Among the tests carried out, an interesting result was observed from X-ray radiography: the structure of the material consisted of fragments of various nature. It is common to find fragments derived from the ingestion of squid (cuttlefish bone and broken beak) which is the favourite food of this animal.

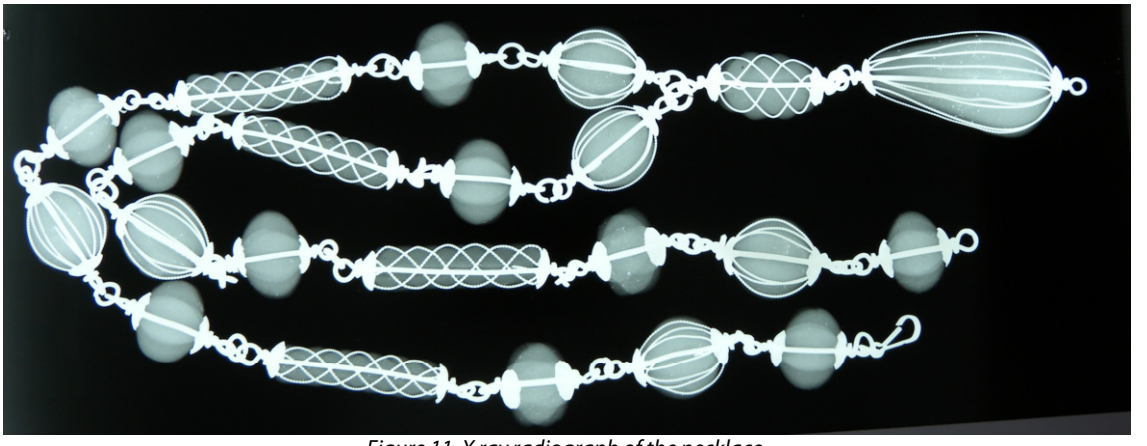

Figure 11. X ray radiograph of the necklace.

EDXRF analysis revealed traces in variable amounts of the elements Na, Mg, Al, Si, S, K, Ca, Ti, Fe, Zn, Cl, Pb, Sr where Na, Cl, Ca, K and Sr are present in higher quantities. To avoid the influence of the precious metal used to assemble the jewel, the analysis was performed on the engraved spheres only. As ambergris is a substance of organic nature, the presence of the given elements is mainly due to the feeding of the animal. In particular the presence of Pb in all analyzed spheres except one is striking: does it reflect pollution or is it a contamination due to the cutting/shaping process?

A thermal probe was used to detect the melting point of the material and it allowed to observe the effects of heat. The material started to soften at about 180°C and melts at about 450°C producing an oily black viscous liquid. The scent released was similar or comparable to that of tobacco. This was a first step in the analysis of this unusual material.

Few references to historical jewels made with this type of material can be found. As an example, a reference dating back to 1632 (Joan Evans – A history of jewellery) described a funerary art jewel made with ambergris (inventory of the Marquis de Removille - chain made of ambergris beads).

Further studies should be performed on this material to better characterize it.

Conclusions

Observation under the microscope clearly allows to identify the different nature of resins and other materials (threads of probable artificial resin) used to imitate the rhinoceros horn, as the appearance is clearly different from that of the natural material.

The hot point test is fairly diagnostic: rhino horn emits a characteristic odour linked to the keratinous substances while resins have a typical, more pungent or sweet smell.

The FTIR spectrum clearly shows the different nature of the materials. Care must be taken to the presence of possible decorative parts or fillers made of artificial resins that lead the object to be of assembled nature.

The use of ambergris in ornamentation is decidedly unusual. Further studies on this type of material are needed in order to better characterize it, preferably on objects that are free from the frame. The hot point allowed us to identify the melting point of the material and the odour emitted in part similar to that of the tobacco. The EDXRF analysis showed the organic nature of the material and the presence of elements related to the environment where sperm whale lives and the type of food. The X-ray necklace highlights the "granular" nature of the material formed from grains of organic substance as well as fragments of material not digested by the animal.

References

Bauer, R., 2013. Gemmological intelligence: imitation rhinoceros horn. The Australian Gemmologist, 25(4), 156-157.

Brady, G.S., Clauser, H.R., 1992. Manuale dei materiali. Tecniche Nuove, Milano, 1200 pp.

Campbell Pedersen, M., 2004. Gem and ornamental materials of organic origin. Elsevier, Oxford, 268 pp.

Campbell Pedersen, M., 2014. Misidentifications and trading loopholes. Gems&Jewellery, 23(4), 16-19.

Reyjal, I., 2010. Une curiositè naturelle: la corne de rhinoceros. Revue de Gemmologie, 174, Dicembre, 25-26.

Shengqinga L., Endongb Z., Lijun L., 2011. Identification of rhinoceros horn and its substitutes. Advanced Materials Research, Vol. 17, 636-639 pp.

Tobin L. Hieronymus, Lawrence M. Witmer, Ryan C. Ridgely, 2006. Structure of White Rhinoceros (Ceratotherium simum) Horn investigated by X-ray computed tomography and histology with implications for growth and external form. Journal of Morphology, 267, 1172–1176 pp.

Villavecchia, V., Eigenmann, G., 1977. Nuovo dizionario di merceologia e chimica applicata. Volume 1 Hoepli, Milano, 514 pp.

Mustard Jasper or Bumble bee stone

Emmanuel Fritsch[1], Joel Ivey[2]

[1]Institut des Matériaux Jean Rouxel CNRS (UMR 6502) & University of Nantes, BP 32229, F-44322 Nantes cedex 3, France; emmanuel.fritsch@cnrs-imn.fr
[2]indoagate.com; jaivey@attglobal.net

Keywords Mustard jasper, Bumble Bee stone, realgar, pyrite, origin of color, volcanic

This decorative rock coming from Indonesia offers an attractive color contrast: opaque bright yellow to orange next to black and/or white (figure 1). Hence its various names. This gem material has been around for a few years, but high numbers of cabochons, beads and larger decorative pieces appeared in the market in 2013 . It is found in the west Java province (Overlin, 2014; Serras Herman, 2014). The general area is riddled with volcanic activity, and the decorative rock comes from the foot of one of the many volcanoes encountered on the island.

Figure 1. Aspect of mustard jasper. Some areas are bright yellow or orange, some are dark gray or black and others are white. The mix of some yellow and some gray gives the mustard-like color appearance. Photo E. Fritsch.

We studied in detail seven cabochons of this material ranging from 10.22 ct to 96.90 ct, representing typical colors. Their refractive index is very difficult to measure, because of micro-porosity, and its specific gravity varies between 2.417 to 2.742. Under ultraviolet radiation part of each sample emits some yellow, while other parts remain inert.

Bubbles appear when a drop of diluted hydrochloric acid is put on its surface proving this material to be essentially a carbonate. Therefore it is not jasper, an opaque form of microcrystalline quartz. It is polycrystalline with a variety of minerals and therefore represents a carbonate rock. The black areas are colored by many black disks, under a millimeter in diameter. The yellow to orange is due to very small yellow dots and sometimes larger ones, even very small cavities, containing orange to even red crystals. The white to near-colorless areas are constituted by the carbonate, which is also the matrix of the two other colored materials. This gem material is not formed from "a mixture of Indonesian volcano lava and sediment" (as stated by Overlin, 2014). The yellow luminescence noted above actually comes from relatively pure and colorless calcite.

A Raman spectrum was obtained using a Bruker MultiRam Fourier Transform Raman spectrometer. The bands of calcite are always present, but additional bands at about 183,194, 220, 343 and 355 cm^{-1} correspond to realgar (AsS), never those of orpiment. The bright yellow color is actually due to the realgar nano-inclusions, and not orpiment, as sometimes mentioned on the basis of color alone, without spectroscopic analysis. When red realgar is ground into nanometric particles its color changes from red to yellow. This has been described in detail for yellow to orange common opal from both Austria- known as "forcherite", and France, near St Nectaire (Gaillou, 2006.)

Inspection with a Jeol 7600 Scannning Electron Microscope equiped with a EDS detector, confirmed that the matrix is indeed a calcium carbonate. Yellow to orange areas are rich in sulfur (S) and arsenic (As). This confirms the Raman findings. Finally the very small black disks in the black areas are identified as pyrite, another sulfide, which occurs as micrometer-size crystals, coalescing in circular groups, which explains the difference in color with the usual golden yellow of pyrite. Such very finely divided sulfides are often called "sooty sulfides" due to their black color.

References

Gaillou E., 2006. Relations between nanostructure, phyical properties and mode of formation of opal A and opal CT [in French] PhD dissertation University of Nantes, pages 181-186. Document downloadable at http://www.gemnantes.fr/fr/recherche/theses/these-gaillou).

Overlin S., 2014. Gem news: Bumble bee "jasper" from Indonesia; Gems & Gemology summer 2014 vol 50 no. 2 pp.166-167.

Serras Herman H., 2014. Bumble bee "jasper" a colorful volcanic lapidary material Rock & Gem, vol. 43, N°8, pp.26-29.

"Electrum": Why was the same word used for amber and for the naturally occurring alloy of gold and silver?

John M. Saul

ORYX, Paris, France; john.saul@wanadoo.fr

Keywords electrum, amber, mythological ages, wandering rocks

In pagan tradition and in myth, the Golden Age was a time when men were immortal. In those times-that-never-were, reproduction was unnecessary and women did not yet exist. By the mythic times of the Age of Silver, Death had come and myth speaks of women and genealogies (Saul, 2013).

The transition from Gold to Silver is not clearly indicated, but a survey of diverse myths shows that that two sub-Ages had been inserted between Gold and Silver. These sub-Ages had mythic and real properties intermediate between gold and silver.

The First sub-Age was of Amber (electrum), in part because amber may have a color intermediate between gold and silver. In myth, this sub-Age is characterized by "woody imagery": amber, resin, trees (including Jupiter's Oak), acorns, acorn-eating pigs, woodpeckers, bees and honey (including Milk and Honey?), spears, javelins, black, black charcoal, ravens, single-bladed axes, carpenter…

The Second sub-Age was of Electrum (the naturally occurring metallic alloy of gold and silver). In myth it was indicated by electrum metal (Rossignol, 1863), alloys, swords, armor, chain mail, white, white charcoal, swans, doves, bees and honey (including Milk and Honey?), double-bladed axes, smiths, son of carpenter…

The transition involved the crossing of a mythic river, celestial or terrestrial, the "River Eridanus", in which amber or electrum metal was supposedly found.

Both sub-Ages were characterized by wars and judgments – two manners of reaching decisions – destined to decide whether humans merited a Return of the Golden Age.

The Golden Age was ruled by Saturn. The Silver Age was ruled by Jupiter/ Zeus. One or both sub-Ages of Electrum were ruled by Mars, god of War and Judgments. These are planetary gods. Planets are "wandering stars" and gold, silver, amber and electrum are "wandering rocks" whose essence "wanders" when heated in a charcoal fire.

References

Rossignol, J.-P., 1863. Les Métaux dans l'Antiquité: Origines religieuses De La Métallurgie, ou les dieux de la Samothrace représentés comme métallurges d'après l'histoire et la géographie De L'Orichalque, histoire du cuivre et de ses alliages suivie d'un appendice sur les substances appelées électre. Auguste Durand, Paris. 392 pp.

Saul, J., 2013. The Tale Told in All Lands. Les 3 Colonnes, Paris, 623 pp.

Infrared spectral characteristics of ambers from three main sources (Baltic Sea, Dominican Republic and Myanmar) and their implications

Guanghai Shi[1], Yan Wang[1], Wei Shi[2], Ruihua Wu[1, 2]

[1] State Key Laboratory of Geological Processes and Mineral Resources, China University of Geoscience, Beijing, China; shigh@cugb.edu.cn
[2] Beijing CUG Gem Testing Center, Beijing, China

Keywords Amber; Origin; Infrared spectra; Myanmar; Baltic; Dominica

Abstract: Infrared spectra of one amber sample from the Baltic Sea, two from the Dominican Republic and three from Myanmar are obtained by specular reflection and KBr Pellet transmission methods. The result shows that small differences in position and intensity of absorption peaks of the infrared spectra could be used to identify the samples among locations, though the spectra of them present similar features in the absorption peak patterns which are caused by C-H vibration of aliphatic series. In the region of 3000~2800 cm^{-1}, two obvious peaks with a weak shoulder peak are observed in the Baltic amber spectrum, whereas there are only two bands in the Dominican samples' and three bands in those from Myanmar's. Between 1740 and 1690 cm^{-1}, one band appears at 1732 cm^{-1} in the spectra of the Baltic amber sample, distinctly different from those of the Dominican and Myanmar ambers which have a doublet at 1730 cm^{-1} and 1695cm^{-1}. For the Dominican amber, the intensity of 1730cm^{-1} is much stronger than that of 1695cm^{-1} feature, the reverse being true for the spectra of Myanmar amber. Within the 1300~1000 cm^{-1} spectral region, Baltic amber can be distinguished from that of the other two origins by a horizontal shoulder between 1250 cm^{-1} and 1175 cm^{-1} (Figure 1), often called "Baltic shoulder", with a well-defined band at 1157 cm^{-1}. Spectra of the Dominican amber show a unique band at 1242cm^{-1} (Figure 2) not reported in the spectra of samples from the other two locations, and spectra of the Myanmar amber have a triplet at 1226 cm^{-1}, 1136cm^{-1} (or 1153cm^{-1}) and approximately 1030cm^{-1} (Figure 3). The ratios of absorption intensity of the 1381 cm^{-1} to the 1456 cm^{-1} feature ($I_{1380cm^{-1}}/I_{1456cm^{-1}}$) are about 0.9, 0.8 and 0.7 respectively for the Baltic, Dominican and Myanmar ambers. These differences of absorption spectra could be used as criteria to separate amber from these three different localities. On the basis of presence and intensity of the bands attributed to exocyclic methylene groups which are at 1643cm^{-1} and 887 cm^{-1}, it is suggested that the Myanmar amber formed earliest, followed by Baltic amber, the Dominican gems being the youngest. Amber's age, plant provenance and geological environment are probably the reasons for the correlation between the amber samples' infrared spectra and localities. These findings strongly suggest that infrared spectroscopy have significance for identifying locality of the amber samples, and thus potentially have archaeological implications in determining the source of ancient amber artifacts without trace.

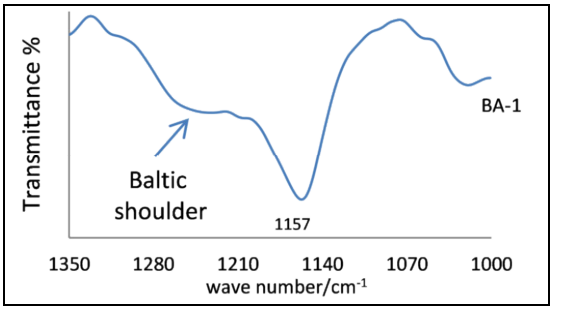

Figure 1. "Baltic shoulder" between 1250 cm^{-1} and 1175 cm^{-1} in Baltic amber sample spectrum.

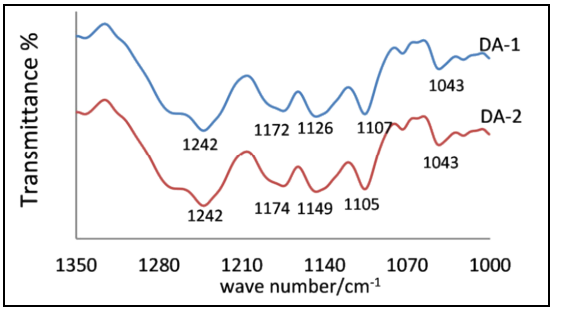

Figure 2. Infrared spectra between 1300 cm^{-1} and 1000 cm^{-1} of Dominican amber samples.

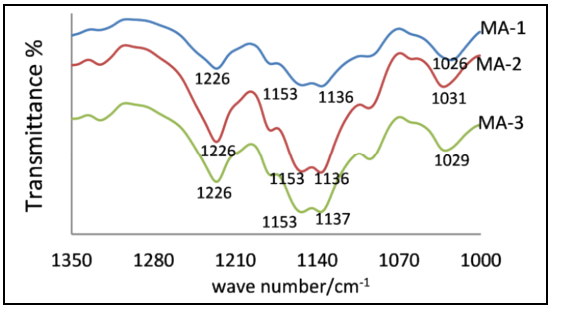

Figure 3. Infrared spectra between 1300 cm^{-1} and 1000 cm^{-1} of Myanmar amber samples.

Jadeite markets in China

Elizabeth Su

Gemsu Rona, Shanghai, China; esu_gems@yahoo.com

Keywords jadeite, market, China

Whole sale markets in China

1. Guangdong province

Yangmei: Yangmei Village was located in the western part of Jieyang, Guangdong Province, China. In the early days, Yangmei Village focused on processing, and as early as the beginning of the last century, Yangmei people started to process a variety of jadeite products for selling, and gradually entered into fields of raw materials auctioning and finished products wholesaling. It has now surpassed Hong Kong to become the largest high-quality jadeite wholesale market in the world. The Yangmei jadeite market features expensive high-quality jadeite products. Prosperity of the Yangmei Market is also due to funds raised by "public shares". As the whole village is a clean system and most villagers are in kinship, when purchasing raw materials from Burma, they would raise funds from relatives and friends, and finished products and sales would be distributed on a fair basis in proportion to fund contribution shares. In this way, Jieyang people normally can easily buy high-grade jadeite raw materials that value up to hundreds of millions or even billions of Chinese yuan, thus ensure the dominant position of the Yangmei Jadeite Market in competition. Yangmei jadeites also reach top engraving level in the industry. As Yangmei developed from the basis of jadestone processing, they have accumulated the most abundant experience in engraving and processing.

Guangzhou: Guangzhou is the largest jadeware wholesale market in the world. Its geographical adjacency to Hong Kong and Macao also brings it unlimited business opportunities. Guangzhou's jadeite market mainly concentrates nearby the Hualin Temple of Liwan District, where there are Hualin Jadeite Street and a number of jadeite buildings such as the new Hualin jadeite building, the old Hualin jadeite building (Xilaixi), Minghui Jewelry & Jade Plaza, etc. Guangzhou's jadeite market is renowned for various choices of cheap fine quality jadeite products. As it is the capital city of Guangdong Province, wholesalers from other markets of Guangdong also transport their goods to Guangzhou for selling, thus Guangzhou market has an abundant variety of jadeite products at different prices for choice, coupled with a relatively complete selection of accessories such as necklaces, buckles, accessory stones, etc.

Pingzhou: Pingzhou is close to Guangzhou, located in the Eastern part of Nanhai District of Foshan City, Guangdong Province. It would take around 40 minutes by shuttle buses and taxis to travel to and from Guangzhou's Hualin Jadeite Market and the Piangzhou Jadeite Market. The Pingzhou Jadeite Market is a single street of around one thousand meters in length, jadeite stores ramify along the street. Thousands of jadeite bracelets are classified by different grades, normally, bracelets made out of the same piece of raw stone are stringed into a circle for easy picking. For wholesale, low-priced bracelets normally are sold in a dozen to dozens per batch and are placed in a bamboo-weaved dustpan so that buyers can pick at will to examine in sunlight; high-priced bracelets are normally sewed with red string in a red cloth bag in single or in double. Finished jadeite products made out of the same piece of raw stone are called "one LOT" in industry terminology, and in wholesale markets, bracelets are normally traded by "one hand"; separate pieces are not sold or would sell for a high price.

Sihui: Sihui is located in Zhaoqing City, Guangdong Province. Sihui mainly focuses on small pieces of low-priced jadeite products that cater to ordinary consumers, thus the production is high. The Tianguang Market is a characteristic farm production market in Sihui; from 3-4 am, sellers would start to stall in the market for peddling. Normally, they would put jadeite goods on a piece of white cloth or in a tray and place them on a simple table, illuminated by emergency lamps or other light sources. Buyers normally examine goods under flashlight, it especially tests buyers' eyesight and makes buyers easily buy lobed or defective goods as the light is quite poor. Sihui market also has many semi-finished products that are merely engraved but not polished. As there is obvious change in transparency in jadeites before- and after-being polished, it requires strong judgment from buyers in buying such semi-finished products. However, as buyers and sellers do not know about the finished effect of polishing, there is a certain degree of luck involved, thus many buyers are willing to try their luck.

2. Yunnan province

Ruili: As a Chinese city bordering Burma, Ruili has been an important city for jadeite trading from the ancient times. Since the reform and opening up, gem traders from Burma, Pakistan, India, Thailand and other peripheral countries and regions started to actively trade in jewellery in Ruili, and jadeite is the most important product. Since March 1998, the Burma government officially permitted the importation of jadeite raw materials into Ruili through the Jiegao Port in the form of border trade, thereby further stimulate the development of jadeite industry in Ruili. For recent years, the Burma government reclaimed the importation of jadeite raw stones and opted for public auctioning in Mandalay. Even so, Ruili is still one of the most important jadeite markets in China as it is advantageously located merely over three hundred miles from Mandalay. Stores on the Jewelry Street focus on retailing of high-grade goods. And the Taili Jewelry Market features foreign jewelers and an abundant variety of products including the wholesaling of different colored gemstones in addition to jadeites. The Jiegao Jade Town features the wholesaling of jadeite raw materials. It opens for business from 5 am each day; jadeite raw stones are transported in batches from Burma to Ruili for buyers' selection in this market. Wholesaling of raw stones would close at around 1-2 pm at noon, while the finished products market would open for business until the afternoon.

Figure 1. Elizabeth Su and friends appraising the jadeite raw materials in Ruili market.

Tengchong: Tengchong is located in the western part of Yunnan Province and is neighboring to Burma which is the place of origin of commercial-grade jadeites. It has been a must-route to pass for jadeite products to enter China since the Ming and Qing Dynasties. Such historical background also made Tengchong become a famous jadeite base. After 1950's, border trade between Tengchong and Burma was forced to break off, and Tengchong only started to resume its position as an import market for jadeite trading until in the 1990's when the Tengchong-Myitkyina highway was constructed. There are mainly two jadeite markets in Tengchong which are the Jewelry Trade Center and the Tengchong Jadeite Town. The number of traders and quality of goods are far off from Guangdong and are also not comparable to Ruili in the same province. Thanks to its unique natural and geological environment, Tengchong has always been a hot travel destination of Yunnan Province, boasting such scenic spots as the Heshun Overseas Chinese Town, the Atami Onsen, etc., and consumers have a long built-up impression of Yunnan Province as the base of jades that forms the saying "Jade Originates from Yunnan". Such combination makes the consumption of clients of travel teams an important pillar for jadeite sales in Tengchong.

Kunming: As the capital city of Yunnan Province, Kunming, like Guangzhou, integrates features of different markets in the province and boasts a relative complete selection of jadeite productions in terms of both quantity and quality.
Kunming jadeite market mainly includes three places, the first one includes the historical Kunming King Star Flowers & Jewelries World and the Kuming Generations King Star Jewelry City, the second one is the Yunnan Mineral & Jewelry Trade Center, and the third one is the Emerald Business Zone of Cuihu District. The first two markets feature small private stores that wholesale and retail a large variety of products at elastic prices, while the Cuihu Jadeite Business Zone features large stores of large jewelry enterprises that cater to retail customers with high-end products.

Retail markets in China

1. Beijing
Beijing is the political, economic and cultural center in China and concentrates a consumer group with highest buying power in the whole nation, thus it also becomes the most import end market for jadeite retailing. Beijing's jadeite market mainly consists of the Beijing International Jewelry Trade Center, the Panjiayuan Antique Market, the Xinjiekou Wanfeng Jewelry City, the Wanfeng Jewelry City, the Guanyuan Jewelry Market, etc. In addition, there are also such famous large jadeite stores in Beijing as Colourful Yunnan, Zhaoyi Jadeite, etc., which sell mid-end and high-end jadeites and jewelries. In terms of style, Beijing consumers tend to buy accessories, bracelets and other bulky products that integrate classical Chinese elements. Beijing consumers normally buy for private collection and gift, for private collection; they would spend more time in selection, while gift buying can be knocked off quickly. In general, Beijing consumers are quick at making a buying decision and would make a buy on the spot if they are fond of a product.

2. Shanghai
Shanghai's jadeite retailing market mainly concentrates in three places such as the Chenghuang Temple, Nanjing West Road and the Bund. In the Chenghuang Temple area, there are such large enterprises as Lao Feng Xiang, East Diamonds, Zhang Tiejun, Chenghuang Jewelry, etc., and there are also small private stores at the second to sixth floors in Zijincheng, their goods focus on popular accessories. Focusing on high-end jadeites, stores on Nanjing West Road and in the Bund Business District are located in high-grade commercial blocks or high-end supermarkets. In terms of style, Shanghai consumers prefer simple, modern, delicate and exquisite articles. Shanghai consumers are rational in consumption, and most of them buy jadeite ornaments for wearing or collection, thus they would visit stores regularly to carefully pick jadeite ornaments that cater to their taste and would go to other similar stores to compare prices. They would only make a buying decision when they feel the prices match their psychology. However, they show a high degree of loyalty once they have faith in a particular store.

References

Zhang Zhifang, 2006. Jadeite book. ISBN 7-222-04824-3.

Bosshart G., 2006. Old and new Jade roads from the Jadeite jade mines in Upper Burma to the vast market-places of Chinese cities. Proceedings 1st International Gem and Jewelry Conference, Gem and Jewelry Institute, Bangkok. 43.

Cecilia Lam, 2005. Jade. ISBN 962-86332-5-2.

Ma Baozhong, 2008. Research of jadeite trading in Yunnan. ISBN 962-450-319-2.

Treated black sapphire

Thanong Leelawatanasuk, Namrawee Susawee, Marisa Maneekrajangsaeng, Saengthip Saengbuangamlam, Supparat Promwongnan, Nicharee Atsawatanapirom, Pantaree Lomthong, Pornsawat Wathanakul

The Gem and Jewelry Institute of Thailand (Public Organization), Bangkok, 10500, Thailand; lpantaree@git.or.th

Keywords treated sapphire, black sapphire, treated corundum

Introduction

Diffusion treated corundum was introduced to the gem market in the late 1970s (Kane et al., 1990). The process involved high-temperature heating of colorless or near-colorless corundum mixed with chemicals in a crucible for a long time. Such a treatment could allow color-causing elements (such as titanium for blue coloration, or chromium for red one) to penetrate into the gem surfaces and produced the desired gem products.

Since late 2013, a variety of gemstone sold as "black sapphire" has entered the market. The result of our preliminary investigation on those stones were quickly reported to the gem community (see GIT'S LAB INFO by Leelawatanasuk and Maneekrajangsaeng, January 2014; Leelawatanasuk et al., 2014). This article is the update of our detailed investigation on this material.

Material and methods

Four "black sapphire" samples (two obtained in late 2013 and the other two in mid 2014) were selected for this study. They were faceted stones come in mixed cut, oval shapes, weighing from 1.44 to 1.91 cts. (Figures 1 and 2). All stones were recorded for standard gemological properties, such as refractive index (RI), specific gravity (SG), pleochroism, fluorescence and internal features under gem microscope with different lighting conditions and immersion method as well as DiamondView™ instrument.

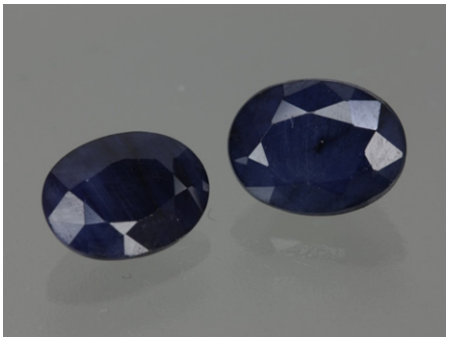

Figure 1. Two very dark blue (nearly black) stones weighing 1.44 ct. (left) and 1.91 ct. (right) obtained in late 2013. Photo: W. Krajae-Jan.

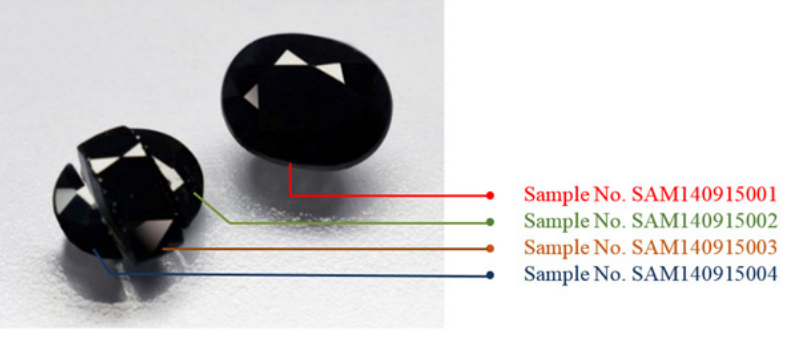

Figure 2. The sliced stone on the left weighs 1.54 ct. altogether, and the one on the right weighs 1.80 ct. obtained in mid 2014. Photo: S. Saengbuangamlam.

For advanced testing, we used a UV-Vis-NIR spectrometer (Model Lambda 950), Fourier Transform Infrared Spectrometer (FTIR, model Nicolet 6700), Soft X-Ray radiograph and Energy Dispersive X-ray Fluorescence Spectrometer (EDXRF, model Eagle III) and Raman Spectroscopy (Renishaw, InVia) to collect specific spectroscopic data.

Results

General properties
The samples appear from extremely dark blue to almost black with low transparency under daylight (Figures 1 and 2). The stones' standard gemological properties are generally consistent with natural sapphire. These four stones possess the RI values of 1.760 – 1.770 and SG values of 3.95 – 4.01. The stones show none to moderate dichroism from very dark blue to dark greenish blue through a dichroscope and inert under both LWUV and SWUV.

Microscopic features
Under magnification with normal illumination, the stones contain many healed fissures which made it difficult to find natural inclusions (Figures 3 and 4 left). However, fiber-optic lighting technique would be very helpful method to find blue to black color concentration along the healed fissures throughout the whole stones (Figures 3 and 4 right).

Due to the lack of transparency of mid 2014 stones, we decided to cut one stone (1.54 ct.) into 3 pieces in order to see more inclusions and provide better results from advanced testing (Figure 2). The polished slabs (~1 mm thick) reveal many features indicating the natural origin of raw material, such as cloud of silk pattern (Figure 5) and repeated twinning (Figure 6).

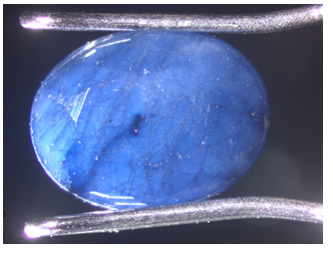

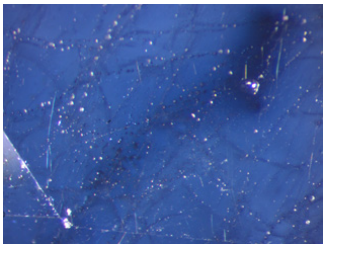

Figure 3. The appearance of stone under a microscope with strong fiber optic light (left, 20x magnification) and a closed-up view of the surface showing dark blue coloration along those healed fissures (right, 40x magnification). photos: M. Maneekrajangsaeng.

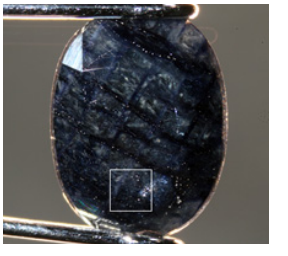

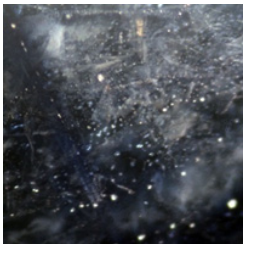

Figure 4. Many healed fissures with color concentration throughout the whole stone, noted also the white spots of residue material left-over along healed fissures after treatment (Sample No. SAM14091500; left, 20x magnification; right, enlargement of the square area on the left, 40x magnification). Photos: S. Saengbuangamlam.

Immersion in di-iodomethane (methylene iodide) reveals the unusual color concentration along healed fissures due to diffusion of color-causing element(s) outward from the fissures into the host sapphire. A Blue color rim was also observed along the stone surface outline indicating color penetration inward from outside of the stone (Figure 7)**.** With high-intensity ultra-shortwave UV radiation of the DiamondView™ (~225 nm), all samples show strong chalky blue fluorescence along the healed fissures (Figures 8 and 9).

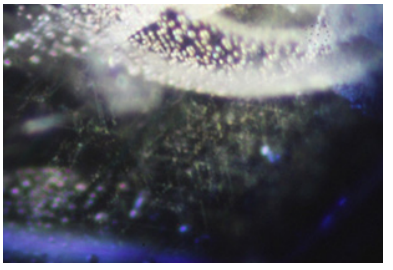

Figure 5. Cloud of silk pattern under dark field illumination of the mid 2014 stone (50x magnification). Photo: N. Atsawatanapirom.

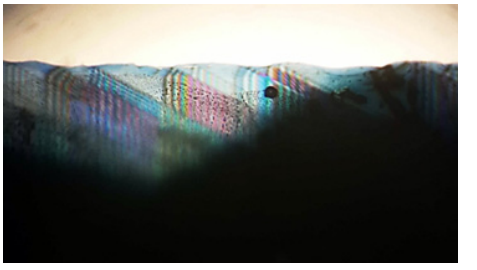

Figure 6. Repeated twinning of the mid 2014 stone seen under immersion in di-iodomethane solution. Photo: S. Saengbuangamlam.

Figure 7. Color concentration along healed fissures and blue color rim along the mid 2014 stone surface outline seen under immersion in di-iodomethane solution. Photos: S. Saengbuangamlam.

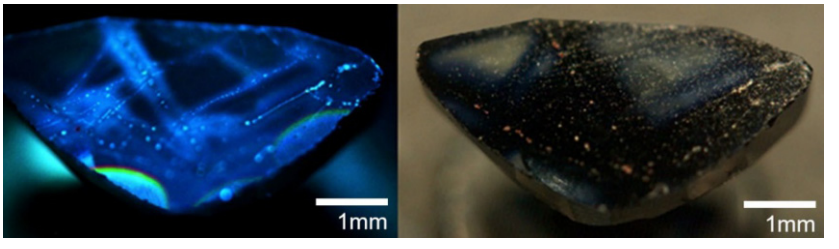

Figure 8. DiamondView™ images showing strong chalky blue fluorescence zones and bright dots in the mid 2014 slab sample no. SAM140915003 (left, SWUV light) that correspond to the dark blue diffusion bands and dots of residue material along the healed fissures (right, normal light). Photos: S. Promwongnan.

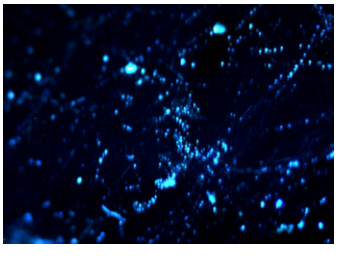

Figure 9. The DiamondView™ image showing chalky bluish glow along the healed fractures of late 2013 stone. Photo: M. Maneekrajangsaeng.

Advanced instrumental analyses

The UV-Vis-NIR spectra of the late 2013 samples reveal iron-related absorption peaks at 377, 388, 450 nm, and Fe^{2+}/Ti^{4+} Intervalent charge transfer (IVCT) band at ~580 nm indicating the stone's 'metamorphic origin' (Figure 10). By contrast, the UV-Vis-NIR spectra of the mid 2014 samples clearly give not only the Fe-related peaks at 377, 388, 450 nm and Fe^{2+}/Ti^{4+} IVCT band at ~580 nm, but also the Fe^{2+}/Fe^{3+} IVCT absorption bands at ~900 nm indicating the stone's 'basaltic origin' (Figure 11). Notably the absorption spectrum of the blue zone shows higher intensity of Fe^{2+}/Ti^{4+} IVCT absorption band near 580 nm than that found in the paler color zone of the same slab sample.

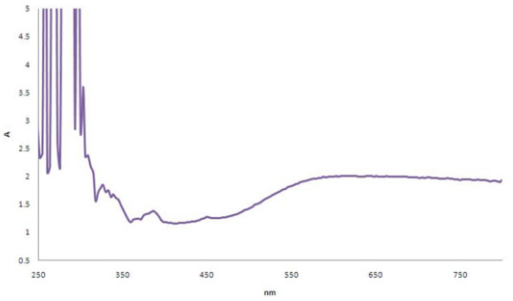

Figure 10. Non-polarized UV-Vis spectrum of late 2013 stone showing small Fe-related absorption peaks at 377/387 and 450 nm and dominant Fe^{2+}/Ti^{4+} IVCT absorption band maximized at around 575 nm.

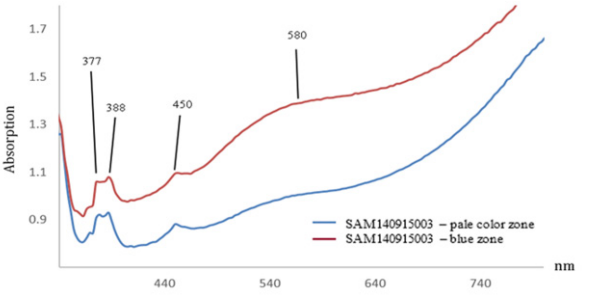

Figure 11. Non-polarized UV-Vis absorption spectra illustrating the differences in the blue and paler color zones of the mid 2014 slab sample no. SAM140915003, the spectra merely displayed up to 800 nm due to signal error at higher nm region.

EDXRF analyses of all samples give the major amounts of Al with minor to trace amounts of Fe, Ti, V, Cr and Ga without Pb, Bi or Ba. For the polished slab (no. SAM140915003), the blue and paler color areas give similar contents of Fe, V, Cr, and Ga, but the amount of Ti content of the blue area is higher than that in the paler color area. The X-ray image shows no high contrast area that are consistent with the chemical analysis result. This implies that no heavy elements (such as lead) were added during the treatment. The Mid-IR spectrum shows absorption pattern usually found for a corundum with two OH-related peaks at 3602 and 3702 cm^{-1}.

Discussion and conclusion

The late 2013 samples are blue to dark blue stones that were treated from starting raw material of metamorphic origin. By contrast, the mid 2014 samples apparently look much darker blue to almost black stones that were treated from starting raw materials of basaltic origin. The starting raw materials could be low-quality, near-colorless-to-pale-colored sapphire with abundant open fissures from both types of origins that were treated by a usual Ti-diffusion technique. Having been heavily fractured materials to begin with, the Ti compound could enter into the stone via open fissures and the Ti-diffusion could have been taken place from the fissures outward into the host corundum while those fissures were also healed during high temperature treatment. Hence, Ti-diffusion technique could create dark blue color zones extending outward from the fissures inside the stone and make them look very similar to a black sapphire. As such, these new products should to be called "diffusion-treated black sapphire", rather than 'black sapphire' in the market

Acknowledgements

The authors would like to express their thanks to Dr. Visut Pisutha-Anond, Ms. Wilawan Atichat, Mr. Surapon Chaiamnuay for help improving this manuscript. Thanks also go to Mr. Pipop Tangjaipak who provided the mid 2014 stones for this study.

References

Kane, R. E., Kammerling, R. C., Koivula, J. I., Shigley, J. E., Fritsch, E., 1990. The identification of blue diffusion-treated sapphires. Gems & Gemology, Vol. 26, No. 2, Summer. 115-133.

Leelawatanasuk, T., Maneekrajangsaeng, M., 2014. A treated stone sold as 'Black Sapphire', GIT LAB INFO, January 2014, 8 p., http://www.git.or.th/2014/eng/testing_center_en/lab_notes_en/glab_en/2014/treated_black_diffused_sapphire.pdf.

Leelawatanasuk, T., Susawee, N., Saengbuangamlam, S., Promwongnan, S., Atsawatanapirom, N., Atichat, W., Pisutha-Arnond, V., Sriprasert, B., 2014. Treated "black sapphire" update, Proceedings of the 4th Gem and Jewelry Conference (GIT 2014), December 8-9, 2014, 126-130.

Synthetic ruby overgrowth on natural corundum

Supparat Promwongnan, Saengthip Saengbuangarmlum, Thanong Leelawatanasuk

The Gem and Jewelry Institute of Thailand (Pub. Org.), Bangkok 10500, Thailand; psupparat@git.or.th

Keywords Synthetic Ruby, Overgrowth, Flux, Diffusion ruby

Introduction

Synthetic ruby has been manufactured by many different techniques, such as flame fusion, hydrothermal or flux processes. Because of the low cost and rapid production process, flame-fusion is, by far, the most common method and is still being used for making large color varieties of man-made corundum sold in the marketplace todays. Nonetheless, other types of synthetic ruby are still available in the trade. For example, a flame-fusion seed crystal with synthetic flux overgrowth in a single stone occasionally appeared in the market and has been reported earlier (Kane, 1985; Gübelin and Koivula, 2005; Sun and Breitzmann, 2014). In early January 2015, an unusual synthetic ruby was encountered in the trade. This stone is somewhat different from the above mentioned synthetics and will be described below.

Sample and procedures

The sample used in this study was a 1.84 ct. faceted (oval, mixed cut) ruby (Figure 1). In the face-up position, the stone appears purplish red similar to a natural ruby. Basic gem instruments were used to collect the stone's standard gemological properties, such as refractive indices, optic sign, specific gravity, pleochroism, long-wave (365 nm) and short-wave (254 nm) ultraviolet fluorescence. The internal features were observed under both normal-type and immersion-type (methylene iodide) microscopes, and fluorescence images were taken by using the DiamondView.

Figure 1. The 1.84-ct. faceted cut ruby used in this study. Photo. by S. Saengbuangamlam.

For collecting some specific spectroscopic data, we used the following advanced instruments: Thermo-Nicolet 6700 Fourier-transform infrared (FTIR) spectrometer, Perkin Elmer Lambda 950 ultraviolet/visible/near-infrared (UV-Vis-NIR) spectrometer, Renishaw inVia Raman micro-spectrometer with a green laser (532 nm excitation) and Energy-dispersive X-ray fluorescence (EDXRF) spectroscopy with an Eagle III system.

Results and discussion

Gemological properties

The stone's standard gemological properties are consistent with those of ruby (see Table 1). The sample shows strong red fluorescence under long-wave UV radiation and moderate pinkish red under short-wave UV radiation.

Table 1. Gemmological properties of synthetic ruby overgrowth on natural corundum

Property	Values and Description
Refractive Index	1.762–1.770 (0.008); Uniaxial Negative
Polariscope Reaction	Doubly Refractive
Specific Gravity (Hydrostatic)	4.02
Pleochroism	Purplish red / orangy red
UV Fluorescence	LW: strong red, SW: moderate pinkish red

Microscopic features

Microscopic examination can disclose many unusual internal features. The stone comprises two parts, a thick, strong red, overgrowth layer and a palercolored core (Figure 2 left). The overgrowth layer shows many tiny, wispy, veil-like fingerprints, typical of synthetic flux-grown ruby (Figure 2 left and center). A roiled effect, due to an irregular growth structure is also present near the boundary between the overgrowth layer and the core (Figure 2 right).

Figure 2. The thick red overgrowth layer clearly seen on the pavilion side of the stone (left, magnified 16X). Higher magnification of the overgrowth layer reveals numerous fine wispy veil-like flux inclusions (center, magnified 25X) and a roiled effect due to the irregular growth structure near the boundary between the overgrowth layer and the core (right, magnified 25X). Photo by S. Promwongnan.

The core area, on the contrary, contains many large planar fingerprints, two-phases fluid inclusions that appeared as drip-like trails and melted crystals, indicating a heat-treated sapphire (Figure 3). These pieces of contrasting evidence lead to the conclusion that this stone is a flux-grown synthetic ruby overgrowth on a heat-treated sapphire seed crystal.

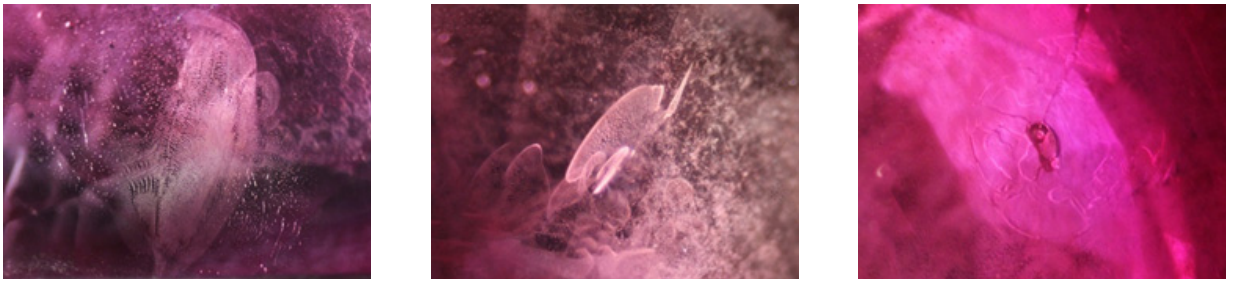

Figure 3. Magnification of the stone's core area showed many natural planar fingerprints (left and center, magnified 20X) and a melted inclusion indicating its natural origin (right, magnified 25X). Photo by S. Promwongnan.

Under an immersion microscope, using low magnification, the complete overgrowth layer all along the core of the stone, appeared as a sharp contact boundary (Figure 4 left). The core occupies a major part of the stone and is near-colorless (Figure 4 right). The overgrowth layer is strong red and rather thick on the pavilion side but very thin on the crown side.

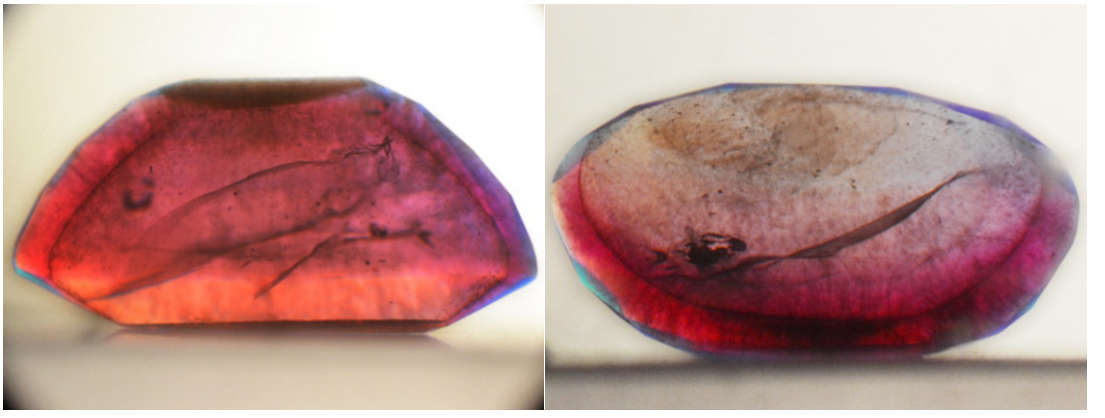

Figure 4. Immersion images clearly showed the near-colorless core occupying a major part of the stone and the thick red color overgrowth layer on the pavilion side (left: side view of the stone, table-down position; right: side view of the stone, tilted-table-facet-up position; immersion in methylene iodide solution under diffuse light-field illumination, magnified 20X). Photo by S. Saengbuangamlam.

Fluorescence images obtained by the DiamondView are also very useful for identification. The image shows a part of the core that reached the surface at the star and bezel facets on one side of the crown (Figure 5). The part that reached the surface was inert to the UV radiation while the overgrowth layer showed an intense, even red fluorescence. Such strong contrasting fluorescence reaction is due to the difference of trace element constituents between the overgrowth layer and the core material (see Table 2). The flux fingerprint inclusions on the table facet also appeared as bright red fluorescence patches on the DiamondView image (Figure 5).

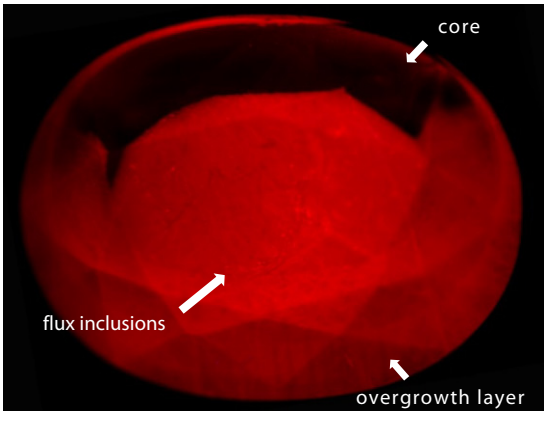

Figure 5. DiamondView image of the stone (face-up) showing the non-fluorescence core reaching the surface at the star and bezel facets above (dark area) in contrast to the intense even red fluorescence overgrowth layer on the table, star and bezel facets below. Note also the bright red fluorescence patches of flux fingerprint inclusions on the table facet. Photo by S. Promwongnan.

Advanced instrument analysis

The Mid-IR spectra give the absorption spectrum commonly found for corundum. The UV-Vis absorption spectra show absorption bands due to Cr^{3+} as typical color-causing element in ruby. Raman analysis also confirms that both synthetic overgrowth layer and natural core part of this stone are corundum.

Semi-quantitative chemical analysis (see Table 2) indicates very low contents of Fe, Ti and Ga but rather high Cr on the overgrowth layer of pavilion side. On the contrary, the core part of the stone reaching the surface at the star

and bezel facets gives relatively higher contents of Fe, Ti and Ga but rather low Cr. Such contrasting results again are consistent with chemical elements commonly found in synthetic flux-grown ruby and natural sapphire, respectively.

Table 2. Trace element contents of the core and overgrowth layer of the stone obtained by EDXRF

Element Oxides (wt.%)	TiO_2	V_2O_5	Cr_2O_3	Fe_2O_3	Ga_2O_3
The overgrowth layer on the pavilion	<0.01	0.01	0.65	<0.01	<0.01
The exposed core area	0.01	<0.01	0.07	0.08	0.01

Conclusion

Based on the aforementioned data, it can be concluded that this stone is a synthetic ruby overgrowth on a natural corundum seed crystal. In fact, this synthetic product is not new but has been circulated in the market since the early 2000s (Smith, 2002). At that time this product was sold under the name "Diffusion ruby", but later most of these gem materials were proved to be synthetic ruby overgrowth on natural sapphire rather than diffusion of chromium into the crystal lattice of corundum. This synthetic product was faded out from the market for a decade. However, the product could re-emerge in the market anytime. Therefore, careful microscopic examination of the stone is necessary to clearly distinguish this type of synthetic stone from a natural ruby. Distinctive inclusions are the sharp contact boundary under immersion and the strong contrasting fluorescence behavior under the DiamondView, between the synthetic overgrowth layer and the natural seed crystal.

Acknowledgements

We would like to express our profound thanks to Dr. Visut Pisutha-Anond, Ms. Wilawan Atichat, Dr. Pornsawat Wathanakul and Mr. Boontawee Sriprasert for their valuable suggestions and their kind reviewing and editing of this article.

References

Gübelin, E.J., Koivula, J.I., 2005. Flux overgrowth on flame-fusion seed crystals, Photoatlas of Inclusions in Gemstones, Vol.2, Opinion Verlag, Basel, Switzerland, p. 352.

Kane, R.E., 1985. A preliminary report on the new Lechleitner synthetic ruby and synthetic blue sapphire, G&G, Vol.21, No.1, p. 35–39.

Smith, C.P., 2002. Diffusion Ruby proves to be synthetic ruby overgrowth on natural corundum, G&G, Vol.38, No.3, p.240-248.

Sun, Z., Breitzmann, H., 2014. Flame-fusion synthetic ruby boule with flux synthetic ruby overgrowth, G&G, Vol.50, No.3, p. 242-243.

www.lithuania.travel photo

INTERNATIONAL GEMMOLOGICAL CONFERENCE

History of the IGC

The International Gemmological Conference (IGC) owes much of its origin to BIBOA (*Bureau International pour la Bijonterie, Orfevrene, Argenterie*), the International Jewellery and Gemstone Federation, the first Congress of which in 1926 recommended and defined use of the term cultured pearl.

Experts from various European gem testing laboratories were invited to attend a series of expert meetings that aimed to formulate the policies of BIBOA. In 1936, at the fifth conference of experts, collaboration among laboratories was acclaimed by traders and they encouraged Laboratory Directors to meet each other at a technical conference from which all commercial delegates would be excluded.

Technical meetings were held annually, and in 1951 a Technical Conference was held in Idar Oberstein to prepare for the next London Congress in 1952. Those attending the 1951 conference included Mr B.W. Anderson, Mr G. Gobel, Dr E. Gubelin, Mr F. Wolf, Mr A. Bonebakker, Mr H. Tillander, Mr A. Strondahl, and Mr O. Dragstead. It has been suggested that the future framework of the IGC was established at this meeting in Idar Oberstein.

The London Congress saw the restructuring of BIBOA in which Gemmological Associations were replaced by National Federal Committees, and BIBOA evolved into BIBOAH—the forerunner of CIBJO, now known as The World Jewellery Federation.

A Technical Conference met at Lugano from 23rd to 25th October 1952 at the initiative of Prof. K. Schlossmacher and Dr. E. Gubelin. Also present at this conference were Messrs B.W. Anderson, A. Bonebakker, O. Dragstead, G. Gobel, K. Siess and H. Tillander. At this historic meeting Dr E. Gubelin proposed creation of a "Committee of an International Gemmological Association" that would consist of one member per country; this member being the Director of a Gem Testing Laboratory, or a gemmologist of the calibre who could attend that meeting. This was agreed to, and this meeting was later considered to be the inaugural meeting of the IGC.

The first meeting of the IGC in Lugano was followed by subsequent meetings in Amsterdam (1953), Copenhagen (1954), London (1955), Munich (1956), Oslo (1957), Paris (1958), Milano (1960), Helsinki (1962), Vienna (1964); Barcelona (1966); Stockholm (1968); Brussels (1970); Vitznau, Switzerland (1972); Washington D. C. (1975), The Hague (1977), Idar Oberstein (1979), Kashiko-Jima (1981), Beruwela, Sri Lanka (1983); Sydney, Australia (1985); Rio de Janeiro (1987), Tremezzo, Italy (1989); Stellenboch (1991), Paris, France (1993); Bangkok, Thailand (1995); Idar Oberstein, Germany (1997); Goa, India (1999); Madrid, Spain (2001), Wuhan, China (2004); Moscow, Russia (2007); Arusha, Tanzania (2009), Interlaken, Switzerland (2011); Hanoi, Vietnam, (2013) and 34th will be held in Vilnius, Lithuania (2015).

Over the history of the IGC, that now in its fourth decade, it can therefore be seen that the International Gemmological Conference is the longest surviving gemmological conference to remain largely in its original format. Over its history, invited delegates representing 33 countries or areas – including Australia, Austria, Belgium, Brazil, Canada, China, Czech Republic, Denmark, England, Finland, France, Greece, Germany, Hong Kong, Israel, India, Italy, Japan, Kenya, Korea, Netherlands, Norway, Russia, Singapore, South Africa, Spain, Sri Lanka, Switzerland, Sweden, Thailand, U.S.A. and Zimbabwe – have been invited to participate in IGC meetings.

During the 20th IGC, which was held in Sydney, Australia, the members present elected nine members to Honorary Members status. The first Honorary Members of the IGC were Oliver Chalmers (Australia), Prof. A. Chikayama (Japan), and Mr R. Crowningshield (U.S.A), Mr. O. Dragsted (Sweden), Prof. Gubelin (Switzerland), Mr. R. T. Liddicoat (U.S.A), Mr. M. Masso (Spain), Dr. F. H. Pough (U.S. A) and Dr. J. M. Saul (Kenya).

In Italy, the IGC logo was designed by Roberto Sambonet and made in gold by Roberto Cusi offered to the conference delegates during the Tremezzo 1989.

In Italy, in 1989, the following rules were agreed for future meetings of the IGC:

1. The prime objective was to be the exchange of gemmological experiences.
2. Gemmology was to be the platform for all topics and was to be regarded as the principal theme.
3. It was decided that attendance at all further Conferences should be by invitation that would be determined where necessary by the Conference Secretary and the Executive Committee.
4. All delegates were to be encouraged to present papers; but this would not be mandatory.
5. All delegates must have a publishing record and all papers at IGC meetings must presented in English, both when written or spoken.
6. The Conference must keep foremost in mind the prime objectives and avoid dilution/confusion of this objective which, if not maintained, could result in a blank organization without true status or credibility.
7. Peripheral commercial activity must be kept to a minimum, and there should be no blatant sponsorship of any kind.

These rules, combined with the original concepts, have been kept as the basis for all conferences since. Any invitation is specific to the person invited and is not transferable.

Rules/Standard Operating Procedures of the IGC

Membership
Membership of the IGC shall consist of:

1. **Honorary Members** are those who are senior members of the IGC and are elected by Delegates on an as-required basis.
2. **Delegates** are those who are elected from Observers, on the recommendation of the Executive Committee, from those Observers who have presented (in English) worthwhile presentations (either lectures, and/or posters) at three successive IGC meetings before becoming eligible for election as a Delegate.
3. **Observers** are those who shall be well published, internationally recognised gemmologists who are invited to attend IGC meetings on the invitation of either the Executive Committee, Delegate/s from the country in which they are resident, or the Conference Secretary of the country in which the IGC meeting is to be held.

   Applications for Observer status, which shall be supported by a pertinent CV and list of publications, should be submitted to the Executive Committee for consideration before any invitation to attend an IGC is offered by the Conference Secretary.

Executive Committee
The day-to-day administration and decision making of the IGC shall be overseen by an Executive Committee that meets formally at IGC meetings, and in between meetings conducts the routine business of the IGC electronically by

email. Following nomination, new members of the Executive Committee shall be elected by majority vote of Delegates at the Business Meeting that follows each IGC.

From time to time, the Executive Committee shall elect a **Chairman** and also one **Honorary Secretary,** who will be responsible for detailed administration and the distribution of decisions of the Executive Committee to Honorary Members and Delegates.

Written minutes shall be kept for all meetings of the Executive Committee and General Business Meetings of Delegates. Copies of these minutes shall be circulated by the Honorary Secretary to eligible Honorary Members and Delegates.

Meetings of the IGC

IGC meetings should be held every two years in a host country approved by Honorary Members and Delegates. Historically these meetings have been held in odd calendar years.

IGC meeting should be timed so as not to clash with other meetings (e.g. IMA meetings) that Delegates are likely to attend.

The venue for IGC meetings should alternate between European and non-European countries.

A country wishing to host an IGC meeting shall submit their proposal first to the Executive Committee and then formally present their proposal to Delegates. The decision to accept or reject a proposal to host an IGC meeting will be made by majority vote of Honorary Members and Delegates present at the IGC Business Meeting, or electronically if an IGC meeting is not being held at the time a decision needs to be made.

Countries hosting IGC meetings shall establish their own administrative structures to ensure the efficient planning and operation of the IGC. Costs involved in hosting an IGC shall be met by Registration Fees paid by Honorary Members, Delegates and Observers attending the meeting, and financial sponsorship from private, institutional and government sources. Day-to-day administration for an IGC shall be the responsibility of an elected Conference Secretary, who shall be either an Honorary Member or Delegate of the IGC.

General responsibilities of the Conference Secretary of each IGC include:

- Planning and implementation for the IGC of:

  pre-conference activities

  post-conference activities

  the formal IGC conference

  associated cultural activities and events

  guest entertainment program

  all finances

  receipt and compilation of abstracts of papers

  publication of proceedings of IGC conference

  implementation of poster presentations
- Obtaining the necessary government permissions and other political factors
- Organisation of formalities required for different foreign visitors in the host country e.g. visas, special permissions etc.

Attendance at IGC meetings, of Delegates and Observers from countries other than the host country, shall be restricted to a maximum of five registrations per country. This restriction does not include Honorary Members.

Each IGC shall consist of a minimum of:

1. Two to three day pre-and post-conference study excursions to areas and facilities of gemmological interest.
2. A 1-day session, prior to the IGC, at which previously nominated delegates and/or observers will be invited to give presentations to gemmologist members of the country hosting the IGC.
3. A five-day professional conference that shall consist of:

   Formal papers of 15 minutes duration, followed by 5 minutes of questions and answers; and,

   Poster presentations that shall be scheduled independently so that adequate time is allowed for each poster to be presented by its author/s and then have its content available for discussion by interested delegates.
4. A Business Meeting for Delegates of a maximum of 1 hour duration that traditionally follows closure of the IGC professional conference.
5. A 1-hour General Discussion session to allow Honorary Members, Delegates and Observers time to exchange opinions on future directions of the IGC.

To minimise duplication of content, the titles and brief outlines of all papers, which an Honorary Member, Delegate or Observer plans present at an IGC meeting, shall be submitted to the Executive for approval. Illustrations used for presentations at IGC meetings shall be presented in CD ROM (not laptop computer), 35 mm slide, or OH projector formats.

If feasible, future meetings of the IGC should be held at the hotel/institution in which the accommodation for Honorary Members, Delegates and Observers has been arranged by the Host country organising committee.

If sufficient seating is available at the venue/s for future IGC lectures, gemmology students from the country hosting the IGC shall be encouraged to attend lectures presented at that IGC.

Addendum to 34th IGC 2015 Proceedings

Residual pressure distribution and visualization of mineral inclusions in corundum: application of photoluminescence spectroscopy in relation to sapphires from New England, New South Wales, Australia

Ahmadjan Abduriyim

Gemological Institute of America (GIA), Tokyo Laboratory; aabduriy@gia.edu

Distribution of residual pressure around mineral inclusions within diamond crystals has been measured by micro-Raman analysis to estimate the depth of origin of diamond (Izraeli et al., 1999; Barron, 2003; Kagi et al., 2009). Corundum, which can form in mantle-crust levels, usually shallower than those of diamond, has the next highest hardness to diamond on Mohs scale, and residual pressure also is observed around inclusions within corundum crystals (Wang et al., 2006; Wathanachchaisaeng et al., 2006; Sutherland et al., 2009; Noguchi et al., 2013).

When a diamond crystal grows inside the mantle, a fragment or fluid from surrounding rocks may be taken into the crystal as an inclusion. At this time, dynamic equilibrium exists between the inclusion and the host diamond, and differential stress is absent (Kagi, 2004). As a diamond travels from depth to the surface, both pressure and temperature decrease. Falling pressure means increase in volume of the crystal, while reduction of temperature means decrease in volume. Relative volume variations in a substance due to alterations of pressure and temperature depend on the contrast between the host and included mineral in terms of compressibility and thermal expansivity respectively. Similarly, an inclusion and surrounding host corundum will show different deformation behavior against temperature and pressure, and this may result in different volume variation after they reach the surface. The inclusion within the corundum may increase in volume within the corundum when taken up to the ground surface, and differential stress acts on the interface between the two materials, thus pressure can remain around the inclusion. Such inclusions provide clues to estimate the mineral formation conditions in the deeper lithosphere. If residual pressure around the inclusion can be measured, it will indicate a potential PT path on which the inclusion was taken into the corundum. Also, by measuring the residual pressure around inclusions in corundum which formed in similar host rock but in a different geographical area, it will enable assessment of their relative depths of formation.

Corundum (Al_2O_3) often contains minor Cr^{3+} which produces a fluorescence spectrum, the so-called R-lines are caused by the cation being excited by a visible light such as a laser. The peak position of these lines is sensitive to pressure so that residual pressure within corundum can be calculated by this fluorescence spectrum (Chai and Brown, 1996). A fluorescence spectrum has the advantages of non-destructive analysis as like Raman spectral analysis but it is shorter measurement period than Raman analysis which gives very weak signals compared with fluorescence from corundum.

In this study, we aimed at investigating how residual pressure was distributed three-dimensionally by measuring residual pressure around mineral inclusions in natural corundum. The materials used for the study came from the New England sapphire field, New South Wales, eastern Australia.

Automorphic zircon, albite, brookite and a pyrochlore group mineral were identified as inclusions in sapphires from Kings Plains mine near Inverell in New South Wales, Australia. Residual pressures around the mineral inclusions had ranges from 0.07GPa to 0.54GPa. Except for brookite, residual pressure distributions

were found to be anisotropic. The anisotropic residual pressure distribution can be explained by anisotropy in thermal expansion and volume elasticity (incompressibility) of host sapphire and inclusions. The length of inclusions was positively correlated with the maximum residual pressure, and zircon inclusions fell in higher (0.47–0.54GPa) and lower (0.07–0.27 GPa) residual pressure groups. This dichotomy is caused by relative orientation between sapphire and zircon. When the c-axis of sapphire and zircon are nearly parallel, residual pressure was higher.

References

Barron L.M., 2003. A simple model for the pressure preservation index of inclusions in diamond, American Mineralogy, 88, pp. 1615–1619.

Chai M., Brown J.M., 1996. Effects of static non-hydrostatic stress on the R line of ruby, Geophysical Research Letters, 23, pp. 3539–3542.

Izraeli E.S., Harris J.W., Navon O., 1999. Raman barometary of diamond formation, Earth and Planetary Science Letters, 173, pp. 351–360.

Kagi H., 2004. The diamond formation condition explored from the inclusion of natural diamond, Journal of Mineralogical and Petrological Sciences, 33, 98–105, in Japanese.

Kagi H., Odake S., Zedgenizov D.A., 2009. Raman spectroscopic estimation of depth of diamond of origin: technical developments and the application, Russian Geology and Geophysics, 50, 1183–1187.

Noguchi N., Abduriyim A., Shimizu I., Kamegata N., Odake S., Kagi H., 2013. Imaging of residual strain distribution around an inclusion in sapphire by combination of micro-Raman photoluminescence spectroscopies, Journal of Raman Spectroscopy, 44(1), pp. 147–154.

Sutherland F.L., Giuliani G., Fallick A.E., Garland M., Webb G., 2009. Sapphire-ruby characteristics, west Pailin, Cambodia: clues to their origin based on trace element and O isotope analysis. Australian Gemmologist, 23(9), pp. 373–432.

Wang W., Scarratt K., Emmett J.L., Breeding C.M. and Douthi T.R., 2006. The effects of heat treatment on zircon inclusions in Madagascar sapphires, Gems & Gemology, 47(2), pp. 134–150.

Wanthanachaisaeng B., Häger T., Hofmeister W. and Nasdala L., 2006. Raman –und flloueszenz –spektropische Eigenschaften von Zircon-Einschlüssen in chrom-haltigen Korunden aus Ilakaka und deren Veränderung durch Hitzebehandlung, Zeitschrift Deutsche Gemmolische Gesellschaft, 55 (3–4), pp. 119–132.